UNIVERSITÀ DELLA CALABRIA

UNIVERSITA' DELLA CALABRIA

Dipartimento di Chimica e Tecnologie Chimiche – CTC

Rende, Italy 2017

Dottorato di Ricerca in

Medicina Traslazionale

CICLO (XXIX)

TRANSITION METAL-BASED COMPLEXES AS
CHEMOTHERAPEUTIC AGENTS. THEORETICAL INVESTIGATION
OF MoA, INTERACTION WITH BIOLOGICAL MOLECULES AND
ENVIRONMENTAL CONDITIONS

AREA 03-Scienze Chimiche, SSD-CHIM03/Chimica generale ed
inorganica

Coordinatore: Ch.mo Prof. Sebastiano Andò

Supervisore: Prof.ssa Emilia Sicilia

Dottoranda: Dott.ssa Ida Ritacco

Abstract

Molti metalli e, conseguentemente, molti complessi metallici svolgono ruoli importanti all'interno di sistemi biologici e biochimici. Oggigiorno, è risaputo che essi rappresentano ingredienti molto importanti per la vita altrettanto quanto i composti organici. Per esempio, i complessi di ferro svolgono un ruolo fondamentale nel trasporto di O_2 nel sangue, i complessi di calcio sono alla base delle ossa, lo zinco è presente nell' insulina che regola la quantità di zucchero nel nostro corpo. Questo è possibile perché i metalli possiedono particolari proprietà chimiche. Infatti, tendono facilmente a perdere elettroni, diventando specie elettron-deficienti più reattive nei confronti di diverse molecole biologiche e più solubili in soluzioni acquose. I metalli non solo sono elementi vitali in molti fenomeni biologici, ma possono anche essere sfruttati per il trattamento di diverse malattie.

L'esempio più importante di questa categoria di composti è il complesso organometallico cisplatino $[Pt(Cl)_2(NH_3)_2]$, il chemioterapico più potente disponibile sul mercato. Scoperto nel 1969 da Rosenberg, esso svolge un ruolo chiave nell' inibizione della divisione cellulare, causando la morte delle cellule tumorali.

Dopo la scoperta della sua attività citotossica, l'applicazione di farmaci metallici nelle varie terapie ha registrato una crescita enorme e la continua ricerca dell'uso di metalli in medicina, in particolare per la cura del cancro, è diventata una disciplina, indicata come Medicinal Inorganic Chemistry.

Dopo la scoperta del cisplatino, altri due farmaci antitumorali a base di platino, derivati del cisplatino, sono stati scoperti: carboplatino e ossaliplatino. Questi complessi esercitano la loro azione citotossica coordinando il DNA e bloccando la divisione cellulare. Tuttavia, anche se questi complessi, di formula generale $[Pt(X)_2(L)_2]$, sono ancora tra i farmaci più frequentemente utilizzati, risultano essere tossici a causa della loro reattività e instabilità.

In questi anni, per superare i problemi relativi all'uso di complessi di Pt(II), l' attenzione è stata concentrata sullo sviluppo di nuovi complessi, generando due diverse categorie di farmaci antitumorali: i complessi di Pt(IV), considerati "profarmaci" e ottenuti per ossidazione dai complessi di Pt(II), e i "farmaci che non contengono platino", come i complessi di iridio, rodio, osmio o rutenio. Le caratteristiche di questi farmaci dovrebbero renderli più inerti, quindi più efficaci dei complessi di Pt(II), e provocare una differenziazione nel meccanismo di azione.

Lo studio teorico dei sistemi biologici ha ormai raggiunto la maturità necessaria per fornire informazioni complementari rispetto a quelle ottenibili sperimentalmente nello studio di molte proprietà e fenomeni. Infatti, l'impressionante sviluppo sia delle metodologie teoriche, sia della tecnologia informatica ha consentito di fornire un importante supporto di studi teorici alle bioscienze. Inoltre, l'uso della teoria del funzionale della densità (DFT), che rappresenta un ottimo compromesso tra accuratezza e costi computazionali, è particolarmente adatto allo studio dei sistemi biologici come dimostrato dal fatto che negli ultimi anni sono stati completati con successo molti studi DFT e sono state affrontate questioni fondamentali nelle simulazioni biologiche.

Scopo di questa tesi è lo studio teorico di farmaci antitumorali contenenti metalli, in particolare complessi di Pt(IV) e Ir(III), delle principali reazioni del farmaco che avvengono dal momento della sua iniezione o somministrazione orale al raggiungimento del suo bersaglio biologico e investigazione del meccanismo di azione che può essere sia quello classico, già proposto per il cisplatino e, quindi, associato all'accumulo cellulare e al legame con il DNA, sia un meccanismo di diversa natura. In alcuni casi, la teoria del funzionale della densità è stata utilizzata come approccio computazionale supportato da calcoli eseguiti a livello Coupled Cluster post Hartree-Fock nella sua versione CCSD(T).

INTRODUCTION

Many metals, and, consequently, many metal complexes play important roles in biological and biochemical systems. It is known, today, that they are very important ingredients in life as well organic compounds. For example, the iron complexes have a fundamental role in the O_2 transport in the blood, the calcium complexes are the basis of the bones, the zinc is present in the insulin, which regulates the amount of sugar in our body. This is possible because metals have particular chemical properties. Indeed, they easily tend to lose electrons, becoming electron deficient species, reactive towards various biological molecules and soluble in water solutions. Metals not only are vital elements in many biological phenomena, but they can be also exploited in therapeutics for a variety of diseases.

The most prominent example of such class of compounds is the organometallic complex cisplatin $[Pt(Cl)_2(NH_3)_2]$, the most potent chemotherapeutic available on the market. Discovered in 1969 by Rosenberg, it plays a key role in the inhibition of cell division, killing the cancer cells. Since its discovery the application of metal drugs for therapeutics has experienced a tremendous and continuous growth and the investigation of the use of metals in medicine, particularly for the treatment of

cancer, has become a discipline that is the Medicinal Inorganic Chemistry.

After the discovery of cisplatin, other two Pt-anticancer drugs, derivatives of cisplatin, have been discovered: carboplatin and oxaliplatin. These complexes exert their cytotoxic action by coordinating to DNA and stopping cell division. However, although these complexes, with general structure $[Pt(X)_2(L)_2]$, are still among the most frequently used drugs, they appear to be toxic, because of their chemical reactivity and instability.

In these years, to overcome Pt(II) complexes disadvantages, the research has turned its attention to the development of new complexes, producing two different anticancer drugs classes: Pt(IV) complexes, which are considered "prodrugs" and are obtained by oxidation of the Pt(II) complexes, and "no-platinum containing drugs", such as iridium, rhodium, osmium or ruthenium complexes. The characteristics of such drugs should both make them more inert and, consequently, more effective than Pt(II) complexes and cause a differentiation in the mechanism of action.

The theoretical investigation of biological systems has now achieved the needed maturity to complement the experimental approaches for the study of a large variety of properties and phenomena. The impressive development accomplished by both theoretical approaches and computer technology provides an

important support to biosciences in many fields. Density Functional Theory (DFT) use represents an optimal compromise between accuracy and computer resources, particularly suitable for the investigation of biological systems. Myriad of DFT studies, indeed, have been successfully completed in recent years and crucial issues in biological simulations have been addressed.

Aim of this PhD thesis is the theoretical study for metal-containing anticancer drugs, particularly Pt(IV) and Ir(III) complexes, of the main reactions in the complicated route of the drug from its injection or oral administration to its biological target and the elucidation of the mechanism of action that could be either the classical one already proposed for cisplatin and thus associated to both cellular accumulation and DNA binding, or could also follow different patterns. The Density Functional Theory is used as computational approach supported, in some cases, by calculations carried out at post Hartree-Fock Coupled Cluster level in its CCSD(T) version.

This PhD thesis is organized in five chapters:

- − Chapter I: Cancer and Anticancer Drugs: General Principles;
- − Chapter II: Theoretical Concepts and Computational Methods;

− Chapter III: Carnosine Role in Inhibition of Platinum II Drugs;

− Chapter IV: Platinum Complexes Hydrolysis;

− Chapter V: A New Class of Anticancer Drugs: Organoiridium(III) Complexes.

List of Papers included in this thesis

1. Collisionally-Induced Dissociation Products of the Protonate Dipeptide Carnosine: Structural elucidation, Fragmentation Pathways and Potential energy surface analysis.

Eslam Moustafa, Ida Ritacco, Emilia Sicilia, Nino Russo, Tamer Shoeib, *Phys. Chem. Chem. Phys.*, 17, 12673-12682, **2015**.

2. Fragmentation Pathways Analysis for the gas Phase Dissociation of Protonated Carnosine-Oxaliplatin Complexes.

Ida Ritacco, Eslam Moustafa, Emilia Sicilia, Nino Russo, Tamer Shoeib, *Dalton Trans*., 44, 4455-4467, **2014**.

3. Mass spectrometric and computational investigation of the protonated carnosine-carboplatin complex fragmentation.

Ida Ritacco, Mohamed Korany, Tamer Shoeib, Nino Russo, Emilia Sicilia, *Inorg. Chem.,* 54, 7885-7897, **2015**.

4. Investigation of the inertness to hydrolysis of Platinum(IV) produgs

Ida Ritacco, Gloria Mazzone, Nino Russo, Emilia Sicilia, *Inorg. Chem.,* **2016,** *55* (4), 1580-1586

5. DFT Investigation of the Mechanism of Action of Organoiridium(III)Complexes As Anticancer Agents

Ida Ritacco, Nino Russo, Emilia Sicilia, *Inorg. Chem.,* **2015**, *54* (22), 10801-10810

6. Hydrolysis in acidic environment and degradation of satraplatin: a joint experimental and theoretical investigation

Ida Ritacco, Tamer Shoeib, Nino Russo, Emilia Sicilia, Submitted *Inorg. Chem.*

7. Hydrolysis of Platinum Compounds: Insights into Reactivity from Accurate Ab Initio Calculations.

Ida Ritacco, Zhen Liu, Jeremy Harvey, Emilia Sicilia, Manuscript in preparation.

Contents

CHAPTER I

Cancer and Anticancer Drugs: General Principles

Introduction

Cancer is a disease caused by abnormal cells present in our body, which multiply uncontrollably. No one knows the causes that originate this phenomenon, but, certainly, environmental, hereditary and related to lifestyle factors can contribute to the tumor onset.

There are two types of cancer: solid tumor, formed by a mass of diseased cells, and liquid tumor, generated by diseased cells present in liquid matrices, such as blood [1]. Furthermore, these tumors can be classified into "malignant and benign tumors", which difference lies in the ability of malignant tumors to generate "metastasis", that is other diseased cells within the body [2]. Cancer is the main cause of death in developed countries, and, in the last years, some types of cancer, such as breast, lung, colon and prostate cancer, have become increasingly common [2].

Currently, cancer is treated by three approaches: surgery, radiation therapy, in which radiations are used to kill the diseased cells, and chemotherapy, in which particular drugs are swallowed either intravenously or orally [3], being the former the most used. So, in this chapter, we will try to explain and understand, in general, how a tumor is generated, what are the drugs most commonly used in chemotherapy, advantages, disadvantages and recent developments of anticancer drugs.

1.1 Creation of a "cell tumor"

A cancer cell is born when the DNA of a healthy cell undergoes mutations [4].

To understand a cancer cell emergence, it is necessary to understand the cell cycle, in which the basis is called phosphorylation, and its phases. The phosphorylation consists of phosphate groups transfer from particular high-energy molecules to various substrates. The enzymes that catalyze this transfer are called "kinases". So, in our body cells, the four phases of the cell cycle are regulated by a set of protein kinases, called CDK (Cyclin-dependent Kinases). The CDK allow the passage from one phase to another and, if they are damaged, an abnormal cell cycle and, consequently, an abnormal cell division will occur. The result is the appearance of an abnormal cell, defined tumor cell [5]. The abnormal cells are eliminated by apoptosis. In the case of tumor cells, the apoptosis phenomenon doesn't occur, so they continue to multiply uncontrollably.

1.1.1 Cancer cells *vs* healthy cells

Cancer cells differ from healthy cells for four reasons [2]:

1. *uncontrolled proliferation*;
2. *loss of functionality*: healthy cells, once they are formed, acquire a specific function that they will carry out for all

their life cycle. In contrast, cancer cells, particularly malignant ones, are all the same and, for that reason, they haven't a specific role. The main consequence is that they lose functionality;

3. *invasiveness*: The tumor cells, in contrast to healthy ones, are located outside of the tissues or organs of origin;

4. *ability to form metastases*, which are small tumors located in body areas different from tumor origin site.

1.2 Cancer therapies

There are several methods for the treatment of cancer. To understand what is the best, it is needed to know and to interpret some information, for example the type and location of the tumor or the patient's health status [6].

1.2.1 Surgery

This treatment is used for tumors that have well-defined characteristics. In fact, they must be solid, small and, in particular, must be localized in the areas of the body easily reached by classical surgery [7].

1.2.2 Radiotherapy

This treatment consists of local irradiation of X-rays (external radiotherapy) or in ingestion of drugs, source of gamma rays

(internal radiotherapy). These rays damage the DNA of diseased cells, which cannot multiply and, so, they die.

Unfortunately, this treatment is not selective. In fact, it damages both cancer cells and healthy cells [7].

1.2.3 Targeted therapies

The use of targeted therapies is based on knowledge of the molecular mechanisms that lead to the development, growth and spread of cancer. They act in a selective way on some of these cellular processes and, for this reason, targeted therapies are defined "smart drugs". Smart drugs are able to specifically coordinate molecular targets that are in cancer cells. In this way the therapy action appears to be selective and healthy cells are not damaged. Basically, the targeted therapies involve the correction of genetic mutations that are the basis of onset tumor, through inhibition or stimulation of the molecular target altered in the diseased cell. So, each genetic mutation underlying the disease has a specific therapy [8].

1.2.4 PDT: Photodynamic therapy

Photodynamic therapy is a non-invasive technique that uses a photosensitizing substance as a drug. The photosensitizer is activated by light at a particular wavelength.

The first step of PDT is the injection of the photosensitizer in the bloodstream. So, the drug enters in the metabolism of cancer cells, which are exposed to light.

At this point, the photodynamic therapy may act in three different ways:

1. *ROS Production*: The photosensitizer, activated by light, releases ROS, that is singlet oxygen, superoxide anion and hydrogen peroxide, which determine the diseased cell apoptosis;

2. *Lack of nutrients*: The photosensitizer can damage the blood vessels of cancer cells, preventing the tumor to receive the necessary nourishment;

3. *Immune system activation*: PDT can activate the immune system to attack cancer cells.

PDT can be used for the treatment of lungs and esophagus cancers. In this case, the light is provided by optical fiber cables inserted into endoscopes. For superficial tumors, such as skin cancers, light-emitting diodes (LEDs) are used.

The main disadvantage of PDT is that the light which is used to activate the photosensitizer cannot pass through more than 1 centimeter of tissue. So, this therapy can be used effectively only for the treatment of skin cancers and small tumors. It cannot be used for the treatment of metastases.

The main advantage of PDT is that healthy tissues are not damaged because diseased tissues are treated in a limited way. Furthermore, PDT may be used with other therapies, such as surgery, radiation therapy, or chemotherapy [9].

1.2.5 Third cancer therapies: Chemotherapy

One of the main advantages of chemotherapy is that it can be used for the treatment of solid tumors, such as testicular cancer, breast, colon, and fluids, such as leukemia, through the use of particular drugs, called "chemotherapeutic drugs". These drugs act on the cells that grow very quickly, i.e. the cancer cells, going to damage some steps of cell division. In this way, the cell replication is hampered and, as a result, the diseased cells die [7,10].

These various therapies can be used separately or can be used in mixed treatments. In fact, in the case of very large tumors, one can think to use radiotherapy or chemotherapy to reduce the tumor, and then to remove it surgically.

1.2.5.1 Chemotherapeutic drugs: classification and Mechanism of Action

Chemotherapy drugs are classified according to their mechanism of action (MoA). In fact, they are divided into [1]:

1. *Antimetabolites*. The mechanism of action consists in the block or change the DNA biosynthetic pathways of cancer cells;

2. *DNA interactive agents*. They are divided into:

   -<u>Alkylating agents</u>, which act by forming covalent bonds with the DNA of diseased cells. In this way, cell replication is blocked;

   -<u>Cross-linking agents</u>, which coordinate the DNA on the same filament (intra-strand cross-linking) or between two different strands (inter-strand cross-linking). Platinum complexes belong to this subclass;

   -<u>Intercalating agents</u>. The intercalation is a type of non-covalent interaction, in which planar molecules are inserted between pairs of the DNA bases;

   -<u>Kinases inhibitors</u>, that is drugs that inhibit kinases;

   -<u>DNA-cleaving agents</u>. They, coordinating the DNA, cause the resolution of the filament to which they bind. From this division free radicals are formed.

3. *Antitubulin agents*. They interfere with the synthesis of microtubules, blocking the nuclear division and causing the death of the diseased cell.

1.2.5.2 Chemotherapeutic drugs administration modes

The chemotherapy consists of "treatment cycles", which can vary from three to eight, depending on the type of cancer and of the drugs used. On these last two factors also depend administration modes of anticancer drugs. In fact, they can be administered intravenously, to date the most widespread way, and by intramuscular or subcutaneous injection. In these cases, the drugs reach the diseased cells by means of transport in the blood. These types of administration have limitations and disadvantages, such as long times of administration, high costs for healthcare and, mainly, possible interaction of drugs with species present in the blood, with the consequent loss of their efficacy. For these reasons, in the last years, it has become always more important the oral administration, consisting in the use of particular drugs [11].

1.2.5.3 Chemotherapeutic drugs resistance

All anticancer drugs listed above, appear to be quite effective in cancer diseases. Unfortunately, in some patients there is the problem of the "resistance", that is the cancer cells survive, despite administration of chemotherapy drug, by adaptations toward the antitumor agent [7]. The resistance phenomenon could increase with the succession of chemotherapy cycles.

Among the many anticancer drugs, some cross-linking agents, in particular platinum complexes, appear to be very effective. So, in the following paragraphs we will focus on the detailed description of platinum complexes, comparing them with complexes having different metals than platinum, but equally effective in the fight against cancer.

1.3 Platinum(II) anticancer drugs

Over the years, the metal-containing compounds have had a fundamental role in the pharmaceutical field, due to their chemical-physical properties. The metals most commonly used in the chemical-pharmaceutical industry are the "transition metals". In fact, they have partially filled d orbitals, which are exploitable in coordination with various ligands due to their interesting electronic properties. Transition metals can be used in the design of new anticancer drugs [12].

The transition metal most commonly used in the anticancer drugs design is Platinum, which, by coordinating various ligands, generates anticancer platinum complexes. The large use of platinum complexes in the treatment of cancer is due to Barnett Rosenberg who, in 1969, discovered, casually, the importance of cisplatin [cis-diamminedichloridoplatinum (II)] in the inhibition of cell division. In fact, during an experiment to analyze the effects of the electric field on the bacterial growth,

he observed that the bacteria proliferation on platinum electrode had ceased. On this electrode, Rosenberg identified the formation of an electrolysis product, identified as Cisplatin (cis-$[Pt(NH_3)_2(Cl)_2]$), considered to be responsible for cellular anti-proliferation. Assuming that the platinum complexes could be used in cancer treatment, Rosenberg and co-workers performed experiments with Sarcoma 180 and the L1210 leukemia. Due to the attained results, in 1971, cisplatin went in the phase I clinical trials and, in 1978, it was approved for use in testicula and ovarian cancer by the US Food and Drug Administration [13,14].

1.3.1 Cisplatin: chemical properties

In cisplatin, the metal ion, that is platinum, has a state of oxidation equal to +2, it has a d^8 electronic configuration, has a coordination number equal to four and cisplatin has a planar-square structure.

The Pt(II) can coordinate the four ligands, two amines and two chlorides, as well as in *cis* position, also in *trans* position, generating, in this way, the transplatin {trans-$[Pt(NH_3)_2(Cl)_2]$} (Fig. 1) [15].
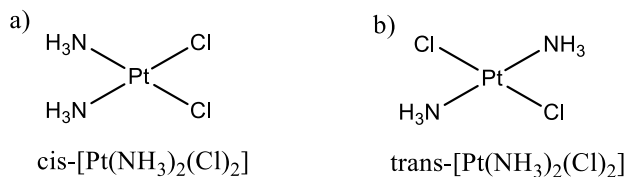
Fig. 1: Chemical structure of a) cisplatin and b) transplatin

Cisplatin, conversely transplatin, can coordinate the DNA of cells. For this reason, it was considered to be an active complex for the inhibition of cell division.

1.3.2 Cell death: Cisplatin action mechanism

Experimental and theoretical studies carried out over the years have provided many information concerning the mechanism of action of cisplatin. Cisplatin, and generally the platinum (II) complexes, induce the death of diseased cells through four steps:

1. *Accumulation inside the cancer cell.* The cisplatin comes into contact with the blood stream of patients intravenously. In plasma, it finds a high concentration of chloride ions (~100 mM), which limits the replacement of its chloride ligands with water molecules (hydrolysis of cisplatin). In this way, the cisplatin preserves its neutrality, necessary requirement for its transport into the cell membranes and, consequently, for the accumulation in the diseased cell. Cisplatin can be transported into the cell membrane by passive diffusion or active transport.

2. *Activation of the drug by hydrolysis.* In the cytoplasm, the concentration of chloride ions decreases (~4 mM). Consequently, the cisplatin chloride ligands are replaced by two molecules of water through an associative substitution reaction (S_N2) (Scheme 1). The loss of chlorides, via hydrolysis, is the step that determines the activation of the drug. In fact, the reaction product, positively charged, is highly reactive towards nucleophiles present inside the cancer cell (**Chapter IV**).

$$cis\text{-}[Pt(NH_3)_2(Cl)_2] + H_2O \rightleftharpoons cis\text{-}[Pt(NH_3)_2(OH_2)(Cl)]^+ + Cl^-$$

$$cis\text{-}[Pt(NH_3)_2(OH_2)(Cl)]^+ + Cl^- + H_2O \rightleftharpoons cis\text{-}[Pt(NH_3)_2(OH_2)_2]^{2+} + 2Cl^-$$
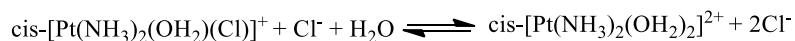
Scheme 1: Hydrolysis reaction of cisplatin

3. *Interaction with DNA.* The literature confirms that the hydrolysis products coordinate the DNA nucleobases of diseased cells, producing structural distortions. Consequently, the cancer cells are no longer able to reproduce themselves, because the DNA transcription is blocked, and, therefore, they die. The main DNA coordination sites are (Fig. 2):

   – the N1 or N7 nitrogens of adenine;
   – The N3 nitrogen of cytosine;

- The N7 nitrogen of guanine.

Theoretical and crystallographic studies have shown that the cisplatin prefers to coordinate the nitrogen N7 of guanine [16] and that it can coordinate the DNA in three different modes (Fig. 3):

- 1,2-intrastrand.
- 1,3-intrastrand;
- interstrand.

The 1,2-adduct intrastrand is the adduct more present in the cancer cell ($\approx$65%) and more reactive, because it induces a significant distortion in the DNA double helix. The 1,3-intrastrand ($\approx$10%) and the interstrand ($\approx$3%) modes are significantly less important [17].

4. *Cell Apoptosis.* Generally, the platinum complex coordination inhibits the DNA replication, causing the death of the cancer cell. This phenomenon is called as "cell apoptosis" and is directly proportional to the cytotoxicity of cisplatin and, in general, to the cytotoxicity of platinum (II) complexes.
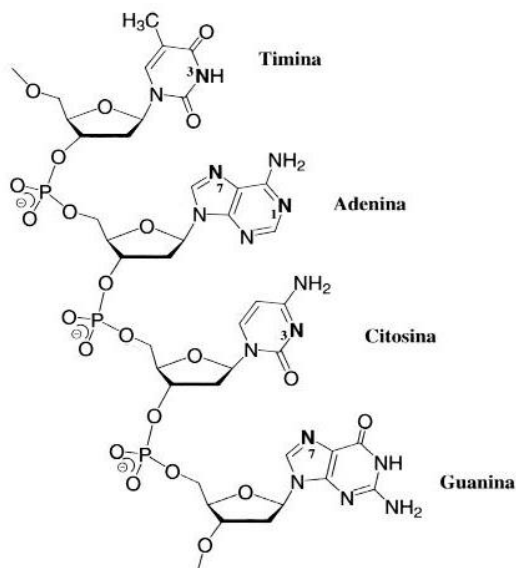
Fig. 2: Cisplatin binding sites in DNA
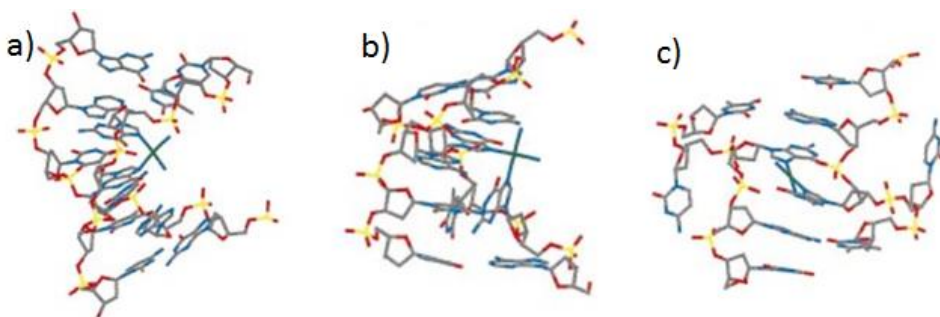
Fig. 3: DNA-Cisplatin adducts. a) 1,2-intrastrand cross-link, b) 1,3-intrastrand cross-link and c) interstrand cross-link.

1.3.3 Cisplatin disadvantages

Although cisplatin appears to be very cytotoxic to certain cancers, *in vivo* and *in vitro* studies have demonstrated that this

drug has many disadvantages. For example, nephro-, oto- and neuro-toxicity, nausea and/or vomiting may occur in patients subjected to this type of chemotherapy. In addition, the cisplatin is not very soluble in aqueous solutions, therefore, the intravenous administration is a limit, and it can be easily complexed from peptides that are in the extra- and intra-cellular environment. Anyway, the main disadvantage of the cisplatin treatment is the resistance of the cancer cell to the drug [17].

1.3.3.1 Cancer cell resistance to cisplatin

Many tumors appear to be resistant to cisplatin, and in general to anti-cancer drugs. In the particular case of cisplatin, the resistance is of two types:

- intrinsic resistance, that means that the tumor cells do not respond to the drug;
- acquired resistance. In this case, the cancer cell becomes resistant after exposure to the drug. For example, the ovarian cancer cells, initially, respond to the action of cisplatin but, in time, acquire resistance to the drug.

The factors that modulate the resistance are three:

1. *Drug changes during its accumulation in the intracellular environment;*

2. *Presence of thiols in the intracellular environment.* A cellular response to the accumulation of cisplatin in the cancer cell is an intracellular increase of thiols concentration. The thiol mainly present in the cells is the glutathione (GSH), which may coordinate the drug, decreasing its cytotoxicity. So, a result of the complexation phenomenon, which will be discussed specifically in Chapter III, is the platinum(II) complex inactivation;

3. *Ability of the cancer cell to repair the DNA structural modifications.* In some cases, the diseased cells are able to survive to DNA damage. It is not clear how this mechanism of cellular resistance develops, but some studies have shown that it happens [18].

Ultimately, cellular resistance to cisplatin is a complicated and multifactorial phenomenon.

1.3.4 Second and third generation drugs

Over the years, research has focused the attention on the design of new platinum (II) complexes, hoping to improve the clinical performance and to overcome the limits of cisplatin. Cleare and Hoeschele, affirmed in their articles that cisplatin derivatives can show antitumor activity only if the structural criteria listed below are fulfilled [19,20]:

- presence of two amine groups in *cis*, because *trans* geometry is not active;

- presence of two leaving groups in *cis* relative to one another;

- the leaving groups must be removed easily;

- the compounds must be neutral at time of administration;

- compounds with alkyl substituents and, at least, one hydrogen atom on the amine ligands are more cytotoxic.

So, the general structure for the new platinum (II) complexes is:
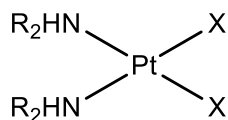
where X are the leaving groups, for example two chlorides or bidentate malonate, while R are hydrogen atoms or alkyl substituents. However, the "rules of thumb" are no longer generally followed because today are known numerous active Pt(II) complexes possessing trans geometry or positive charge.

1.3.4.1 Second generation platinum drugs: Carboplatin

Carboplatin [cis-diammine(1-1-cyclobutanedicarboxylato) platinum(II)] is called second-generation drug and it has been developed to overcome the toxicity limits of cisplatin (Fig. 4).
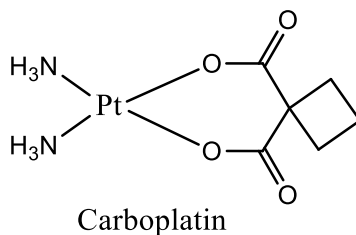
Carboplatin

Fig. 4: Chemical structure of Carboplatin

The carboplatin MoA is very similar to that of cisplatin. However, carboplatin undergoes hydrolysis more slowly than cisplatin for the presence of the bidentate ligand cyclobutanedicarboxylate [21]. Therefore, being the carboplatin less reactive than cisplatin, it is also less toxic. Indeed, neuro- and oto-toxicity appear to be less evident after carboplatin treatment. This allows using higher doses of the drug during chemotherapy cycles. Currently, carboplatin is the drug most widely used for the treatment of ovarian cancer [22]. It appears to be not very effective against bladder, head and testicles cancer. In these cases, the drug most used is cisplatin.

The main disadvantage of carboplatin is the cell resistance [23]. Furthermore, the use of high doses of this drug can generate phenomena of myelosuppression (decreased production of cells in the blood by the bone marrow) and thrombocytopenia (decreased production of platelet). Another carboplatin problem is the possible complexation of the drug in the extra- or intra-cellular environment (**Paper III**).

1.3.4.2 Third generation platinum drugs: Oxaliplatin

Oxaliplatin [trans-(1R,2R-Diaminocyclohexane)oxalato platinum(II)] was developed to overcome cellular resistance limitations of cisplatin and carboplatin. Oxaliplatin is a cisplatin derivative having two bidentate ligands, that is 1R, 2R-diaminocyclohexano ligand (DACH) and the oxalate group as a leaving group (Fig. 5).
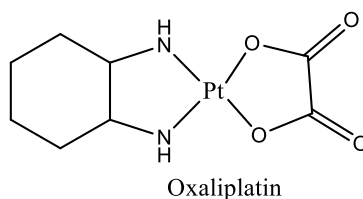
Oxaliplatin

Fig. 5: Chemical structure of Oxaliplatin

The presence of the oxalate reduces the drug reactivity, limiting its toxicity, while the presence of the DACH increases the oxaliplatin lipophilicity, favoring its accumulation in the cytoplasm by passive absorption.

Oxaliplatin, as carboplatin, is hydrolyzed more slowly than cisplatin [24] and the hydrolysis product interacts with the DNA of the cancer cell to form the DNA-oxaliplatin adduct. This adduct is much more efficient in the inhibition of cell replication compared to cisplatin-DNA and DNA-carboplatin adducts, because the DACH ligand has a higher lipophilicity and steric hindrance [18]. To date, the oxaliplatin is used for the treatment

of breast, stomach, pancreas and, in combination with other drugs, to the colon cancers. Similarly to cisplatin and carboplatin, the main problem of oxaliplatin is its complexation by means of peptides that are in the extra- or intra- cellular environment (**Paper II**).

Cis-, Carbo- and Oxaliplatin play a key role in the fight against various cancers. However, their clinical use is limited due to their toxicity and cellular resistance. In addition, the research of new and more effective platinum(II) drugs did not produce satisfactory results, except in rare cases [25,14].

The requirement to develop platinum drugs strongly cytotoxic, has encouraged researchers to a clinical investigation of platinum(IV) complexes as anticancer prodrugs.

1.4 Platinum(IV) prodrugs. General aspects

The platinum(IV) complexes are anticancer prodrugs of structure $[PtA_2L_2X_2]$, that show a low-spin d^6 octahedral geometry. These compounds are obtained by adding the axial ligands (X) to the platinum(II) complexes through oxidative addition. The axial ligands can be chloro, hydroxo or carboxylato groups and they regulate the pharmacological properties of platinum(IV) complexes, such as lipophilicity, reduction potentials, charge, selectivity and accumulation in the

cancer cell. Instead, the equatorial ligands, that is amine ligands (A) and leaving groups (L), determine the prodrugs cytotoxicity. The platinum(IV) prodrugs are more inert than platinum(II) drugs, therefore, more stable and, consequently, less reactive. This all translates into a lower tendency to hydrolysis or substitution of the ligands in the blood, after the intravenous administration and intra-cellular environment. Due to this low reactivity, the platinum(IV) complexes may be taken orally and accumulate in the cytosol in higher quantities than platinum(II) complexes.

In cancer cells, platinum(IV) prodrugs are activated by reduction, which consists in the release of the two axial ligands and the real drug, that is the platinum(II) complex. Then, this complex coordinates the final target, i.e. the DNA (Scheme 2) [26].
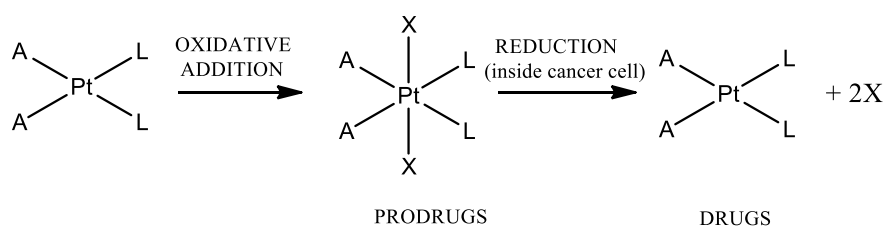
Scheme 2: Synthesis and reduction of platinum(IV) complexes

According to various studies, in the cytoplasm, the reduction of the platinum(IV) complexes occurs due to glutathione (GSH) and ascorbate as reducing agents. The reduction is considered

the activation step of the platinum(II) drugs, because it favors the transition from the platinum(IV) complexes, kinetically inert and not very reactive, to platinum(II) complexes, kinetically labile, and, therefore, more cytotoxic of platinum(IV) prodrugs [27].

The intracellular reduction rate of the platinum(IV) complexes depends on the type of cell and on the ligands coordinated to the metal, which define the coordination sphere of the complex.

Generally, the platinum(IV) prodrugs have many advantages compared to the platinum(II) complexes [13]: due to their stability they could be assumed orally, they have fewer side effects than the platinum(II) complexes and the axial ligands can be modified to improve and increase the pharmacological properties of the complex.

Platinum(IV) anticancer complexes can be divided into three categories based on the type of axial ligands:

- Complexes with non-bioactive axial ligands;
- Complexes with bioactive axial ligands;
- Photoactivatable complexes.

1.4.1 Platinum(IV) complexes with non-bioactive axial ligands

The main platinum(IV) complexes that do not exhibit bioactive axial ligands are Tetraplatin, iproplatin and satraplatin, formally called JM-216 (Fig. 6).

a) Tetraplatin   b) Iproplatin   c) Satraplatin
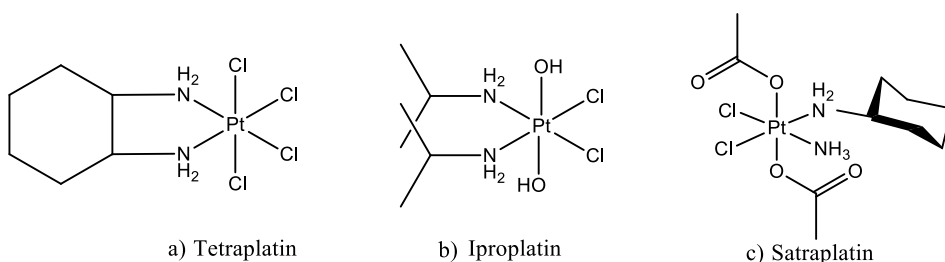
Fig. 6: Chemical structure of a) tetraplatin, b) iproplatin and c) satraplatin

Clinically, tetraplatin and iproplatin have been abandoned because the former exhibited a strong neurotoxicity, while the latter was less active than cisplatin and carboplatin.

Satraplatin, instead, has been the first platinum(IV) complex to be administered orally, because being inert and, therefore, stable, accumulates in large quantities in the cancer cell and do not exhibit cellular resistance.

From satraplatin, by reduction, a highly active platinum(II) complex is formed, i.e. the amminedichlorido (cyclohexylamine) platinum(II) (JM-118). As it happens for the cis-, carbo- and

oxaliplatin, inside the cancer cell JM118 undergoes hydrolysis and, subsequently, interacts with DNA, generating the DNA-JM118 adduct and inhibiting cell division (Scheme 3).
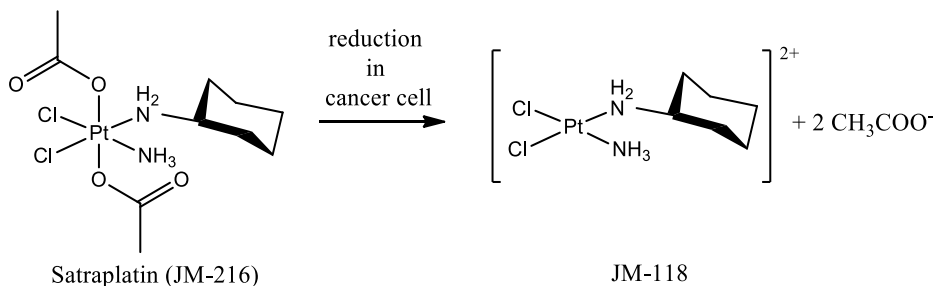
Schema 3: Satraplatin reduction

Although satraplatin is responsible for the regression of various cancers, such as prostate cancer, it is not used as a chemotherapeutic drug because it does not guarantee patient survival. The satraplatin can be used in combination with other drugs for the treatment of prostate cancer, lungs cancer and small solid tumors [13].

1.4.2 Platinum(IV) complexes with bioactive axial ligands

The selectivity of platinum(IV) complexes towards the cancerous tissues or intracellular targets depends heavily on the axial ligands [13]. An example of a bioactive axial ligand is estradiol. The platinum(IV) complex, shown in Figure 7, which has estradiol in axial position, turns out to be highly cytotoxic towards the breast and ovarian cancer cells, because the estrogen

released after the intracellular reduction of the platinum(IV) complex encourages HMGB1 protein expression [28].

Another complex belonging to this category is the platinum(IV) prodrugs with ethacrynic acid in the axial position (Fig. 7), developed to overcome the limitations related to cellular resistance. In fact, the ethacrynic acid is an inhibitor of glutathione-S-transferase [29].

Subsequently, Lippard and co-workes proposed as platinum(IV) prodrug with bioactive axial ligands the Mitaplatin, a platinum(II) complex which has dichloroacetates in the axial position (Fig. 7). The dichloroacetates, once released into the cancer cells by reduction, change the mitochondrial membrane potential, causing apoptosis of cancer cell [30].

Pt(IV)- estradiol   Pt(IV) complex with ethacrynic acid   mitaplatin
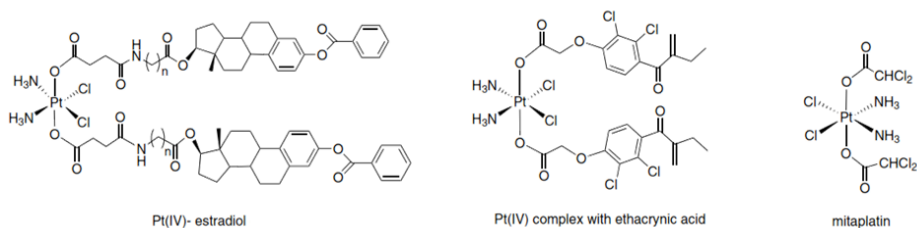
Fig. 7: Chemical structure of Platinum(IV) complexes with bioactive axial   ligands

1.4.3 Photoactivatable platinum(IV)

Platinum(IV) complexes activated directly into the tumor tissue by irradiation are defined photoactivable complexes. These

complexes are inert in the dark and do not show interaction with the glutathione that is in the cancer cell. Furthermore, in the active and cytotoxic form, they have azides and amines in *trans* between them and the hydroxyl groups in axial position (Fig. 8). Amines, that are in the equatorial position, may be replaced by pyridine, which makes the complexes more cytotoxic and more resistant to irradiation [31].

The MoA differs from that of platinum(IV) and platinum(II) complexes. In this case, a drug photodecomposition takes place through the transfer of one electron from each azido ligand to platinum, generating N_2 and platinum(II) complex (Scheme 4). The latter, then, by interacting with the DNA of the cancer cell, generates the Pt-DNA adduct [13].

photoactivatable Pt(IV) complexes
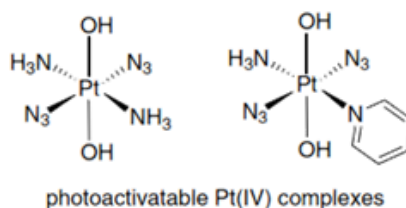
Fig. 8: Chemical structure of Photoactivatable Platinum(IV) complexes.
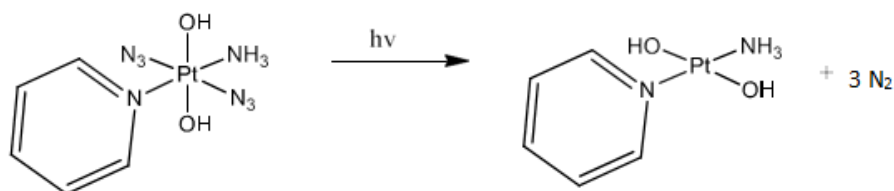
Scheme 4: Possible mechanism for the photoreaction of a generic photoactivatable platinum(IV) upon irradiation with UVA.

1.4.4 Platinum(IV) complexes reduction

Since many years, the literature affirms that the antitumour activity of platinum(IV) complexes is directly proportional to their ability to reduce themselves in the cancer cell. So, to understand the biological activity of these prodrugs it is necessary to understand what are the factors that influence their reduction. Generally, the reduction of the platinum(IV) complexes involves the loss of the two axial ligands and the release of the platinum(II) drug, which, by binding to DNA, stops cell replication and induces cellular apoptosis.

The reduction depends on the structure of the prodrug, therefore on the nature of axial and equatorial ligands, and on the reducing agents involved in the process. A measure of the platinum(IV) complexes reduction can be obtained through cyclic voltammetry experiments. Indeed, Choi et al. explained that the reduction kinetics strongly depends on the reduction potentials of the complexes submitted to voltammetric analysis [32].

Furthermore, it is worth mentioning that the reduction Pt(IV)-Pt(II) is irreversible, therefore, to define the reduction potential of platinum(IV) complexes all the rules of the irreversible cyclic voltammetry must be observed [33,34].

Cyclic voltammetry studies have confirmed the relationship between the nature of the ligands and the reduction degree. According to these studies, the axial ligands have a greater influence on the reduction kinetics than the equatorial ligands. For example, platinum(IV) complexes, which have chlorides in axial position and have reduction potential of about E=-4mV, are reduced more easily than complexes that in axial position have carboxylate groups ($-250 \leq E \geq -350$) or hydroxides (E=-664mV). Then, higher is the negativity of reduction potential, lower is the reduction kinetic of the prodrugs. The variation of the equatorial ligands has an influence next to nothing on the reduction kinetics.

The main reducing agents, inside the cancer cell, are glutathione and ascorbic acid, although the reduction mechanism of the platinum(IV) to platinum(II) complexes is not clear. It is thought that the reduction of the platinum(IV) complexes using glutathione and/or ascorbic acid can occur with inner- or outer-sphere electron-transfer mechanisms [35-37].

The inner-sphere electron-transfer mechanism proceeds through the formation of a strong covalent bond between the oxidant and

reductant species. This covalent bond is seen as an ideal bridge, due to which the reductant species can transmit electrons to the oxidant species. In a chemical reaction, the "bridge structure" can be a very stable minimum, a reaction intermediate or a transition state.

The outer-sphere electron-transfer mechanism does not require for the formation of bridges between oxidizing and reductant species, but consists in an electron transfer from the reaction environment to the oxidizing species.

The reaction can also be catalyzed by Pt(II) [38].

1.4.4.1 Reduction by glutathione: mechanistic hypothesis

The reduction mechanism of the platinum(IV) complexes by glutathione should proceed with the formation of a covalent bond between the axial ligand of the complex and the glutathione sulfur, favoring an electron transfer from the reductant species to the axial ligand. In this way, the electronic density of the axial ligand is shifted to the metal center, making the Pt-axial ligand bond weaker and the release of the axial ligand easier. For example, Ranford et al. suggested that the reduction of the complex $[PtCl_2(OCOCH_3)_2(NH_3)_2]$ by glutathione, occurs via the formation of a bridge between the sulfur of the reductant species and the acetate oxygen coordinated to platinum (Fig. 9).

After bridge formation, there is an electrical charge transfer from glutathione, which is considered as a nucleophile, to the axial ligand and, subsequently, to the platinum. This weakens the acetate-Pt bond and facilitates the axial ligand release [39,27].
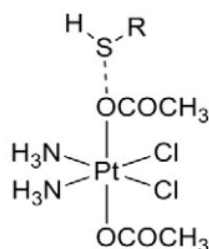
Fig. 9: Transition state form in the case of the interaction [PtCl$_2$(OCOCH$_3$)$_2$(NH$_3$)$_2$] and Glutathione

Starting from the transition state, shown in Figure 9, two hypothesis of mechanism have been proposed.

The first hypothesis proposes the formation of an intermediate, following the release of the first axial ligand, in which the platinum is pentacoordinated and it has an oxidation number equal to +3. Then, from this minimum, by interaction with another glutathione and release of the second axial ligand, the platinum(II) drug would be released (Scheme 5a).

The second hypothesis proposes a concerted mechanism, that is the release of the first axial ligand, due to glutathione, and, simultaneously, the release of the second axial ligand to form the corresponding platinum(II) complex (Scheme 5b).
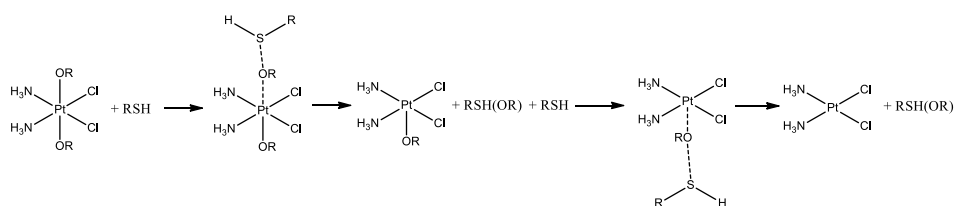
Scheme 5a: First hypothesis of platinum(IV) complexes reduction
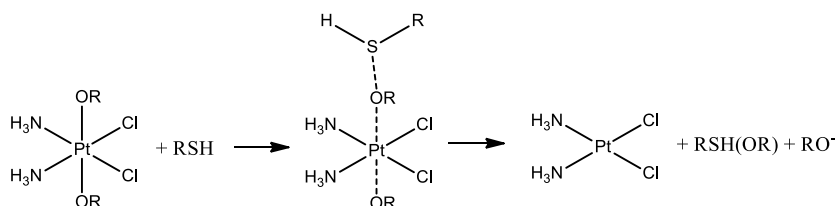
Scheme 5b: Second hypothesis of platinum(IV) complexes reduction

1.4.4.2 Reduction by ascorbate: mechanistic hypothesis

In the case of reduction by ascorbate, the hypothesis of mechanism proposes an outer sphere electron transfer as result of the interaction between the platinum(IV) complex and the reductant agent. It is not clear how the electron transfer occurs, but it has been hypothesized that the reductant species releases two electrons to the reaction environment, and, subsequently, these electrons are transferred from reaction environment to the

platinum(IV) complex, causing the release of the axial ligands together with the drug (Scheme 6) [27,37].
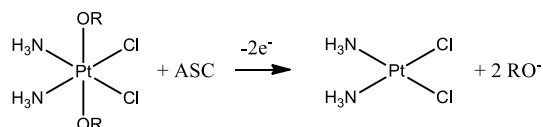
Scheme 6: Platinum(IV) complexes reduction by ascorbate

1.4.4.3 Basolo reduction

Basolo studied the reduction of some platinum(IV) complexes, such as $[Pt(en)_3]^{4+}$ (en = ethylenediamine), by $[Cr(bipy)_3]^{2+}$ (bipy = 2,2′-bipyridine). Basolo affirmed that this reduction occurs through an outer-sphere mechanism, in which there is an electron transfer to generate a Pt(III) intermediate, without, however, direct interaction with the reductant species. The Pt(III) could react rapidly with another $[Cr(bipy)_3]^{2+}$ to yield Pt(II) complex. When the platinum(IV) complex has chloride ligands in the axial position, such as $[Pt(NH_3)_5Cl]^{3+}$, it is suggested an inner sphere mechanism where one axial chloride is coordinated to the complex of Cr(II), forming a bridge. He also suggested a two electron reduction mechanism to yield Pt(II) and Cr(IV) complexes with the latter that is reduced directly to Cr(II) [38].

The Basolo reduction mechanism can also be applied when the reductant species is a platinum(II) complex.

To date, only the Basolo reduction mechanism is supported by experimental and theoretical data (**Paper IV**). Unfortunately, this mechanism has limitations, because it can be used only when the platinum(IV) complexes has certain types of axial ligands.

As regards the reduction mechanisms by glutathione and ascorbate only few experimental data are available that are not supported by theoretical data. For this reason, future studies should be devoted to the design of prodrugs inert to hydrolysis (**Paper IV**), the interaction of this complexes with proteins that are in the blood and cancer cells and the understanding of their reduction mechanism.

1.5 Non-platinum anticancer drugs

Currently, only the platinum-based drugs have been approved for clinical practices. However, in the last years, research has turned its attention to the study of new metal-containing complexes. These non-platinum complexes have low toxicity and high activity against tumors that appear to be resistant to cisplatin. Inside the cancer cells, these drugs, which contain

main group or transition metals, can act on different targets, such as DNA, enzymatic functions, and/or the formation of ROS.

The metals most frequently used for this purpose are ruthenium(II) and ruthenium(III), gold(I) and gold(III), copper(II), and iridium(III) [40,41]. The iridium (III) seems to be an excellent candidate for the development of new anticancer drugs, due to its peculiar characteristics (**Paper VI**).

1.5.1 Ruthenium complexes as anticancer drugs

Ruthenium(II) and Ruthenium(III) exhibit antitumor activity. The ruthenium(II) forms penta- and hexa-coordinated complex, while the ruthenium(III) forms only hexa-coordinated complexes. Furthermore, ruthenium(III) is considered a prodrug, because, as confirmed by in vivo experiments, before reaching the final target, it is always reduced to ruthenium(II).

The most studied ruthenium(II) complexes, due to their high cytotoxic activity, are those having arene ligands. The cytotoxic activity of ruthenium complexes should be based on their ability to interact with the DNA of cancer cells or result from other interaction types. The ruthenium(II) complexes exhibit cytotoxic activity similar to that of carboplatin and lower than that of cisplatin.

In most cases, the ruthenium(II) complexes have, in addition to arene ligands, a chloride ligand. It seems that the hydrolysis is

the fundamental step for the activation of these complexes. In fact, they may undergo rapid hydrolysis leading to the loss of the chloride ligand and to the rapid interaction with aminoacids and various nucleobases.

The more cytotoxic ruthenium(III) complexes, are those that have indazole ligands, able to interact with the DNA of cancer cells and to induce apoptosis via the intrinsic mitochondrial pathways [40,41].

1.5.2 Gold complexes as anticancer drugs

Gold(I) complexes which have phosphine ligands are used as anticancer drugs, because they are inhibitors of the enzyme thioredoxin reductase (TR). This enzyme is present in high concentrations in cancer cells and promotes the diseased cells proliferation. The inhibition of TR enzyme by gold(I) complexes causes cell apoptosis.

Gold(III) complexes have a chemical behavior very similar to that of the platinum(II) complexes. In fact, gold(III) complexes are isoelectronic with platinum(II) complexes, although gold(III) complexes in the physiological environment undergo rapid hydrolysis and subsequent reduction to gold(I). For this reason, over the years, gold(III) complexes more inert to hydrolysis and, then, to reduction have been designed [40,41].

1.5.3 Copper complexes as anticancer drugs

Many copper(II) complexes, containing N-, S-, and/or O-ligands, have a good cytotoxic activity. The action mechanism of copper(II) complexes is not yet clear, but it is assumed that these complexes cause cellular apoptosis by interacting with the DNA or by inhibiting the enzymes that are, in high amounts, inside the cancer cell.

The use of copper(I) complexes as anticancer drugs is limited by their low stability and by their tendency to be oxidized [40,41].

1.5.4 Iridium complexes as anticancer drugs

In the last years, a great deal of efforts has been devoted to the study of new anticancer drugs containing iridium as a metal center. In particular, iridium(III) complexes seem to be very inert and less reactive. While ruthenium complexes are stabilized by the presence of arene ligands, iridium(III) complexes are stabilized by the presence of the pentamethylcyclopentadienyl ligand (Cp*), which is negatively charged. Furthermore, half-sandwich organoiridium(III) cyclopentadienyl complexes of general formula $[(\eta^5 - Cp^x)Ir(III)- (X^\wedge Y)Z]^{0/+}$, where $Cp^x = Cp^*$, Cp^{xph} (tetramethyl-(phenyl)-cyclopentadienyl) or Cp^{xbiph} (tetramethyl(biphenyl)-cyclopentadienyl), $X^\wedge Y$=bidentate ligand with nitrogen, oxygen,

and/or carbon donor atoms, and Z=Cl, H_2O, or pyridine (py), have high cytotoxicity.

These complexes can undergo hydrolysis, losing the Z ligand, and, subsequently, can interact with the DNA of the cancer cell, or to produce ROS, by interacting with other species that are in the cancer cell, increasing the intracellular oxidative stress. In both cases cellular apoptosis occurs (**Paper VI**).

REFERENCES CHAPTER I

[1] Nussbaumer, S., Bonnabry, P., Veuthey, J. L., Fleury-Souverain, S., *Talanta* **2011**, 85, 2265-2289.

[2] Rapporti Associazione Italiana Registri Tumori.

[3] Shewach, D. S., Kuchta, R. D., *Chem. Rev.* **2009**, 109, 2859-2861.

[4] Evan, G. I., Vousden, K. H., *Nature* **2001**, 411, 342-348.

[5] Collins, K., Jacks, T., Pavletich N. P., *PNAS USA* **1997**, 94, 2776-2778.

[6] World Health Organization (WHO), *Geneva: World Health Organization* **1979**, 48.

[7] Smith, H. J., *Introduction to the Principles of Drug Design and action-Harwood academic publishers,* III edition, **1998**, 1-568.

[8] Urruticoechea, A., Alemany, R., Balart, J., Villanueva, A., Viñals, F., Capellá, G., *Current Pharmaceutical Design*, **2010**, 16, 3-10.

[9] Wilson, B. C., *Canadian Journal of Gastroenterology*, **2002**, 16(6), 393–396.

[10] Johnstone, R. W., Ruefli, A. A., Lowe S. W., *Cell* **2002**, 108, 153-164.

[11] Steward, D. J., *Prog. Exp. Tumor Res.* **1984**, 28, 32-50.

[12] Baile, M. B., Kolhe, N. S., Deotarse, P. P., Jain, A. S., Kulkarni, A. A., *International Journal of Pharma Research & Review* **2015**, 4 (8), 59-66.

[13] Dilruba, S., Kalayda, G. V., *Cancer Chemother Pharmacol* **2016**, 77 (6), 1103-1124.

[14] Wong, E., Giandomenico, C. M., *Chem. Rev.* **1999**, 99, 2451-2466.

[15] Alderden, R. A., Hall, M. D., Hambley, T. W., *Journal of Chemical Education* **2006**, 83, 728-734.

[16] Alberto, M. E., Butera, V., Russo, N., *Inorg. Chem.* **2011**, 50 (15), 6965-6971.

[17] Jamieson, E. R., Lippard, S. J., *Chem. Rev.* **1999**, 99, 2467-2498.

[18] Perez, R. P., *Eur. J. Cancer* **1998**, 34, 1535-1542.

[19] Cleare, M. J., Hoeshcele, J.D., *Plat. Met. Rev.* **1973**, 17, 2-13.

[20] Cleare, M. J., Hoeshcele, J.D., *Bioinorg. Chem.* **1973**, 2, 187-210.

[21] Pavelka, M., Lucas, Maria Fatima A., Russo, N., *Chem. Eur. J.* **2007**, 13, 10108-10116.

[22] Ozols R. F., Bundy B. N., Greer B. E., Fowler J. M., Clarke-Pearson D., Burger R. A., Mannel R. S., DeGeest K., Hartenbach E. M., Baergen R., *J. Clin. Oncol.* **2003**, 21, 3194-3200.

[23] Stewart, D. J., *Crit. Rev. Oncol. Hematol.* **2007**, 63, 12-31.

[24] Lucas, Maria Fatima A., Pavelka, M., Alberto, M., Russo, N., *J. Phys. Chem.* **2009**, 113, 831-838.

[25] Galanski, M., Jakupec, M. A., Keppler, B. K., *Curr. Med.* **2005**, 12, 2075-2094.

[26] Wexselblatt, E., Yavin, E., Gibson D., *Angew. Chem. Int. Ed.* **2013**, 52, 6059-6062.

[27] Wexselblatt, E., Gibson D., *J. Inorg. Biochem.* **2012**, 117, 220-229.

[28] He, Q., Liang, C. H., Lippard, S. J., *Proc. Natl. Acad. Sci. USA* **2000**, 97, 5768-5772.

[29] Ang, W. H., Khalaila, I., Allardyce, C. S., Juillerat-Jeanneret, L., Dyson, P. J., *J. Am. Chem. Soc.* **2005**, 127, 1382-1383.

[30] Dhar, S., Lippard, S. J., *Proc. Natl. Acad. Sci. USA* **2009**, 106, 2219-2220.

[31] Butler, J. S., Sadler, P. J., *Curr. Opin. Chem. Bio.* **2013**, 17, 175-188.

[32] Choi, S., Filotto, C., Bisanzo, M., Delaney, S., Lagasee, D., Whitworth, J. L., Jusko, A., Li, C., Wood, N. A., Willingham, J., Schwenker, A., Spaulding, K., *Inorg. Chem.* **1998**, 37, 2500.

[33] Mabbott, G. A., *J. Chem. Educ.* **1983**, 60 (9), 697.

[34] Evans, D. H., O'Connel, K. M., Petersen, R. A., Kelly, M. J., *J. Chem. Educ.* **1983**, 60 (4), 290.

[35] Hall, M. D., Hambley, T. W., *Coordination Chemistry Reviews* **2002**, 232, 49-67.

[36] Johnstone, T. C., Suntharalingam, K., Lippard, S. J., *Chem. Rev.* **2016**, 116 (5), 3436-3486.

[37] Ejehi, Z., Ariafard, A., *Chem. Commun.*, **2017**, DOI: 10.1039/ C6CC07834F.

[38] Basolo., *Chem. Rev.* **2016**, 116 (5), 3436-3486.

[39] Chen, L., Lee, P. F., Ranford, J. D., Vittal, J. J., Wong, S. Y., *J. Chem. Soc. Dalton* **1999**, 1209-1212.

[40] Trudu, F., Amato, F., Vanhara, P., Pivetta, T., Pena-Mèndez, E. M., Havel, J., *Journal of applied biomedicine* **2015**, 13, 79-103.

[41] Ott, I., Gust, R., *Arch. Pharm. Chem. Life Sci.* **2007**, 340, 117-126.

CHAPTER II

**Theoretical Concepts and
Computational Methods**

Introduction

The main goal of theoretical chemistry is to explore the electronic structure and properties of more or less complex systems.

Quantum mechanics emerged in the beginning of the twentieth century as a new discipline because of the need to describe phenomena, which could not be explained using Newtonian mechanics or classical electromagnetic theory. These phenomena include the photoelectric effect, blackbody radiation and the rather complex radiation from an excited hydrogen gas. These and other experimental observations led to the concepts of quantization of light into photons, the particle-wave duality, the de Broglie wavelength and the fundamental equation describing quantum mechanics, namely the Schrödinger equation.

Particles defined as "quantum systems" are described by a wave function (ψ) [1], that is a mathematical object that contains all the information of the system under examination. A quantum system can be described by the *non-relativistic time-independent Schrödinger equation* [2]:

$$\hat{H}\psi = E\psi \qquad\qquad (2.1)$$

where $\hat{H}$ is the Hamiltonian operator for a system of nuclei and electrons described by position vectors R_A and r_i, respectively.

In atomic units, the Hamiltonian for N electrons and M nuclei is

$$\hat{H} = -\sum_{i=1}^{N}\frac{1}{2}\nabla_i^2 - \sum_{A=1}^{M}\frac{1}{2M_A}\nabla_A^2 - \sum_{i=1}^{N}\sum_{A=1}^{M}\frac{Z_A}{r_{iA}} + \sum_{i=1}^{N}\sum_{j>1}^{N}\frac{1}{r_{ij}} + \sum_{A=1}^{M}\sum_{B>A}^{M}\frac{Z_A Z_B}{R_{AB}} \quad \textbf{(2.2)}$$

In Eq. (2.2) the first term is the operator for the kinetic energy of the electron; the second term is the operator for the kinetic energy of nuclei; the third term is the coulomb attraction between electrons and nuclei; the fourth and fifth terms are the repulsion between electrons and nuclei, respectively.

Due to the *Born-Oppenheimer* approximation [3], in equation (2.2), the second term can be neglected and the last term can be considered constant. The remaining terms in (2.2) compose the electronic Hamiltonian, that is the Hamiltonian describing the motion of N electrons in the field of M point charges.

$$\hat{H}_{elec} = -\sum_{i=1}^{N}\frac{1}{2}\nabla_i^2 - \sum_{i=1}^{N}\sum_{A=1}^{M}\frac{Z_A}{r_{iA}} + \sum_{i=1}^{N}\sum_{j>1}^{N}\frac{1}{r_{ij}} \quad \textbf{(2.3)}$$

Quantum chemistry tries to find approximate solutions to the electronic Schrödinger equation, because it can be solved exactly only for one- electron systems, such as hydrogen atom or H_2^+ molecule.

2.1 The Slater determinant

A single electron is described by the wave function $\psi(r,s)$, *spin orbital,* that define both its spatial distribution, $\psi(r)$, and its spin, $\alpha(s)$ or $\beta(s)$.

$$\psi(r,s) = \begin{cases} \psi(r)\alpha(s) \\ or \\ \psi(r)\beta(s) \end{cases} \tag{2.4}$$

For a system of N electrons, the total electronic wave function is equal to the product of the wave functions of each electron and it is known as *Hartree Product*. The Hartree product doesn't respect the *antisymmetry principle* (a general statement of the *Pauli exclusion principle*) that requires that electronic wave functions be antisymmetric with respect to the interchange of the space and spin coordinates of any two electrons [4]. So, the *Slater determinant* has been introduced as the simplest antisymmetric wave function which can describe the ground state of an N-electron system:

$$\psi_N^{SD} = \frac{1}{\sqrt{N!}} \begin{vmatrix} \psi_i(r_1,s_1) & \psi_j(r_1,s_1) & \dots & \psi_j(r_1,s_1) \\ \psi_i(r_1,s_1) & \psi_j(r_2,s_2) & \dots & \psi_k(r_2,s_2) \\ \vdots & \vdots & & \vdots \\ \psi_i(r_N,s_N) & \psi_j(r_N,s_N) & \dots & \psi_k(r_N,s_N) \end{vmatrix} \tag{2.5}$$

The Slater determinant incorporated both exchange effects, arising from the requirement that $|\psi|^2$ be invariant to the exchange of the space and spin coordinates of any two electrons,

and correlation effect, which means that the motion of two electrons with parallel spins is correlated while the motion of electrons with opposite spins remains uncorrelated [5].

2.2 The Hartree-Fock approximation

To find and to describe approximate solutions to the electronic Schrödinger equation results to be very difficult. To try to solve this problem another approximation is used, that is the Hartree-Fock (HF) approximation [6-9]. The simplest antisymmetric wave function, which can be used to describe the ground state of an N-electron system, is a single Slater determinant.

The variation principle states that the best wave function, of this functional form, is the one which gives the lowest possible energy and, in the Slater Determinant wave function, the variational flexibility is in the choice of spin orbitals.

Minimizing the energy with respect to the choice of spin orbitals lead to the HF equation, that is an eigenvalue equation of the form:

$$f(i)\psi(r_i s_i) = \varepsilon\psi(r_i s_i) \qquad \textbf{(2.6)}$$

where *f(i)* is the Fock operator that includes a one-electron contribute for the kinetic energy of ith electron and for the coulomb attraction between the ith electron and nucleus, and a

two-electron contribute that measure the "field" seen by the ith electron due to the presence of the other electrons on the other spin orbitals.

Thus the Hartree-Fock equation depends on its eigenfunctions, so it is a non-linear equation that must be solved iteratively, using the self-consistent-field (SCF) method. However, with the HF approach the motion of the electrons with opposite spins remains not correlated.

Electron correlation can be included explicitly with well-known extensions collectively called post-Hartree-Fock methods [10], like *Moller-Plesset perturbation theory (MP)*, the *generalized valence bond method (GVB), configuration interaction (CI), multiconfigurational self–consistent field (MCSCF) and coupled cluster theory (CC)*.

These approaches improve the level of accuracy but become computationally much more demanding and thus are only suitable for relatively small systems. To handle larger systems an alternative approach has been developed.

2.3 Density functional theory (DFT)

Density Functional Theory (DFT) allows to deal with large molecular systems, including the electron correlation, with a computational demanding much lower than post-HF methods.

These DFT vantages are due to the use of the *electron density* $\rho(r)$ as basic variable.

$$\rho(r) = N \int \dots \int |\psi(x_1, x_2, \dots x_N)|^2 dx_1 \, dx_2 \dots dx_N \qquad \textbf{(2.7)}$$

In contrast to the wave function, ψ_N, that depends on 3N variable excluding the spin variable, the electron density $\rho(r)$ depends on 3 variables only, also for many-electron systems.

In 1964, Hohenberg-Kohn introduced the existence of an unique relationship between $\rho(r)$ and all fundamental properties of a given system [11].

2.3.1 The Hohenberg-Kohn theorems

The *first Hohenberg-Kohn theorem* [11] affirms that every observable of a quantum mechanical system can be calculated exactly from the ground-state electron density $\rho(r)$, so every observable can be written as a functional of the ground-state electron density $\rho(r)$.

For a system defined by an external potential *v(r),* acting on the electrons due to the nuclear charges, the energy E_v can be written as functional of the electron density.

Within the Born Oppenheimer approximation, E_v can be splitted into three terms, which are kinetic energy *T*, electron-electron repulsion E_{ee} and the nuclei-electron attraction *V*:

$$E_v[\rho] = T[\rho] + E_{ee}[\rho] + V[\rho] = T[\rho] + E_{ee}[\rho] + \int \rho(r)v(r)dr \quad \text{(2.8)}$$

Since the terms T and E_{ee} depend exclusively on the coordinates of the electrons and their forms are the same for all systems, depending only on the number of electrons, they are grouped together into the universal Hohenberg and Kohn functional $F^{HK}[\rho]$.

$$F^{HK}[\rho] = T[\rho] + E_{ee}[\rho] \quad \text{(2.9)}$$

F^{HK} contains the functional for the kinetic energy $T[\rho]$ and that for the electron-electron interaction $E_{ee}[\rho]$. The explicit form of both these functionals are unknown.

However from term $E_{ee}[\rho]$ can be extracted at least, analytically, the classical part $J[\rho]$ that measures the coulomb electron-electron interaction, whereas $Vq[\rho]$ is a measure of the non-classical electronic interaction:

$$E_{ee}[\rho] = J[\rho] + Vq[\rho] = \frac{1}{2}\iint \frac{\rho[r]\rho[r']}{|r-r'|} dr \, dr' + Vq[\rho] \quad \text{(2.10)}$$

The complete form of the ground state energy associated with the density $\rho(r)$, is the functional

$$E_v[\rho] = F^{HK}[\rho] + \int \rho(r)v(r)dr = T[\rho] + \frac{1}{2}\iint \frac{\rho[r]\rho[r']}{|r-r'|} dr \, dr' + Vq[\rho] +$$
$$+ \int \rho(r)v(r)dr \quad \text{(2.11)}$$

The *second Hohenberg-Kohn theorem* [11], affirms that for a trial electron density $\tilde{\rho}(r)$, the energy is higher or equal to the real energy of system:

$$E_0 \leq E_v\,[\tilde{\rho}] \qquad\qquad \textbf{(2.12)}$$

where E_0 is the correct energy and $E_v[\tilde{\rho}]$ is the energy, written as functional of trial electron density $\tilde{\rho}(r)$, of a system with an external potential v(r).

So, this theorem states the variational principle for the DFT theory. The applicability of the variational principle is limited to the ground state. Hence the strategy cannot be easily transferred to the problem of excited states. According to the two theorems, the energy can be known exactly when the electron density of the system is exact.

2.3.2   The Kohn-Sham equations

The explicit form of the functional $F^{HK}[\rho]$ is the major challenge of DFT. Since only the *J[ρ]* term is known, the main problem is to find the expression for *T[ρ]* and *Vq[ρ]*.

In 1927 Thomas and Fermi provided the first example of density functional theory. However the performance of their model had a deficiency due to the poor approximation of the kinetic energy.

To solve this problem Kohn and Sham proposed, in 1965, a new approach [12].

They considered a reference system whit non-interacting electrons, having the same density of the real, interacting one.

For the reference system, both the kinetic energy and ground-state electron density can be written using one-electron orbital:

$$T_s[\rho] = \sum_{i=1}^{N} < \psi_i \left| -\frac{1}{2} \nabla_i^2 \right| \psi_i > \qquad (2.13)$$

$$\rho[r] = \sum_{i=1}^{N} \sum_{s} |\psi_i(r,s)|^2 \qquad (2.14)$$

The kinetic energy of the real system can be expressed as sum of two contributes: the kinetic energy of the reference system $T_s[\rho]$ and the kinetic energy that measures the electron correlation $T_c[\rho]$

$$T[\rho] = T_s[\rho] + T_c[\rho] \qquad (2.15)$$

Consequently a new redefinition of the universal functional can be introduced:

$$F[\rho] = T_s[\rho] + J[\rho] + E_{xc}[\rho] \qquad (2.16)$$

Where $E_{xc}[\rho]$ is the exchange and correlation functional that represents the sum of the terms having an unknown analytically form: i) the difference between the exact kinetic energy and the

kinetic energy of the reference system; ii) the non-classical electron-electron interaction; iii) the self-interaction correction. So the exchange and correlation functional can be defined as

$$E_{xc}[\rho] = (T[\rho] - T_s[\rho]) + (E_{ee}[\rho] - J[\rho]) \qquad \textbf{(2.17)}$$

Including all these considerations the expression of energy for the real, interacting system is

$$E_v[\rho] = T_s[\rho] + J[\rho] + E_{xc}[\rho] + \int \rho(r)v(r)dr \qquad \textbf{(2.18)}$$

The only term for which no explicit form can be given is E_{xc}. Applying the variational method, imposing the wave function orthogonality condition and using the Lagrange multipliers method, the Kohn-Sham equations have been obtained:

$$-\frac{1}{2}\nabla_i^2 + v_s(r)\psi_i{}^{KS} = \varepsilon_i\psi_i{}^{KS} \qquad \textbf{(2.19)}$$

Where v_s is the local potential for the single particle that includes the exchange and correlation potential, v_{xc}, defined as the functional derivative of E_{xc} with respect to $\rho(r)$. So v_s depends on the density and therefore the Kohn-Sham equations have to be solved iteratively.

$$v_{xc} = \frac{\delta E_{xc}[\rho]}{\delta\rho(r)} \qquad \textbf{(2.20)}$$

Kohn-Sham equations led to a formalism that is exact and computationally accessible. The only one lack is the fact that the explicit form of the functional *Exc* is unknown. The major challenge in DFT is to find e improve approximate model for this unknown functional. Although there is no exact solution of this functional, an approximate functional have been proposed. One approach to calculate the functional *Exc* is the *Local (Spin) Density Approximation* (L(S)DA). This approach is based on assuming that the density ρ varies very slowly and locally with position and can thus be treated as a homogeneous electron gas[7]. In fact, the exchange energy of an electron gas with uniform density can be calculated exactly. Unfortunately, the L(S)DA approximation cannot be used for systems with no uniform electronic distribution. In this case, to yield accurate chemical description, *Gradient Corrected or Generalized Gradient Approximation (GGA)* was introduced. This approximation depend not only on the density ρ, but also on the gradient Δ_ρ.

The development of GGA methods is based on two different approaches:

1. *Semiempirical approach*. This approach was proposed by Becke [13-18]. The basic idea is to choose a flexible mathematical functional form depending on one or more parameters to molecular thermochemical data. Exchange functionals of this category are for example Becke88 (B),

Perdew-Wang (PW) and modified-Perdew-Wang (MPW) [19-23];

2. *Nonempirical approach*. This approach was proposed by Perdew and it provides that the development of exchange-correlation functionals should depend on principles derived by quantum mechanics. Exchange functionals of this category are for example Perdew 86 (P), Perdew-Burke-Ernzerhof (PBE) and modified-Perdew-Burke-Ernzerhof (mPBE) [24-26].

GGA functionals have been shown to give more accurate predictions for thermochemistry than LSDA ones, but they still underestimate barrier heights. LSDAs and GGAs are "local" functionals because the electronic energy density at a single spatial point depends only on the behaviour of the electronic density and kinetic energy at and near that point [27].

Local functional can be mixed with non-local HF exchange (calculated via Kohn-Sham orbitals) leading to the hybrid functionals, that are often more accurate than local functional especially for main group thermochemistry.

One popular group of hybrid methods is Becke 3 parameter functional (*B3*), with the three empirical fitted parameters A,B and C:

$$E_{XC}^{B3} = (1-A)E_x^{Dirac-Slater} + AE_x^{HF} + BE_x^{B88} + E_c^{VWN} + C\Delta E_C^{GGA} \quad \textbf{(2.21)}$$

where Δ indicates that $\Delta\rho$-dependent fractions of corresponding functionals are included. B88 is a widely used gradient correction to exchange by Becke.

LSDA exchange, $E_x^{Dirac-Slater}$, is given by the Dirac-Slater formula for a uniform electron gas, and LSA correlation energy E_c^{VWN} is the functional by Vosko, Wilk an Nusair (VWN) [28].

When ΔE_C^{GGA} gradient correction to correlation in eq. (2.21) is Lee, Yang and Parr functional (LYP) [29], the approximate functional is known as B3LYP. So A determines the extent of replacement of the Slater local exchange $E_x^{Dirac-Slater}$ by the exact HF exchange E_x^{HF}; B controls the addition of Becke's gradient-correction to the exchange functional E_x^{B88}; C defines the weight of the LYP correlation E_C^{LYP} and the VWN correlation E_c^{VWN} functionals.

In recent years, new density functionals have been developed, belonging to the M05-class and M06-class functionals (including M05, M052X, M06L, M06, M062X, M06HF) [30]. In this thesis, the B3LYP and M06L functionals are used to investigate the various reaction mechanisms.

2.4 Coupled cluster approximation

The coupled cluster (CC) is an *ab initio* post-Hartree-Fock method used to describe small and medium-sized systems. This method introduces a correction factor in the molecular orbital that considers electron-electron repulsive forces. This factor is represented by an exponential operator $(e^{\hat{T}})$.

The fundamental equation in the CC theory is:

$$\psi(CC) = e^{\hat{T}} \, \Phi_0 \qquad (2.21)$$

where $\psi(CC)$ is the exact non-relativistic ground-state molecular electronic wave function, Φ_0 is the normalized ground-state Hartree-Fock wave function, the operator $e^{\hat{T}}$ is defined by the Taylor-series expansion:

$$e^{\hat{T}} = 1 + \frac{\hat{T}}{1!} + \frac{\hat{T}^2}{2!} + \frac{\hat{T}^3}{3!} + \cdots = \sum_{k=0}^{\infty} \frac{\hat{T}^k}{k!} \qquad (2.22)$$

and the cluster operator $\hat{T}$ is

$$\hat{T} = \hat{T}_1 + \hat{T}_2 + \ldots + \hat{T}_n \qquad (2.23)$$

where n is the number of electrons in the molecule and $\hat{T}_1$ is the operator of all single excitations, $\hat{T}_2$ is the operator of all double excitations and so forth.

If, in eq. (**2.22**) $\hat{T} = \hat{T}_1$, the method considers only the single excitations and it is indicated by the acronym (CCS). If, in eq. (**2.22**) $\hat{T} = \hat{T}_1 + \hat{T}_2$, the method considers the single and doubles excitations and it is indicated by the acronym (CCSD). Finally, including also $\hat{T}_3$ the method considers the single, doubles and triples excitations and it is indicated by the acronym (CCSD(T)) [31,32].

REFERENCES CHAPTER II

[1] Green, N. J. B., *Quantum Mechanics 1: Foundations,* Oxford University, **1997**, page 6.

[2] Schrödinger, E., *Ann. Physik., * **1926**, 79, 361.

[3] Born, M., Oppenheimer, J. *Ann. Physik.,* **1927**, 84, 457.

[4] Pauli, W. *Z., Physik.* **1925**, 31, 765.

[5] Szabo, A., Ostlund, N. S., *Modern Quantum Chemistry*, Dover Publication: New York, **1989**.

[6] Hartree, D., *Proc. Cambridge Phil. Soc*., **1928**, 24, 89.

[7] Hartree, D., *Proc. Cambridge Phil. Soc.,* **1928**, 24, 111.

[8] Hartree, D., *Proc. Cambridge Phil. Soc*., **1928**, 24, 426.

[9] Fock, V. *Z., Physik.,* **1930**, 61, 126.

[10] Bartlett, R. J., Stanton, J., *In Reviews in Computational Chemistry*; Lipkowitz, K. B., Boyd, D.B.: Eds., VCH Publishers: New York, **1994**, Vol.V.

[11] Hohenberg, P., Kohn, W., *Phys. Rev. B,* **1964**, 136, 864.

[12] Kohn, W., Sham, L., *J. Phys. Rev. A* **1965**, 136, 1133.

[13] Becke, A. D., *J. Chem. Phys.* **1986**, 84, 4524.

[14] Becke, A. D., *J. Chem. Phys.* **1992**, 96, 2155.

[15] Becke, A. D., *J. Chem. Phys.* **1992**, 97, 9173.

[16] Becke, A. D., *J. Chem. Phys.* **1993**, 98, 5648.

[17] Becke, A. D., *J. Chem. Phys.* **1996**, 104, 1040.

[18] Becke, A. D., *J. Chem. Phys.* **1997**, 107, 8544.

[19] Becke, A. D., *Phys. ReV. A*, **1988**, 38, 3098.

[20] Perdew, J. P., Wang, Y., *Phys. ReV. B*, **1986**, 33, 8800.

[21] Adamo, C., Barone, V., *J. Chem. Phys.,* **1998**, 108, 664.

[22] Handy, N. C., Cohen, A., *J. Mol. Phys.,* **2001**, 99, 403.

[23] Xu, X., Goddard, W. A., III. *Proc. Natl. Acad. Sci.* U.S.A., **2004**, 101, 2673.

[24] Perdew, J. P., *Phys. ReV. B*, **1986**, 33, 8822.

[25] Perdew, J. P., Burke, K., Ernzerhof, M., *Phys. ReV. Lett.*, **1996**, 77, 3865.

[26] Adamo, C., Barone, V., *J. Chem. Phys.,* **2002**, 116, 5933.

[27] a) van Leeuwen, R., Baerends, E.J., *Phys. Rev. A*, **1994**, 49, 2421; b) Becke, A. D., *J. Chem. Phys.,* **1998**, 109, 2092; c) Mori-Sanchez, P., Cohen, A. J., Yang, W., *J. Chem. Phys*., **2006**, 124, 91102/1.

[28] Vosko, S. H.,Wilk, L., Nusair, M., *Can. J. Phys*. **1980**, 58, 1200.

[29] Lee, C., Yang, W., Parr, R.G., *Phys. Rev. B* **1988**, 37, 785.

[30] Zhao, Y., Truhlar, D. G., *Acc. Chem. Res.,* **2008**, 41(2), 157.

[31] Barlett, R. J., *J. Phys. Chem.*, **1989**, 93, 1697.

[32] Noga, J., Barlett, R. J., *J. Phys. Chem.*, **1987**, 86, 7041.

CHAPTER III

Carnosine Role in the Inhibition of Platinum(II) Drugs

Introduction

The dipeptide L-carnosine (*β*-alanyl-L-histidine) is present in different body areas such as in skeletal and cardiac muscles, in brain tissue, in olfactory bulb, in hippocampus and in the stomach. It is also present in the cytosol of cells due to its water solubility [1-6].

The different electron rich sites of carnosine dipeptide can act as potential binding sites to various metal cations such as the carboxylic, amino, and amide groups as well as the histidine imidazole moiety. The pK_a values of these groups are approximately 2.6 for the carboxylic, 6.8 for the nitrogen of imidazole and 9.4 for the amino group. Due to this pK_a large range, carnosine can exist in several different tautomeric forms [7].

Carnosine plays many biological roles. It is known that carnosine has an anti-glycating effect, which can help in minimizing the effects of some diseases such as diabetes and Alzheimer [8]. It can react with several highly reactive species, such as hydroxyl, superoxide and molecular oxygen free radicals, especially in the water-rich environment inside the body, so it has an antioxidant activity [3, 9, 10] and it also has significant anti-inflammatory, antihypertensive, anti-aging, neurological and wound healing effects [11]. Carnosine is also able to buffer the increase of acidity, generated by lactic acid

formation, inside muscle tissue during muscle stress [12]. It is also reported that carnosine can act as a metal ion chelator, such as iron, calcium, and especially copper and zinc [13]. For that reason, carnosine is used for the treatment of diseases such as Wilsons disease[14] and Alzheimers.

Recently, it has been shown that carnosine may be involved in complexation of platinum anti-cancer drugs. Different studies have shown that carnosine may inhibit the cytotoxic action of oxaliplatin and carboplatin through the formation of complexes, defined fragmentation products, that are less cytotoxic than oxaliplatin and carboplatin alone [15]. Furthermore, this complexation reduces the efficacy of the Pt-drugs [7]. More recently, it has been reported that some fragments originating from carnosine can prevent cell proliferation in colon cancer cells [16,17]. As a consequence it should be of interest to gain information on the carnosine fragmentation mechanisms.

Various mass spectrometric techniques utilizing electrospray ionization and chip nanospray have been previously employed to study the interaction of oxaliplatin and carboplatin with carnosine. In particular, the technique that provides information about the fragmentation of carnosine, carnosine-oxaliplatin and carnosine-carboplatin complexes is the collision induced dissociation (CID). This technique involves the fragmentation of gas phase ions. The ions are generally accelerated in a vacuum

by an electric potential and made to collide with neutral molecules in the gas phase (usually helium, nitrogen or argon). In the collision the kinetic energy is converted into internal energy and this causes the damage of one or more bonds and the ion fragmentation.

3.1 Aim of the study

In this Chapter, the outcomes of a detailed theoretical investigation of the protonated complexes of oxaliplatin and carboplatin with carnosine as well as their collision induced fragments will be presented together with the results of a thorough computational analysis of the CID products of protonated carnosine. Particularly, potential energy surfaces (PESs) for the gas phase dissociation of the protonated carnosine-oxaliplatin and carnosine-carboplatin complexes have been described. Calculated potential energy surfaces of the dissociation processes have been compared with the outcomes of the energy resolved collision induced dissociation of the protonated carnosine-oxaliplatin and carnosine-carboplatin complexes (**Paper II-III**). Furthemore, the CID products of protonated carnosine have been quantum-mechanically scrutinized to elucidate the structures of these products and their precursors as well as to provide an accurate description of the energy profiles for these dissociation pathways (**Paper I**).

3.2 Collisionally-Induced Dissociation Products of the Protonated Dipeptide Carnosine: Structural elucidation, Fragmentation Pathways and Potential energy surface analysis (Paper I).
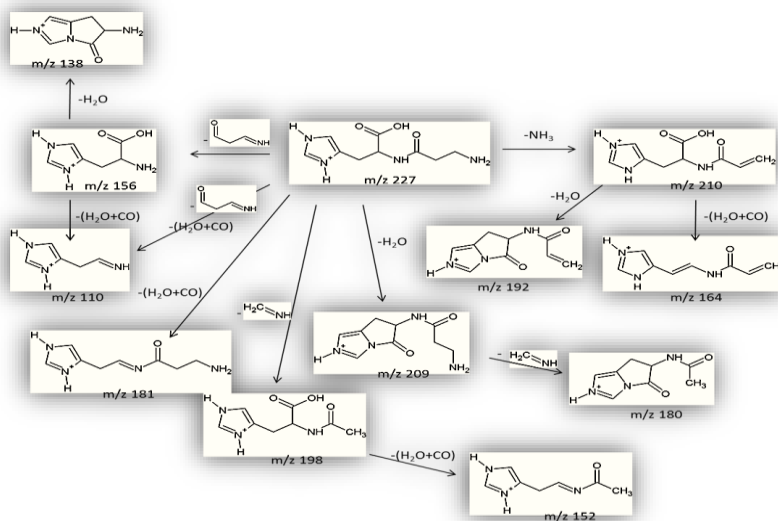
The use of the collision induced dissociation (CID) technique involves the fragmentation of ions in gas phase. For this reason, to analyze the carnosine fragmentation with this technique its protonated form ([carnosine+H]$^+$) must be considered. Carnosine has different protonation sites: carboxylic, amino, amide groups and imidazole moiety of histidine.

Theoretical calculations show that the most stable structure of the protonated carnosine is one in which the protonation site is the imidazole moiety of histidine [18,7,19].

This structure is that of the precursor fragment and it is labeled as **227**, which indicates the ratio between the mass and the charge of the ion. Collision-induced dissociation experiments are shown to yield eleven different fragment ions. Therefore, the formation mechanism of each fragment has been theoretically examined, employing different levels of theory, that is B3LYP, M06, M06 single point and MP2 single point. Relative gas-phase free energies of minima and transition states have been calculated with respect to the most stable conformer of [carnosine+H]⁺, **227**. In **Paper I**, only the fragmentation mechanisms at lower energies are reported. The adopted computational protocols give comparable energetic trends and are all able to elucidate the fragmentation mechanisms, which account for all experimental data. In the case of single point M06 and MP2 calculations on previously optimized B3LYP structures, the description of the energy profiles in some regions appear to be significantly different.

3.3 Fragmentation Pathways Analysis for the Gas Phase Dissociation of Protonated Carnosine-Oxaliplatin Complexes (Paper II)
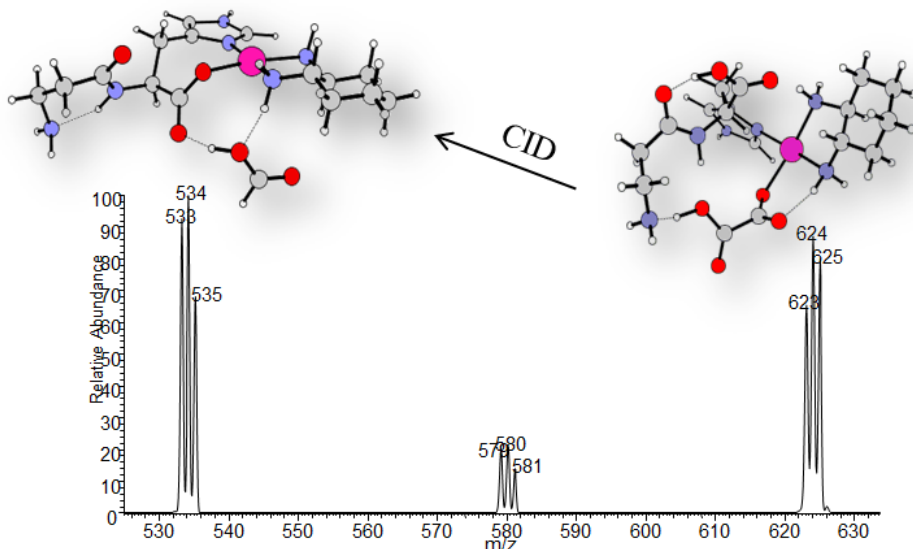
The carnosine may be involved in complexation of platinum anti-cancer drugs. In fact, recent studies have shown that carnosine can inhibit the cytotoxic action of the third generation chemotherapeutic drug oxaliplatin through the formation of complexes that are less cytotoxic than oxaliplatin alone [15] being the consequence of such complexation the fragmentation of the drug.

Also in this case, in order to study the interactions between oxaliplatin and the carnosine dipeptide collision induced dissociation (CID) technique has been used [20,21]. Therefore,

the protonated form of the carnosine-oxaliplatin complex, [Carnosine+ OxPt+H]$^+$, called in **Paper II** precursor fragment **1A,** has been considered. The fragmentation mechanism of the **1A** complex has been theoretically examined at DFT level, adopting the hybrid exchange-correlation B3LYP functional and, for all the atoms, the LANL2DZ basis sets. In this paper three fragmentation mechanisms of protonated carnosine-oxaliplatin complex, [Carnosine+ OxPt+H]$^+$, have been reported and investigated theoretically together with the formation mechanisms of protonated oxaliplatin, [OxPt+H]$^+$, and protonated carnosine, [Carnosine+H]$^+$, from the same precurson ion through loss of neutral carnosine and neutral oxaliplatin, respectively. Furthermore, a comparison between the calculated potential energy surfaces of the dissociation process and the energy resolved collision induced dissociation of the protonated carnosine-oxaliplatin complex has been also reported.

3.4 Mass Spectometric and Computational Investigation of the Protonated Carnosine-Carboplatin Complex Fragmentation (Paper III)
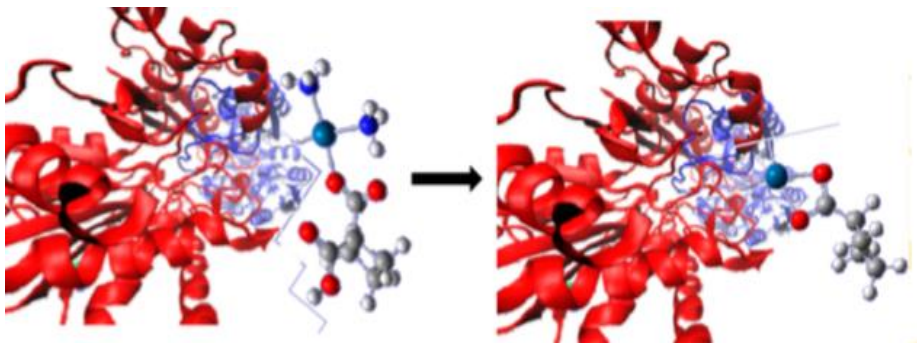
Carboplatin is a platinum anticancer drug used for the treatment of many human cancers. Inside the cancer cell, the carboplatin-DNA interaction has been widely investigated [22-25].

Carboplatin, likewise oxaliplatin, can generate undesired interactions with polypeptides, such as carnosine. Also in this case, the interaction between carnosine and carboplatin, generating a carnosine-carboplatin complex, causes the loss and deactivation of the drug, before it arrives at the ultimate target, due to its fragmentation. Experimentally, in order to study the interactions between carboplatin and carnosine dipeptide the collision induced dissociation (CID) technique has been used. The fragmentation pathways of the protonated carnosine-carboplatin complex, [Carnosine+CarbPt+H]$^+$, **1A** precursor, have been investigated in **Paper III**. A detailed description of

the fragmentation pathways for the gas phase dissociation of the protonated carboplatin−carnosine complex and a comparison between calculated potential energy surfaces for the dissociation processes and collision-induced dissociation (CID) experiments have been reported. Different fragmentation mechanisms have been investigated and the free-energy fragmentation pathways have been calculated by using DFT at the B3LYP/LANL2DZ level.

REFERENCES CHAPTER III

[1] Gulewitsch, W., Amiradzibi, S., *Ber. Deut. Chem. Ges.,* **1900**, 33, 1902-1903.

[2] Severina, I., Bussygina, O., Pyatakova, N., *Biochemistry-Moscow,* **2000**, 65, 783-788.

[3] Kohen, R., Yamamoto, Y., Cundy, K., Ames, B., *Proc. Natl. Acad. Sci. U. S. A.*, **1988**, 85, 3175-3179.

[4] Gariballa, S. E., Sinclair, A. J., *Age and Aging* , **2000**, 29, 207-210.

[5] Horning, M., Blakemore, L., Trombley, P., *Brain Res.,* **2000**, 852, 56-61.

[6] Nino, M., *Journal of cosmetics, dermatological sciences and applications*, **2011**, 1, 177.

[7] Moustafa, E. M., Korany, M., Mohamed, N. A, Shoeib, T., *Inorganica Chimica Acta*, **2014**, 421, 123-135.

[8] Reddy, V. P., Garrett, M. R., Perry, G., Smith, M. A., *Sci. Aging Knowledge Environ.*, 2005, 18, pe12.

[9] Hartman, P., Hartman, Z., Ault, K., *Photochemistry and photobiology*, **1990**, 51, 59-66.

[10] Pavlov, A., Revina, A., Dupin, A., Boldyrev, A., Yarpolov, A., *Biochimica et biophysica acta*, **1993**, 1157, 304-312.

[11] Kovacs-Nolan, J., Mine, Y., *Animal Muscle-Based Bioactive Peptides, Bioactive Proteins and Peptides as*

Functional Foods and Nutraceuticals, Wiley-Blackwell, **2010**, pp. 225–231.

[12] Suzuki, Y., Ito, O., Mukai, N., Takahashi, H., Takamatsu, K., *Jpn. J. Physiol.*, **2002**, 52, 199–205.

[13] Boldyrev, A., Severin, S., *Adv. Enzyme Regul.*, **1990**,30, 175**.**

[14] Kang, J., Kim, K., Choi, S., Kwon, H., Won, M., Kang, T., *Mol. Cells*, **2002**, 13, 498–502.

[15] Moustafa, E. M., Camp, C. L., Youssef, A. S., Amleh, A., Reid, H. J., Sharp, B. L., Shoeib, T., *Metallomics*, **2013**, 5, 1537–1546.

[16] Iovine, A., Iannella, M. L., Nocella, F., Pricolo, M. R., Bevilacqua, M. A., *Cancer Lett.*, **2012**, 315, 122–128.

[17] Horii, Y., Shen, J., Fujisaki, Y., Yoshida, K., Nagai, K., *Neurosci. Lett.*, **2012**, 510, 1-5.

[18] Menges, F., Riehn, C., Niedner-Schatteburg, G., *Z. Phys. Chem.* , **2011**, 225, 595-609.

[19] Grégoire, G., Gaigeot, M. P., Marinica, D. C., Lemaire, J., Schermann, J. P., Desfrançois, C., *Phys. Chem. Chem. Phys*., **2007**, 9, 3082-3097.

[20] Hartinger, C. G., Groessl, M., Meier, S. M., Casini, A., Dyson, P. J., *Chem. Soc. Rev*., **2013**, 42, 6186.

[21] Groessl, M., Hartinger, C. G., *Anal. Bioanal. Chem.*, **2013**, 405, 1791.

[22] Knox, R. J.; Friedlos, F.; Lydall, D. A.; Roberts, J, *J. Cancer Res.,* **1986**, 46, 1972.

[23] Jamieson, E. R.; Lippard, S. *J. Chem. Rev.*, **1999**, 99, 2467−2498.

[24] Tewey, K. M.; Chen, G. L.; Nelson, E. M.; Liu, L. F. *J. Biol. Chem.*, **1984**, 259, 9182−9187.

[25] Johnstone, T. C.; Park, G. Y.; Lippard, S. *J. Anticancer Res.,* **2014**, 34, 471−476.

Paper I

"Collision-induced dissociation products of the protonated dipeptide carnosine: structural elucidation, fragmentation pathways and potential energy surface analysis"

Eslam Moustafa, Ida Ritacco, Emilia Sicilia, Nino Russo, Tamer Shoeib.

Collision-induced dissociation products of the protonated dipeptide carnosine: structural elucidation, fragmentation pathways and potential energy surface analysis†

Eslam M. Moustafa,[a] Ida Ritacco,[b] Emilia Sicilia,[b] Nino Russo[bc] and Tamer Shoeib*[ad]

Collision-induced dissociation (CID) experiments on protonated carnosine, [carnosine + H]$^+$, with several collision energies were shown to yield eleven different fragment ions with the generation of product ions [carnosine−H$_2$O + H]$^+$ and [carnosine−NH$_3$ + H]$^+$ being the lowest energy processes. Energy-resolved CID showed that at slightly higher collision energies the ions [histidine + H]$^+$ and [histidine−H$_2$O−CO + H]$^+$ are formed. At even higher energies four other product ions were observed, however, attained relatively lower abundances. Quantum chemistry calculations, carried out at different levels of theory, were employed to probe fragmentation mechanisms that account for all the experimental data. All the adopted computational protocols give similar energetic trends, and the range of the calculated free energy barrier values for the generation of all the observed product ions is in agreement with the fragmentation mechanisms offered here.

Introduction

The dipeptide β-alanine-L-histidine, also known as carnosine, is a naturally occurring substance synthesized by endogenous carnosine synthetase discovered more than 100 years ago.[1] It is present at elevated levels in human skeletal and cardiac muscles as well as in brain tissues[2–5] and is typically concentrated in the cytosol of cells due to its water solubility.[6] Although not much is known about its physiological function, several possible roles have been considered since its first discovery[7,8] such as pH-buffering,[9] metal chelation[10] or neurotransmitter function.[11] Carnosine is also reported to have antioxidant activity due to its ability to react with several highly reactive species, such as hydroxyl, super oxide and molecular oxygen free radicals, especially in the water rich environment inside the body.[3,12,13] More recently, carnosine was shown to play a role in the detoxification of the anti-cancer drug oxaliplatin, one of the most commonly used Pt-anticancer chemotherapeutic agents.[14] Additionally, it was shown that complexes formed between carnosine and oxaliplatin reduce the efficacy of the Pt-drug causing increased viability in cancer cells.[14]

The interaction of carnosine with metals of biological relevance was the subject of several studies including the report on metal binding energies to the peptide and providing structural elucidation of the complexes and the resulting collision induced dissociation (CID) products.[14–21] Studies of the CID products of protonated carnosine, on the other hand, have received considerably less attention. In general, the observed fragmentation patterns generated from protonated peptide ions typically depend on several factors including the amino acid composition, the size of the peptides, the excitation method used and the charge of the ions.[22] CID of protonated peptides employing soft ionization techniques such as electrospray and matrix assisted laser desorption proved useful for determining amino acid sequences. This in turn increased the interest in the fragmentation pathways of protonated peptides and the mechanisms of product ion formation which spurred several studies on protonated α-amino acids,[23–30] while studies on β-amino acids or peptides that contain them remain very sparse.[31,32]

Relatively simple CID mass spectra are generated due to the fragmentation of protonated aliphatic α-amino acids which mainly show their respective iminium ions produced *via* the concomitant loss of H$_2$O and CO. Hydroxylic and acidic α-amino acids lose H$_2$O through the OH and COOH groups in their side chains in addition to the concomitant loss of H$_2$O

[a] *Department of Chemistry, The American University in Cairo, New Cairo 11835, Egypt*

[b] *Dipartimento di Chimica Universita della Calabria, Via P. Bucci, cubo 14c, 87036 ArcaVacata di Rende (CS), Centro di Calcolo ad Alte Prestazioni per Elaborazioni Parallele e Distribute – Centro d'Eccellanza MIUR, Rende 87036, Italy*

[c] *Division de Ciencias Basicas e Ingenieria, Departamento de Quimica, Universidad, Autonoma Metropolitana-Iztapalapa, Av. San Rafael Atlixco No. 186, Col. Vicentina, CP 09340, Mexico, Distrito Federal, Mexico*

[d] *Centre for Analytical Science, Department of Chemistry, Loughborough University, Loughborough, Leicestershire LE11 3TU, UK. E-mail: T.Shoeib@aucegypt.edu*

This journal is © the Owner Societies 2015

Phys. Chem. Chem. Phys., 2015, **17**, 12673–12682 | **12673**

and CO. Basic α-amino acids such as arginine and lysine have a nitrogen on the side chain as the favoured site of protonation[30] thus one of the major fragmentation pathways in these amino acids involves the loss of NH_3 and, in the case of protonated arginine, guanidine.[23,24] Facile elimination of NH_3 is observed in all aromatic α-amino acids, with the exception of protonated histidine in addition to the concomitant elimination of H_2O and CO.[23,33–36] At higher collision energies, subsequent to the elimination of NH_3 the loss of H_2O, CO, CO_2 and CH_2CO is observed, while the loss of HCN, $HCNH_2$, and NH_3 occurs subsequent to the concomitant loss of H_2O and CO.[26]

Protonated peptide fragmentation under low-energy collision conditions is believed to be charge induced, and electron rearrangements involved in decomposition of an activated ion into two or more fragments are assumed to be triggered by localization of the charge on specific sites within the molecular structure of the decomposing ions.[22] Thus, the observation of a large number of product ions typically implies that there is a heterogeneous population of fragmenting precursor isomers. This situation is likely since peptides contain multiple functional groups and each of them can act as a protonation site. In the case of carnosine these sites include the carboxylic, amino, and amide groups as well as the imidazole moiety of histidine. The average pK values of these groups are 2.64 for the carboxylic group, 6.77 for the *tele* nitrogen of imidazole and 9.37 for the amino group.[10] This large range of values may explain the fact that carnosine can exist in several different tautomeric forms. In addition to possibly having a large population of fragmenting precursor isomers it is also possible, however, for inter-conversions between these protonated isomers to occur if low energy barriers are required, which can also contribute to the formation of a large number of collisionally-induced fragment ions.

In this paper, we report for the first time on a detailed examination of the CID products of protonated carnosine and employ quantum chemistry calculations to rationalize the observed fragmentation patterns.

Instrumentation

An LTQ linear ion trap mass spectrometer (Thermo Electron, San Jose, CA, USA) and an Acquity TQ tandem quadrupole mass spectrometer (Waters, MA, USA), both equipped with electrospray ionisation interfaces, were used in this work. Carnosine, HPLC-grade water and methanol were all purchased from Sigma-Aldrich, UK. Deuterium exchange experiments were carried out in solutions that contain deuterium oxide (99.9%) and CH_3OD (99.5%), both from Sigma-Aldrich. The LTQ resolving powers achieved were in the order of 1500 while the upper instrumental error limit in measurements was 0.2 m/z units. The LTQ autotune routine was used to obtain the lens, quadrupole and octupole voltages for the maximum transmission of the ions of interest. Helium gas, admitted into the ion trap at a maintained pressure of approximately 10^{-3} Torr, was used as the buffer gas to improve the trapping efficiency and as the collision gas for collision-induced dissociation experiments performed here.

Experiments designed to elucidate ion structures or fragmentation pathways on the LTQ were performed as follows: the ion of interest was selected then collisionally activated by setting the activation amplitude to 25–35% of the maximum voltage available (determined empirically), and the activation Q setting (used to adjust the frequency of the RF excitation voltage) was set to 0.25 units.

The Acquity TQ was operated in the positive ion mode, with typical values of cone and extractor voltages set to 30 and 3 respectively. The capillary voltage was optimised day-to-day for maximum signal transmission and spray stability, and the optimised range was typically 2200–2500 volts. The de-solvation gas was usually set to a flow of 250 L h^{-1} and a temperature of 150 °C. Argon was used as the collision gas at a typical flow rate of 0.15 ml min^{-1}. Ions sampled from the electrospray suffered many collisions in an attempt to achieve effective thermalization in the lens region, being from the orifice/skimmer to the first r.f. only quadrupole. The bias potential in this lens region was set up to strike a compromise between signal transmission and minimal collisional heating. The precursor ions underwent multiple collisions with argon to produce tandem mass spectra at collision energies in the range 0–30 eV in the lab frame having both Q1 and Q3 operated at unit resolution with a typical dwell time of 25 milliseconds per transition. Both instruments described here were previously successfully employed by us using the exact setup described to elucidate structures of metal and non-metal containing biological ligands.[37–39] While some of our previous studies were conducted under single collision conditions[40–42] the experiments reported here were all performed under multiple collision conditions.

Computational methods

All molecular orbital calculations were performed using GAUSSIAN 09.[43] The structures were fully optimized without symmetry constraints by means of density functional theory (DFT) using the hybrid Becke's three-parameter exchange functional and the correlation functional from Lee, Yang and Parr (B3LYP)[44–46] in conjunction with the standard Pople basis set 6-311++G(d,p).[47–49] All the stationary points reported here were further characterized by harmonic frequency analysis to have the appropriate number of imaginary frequencies, which are none for local minima and one for first-order saddle points. Intrinsic reaction coordinate calculations[50] were run to connect the transition state geometries with those of the corresponding minima. All species considered in this work were in the singlet state and thus all calculations performed were on closed shell species. The spin has been conserved through all the reactions described within the manuscript. Total energies, zero-point energies, thermal corrections and entropies are given in the ESI,† Tables S1–S4. Long and weak interactions such as hydrogen bonds are often difficult to be accurately described by DFT theory. However, studies employing DFT calculations with the B3LYP functional accurately detail hydrogen bonding in small systems such as hydrogen fluoride dimers, clusters of cyanoacetylene and

12674 | *Phys. Chem. Chem. Phys.*, 2015, **17**, 12673–12682

This journal is © the Owner Societies 2015

hydrogen cyanide as well as in water dimers and complexes.[51–54] The B3LYP and 6-31++G(d,p) combination was successfully used to model internal hydrogen bonding within a protonated triglycine and to demonstrate the validity of the "mobile proton" model in the tripeptide,[55] while the B3LYP/6-311++G(2d,2p) level of theory was shown to predict the existence of a hydrogen bonding stabilised zwitterionic form of protonated carnosine in the gas phase.[21] With the aim of comparing, however, both single point MP2 (frozen core)[56] and M06[57] calculations were carried out by using the same 6-311++G(d,p) basis set on optimized B3LYP/6-311++G(d,p) geometries. The hybrid M06 exchange–correlation functional was employed here as it is specifically designed to accurately describe non-covalent interactions. Additionally, the M06 functional along with the 6-311++G(d,p) basis set was employed to perform full optimization followed by frequency calculations of geometrical structures of minima and transition states and to map the fragmentation pathways on the corresponding PESs. For the sake of clarity, from this point forward the used levels of theory B3LYP/ 6-311++G(d,p), M06/6-311++G(d,p), M06/6-311++G(d,p)//B3LYP/ 6-311++G(d,p) and MP2/6-311++G(d,p)//B3LYP/6-311++G(d,p) will be indicated as B3LYP, M06, M06SP, and MP2SP, respectively.

Results and discussion

Electrospraying a 1 mM solution of carnosine on a 1 : 1 (v/v) water–methanol solution generated the mass spectra shown

and assigned in Fig. 1 (see panel A). The MS^2 spectra of [carnosine + H]$^+$, for which the potential energy surfaces were extensively studied and found to be relatively flat containing several low energy structures,[21] are shown in Fig. 1 (see panel B). Collision-induced dissociation experiments are shown to yield eleven different fragment ions as shown in Fig. 1 (see panel B) and Fig. 2. It is important to note that the results shown in Fig. 1 and 2 were produced by two different mass spectrometers operated with two different collision gases and not under single collision conditions. Thus even at the same values of E_{lab} no direct comparison of ion intensities between the two figures is possible. Although many pathways leading to the formation of such fragments were examined, only those at lower energies are reported here. Relative gas-phase free energies of minima and transition states are calculated with respect to the most stable conformer of [carnosine + H]$^+$, **227**, shown in Fig. 3 and 4, which has also been previously reported as the lowest energy species of protonated carnosine[17,21,58] obtained by protonation at the *pros* imidazole nitrogen of the imidazole ring of the histidine residue and containing two pseudo rings. The first is a pseudo eight membered ring due to the formation of a hydrogen bond between the hydrogen atom of the protonated *pros* imidazole nitrogen and the amide carbonyl oxygen atom. The second of such pseudo rings is formed by the formation of a hydrogen bond between the hydrogen atom of the amide nitrogen and the nitrogen atom of the amino group. The outcomes of all the employed levels
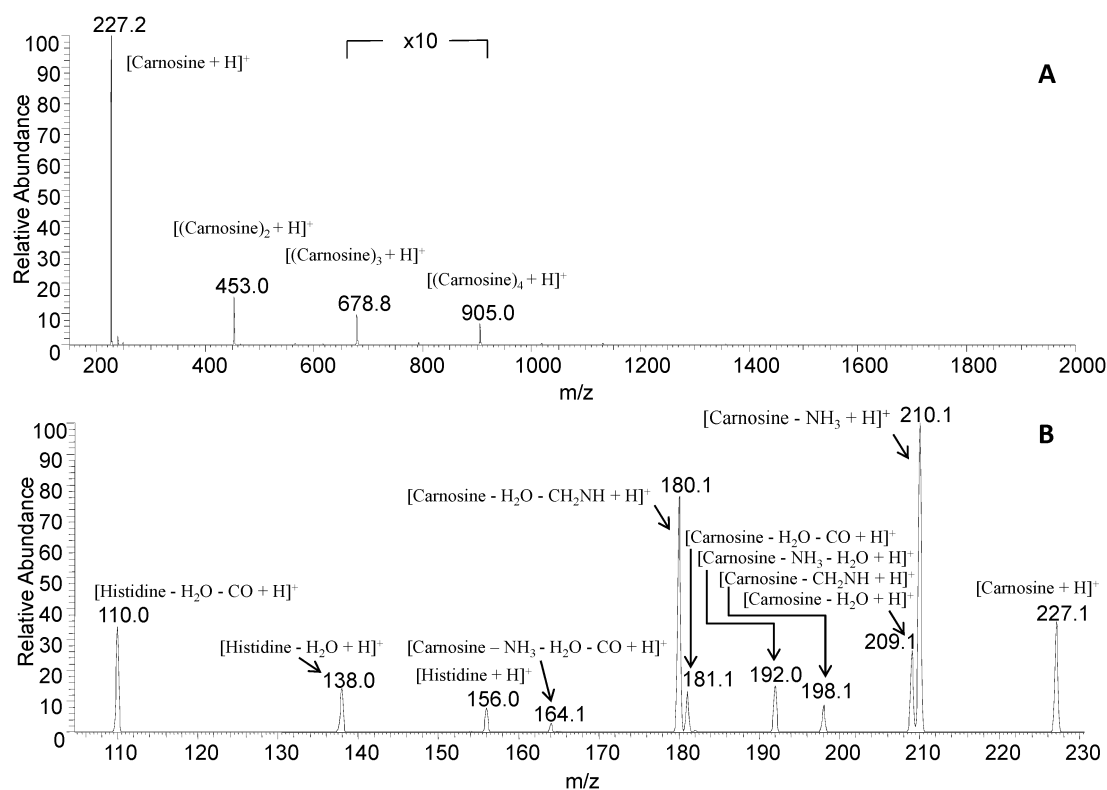

Fig. 1 Panel A, full scan MS spectrum of a 1 mM carnosine in a (1 : 1) (v/v) water/methanol solution without allowing for incubation time. Panel B, MS^2 spectrum of the ion [carnosine + H]$^+$ generated at 25 eV in the lab frame. Both mass spectra were generated by an LTQ linear ion trap using helium as a collision gas as described in the Instrumental section.
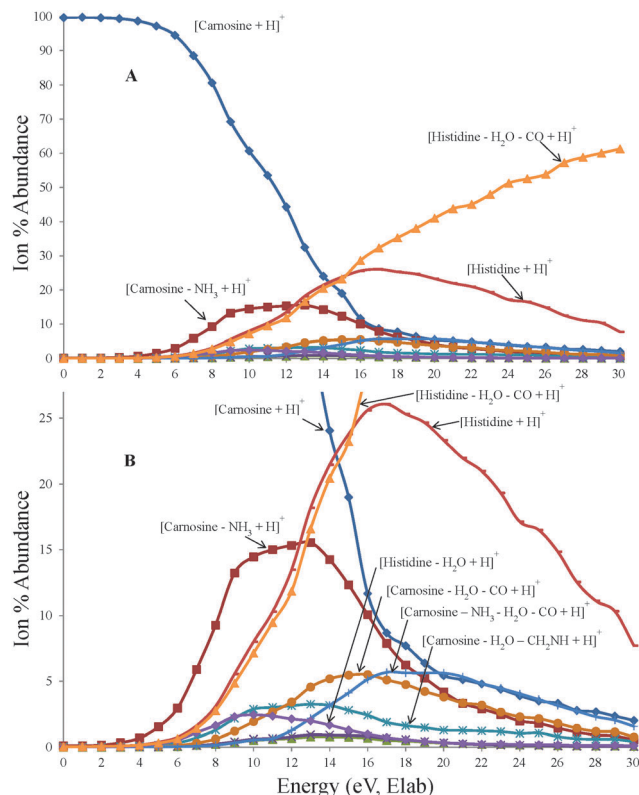
Paper

Fig. 2 Energy-resolved collision induced dissociation curves of [carnosine + H]$^+$ as obtained on the Aquity TQ tandem mass spectrometer employing argon as a collision gas as described in the Instrumental section. Y-axis is (ion abundance)/(total ion abundance) expressed as a percentage. Panel A shows the full curve, while panel B shows an expanded view for clarity. Only ions attaining relative intensities above 2.5% are labelled.
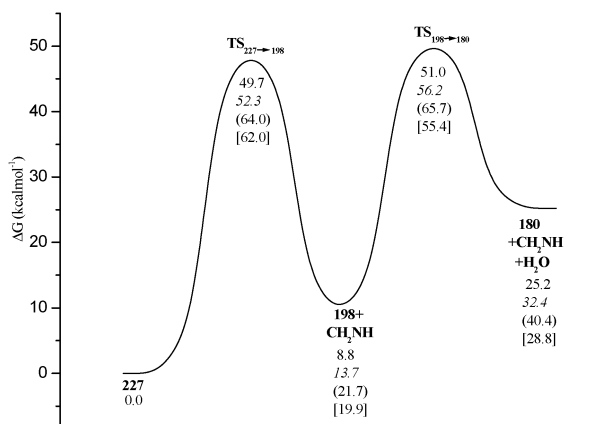

Fig. 3 B3LYP free energy profile for the fragmentation of [carnosine + H]$^+$ to give the ion at m/z 180 and its precursor at m/z 198. Relative free energies at 298 K are in kcal mol^{-1} and calculated with respect to the most stable conformer, **227**, of protonated carnosine. M06, M06SP and MP2SP values are reported in italics, brackets and square brackets, respectively.

of theory, that is B3LYP, M06, M06SP and MP2SP, are reported and discussed.

Many of the fragment ions observed in the MS^2 spectra shown in Fig. 1 (see panel B) were previously reported.[17,18] The MS^2

spectra of [carnosine-d_5 + D]$^+$ in which carnosine has all its labile hydrogen atoms exchanged with deuterium atoms are shown in Fig. S1 of the ESI.†

[Carnosine–CH$_2$NH + H]$^+$

The ion at m/z 198 shown in panel B of Fig. 1, which is labeled [carnosine–CH$_2$NH + H]$^+$, is shown to be formed from the most stable conformer of [carnosine + H]$^+$, **227**, through the transition state **TS$_{227\rightarrow198}$** with an associated barrier of 49.7, 52.3, 64.0 and 62.0 kcal mol^{-1} calculated at the B3LYP, M06, M06SP and MP2SP levels, respectively, as shown in Fig. 3. Schematic representations and optimised structures at the B3LYP level of all involved species are shown in Fig. 4 and Fig. S2 in the ESI,† respectively. This ion is shown to correspond to the signals at m/z 203 and 204 at a ratio of 4:1 in the CID spectrum of the deuterium-incorporated complex shown in Fig. S1 (ESI†). This indicates that the loss of a single deuterium atom most likely on the nitrogen atom of the eliminated CH$_2$ND to be the dominant pathway but that evidence of gas phase H/D exchange prior to the elimination reaction is observed.

[Carnosine–CH$_2$NH–H$_2$O + H]$^+$

The subsequent elimination of H$_2$O from the ion [carnosine–CH$_2$NH + H]$^+$ to produce [carnosine–CH$_2$NH–H$_2$O + H]$^+$, which is observed at m/z 180 in Fig. 1, corresponds to a signal cluster at m/z 183, 184, 185 and 186 in the CID spectrum of the deuterium-incorporated complex shown in Fig. S1 (ESI†). This cluster indicates the loss of up to three deuterium atoms most likely due to the elimination of CH$_2$ND and D$_2$O as consistent with the proposed fragmentation pathway. The presence of such a signal cluster is also an indication of a significant H/D gas phase scrambling prior to the elimination reaction observed. This partial H/D gas phase scrambling has been previously reported in the CID of protonated and metal ion bound-aromatic amino acids including histidine and tryptophan.[25,26,42] Mechanisms rationalising this observed H/D scrambling were reported[42] in which it is assumed that the forward and reverse rates of each of the steps are fast, an assumption that is reasonable as hydride transfers typically have fast reaction rates.[25] The proposed fragmentation pathway to produce [carnosine–CH$_2$NH–H$_2$O + H]$^+$ is shown in Fig. 3 to go through a transition state calculated to be at 51.0, 56.2, 65.7 and 55.4 kcal mol^{-1} at the B3LYP, M06, M06SP and MP2SP levels relative to structure **227**, respectively. It is important to note that for three of the used computational protocols, the second transition state shown in Fig. 3 is calculated to be very slightly higher in energy than the first transition state shown in the figure. This energy difference where **TS$_{198\rightarrow180}$** is shown to be higher than **TS$_{227\rightarrow198}$** is calculated to be at a maximum of 3.9 kcal mol^{-1} at the M06SP level, while at the MP2SP level the order is shown to be reversed with **TS$_{198\rightarrow180}$** being lower by 6.6 kcal mol^{-1}. This may consequently explain the relatively low abundance observed for the ion [carnosine–CH$_2$NH + H]$^+$.

[Carnosine–NH$_3$ + H]$^+$

The CID curve shown in Fig. 2 reveals that the loss of the NH$_3$ pathway to produce the ion at m/z 210 from the precursor
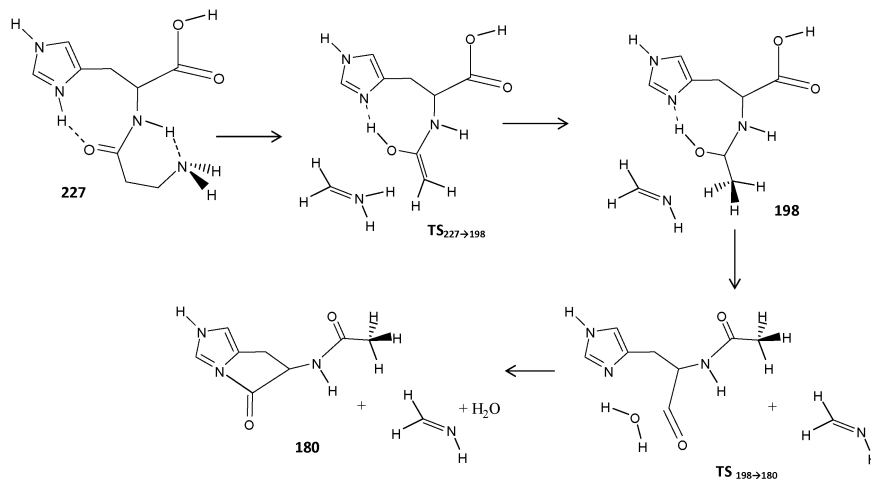
Fig. 4 Proposed mechanism for the collision induced fragmentation of [carnosine + H]$^+$ to produce the fragments observed at m/z 198 and 180.
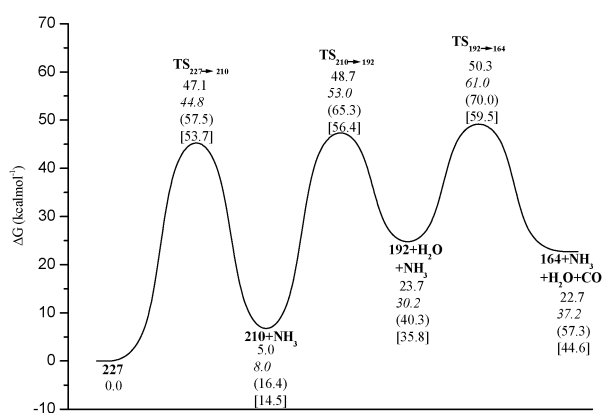

Fig. 5 B3LYP free energy profile for the fragmentation of [carnosine + H]$^+$ to give the ion at m/z 164 and its precursors at m/z 210 and 192. Relative free energies at 298 K are in kcal mol^{-1} and calculated with respect to the most stable conformer, **227**, of protonated carnosine. M06, M06SP and MP2SP values are reported in italics, brackets and square brackets, respectively.

[carnosine + H]$^+$ at m/z 227 as shown in Fig. 1 is among the lowest energy processes. The CID spectrum of the deuterium-incorporated complex shown in Fig. S1 (ESI†) indicates the loss of ND$_3$, NHD$_2$ and NH$_2$D to be evident at an approximate ratio of 5:4:1. This significant H/D scrambling prior to the elimination of NH$_3$ was previously reported in metal ion containing and protonated amino acids.[26,42] The calculated energy profile for this reaction is shown in Fig. 5, and the corresponding schematic representations and optimised structures at the B3LYP level of all involved species are shown in Fig. 6 and Fig. S3 in the ESI,† respectively. The loss of NH$_3$ from [carnosine + H]$^+$ to form [carnosine−NH$_3$ + H]$^+$ observed at m/z 210 in Fig. 1 is shown to go through the transition state **TS**$_{227 \to 210}$ in which the hydrogen bond between the hydrogen atom of the amide nitrogen and the nitrogen atom of the neutral amino group of structure **227** is no longer present and a 1,3-hydride shift to the terminal amino nitrogen takes place. This transition state **TS**$_{227 \to 210}$ leads to the release of NH$_3$ and the formation of an ion molecule adduct as shown in structure **210** in Fig. 6 and Fig. S3 (ESI†), in which the

remaining ion forms a hydrogen bond with the newly liberated NH$_3$ molecule through the hydrogen of the amide atom. This rather long and weak hydrogen bonding interactions, at 1.977 and 1.937 Å as optimized at the B3LYP and M06 levels, respectively, are then very easily broken to produce the ion observed at m/z 210. The production of this ion is shown to be among the lowest processes calculated here, requiring an activation barrier of 47.1 kcal mol^{-1}, at the B3LYP level, calculated with respect to the lowest energy form of protonated carnosine, as shown in Fig. 5. This same energy barrier is calculated to be 44.8, 57.5 and 53.7 kcal mol^{-1} at the M06, M06SP and MP2SP levels respectively.

All efforts to locate a 'loose' transition state for the direct removal of NH$_3$ from structure **227** in Fig. 6 and Fig. S3 (ESI†) resulted in a concerted transition state for the simultaneous shifting of two hydrogen atoms – the first from the amide nitrogen to the terminal amino nitrogen, forming the NH$_3$ group which is subsequently lost as a neutral fragment, while the second being one of the two hydrogen atoms on the CH$_2$ group adjacent to the CO shifting to the amide nitrogen atom. This step was calculated at the B3LYP level of theory to have a barrier of 72.1 kcal mol^{-1} relative to structure **227** of Fig. 6 and Fig. S3 (ESI†). The second step in this pathway is the removal of NH$_3$ involving a subsequent transition state which was calculated to have a barrier of 37.3 kcal mol^{-1} relative to structure **227** of Fig. 6 and Fig. S3 (ESI†). This process detailed here is shown in Fig. S5 (ESI†) and is calculated to be less viable than the one previously described in Fig. 5 and 6 for the loss of NH$_3$.

[Carnosine−NH$_3$−H$_2$O + H]$^+$

The subsequent loss of H$_2$O from the ion [carnosine−NH$_3$ + H]$^+$ observed at m/z 210 in Fig. 1 is shown in Fig. 5 to occur by overcoming the transition state **TS**$_{210 \to 192}$ schematically shown in Fig. 6 and Fig. S3 (ESI†), in which the backbone of the dipeptide is rearranged to allow for the carbonyl oxygen atom of the –COOH group to abstract the hydrogen atom from the *pros* nitrogen of the imidazole ring which in turn allows for the elimination of H$_2$O and the formation of a bond between the carbon atom of the remaining carbonyl group and the
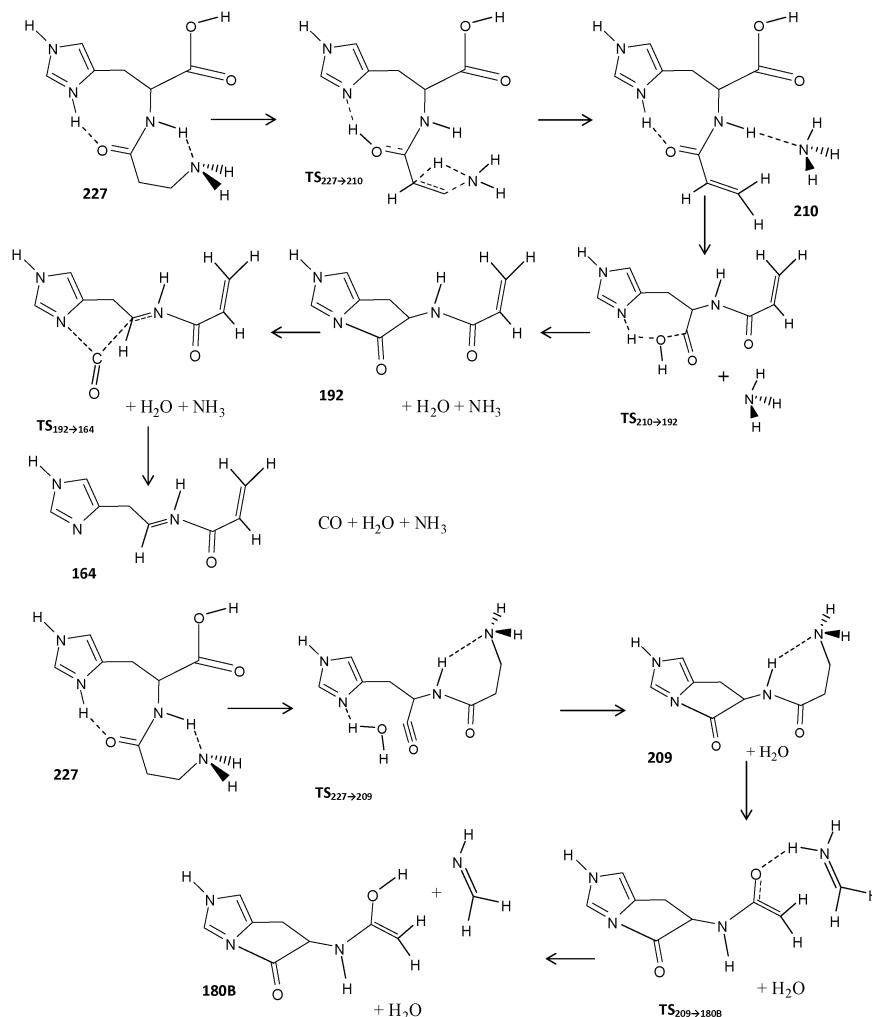
Fig. 6   Proposed mechanism for the collision induced fragmentation of [carnosine + H]$^+$ to produce the fragments observed at m/z 210, 192 and 164.

pros nitrogen of the imidazole ring resulting in the formation of a five-member ring within the ion [carnosine–NH$_3$–H$_2$O + H]$^+$ which is observed at m/z 192. The corresponding signal cluster for this ion in the CID spectrum of the deuterium-incorporated complex shown in Fig. S1 (ESI†) indicates the loss of one, two, three, four or five deuterium atoms at a ratio of 1 : 6 : 10 : 3 : 2 which is consistent with the mechanism proposed here. The transition state **TS$_{210 \to 192}$** for this process is calculated to be only very slightly higher in energy than the transition state **TS$_{227 \to 210}$** responsible for the generation of the ion [carnosine–NH$_3$ + H]$^+$ at m/z 210.

[Carnosine–NH$_3$–H$_2$O–CO + H]$^+$

The subsequent loss of CO from the ion [carnosine–NH$_3$–H$_2$O + H]$^+$ produces the ion [carnosine–NH$_3$–H$_2$O–CO + H]$^+$ observed at m/z 164 in Fig. 1. This process in which the CO moiety in the five-member ring of the ion [carnosine–NH$_3$–H$_2$O + H]$^+$ is eliminated, as it is shown in Fig. 5 and 6, to produce structure **164** going through the transition state **TS$_{192 \to 164}$** is calculated to be at 50.3 kcal mol^{-1} at the B3LYP level relative to

structure **227**, this value increases to 61.0, 70.0 and 59.5 at the M06, M06SP and MP2 levels respectively.

[Carnosine–H$_2$O + H]$^+$ and [carnosine–H$_2$O–CO + H]$^+$

The ion at m/z 209 shown in panel B of Fig. 1 is shown in Fig. 7 to be produced initially at relatively low collision energies; however, it does not attain any significant relative abundance. This ion was assigned to be due to the loss of H$_2$O from the precursor [carnosine + H]$^+$ at m/z 227 shown in Fig. 1, the corresponding signal for this ion in the CID spectrum of the deuterium-incorporated complex shown in Fig. S1 (ESI†) is observed at m/z 213 and 214 indicating the loss of D$_2$O and HOD respectively. This ion is proposed to be formed by overcoming the barrier relative to the transition state **TS$_{227 \to 209}$** shown in Fig. 7 in which a very similar rearrangement to the transition state **TS$_{210 \to 192}$** is observed where H$_2$O is eliminated from [carnosine–NH$_3$ + H]$^+$. Here, however, the resulting ion [carnosine–H$_2$O + H]$^+$ is observed at m/z 209 as shown in Fig. 1 and the barrier for the corresponding transition state was calculated to be 43.0, 42.0, 52.0 and 43.2 kcal mol^{-1} at the
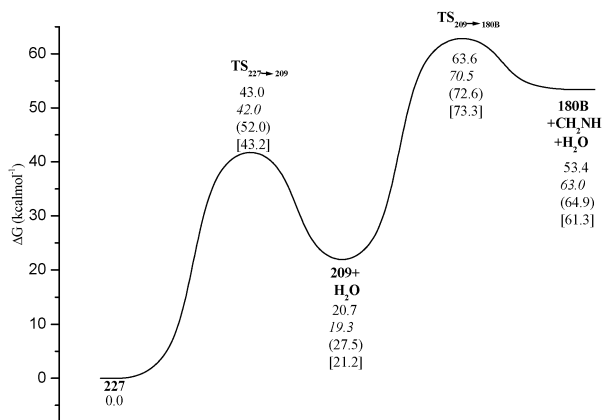
Fig. 7 B3LYP free energy profile for the fragmentation of [carnosine + H]$^+$ to give the ion at m/z 180 and its precursor at m/z 209. Relative free energies at 298 K are in kcal mol^{-1} and calculated with respect to the most stable conformer, **227**, of protonated carnosine. M06, M06SP and MP2SP values are reported in italics, brackets and square brackets, respectively.

Fig. 8 B3LYP free energy profile for the fragmentation of [carnosine + H]$^+$ to give the ion at m/z 110 and its precursors at m/z 138, 156 and 227. Relative free energies at 298 K are in kcal mol^{-1} and calculated with respect to the most stable conformer, **227**, of protonated carnosine. M06, M06SP and MP2SP values are reported in italics, brackets and square brackets, respectively.
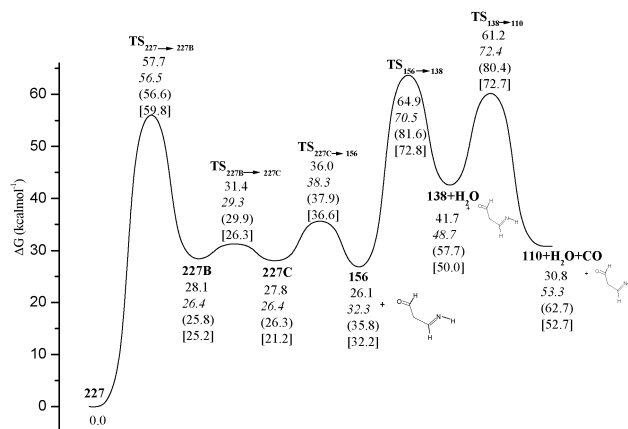
B3LYP, M06, M06SP and MP2 levels, respectively, which is in line with our experimental observation of the formation of the ion at m/z 209 being a relatively low energy process.

The subsequent neutral loss of CH$_2$NH from the resulting ion [carnosine–H$_2$O + H]$^+$ at m/z 209 is shown to proceed via a C–C bond cleavage and a hydride transfer of one of the hydrogens on the terminal amino nitrogen atom to a carbonyl oxygen atom on the peptide to produce the observed ion [carnosine–H$_2$O–CH$_2$NH + H]$^+$ at m/z 180 and the neutral fragment CH$_2$NH as shown in Fig. 6 and Fig. S3 (ESI†). While this process may be consistent with the signal cluster at around m/z 184 in the CID spectrum of the deuterium-incorporated complex shown in Fig. S1 (ESI†), this pathway proceeds through the transition state **TS$_{209 \to 180B}$** shown in Fig. 7, which is calculated to be 63.6, 70.5, 72.6 and 73.3 kcal mol^{-1} as calculated at the B3LYP, M06, M06SP and MP2 levels, respectively with respect to structure **227** to produce structure **180B** shown in Fig. 6, Fig. S3 (ESI†) and Fig. 7. This is compared to the favoured production route of structure **180** via the pathway shown in Fig. 3 which proceeds through the transition state **TS$_{198 \to 180}$** calculated at 51.0, 56.2, 65.7 and 55.4 kcal mol^{-1} for the same levels of theory respectively.

The loss of CO from the ion [carnosine–H$_2$O + H]$^+$ at m/z 209 produces the ion [carnosine–H$_2$O–CO + H]$^+$ which is observed at m/z 181 in Fig. 1, and the corresponding signals at m/z 185 and 186 in the CID spectrum of the deuterium-incorporated complex shown in Fig. S1 (ESI†) are consistent with the loss of D$_2$O and HOD respectively. The barrier for this process was not reported here, however, the barrier to the formation of the ion [carnosine–H$_2$O–CO + H]$^+$ directly from [carnosine + H]$^+$ was calculated to be 58.6 kcal mol^{-1} at the B3LYP level.

[Histidine + H]$^+$, [histidine–H$_2$O + H]$^+$ and [histidine–H$_2$O–CO + H]$^+$

The last three ions observed at m/z values of 156, 138 and 110 as shown in panel B of Fig. 1 are labeled [histidine + H]$^+$, [histidine–H$_2$O + H]$^+$ and [histidine–H$_2$O–CO + H]$^+$ respectively.

The formation of [histidine + H]$^+$ observed at m/z 156 through the loss of CH(O)CH$_2$CHNH from [carnosine + H]$^+$ is consistent with the ion cluster at around m/z 161 in the CID spectrum of the deuterium-incorporated complex shown in Fig. S1 (ESI†) corresponding to the loss of two, one or none of the deuterium atoms from the precursor ion [carnosine-d_5 + D]$^+$ at a ratio of 2:6:1. This is consistent with the pathway for the formation of this ion proposed here as shown in Fig. 8 and 9 as well as Fig. S4 in the ESI,† to initially involve two rearrangement steps of the precursor ion [carnosine + H]$^+$. The first of these rearrangement steps goes through the transition state **TS$_{227 \to 227B}$** and is calculated to require 57.7 kcal mol^{-1} when the B3LYP protocol is used, relative to structure **227**. This barrier is, in fact, calculated to be significantly higher in energy than that needed for the eventual formation of the ion [histidine + H]$^+$ observed at m/z 156 in Fig. 1 panel B as shown in structure **156** in Fig. 8 and 9 from the rearranged form of the ion [carnosine + H]$^+$ in structure **227C**. The corresponding transition state for this process **TS$_{227C \to 156}$** is calculated at the B3LYP, M06, M06SP and MP2SP levels to be 36.0, 38.3, 37.9 and 36.6 kcal mol^{-1} relative to structure **227** respectively. In turn, the loss of H$_2$O from [histidine + H]$^+$ to produce [histidine–H$_2$O + H]$^+$ as observed at m/z 138 in Fig. 1 panel B and at m/z 141 and 142 in the CID spectrum of the deuterium-incorporated complex shown in Fig. S1 (ESI†) corresponding to the retention of 3 and 4 deuterium atoms, respectively, is observed to go through the transition state **TS$_{156 \to 138}$** calculated at 64.9, 70.5, 81.6 and 72.8 kcal mol^{-1}, respectively, at the same levels of theory. Finally, the subsequent loss of CO from [histidine–H$_2$O + H]$^+$ to produce the smallest observed ion [histidine–H$_2$O–CO + H]$^+$ at m/z 110 in Fig. 1 panel B and at m/z 113 and 114 in the CID spectrum of the deuterium-incorporated complex shown in Fig. S1 (ESI†) again corresponding to the retention of 3 and 4 deuterium atoms, respectively, is shown to involve a transition state at 62.1, 72.4, 80.4 and 72.7 kcal mol^{-1} for B3LYP, M06,
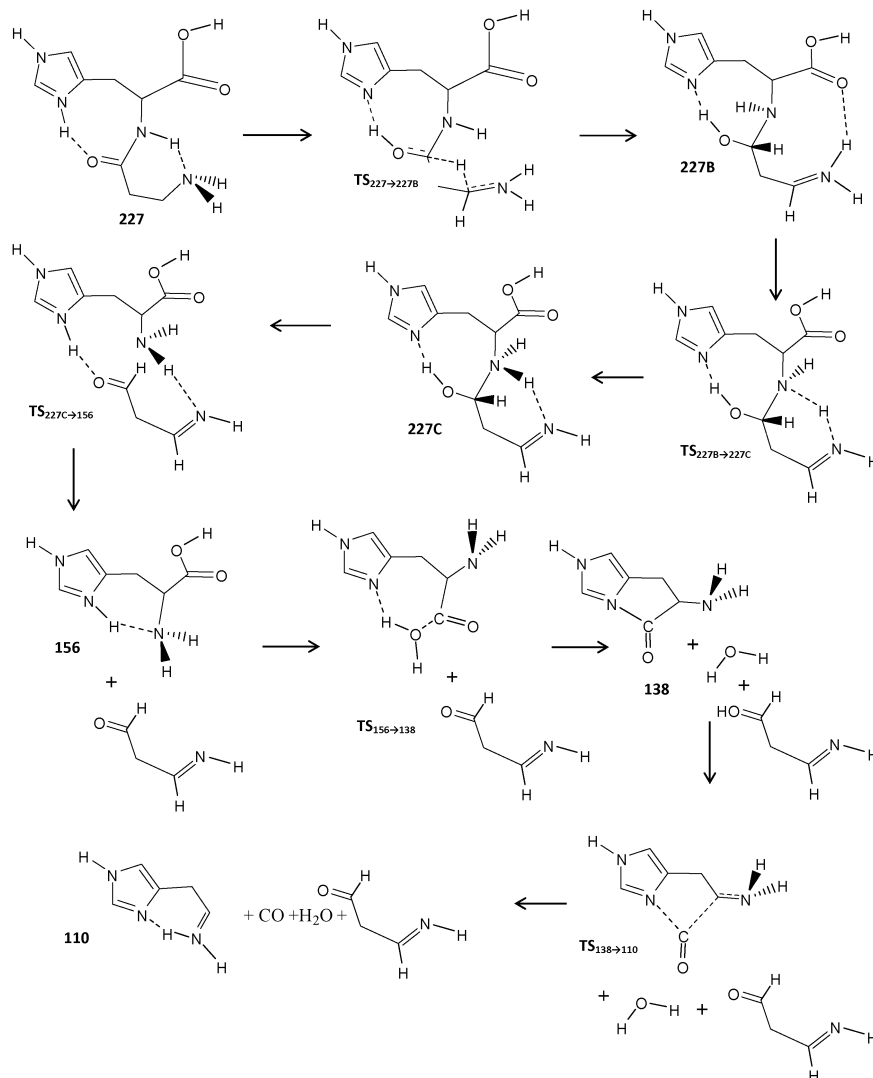
Fig. 9 Proposed mechanism for the collision induced fragmentation of [carnosine + H]$^+$ to produce the fragment ion observed at *m/z* 156, 138 and 110.

M06SP and MP2SP, respectively, relative to structure **227** which is 19.3, 14.5, 23.1 and 17.9 kcal mol^{-1} lower than the barrier needed to produce its precursor. This may explain the observations presented in the collision induced dissociation curve of Fig. 2 in which the ion [histidine–H$_2$O + H]$^+$ at *m/z* 138 is shown not to attain any significant abundance, while the ions [histidine + H]$^+$ and [histidine–H$_2$O–CO + H]$^+$ at *m/z* values of 156 and 110, respectively, reach significant relative abundances.

The results of the computational analysis of the fragmentation pathways reported here show that all the adopted computational protocols are able to reproduce and rationalize the experimental evidence and give comparable energetic trends. However, the description of the calculated energy profiles in terms of relative energies of the intercepted stationary points, calculated with respect to the reference energy of structure **227**, appears to be significantly different when single point calculations are carried out on previously optimized geometries with the risk that the main features of the fragmentation PESs might not be captured.

Conclusions

Collision-induced dissociation experiments on protonated carnosine, [carnosine + H]$^+$, with several collision energies were shown to yield eleven different fragment ions with the product ions [carnosine–H$_2$O + H]$^+$ and [carnosine–NH$_3$ + H]$^+$ to be the lowest energy processes. The MS^2 spectra of [carnosine-*d$_5$* + D]$^+$ in which carnosine has all its labile hydrogen atoms exchanged with deuterium atoms provided some insights into the CID mechanisms although a significant gas phase H/D scrambling prior to fragmentation was evident. The outcomes of the present combined theoretical and experimental investigation of the fragmentation pathways show that the lowest energy species for protonated carnosine found here is the same as that previously proposed.[17,21,58] The adopted computational protocols give comparable energetic trends and are all able to elucidate the fragmentation mechanisms, which account for all experimental data. However, when single point M06 and MP2 calculations on previously optimized B3LYP structures are carried out,

the description of the energy profiles in some regions was significantly different.

Acknowledgements

References

1   W. Gulewitsch and S. Amiradzibi, *Ber. Dtsch. Chem. Ges.*, 1900, **33**, 1902–1903.
2   I. Severina, O. Bussygina and N. Pyatakova, *Biochemistry*, 2000, **65**, 783–788.
3   R. Kohen, Y. Yamamoto, K. Cundy and B. Ames, *Proc. Natl. Acad. Sci. U. S. A.*, 1988, **85**, 3175–3179.
4   S. E. Gariballa and A. J. Sinclair, *Age Ageing*, 2000, **29**, 207–210.
5   M. Horning, L. Blakemore and P. Trombley, *Brain Res.*, 2000, **852**, 56–61.
6   M. Nino, *J. Cosmet., Dermatol. Sci. Appl.*, 2011, **1**, 177.
7   A. A. Boldyrev, *Biochemistry*, 2000, **65**, 751–756.
8   A. Guiotto, A. Caderan, P. Ruzza and G. Borin, *Curr. Med. Chem.*, 2005, **12**, 2293–2315.
9   E. C. Smith, *J. Physiol.*, 1938, **92**, 336–343.
10 E. J. Baran, *Biochemistry*, 2000, **65**, 789–797.
11 N. S. Nadi, J. D. Hirsch and F. L. Margolis, *J. Neurochem.*, 1980, **34**, 138–146.
12 P. Hartman, Z. Hartman and K. Ault, *Photochem. Photobiol.*, 1990, **51**, 59–66.
13 A. Pavlov, A. Revina, A. Dupin, A. Boldyrev and A. Yarpolov, *Biochim. Biophys. Acta*, 1993, **1157**, 304–312.
14 E. M. Moustafa, C. L. Camp, A. S. Youssef, A. Amleh, H. J. Reid, B. L. Sharp and T. Shoeib, *Metallomics*, 2013, **5**, 1537–1546.
15 P. Mineo, *Rapid Commun. Mass Spectrom.*, 2002, **16**, 722–729.
16 M. Bjorn Reinhard, *Chemistry of Microsolvated Metal Ions*, PhD thesis, Kaiserslautern University of Technology, Germany, 2003.
17 F. Menges, C. Riehn and G. Niedner-Schatteburg, *Z. Phys. Chem.*, 2011, **225**, 595–609.
18 P. G. Peiretti, C. Medana, S. Visentin, V. Giancotti, V. Zunino and G. Meineri, *Food Chem.*, 2011, **126**, 1939–1947.
19 S. A. Klyuev, *Biofizika*, 2006, **5**, 669–672.
20 S. D. Demukhamedova, *J. Struct. Chem.*, 2010, **51**, 824–832.
21 E. M. Moustafa, M. Korany, N. A. Mohamed and T. Shoeib, *Inorg. Chim. Acta*, 2014, **421**, 123–135.
22 B. Paizs and S. Suhai, *Mass Spectrom. Rev.*, 2005, **24**, 508–548.
23 N. N. Dookeran, T. Yalcin and A. G. Harrison, *J. Mass Spectrom.*, 1996, **31**, 500–508.
24 T. Yalcin and A. G. Harrison, *J. Mass Spectrom.*, 1996, **31**, 1237–1243.
25 F. Rogalewicz, Y. Hoppilliard and G. Ohanessian, *Int. J. Mass Spectrom.*, 2000, **195–196**, 565–590.
26 H. El Aribi, G. Orlova, A. C. Hopkinson and K. W. M. Siu, *J. Phys. Chem. A*, 2004, **108**, 3844–3853.
27 R. A. J. O'Hair, M. L. Styles and G. E. Reid, *J. Am. Soc. Mass Spectrom.*, 1998, **9**, 1275–1284.
28 H. Lioe, R. A. J. O'Hair and G. E. Reid, *J. Am. Soc. Mass Spectrom.*, 2004, **15**, 65–76.
29 I. P. Csonka, B. Paizs and S. Suhai, *J. Mass Spectrom.*, 2004, **39**, 1025–1035.
30 Z. B. Maksik and B. Kovacevic, *Chem. Phys. Lett.*, 1999, **307**, 497–504.
31 A. K. Y. Lam, S. H. Ramarathinam, A. W. Purcell and R. A. J. O'Hair, *J. Am. Soc. Mass Spectrom.*, 2008, **19**, 1743–1754.
32 E. R. Talaty, T. J. Cooper, S. Osburn and M. J. Van Stipdonk, *Rapid Commun. Mass Spectrom.*, 2006, **20**, 3443–3455.
33 T. Shoeib, A. Cunje, A. C. Hopkinson and K. W. M. Siu, *J. Am. Soc. Mass Spectrom.*, 2002, **13**, 408–416.
34 H. Lioe and R. A. J. O'Hair, *Org. Biomol. Chem.*, 2005, **3**, 3618–3628.
35 E. Uggerud, *Theor. Chim. Acta*, 1997, **97**, 313–316.
36 F. Rogalewicz, Y. Hoppilliard and G. Ohanessian, *Int. J. Mass Spectrom.*, 2000, **195–196**, 565–590.
37 I. Ritacco, E. M. Moustafa, E. Scicilia, N. Russo and T. Shoeib, *Dalton Trans.*, 2015, **44**, 4455–4467.
38 S. L. Kerr, T. Shoeib and B. L. Sharp, *Anal. Bioanal. Chem.*, 2008, **391**, 2339–2348.
39 T. Shoeib, D. W. Atkinson and B. L. Sharp, *Inorg. Chim. Acta*, 2010, **363**, 184–192.
40 T. Shoeib, I. K. Chu, Y.-P. Tu, A. C. Hopkinson and K. W. M. Siu, *Eur. J. Mass Spectrom.*, 2000, **6**, 187–192.
41 C. F. Rodriquez, X. Guo, T. Shoeib, A. C. Hopkinson and K. W. M. Siu, *J. Am. Soc. Mass Spectrom.*, 2000, **11**, 967–975.
42 T. Shoeib, J. Zhao, H. El Aribi, A. C. Hopkinson and K. W. M. Siu, *J. Am. Soc. Mass Spectrom.*, 2013, **24**, 38–48.
43 M. J. Frisch, G. W. Trucks, H. B. Schlegel, G. E. Scuseria, M. A. Robb, J. R. Cheeseman, G. Scalmani, V. Barone, B. Mennucci, G. A. Petersson, H. Nakatsuji, M. Caricato, X. Li, H. P. Hratchian, A. F. Izmaylov, J. Bloino, G. Zheng, J. L. Sonnenberg, M. Hada, M. Ehara, K. Toyota, R. Fukuda, J. Hasegawa, M. Ishida, T. Nakajima, Y. Honda, O. Kitao, H. Nakai, T. Vreven, J. A. Montgomery Jr., J. E. Peralta, F. Ogliaro, M. Bearpark, J. J. Heyd, E. Brothers, K. N. Kudin, V. N. Staroverov, R. Kobayashi, J. Normand, K. Raghavachari, A. Rendell, J. C. Burant, S. S. Iyengar, J. Tomasi, M. Cossi, N. Rega, J. M. Millam, M. Klene, J. E. Knox, J. B. Cross, V. Bakken, C. Adamo, J. Jaramillo, R. Gomperts, R. E. Stratmann, O. Yazyev, A. J. Austin, R. Cammi, C. Pomelli, J. W. Ochterski, R. L. Martin, K. Morokuma, V. G. Zakrzewski, G. A. Voth, P. Salvador, J. J. Dannenberg, S. Dapprich, A. D. Daniels, Ö. Farkas, J. B. Foresman, J. V. Ortiz, J. Cioslowski and D. J. Fox, *Gaussian 09, Revision A.1*, Gaussian Inc, Wallingford CT, 2009.
44 A. Lee, W. Yang and R. G. Parr, *Phys. Rev. B: Condens. Matter Mater. Phys.*, 1988, **37**, 785–789.
45 A. D. Becke, *Phys. Rev. A: At., Mol., Opt. Phys.*, 1988, **38**, 3098–3100.

46 A. D. Becke, *J. Chem. Phys.*, 1993, **98**, 5648–5652.

47 R. Krishnan, J. S. Binkley, R. Seeger and J. A. Pople, *J. Chem. Phys.*, 1980, **72**, 650–654.

48 J. P. Blaudeau, M. P. McGrath, L. A. Curtiss and L. Radom, *J. Chem. Phys.*, 1997, **107**, 5016–5021.

49 T. Clark, J. Chandrasekhar and P. V. R. Schleyer, *J. Comput. Chem.*, 1983, **4**, 294–301.

50 K. Fukui, *Acc. Chem. Res.*, 1981, **14**, 363–368.

51 R. C. Guedes, P. C. Do Couto and B. J. C. Cabral, *J. Chem. Phys.*, 2003, **118**, 1272–1281.

52 R. K. Milburn, A. C. Hopkinson and D. K. Bohme, *J. Am. Chem. Soc.*, 2005, **127**, 13070–13078.

53 X. Xu and W. A. Goddard, *J. Phys. Chem. A*, 2004, **108**, 2305–2313.

54 K. Schoone, J. Smets, R. Ramaekers, L. Houben, L. Adamowicz and G. Maes, *J. Mol. Struct.*, 2003, **649**, 61–68.

55 H. El Aribi, C. F. Rodriquez, D. R. P. Almeida, Y. Ling, W. W. N. Mak, A. C. Hopkinson and K. W. M. Siu, *J. Am. Chem. Soc.*, 2003, **125**, 9229–9236.

56 C. Moller and M. S. Plesset, *Phys. Rev.*, 1934, **46**, 618–622.

57 Y. Zhao and D. G. Truhlar, *Theor. Chem. Acc.*, 2008, **120**, 215–241.

58 G. Grégoire, M. P. Gaigeot, D. C. Marinica, J. Lemaire, J. P. Schermann and C. Desfrançois, *Phys. Chem. Chem. Phys.*, 2007, **9**, 3082–3097.

12682 | *Phys. Chem. Chem. Phys.*, 2015, **17**, 12673–12682

This journal is © the Owner Societies 2015

Paper II

"Fragmentation Pathways Analysis for the gas Phase Dissociation of Protonated Carnosine-Oxaliplatin Complexes"

Ida Ritacco, Eslam Moustafa, Emilia Sicilia, Nino Russo, Tamer Shoeib.

Dalton Transactions

An international journal of inorganic chemistry

[Carnosine + OxPt + H]⁺

CID

[Carnosine + H]⁺

[OxPt − CO₂ + H]⁺

[Carnosine + OxPt − CO₂ + H]⁺

[Carnosine − NH₃ − H + Pt(dach)]⁺

[OxPt + H]⁺

[Carnosine − H + Pt(dach)]⁺
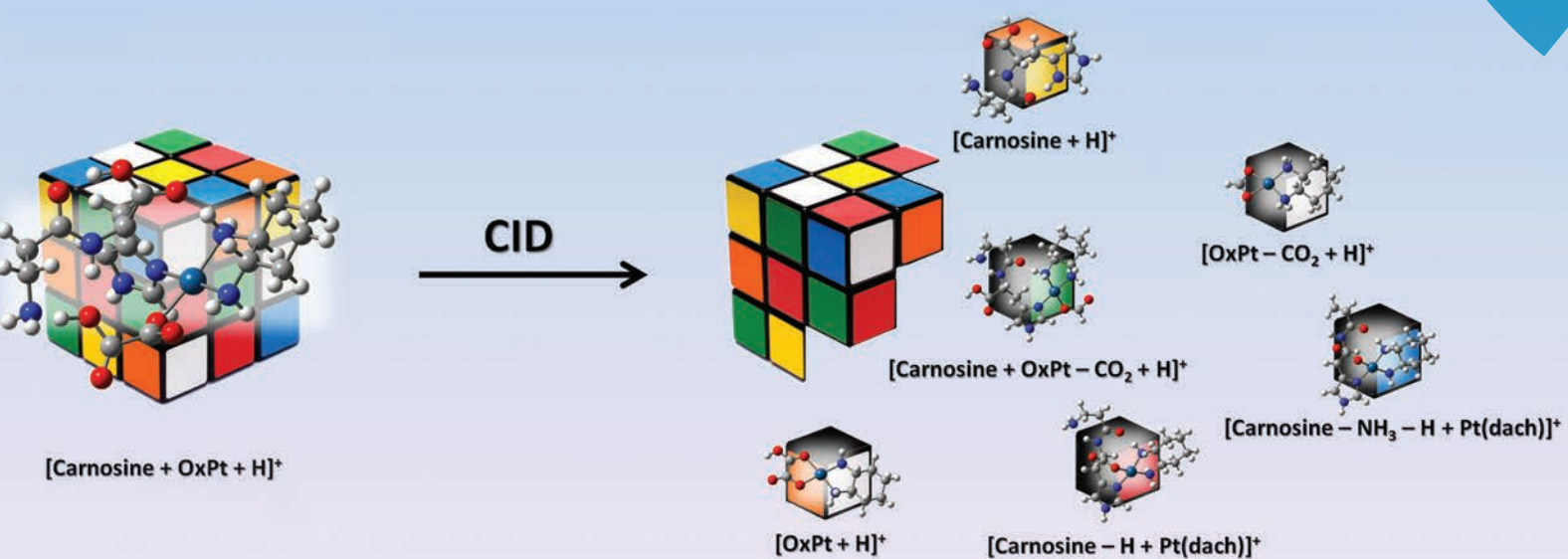
ROYAL SOCIETY
OF CHEMISTRY

Fragmentation pathways analysis for the gas phase dissociation of protonated carnosine-oxaliplatin complexes†

Ida Ritacco,[a] Eslam M. Moustafa,[b] Emilia Sicilia,[a] Nino Russo[a] and Tamer Shoeib*[b,c]

Collision-induced dissociation (CID) experiments on the protonated carnosine-oxaliplatin complex, [Carnosine + OxPt + H]$^+$ using several collision energies were shown to yield nine different fragment ions. Energy-resolved CID experiments on [Carnosine + OxPt + H]$^+$ showed that the generation of the product ion [Carnosine − H + Pt(dach)]$^+$ (where dach is 1,2-diaminocyclohexane) is the lowest energy process. At slightly higher collision energies, the loss of neutral carnosine from [Carnosine + OxPt + H]$^+$ to produce [OxPt + H]$^+$ was observed, followed by the loss of oxaliplatin from the same precursor ion to produce [Carnosine + H]$^+$. At significantly higher energies, the ion [OxPt − CO$_2$ + H]$^+$ was shown to be formed, while the last two investigated ions [Carnosine + OxPt − CO$_2$ + H]$^+$ and [Carnosine − NH$_3$ − H + Pt(dach)]$^+$ did not attain any significant relative abundance. Density functional calculations at the B3LYP/LANL2DZ level were employed to probe the fragmentation mechanisms that account for all experimental data. The lowest free energy barriers for the generation of each of the ions [Carnosine − H + Pt(dach)]$^+$, [OxPt + H]$^+$, [Carnosine + H]$^+$, [Carnosine + OxPt − CO$_2$ + H]$^+$ and [Carnosine − NH$_3$ − H + Pt(dach)]$^+$ from [Carnosine + OxPt + H]$^+$ according to the fragmentation mechanisms offered here were calculated to be 31.9, 38.8, 49.3, 75.2, and 85.6 kcal mol^{-1}, respectively.

Introduction

The endogenous dipeptide L-carnosine (β-alanyl-L-histidine)[1–3] is found in different organs such as the stomach and kidney, and also at elevated levels in skeletal and cardiac muscles as well as in brain tissue in the olfactory bulb and hippocampus.[4,5] Owing to its water solubility, carnosine levels are found to be particularly elevated in the cytosolic cellular fractions.[6] Since its discovery, there have been many investigations on its biological functions. It is presently known, for example, that carnosine is able to interact with aldehydes generated inside the body as a result of glycation reactions, which occur between reducing sugar and different body proteins.[7–9] This helps in protecting body proteins, giving carnosine its anti-glycating effect,[7–9] which in turn can help in minimizing the effects of some diseases such as diabetes and Alzheimer's.[10] Carnosine also has significant anti-inflammatory, antihypertensive, anti-aging, neurological and wound healing effects,[11] in addition to possessing unique antioxidant properties, due to its ability to interact with highly reactive species such as hydroxyl, super oxide and molecular oxygen free radicals, especially in the water rich environment inside the body. These antioxidant properties are prominent in the ability of carnosine to hinder lipid peroxidation, which helps in preserving the integrity of body membranes. Carnosine is also known for its buffering capability, being able to buffer the increased acidity generated by lactic acid formation inside muscle tissue during muscle stress.[12] It is also reported that carnosine can act as an effective heavy metal ion chelator and is able to interact with the circulating metals ions within the body such as iron, calcium, metal containing enzymes and especially copper and zinc.[13] These metal chelating properties make carnosine an effective agent in the prevention and partial reversal of cataracts[14] and in the treatment of Wilson's disease[15] and Alzheimer's disease. The ability of carnosine to bind Zn^{2+} has been found to help modulate neuronal excitability by preventing the Zn^{2+} inhibition of neurotransmitter receptors.[16] In fact, polaprezinc, a commercially available carnosine-zinc(II) drug complex is marketed for its effective anti-ulcer properties and the ability to improve gastric health.[17–19]

Additionally, it has been shown that carnosine acts as a neuroprotector[20,21] and can retard tumour growth in mouse models.[22] More recently, it has been reported that carnosine

[a]Dipartimento di Chimica UniVersita della Calabria, Via P. Bucci, cubo 14c, 87036 Arca Vacata di Rende (CS), Centro di Calcolo ad Alte Prestazioni per Elaborazioni Parallele e Distribuite - Centro d'Eccellenza MIUR, Rende 87036, Italy
[b]Department of Chemistry, The American University in Cairo, New Cairo 11835, Egypt
[c]Centre for Analytical Science, Department of Chemistry, Loughborough University, Loughborough, Leicestershire LE11 3TU, UK. E-mail: T.Shoeib@aucegypt.edu
† Electronic supplementary information (ESI) available. See DOI: 10.1039/c4dt02217c

can prevent cell proliferation in colon cancer cells.[23,24] However, it has also been shown that carnosine may be involved in complexation with and sequestering of platinum anti-cancer drugs. Specifically, *in vitro* studies on hepatocellular carcinoma HepG2 cells have shown that carnosine may inhibit the cytotoxic action of the third generation chemotherapeutic drug, oxaliplatin, most likely through the formation of complexes that are less cytotoxic than oxaliplatin alone.[25]

Mass spectrometry has proven to be an invaluable technique in studying the interactions between anticancer platinum containing metallodrugs and biomolecules, including DNA, proteins and peptides on a molecular level (for recent reviews, see ref. 26 and 27). This is especially important as an understanding of these interactions allows for a better informed design of future drugs. Studies of anticancer platinum metallodrugs interactions with DNA have been most prevalent as DNA is considered to be the ultimate pharmacological target for such drugs.[28–30] However, recently other targets such as proteins and peptides that often play a role in the toxicological profile of platinum anticancer drugs have been considered. Recent examples include the successful use of Fourier transform ion cyclotron resonance mass spectrometry (FT-ICR-MS) with electron capture detection (ECD) to identify the binding sites of cisplatin to several proteins and peptides.[31] In this study, side chain losses from the charge-reduced platinum species provided characteristic indicators for the localization of the Pt-binding sites to certain amino acid residues.[31] In other studies, inductively coupled plasma mass spectrometry (ICP-MS) was employed in the study of cisplatin binding to the model protein cytochrome C which is a relatively small and well-characterized protein[32] as well as to plasma proteins being among the major metabolic pathways of this metallodrug.[33] Coupling capillary electrophoresis to ICP-MS, on the other hand, allowed for the examination of the interactions of different candidate platinum anticancer drugs with human serum albumin (HSA), including measurements of the kinetics of binding and the determination of the number of drug molecules attached to HSA.[34] A similar study where the identification of products formed upon the binding of cisplatin, carboplatin and oxaliplatin with proteins like β-lactoglobulin, HSA and haemoglobin was examined by employing liquid chromatography electrospray ionization time of flight mass spectrometry (LC-ESI-TOF-MS).[35] Finally, electrospray ionization with tandem mass spectrometry (ESI-MS/MS) was employed to provide structural information and examine the dissociation pathways for the main reaction products of cisplatin with several sulphur containing peptides.[36]

Specifically, a study on the interactions of oxaliplatin with carnosine as well as two of its derivatives, β-alanyl-*N*-methylhistidine (anserine) and *N*-acetylcarnosine (NAC) was recently reported, which employed various mass spectrometric techniques utilizing electrospray ionization and chip nanospray.[25] In this study, a detailed characterization of the protonated complexes of oxaliplatin with each of the three dipeptide ligands as well as their collision induced fragments was presented.[25] In the present paper, an analysis of the potential energy surfaces (PESs) for the gas phase dissociation of the protonated carnosine-oxaliplatin complex is presented. A comparison between the calculated potential energy surfaces of the dissociation process and the energy resolved collision induced dissociation of the protonated carnosine-oxaliplatin complex is also reported.

Instrumentation

A tandem quadrupole mass spectrometer, an Acquity TQ (Waters, MA, USA) equipped with an electrospray ionisation interface was used in this work. The instrument was operated in the positive ion mode, with the typical values of the cone and extractor voltages set to 30 and 3 respectively. The capillary voltage was optimised day to day for maximum signal transmission and spray stability, the optimised range was typically 2200–2500 volts. The de-solvation gas was usually set at a flow of 250 L h^{-1} and a temperature of 150 °C. Argon was used as the collision gas at a typical flow rate of 0.15 mL min^{-1}. Ions sampled from the electrospray suffered many collisions in an attempt to achieve effective thermalization in the lens region, which were from the orifice/skimmer to the first r.f. only quadrupole. The bias potential in this lens region was set up to strike a compromise between signal transmission and minimal collisional heating. The precursor ions underwent multiple collisions with argon to produce the tandem mass spectra obtained at collision energies in the range of 0–25 eV in the lab frame, which has both Q1 and Q3 operating at unit resolution with a typical dwell time of 25 milliseconds per transition.

Reagents

Carnosine, HPLC-grade water and methanol were all purchased from Sigma-Aldrich, UK while oxaliplatin was obtained from Sanofi-Synthelabo Limited, UK.

Computational methods

Geometry optimizations without symmetry constraints as well as frequency calculations for all the reactants, intermediates, products and transition states were performed at the Density Functional level of theory by using the hybrid exchange-correlation B3LYP functional[37–40] as implemented in the GAUSSIAN03[41] code. For all the atoms, the LANL2DZ[42–44] basis sets were employed. The recent successful use of the LANL2DZ basis set has been proven by the calculation of both the structural details of gold based drug complexes with cysteine and selenocysteine[45] and the geometrical features and thermodynamic properties of Cd^{2+} complexes with GSH.[46] The same basis set was used to gain insight into the decomposition pathways of the photo-activated Pt containing anticancer complexes[47] and to obtain excellent agreement with the experimental Raman and IR data of Pt-carboplatin complexes.[48] The use of the B3LYP/LANL2DZ computational protocol in investigating transition metals containing compounds is well established.[49–61] In fact, it was recently used to successfully investigate the structures of the anti-arthritic drug, auranofin and its complexes with cysteine;[45] to model CO adsorption on Pt nanoclusters;[62] to obtain structural information and

binding energies for the complexation of *cis*- and *trans*-Pt(NH$_3$)$_2$Cl$^+$ to guanine;[57] to investigate monomeric complexes between cisplatin and glutathione;[63] to obtain excellent agreement with the X-ray data for cisplatin analogues[64] and oxaliplatin analogues;[65] as well as to examine the mechanism of the Pt and Pd catalysed coupling and cyclopropanation reactions between olefins.[66] Most recently, this level of theory was used to study the interactions of the anti-cancer Pt containing drug oxaliplatin with each of the cytoplasmic thiol containing tripeptide ligands γ-L-glutamyl-L-cysteinyl-glycine (GSH)[67] as well as the biologically active β-alanine-L-histidine dipeptide carnosine.[25] In another recent study, this level of theory has been employed to study the binding modes and binding energies of carnosine to various biologically relevant metal cations as well as to some Pt based anticancer drugs. The Pt^{2+} binding energy to carnosine was calculated in that study *via* seven different levels of theory being B3P86/LANL2DZ, B3PW91/LANL2DZ, B3LYP/SDD, B3P86/SDD, B3PW91/SDD, B3LYP/LANL2DZ// 6-31G(d) and M06/SDD//6-311G(d,p). It was determined that all the values obtained for the Pt^{2+} binding energies with the exception of those obtained using B3P86/SDD exhibited relatively small deviation.[68] In addition, the bond dissociation energy of the Pt$^+$–CH$_2$ bond was also calculated at five different levels of theory, and the results were shown to exhibit very small variations.[68] Importantly, all the results were, with the exception of the value calculated at the B3P86/LANL2DZ level of theory, shown to be within 2.3 kcal mol^{-1} of the experimentally determined value.[68,69]

For each optimized stationary point, vibrational analysis was performed to establish its nature either as a minimum (no imaginary frequencies) or a first order saddle point (one imaginary frequency). The vibrational mode associated to the imaginary frequency of each intercepted transition state was shown to correspond to the correct movement of the involved atoms. In addition, the intrinsic reaction coordinate (IRC)[70,71] method was used to show that each located transition state is properly connected to its respective reactants and products along the imaginary mode of vibration. The calculated total electronic energies, zero-point energies, thermal corrections and entropies for all the stationary points are given in ESI Tables S1–S4.†

Results and discussion

The electrospraying of a 2 : 1 mM solution mixture of carnosine with oxaliplatin in 1 : 1 (v/v) water–methanol solvent system generated the mass spectra shown and assigned in the top panel of Fig. 1. The mass selection and subsequent
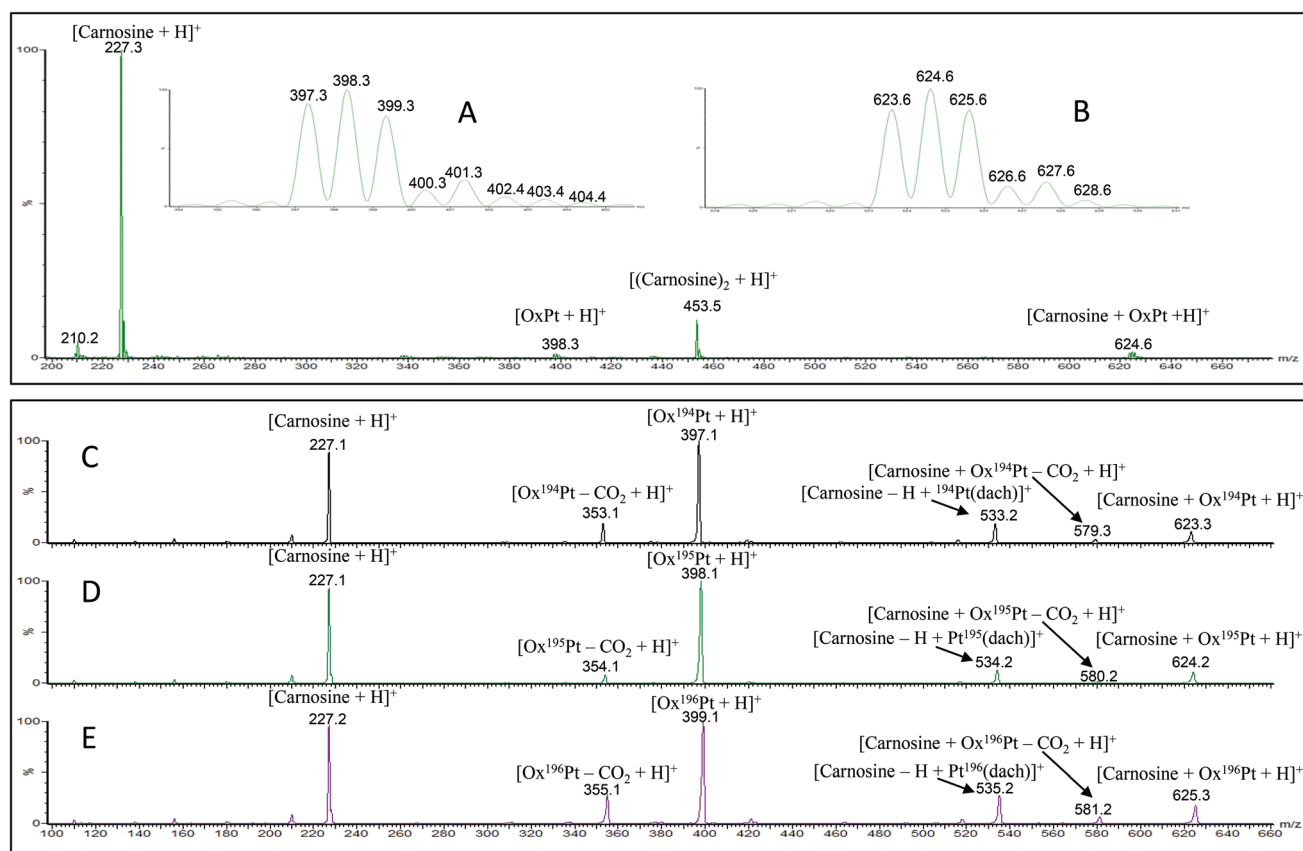

Fig. 1 Top panel, full scan MS spectrum of a (2 : 1) molar mixture of Carnosine and OxPt in a (1 : 1) (v/v) water–methanol solution without allowing for incubation time. The signals assigned as [OxPt + H]$^+$ and [Carnosine + OxPt + H]$^+$ are each expanded and normalized to 100% in inserts A and B respectively for clarity. Bottom panel, MS^2 spectrum of the ion [Carnosine + OxPt + H]$^+$ generated at 25 eV in the lab frame. Sub-panels C, D and E show the CID patterns obtained due to the isotopes ^{194}Pt, ^{195}Pt and ^{196}Pt of [Carnosine + OxPt + H]$^+$ respectively.

collision induced dissociation (CID) of the ion [Carnosine + OxPt + H]$^+$ resulted in the MS^2 spectra shown in the bottom panel of Fig. 1. Performing the CID experiments on the [Carnosine + OxPt + H]$^+$ containing the three most abundant isotopes of platinum ^{194}Pt, ^{195}Pt and ^{196}Pt confirms that there is no difference in the fragmentation pathways among the three platinum isotopes, but significantly allows for a quick identification of the product ions that contain the platinum metal. The product ions labelled in Fig. 1 and their precursor ions [Carnosine +

OxPt + H]$^+$ were all previously reported and identified.[25] The energy-resolved CID spectra shown in Fig. 2 reveals that [Carnosine + OxPt + H]$^+$ initially loses the elements of HOC$_2$O$_2$OH to produce the ion [Carnosine − H + Pt(dach)]$^+$ as the lowest energy process. The neutral species lost in this case, which constitutes the elements of HOC$_2$O$_2$OH, may be lost as one molecule or as a combination of CO$_2$ and HCOOH or CO$_2$, H$_2$O and CO. At slightly higher collision energies, the loss of neutral carnosine from [Carnosine + OxPt + H]$^+$ to produce

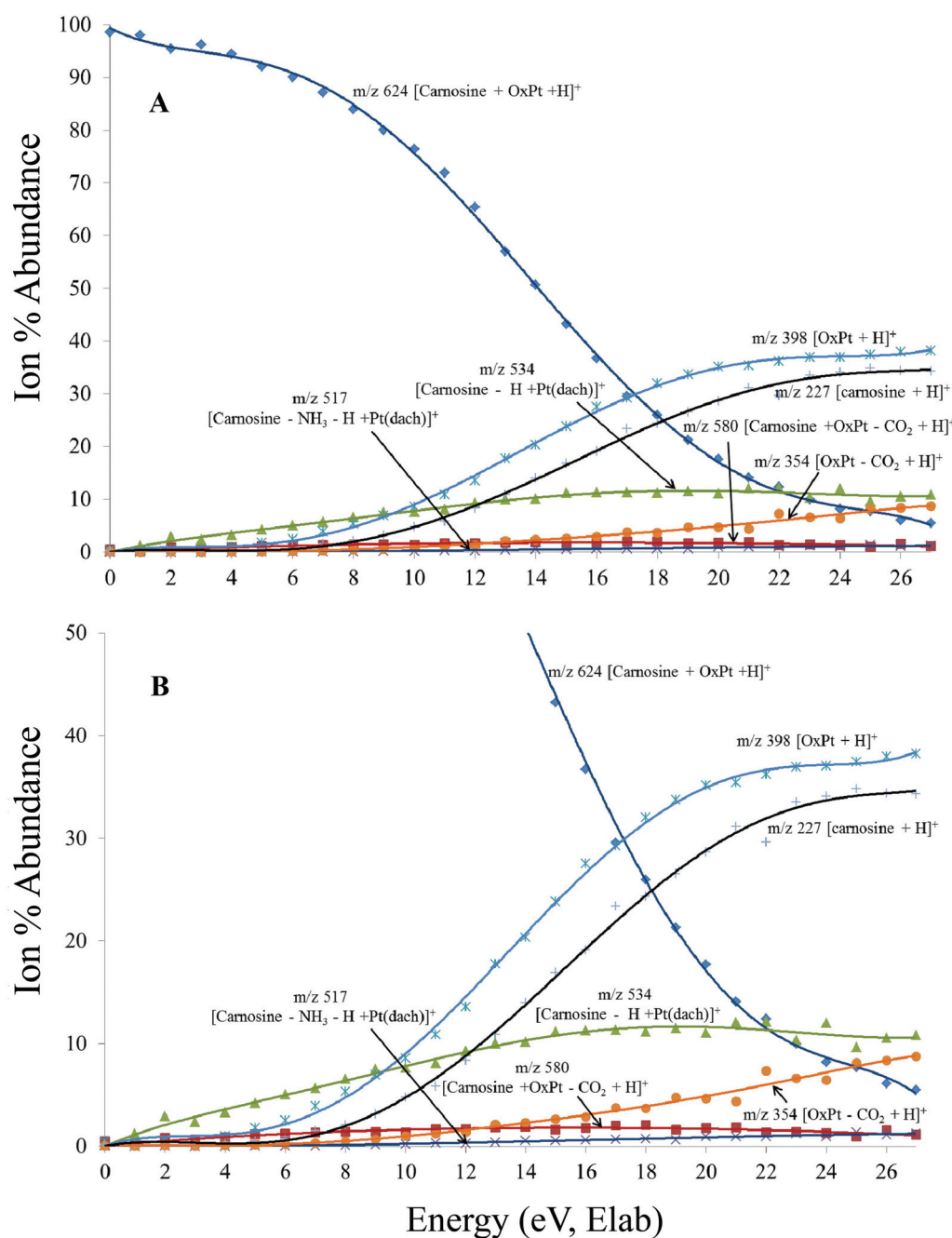**Fig. 2** Energy-resolved collision induced dissociation curves of [Carnosine + OxPt + H]$^+$. *Y*-axes are (ion abundance)/(total ion abundance) expressed as a percentage, *m/z* values refer to the complexes containing ^{195}Pt. panel A shows the full curve, while panel B shows an expanded view for clarity.

$[OxPt + H]^+$ can be observed followed by the loss of oxaliplatin from the same precursor ion to produce $[Carnosine + H]^+$. It is interesting to note that even at the highest collision energies employed here, no evidence of declining relative abundances of these three fragment ions were observed, and in fact in all three cases, no clear maximum was reached. This indicates that subsequent fragmentation reactions of these three product ions, due to tertiary collisions, may be considered to have a minimum contribution to the observed overall fragmentation pattern. At significantly higher energies, however, the ion $[OxPt − CO_2 + H]^+$ is shown to be initially formed, reaching a modest 9% relative abundance while its most likely precursor $[Carnosine + OxPt − CO_2 + H]^+$ as well as the last ion observed $[Carnosine − NH_3 − H + Pt(dach)]^+$ were shown to not attain any significant relative abundance.

Fragmentation mechanism 1

Two mechanisms are presented for the loss of CO_2 from $[carnosine + OxPt + H]^+$ (see Fig. 3 and 4 as well as Scheme 1). In

Fig. 3 Potential energy surface for the fragmentation of the protonated carnosine-oxaliplatin complex, ion **1A**. Structure labels are in bold, top numbers are in kcal mol^{-1} while bottom numbers in parentheses are in kJ mol^{-1}.
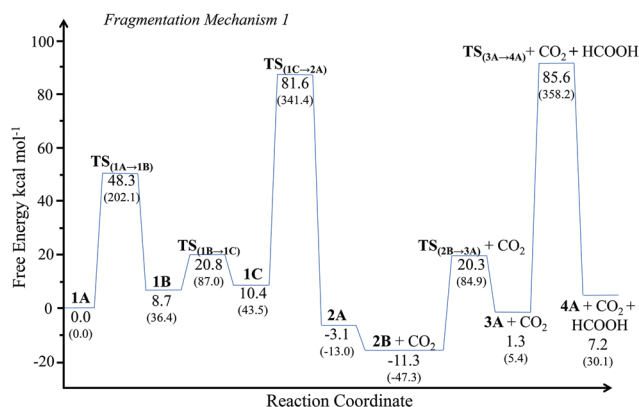

Fig. 4 Potential energy surface for the fragmentation of the protonated carnosine-oxaliplatin complex, ion **1A**. Structure labels are in bold, top numbers are in kcal mol^{-1} while bottom numbers in parentheses are in kJ mol^{-1}.

both the mechanisms, the initial starting point is the precursor ion [carnosine + OxPt + H]$^+$ in its lowest gas phase conformation, structure **1A** as shown in Fig. 7–9 and Schemes 1–3. This conformer of the protonated carnosine-oxaliplatin complex was previously shown to be the global minimum on this potential energy surface.[25] Structure **1A** involves Pt coordination to the *pros* nitrogen atom of the histidine ring of carnosine and formal protonation of one of the carbonyl oxygen atoms of the oxalate moiety of oxaliplatin. This protonation arrangement results in a strong hydrogen bond with the terminal amino nitrogen of carnosine as demonstrated by a 1.315 Å bond length, see Fig. 7–9. The Pt coordination on the *pros* nitrogen atom of the histidine ring of carnosine is consistent with an earlier study examining the silver ion binding energies of all 20 α-amino acids, which showed that histidine had the third highest silver ion binding energy being lower than that of arginine and only slightly lower than that of lysine.[60] The lowest energy conformer of the Ag$^+$-histidine complex in that study also showed Pt-coordination to the *pros* nitrogen atoms of the histidine ring.[60] Structure **1A**, as shown in Fig. 7–9 and Schemes 1–3, is stabilised by three strong hydrogen bonds, in addition to the one to the terminal amino nitrogen of the carnosine dipeptides. The number and, more importantly, the strength of these hydrogen bonds, with the longest being 1.886 Å, make structure **1A** a relatively rigid conformer. This is evident from the fact that structure **1A** was calculated to have the lowest entropy value of all the conformers of [carnosine + OxPt + H]$^+$ (see Tables S1–S4†). This is in line with a previous study that showed that structure **1A** had the second lowest calculated entropy value of twenty five conformers of this complex.[25]

The initial step in the first path proposed for the loss of CO_2 to produce the ion $[Carnosine + OxPt − CO_2 + H]^+$ is shown in Fig. 3 and 7 as well as Scheme 1, involving the breaking of the hydrogen bond to the terminal amino nitrogen atom of the carnosine dipeptide and migration of the proton from its initial position on one of the carbonyl oxygen atoms to the other carbonyl atom, both of the oxalate moiety of oxaliplatin (see **TS$_{(1A→1B)}$** in Fig. 7 and Scheme 1). The concerted hydrogen bond breaking and hydrogen migration result in the corresponding transition state **TS$_{(1A→1B)}$** to be 48.3 kcal mol^{-1} higher in free energy relative to **1A**. This transition state leads to the formation of the minimum structure **1B** (see Fig. 7 and Scheme 1), which is 8.7 kcal mol^{-1} higher in free energy relative to **1A**, and shows the retention of three of the hydrogen bonds shown in **1A** while no evidence of hydrogen bonding to the terminal amino nitrogen atom is observed. The hydrogen atom is now, in fact, fully migrated to the other carbonyl oxygen atom of the oxalate moiety. A simple rearrangement *via* the rotation of the resulting OH group produces the transition state **TS$_{(1B→1C)}$** shown in Fig. 7 and Scheme 1, which is calculated to be 20 kcal mol^{-1} higher in energy with respect to **1A**. This transition state in turn leads to the minimum structure **1C** (see Fig. 3 and 7 as well as Scheme 1) in which the OH group is rotated. The highest barrier to CO_2 elimination in this mechanism results from the subsequent transition state
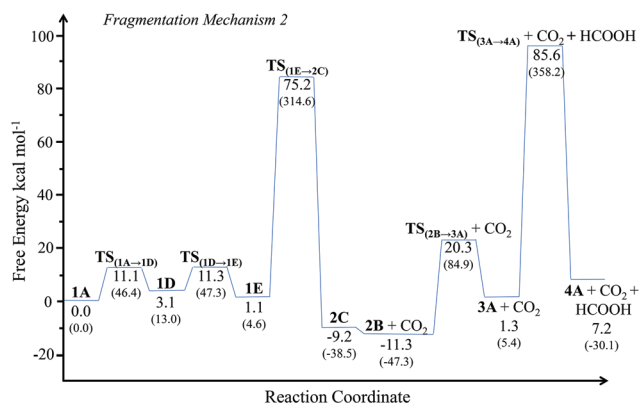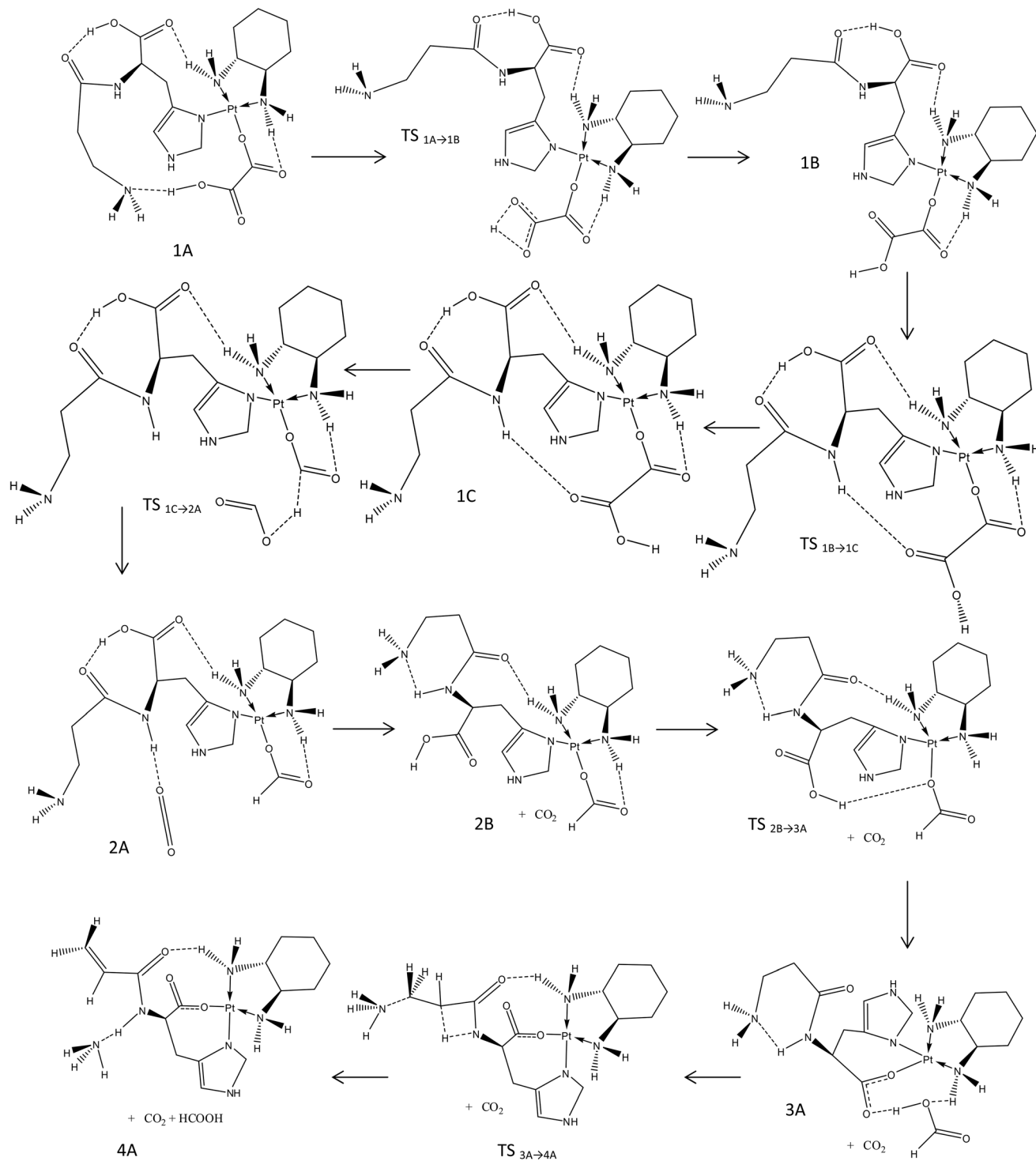
Scheme 1 Proposed mechanism 1 for the collision induced fragmentation of [Carnosine + Oxaliplatin + H]$^+$.

TS$_{(1C \rightarrow 2A)}$ (see Fig. 3 and 7 as well as Scheme 1), which involves the breakage of the C–C bond of the oxalate moiety and the migration of the "inside" proton of the OH group of the oxalate from the oxygen atom to the carbon atom of the newly formed HCOO group. This transition state which involves the simultaneous breaking of two bonds and the formation of a new one is not surprisingly high in energy, and presents a

barrier of 71.2 kcal mol^{-1} relative to its associated starting minimum structure **1C**. This transition state leads to the minimum structure **2A**, Fig. 7, in which the newly formed HCOO group is attached to the Pt centre through a carbonyl oxygen atom, and the CO_2 molecule is now formally eliminated. The released CO_2 molecule is shown in Fig. 7 and Scheme 1 to be held to the amidic hydrogen atom of structure

2A by a relatively weak hydrogen bond, with a bond length of 1.967 Å. Removing the eliminated CO_2 molecule and allowing simple rotations about the single bonds produces conformer **2B** of the ion $[Carnosine + OxPt − CO_2 + H]^+$, which in combination with CO_2 is 8.2 kcal mol^{-1} lower in free energy relative to **2A**. Structure **2B** is shown to be connected to the transition state $TS_{(2B→3A)}$ in which the Pt-carbonyl oxygen atom bond is broken. This carbonyl oxygen atom simultaneously abstracts the hydrogen atom of the OH group of carnosine, causing the elimination of a HCOOH group and the formation of structure **3A**, which corresponds to the ion $[Carnosine − H + Pt(dach)]^+$. The highest barrier calculated in this mechanism is for the process of NH_3 elimination from structure **3A** through $TS_{(3A→4A)}$, which involves two concomitant 1,2-hydrogen shifts and results in the formation of structure **4A**, which corresponds to the ion $[Carnosine − NH_3 − H + Pt(dach)]^+$ as shown in Fig. 3 and 7 as well as Scheme 1. This transition state is shown to be 85.6 kcal mol^{-1} higher in energy than the **1A** global minimum on the PES.

Fragmentation mechanism 2

The initial step in the second path proposed for the loss of CO_2 from $[Carnosine + OxPt + H]^+$ is shown in Fig. 4 and 8 as well as Scheme 2. In analogy with the proposed first mechanism, the initial step here also involves breaking of the hydrogen bond with the terminal amino nitrogen atom of the carnosine dipeptide. However, unlike in mechanism 1, the proton retained by the carbonyl oxygen atom does not move from its initial position, as shown in structure $TS_{(1A→1D)}$ in Fig. 8 and Scheme 2. This transition state is only 11.1 kcal mol^{-1} higher in free energy relative to the starting structure **1A** and leads, as shown in Fig. 8, to the formation of structure **1D**, which is internally stabilised by four hydrogen bonds and is higher in free energy relative to structure **1A** by only 3.1 kcal mol^{-1}. Two simple rotations about the H–O and C–C bonds in the oxalate moiety convert structure **1D** into **1E** through the transition state $TS_{(1D→1E)}$, whose structure is shown in Fig. 8 and Scheme 2, overcoming a free energy barrier of 8.2 kcal mol^{-1} as shown in Fig. 4. The elimination of CO_2 from the **1E** conformer of the ion $[carnosine + OxPt + H]^+$ by means of breaking the C–C bond of the oxalate moiety and the migration of the "inside" proton of the OH group of the oxalate from the oxygen atom to the carbon atom of the newly formed HCOO group takes place *via* the transition state $TS_{(1E→2C)}$ in Fig. 8 and Scheme 2. This transition state for the elimination of CO_2 involves a free energy barrier of 74.1 kcal mol^{-1} relative to the starting point structure **1E**. This barrier for the elimination of CO_2 is 2.9 kcal mol^{-1} higher in energy than that shown in Fig. 3, which is detailed in mechanism 1. However, it involves the transition state $TS_{(1E→2C)}$, shown in Fig. 8 and Scheme 2, which is 6.4 kcal mol^{-1} lower in energy relative to the reference energy of the starting structure **1A** on the free energy scale. Similar to mechanism 1, here, the transition state $TS_{(1E→2C)}$ leads to the minimum structure **2C** for the ion $[Carnosine + OxPt − CO_2 + H]^+$ in which the newly formed HCOO group is attached to the Pt centre through a

carbonyl oxygen atom, and the CO_2 molecule is formally eliminated. The eliminated CO_2 molecule is shown in structure **2C** in Fig. 8 and Scheme 2 to be held by a very weak hydrogen bond at a distance of 2.289 Å to the hydrogen atom retained by the HCOO group. Removing the eliminated CO_2 molecule and allowing simple rotations about the single bonds produces the same conformer **2B** as in mechanism 1 (see Fig. 8 and Scheme 2), which together with CO_2 is 2.1 kcal mol^{-1} lower in free energy relative to **2C**. The remainder of the path of mechanism 2, involving the elimination of HCOOH and NH_3 groups is identical to that described previously in mechanism 1. The formation of structure **4A**, corresponding to the ion $[Carnosine − NH_3 − H + Pt(dach)]^+$ as seen in mechanisms 1 and 2, is shown to involve the highest barriers in these mechanisms. These barriers, in fact, are 85.6 kcal mol^{-1} higher in free energy relative to the **1A** global minimum on either of these surfaces. This agrees with the energy-resolved CID data that shows the ion $[Carnosine − NH_3 − H + Pt(dach)]^+$ to be produced at significantly high energies and not attaining any significant relative abundance.

Fragmentation mechanism 3

Both the mechanisms 1 and 2 show that the formation of the ion $[Carnosine − H + Pt(dach)]^+$ *via* the sequential eliminations of CO_2 and HCOOH from $[carnosine + OxPt + H]^+$ entails high free energy barriers of 81.6 and 75.2 kcal mol^{-1}, respectively above the **1A** global minimum. This is, however, not consistent with the energy-resolved CID data shown in Fig. 2, which indicate that the ion $[Carnosine − H + Pt(dach)]^+$ is easily produced at low collision energies. This inconsistency led us to investigate a mechanism in which the starting structure **1A** is interconverted to **1D** through the transition state labelled $TS_{(1A→1D)}$ in the same fashion as previously described in mechanism 2. However, the structure **1D** shown in Fig. 9 and Scheme 3 in this case undergoes a transformation in which the Pt–O bond connecting the Pt metal to the oxalate moiety is broken and replaced by a Pt bond to the carbonyl oxygen atom of the carnosine dipeptide, as shown in structure **1F** in Fig. 9 and Scheme 3. This leaves the oxalate moiety to form a 1.572 Å hydrogen bond, through one of its carbonyl oxygen atoms, to one of the hydrogen atoms of the amino groups of the dach ligand and another 1.540 Å hydrogen bond, through the oxygen atom of its OH group, to the hydrogen atom of the OH group of the carnosine peptide. This transformation to produce structure **1F** is shown to pass through the transition state $TS_{(1D→1F)}$, which is calculated to be 31.9 kcal mol^{-1} in free energy higher than structure **1A**, as shown in Fig. 5. Structure **1F** undergoes a simple rotation about a single bond involving a free energy barrier of only 6 kcal mol^{-1} in order to produce structure **1G** in which the OH hydrogen of the oxalate moiety is on the "inside", while both hydrogen bonds to the oxalate moiety are retained. The resulting structure **1G** (see Fig. 9 and Scheme 3) is shown to undergo a further transformation by which the "inside" hydrogen atom of the oxalate moiety is transferred to the opposing carboxylic oxygen atom of the oxalate while leaving the now

Fig. 5 Potential energy surface for the fragmentation of the protonated carnosine-oxaliplatin complex, ion **1A**. Structure labels are in bold, top numbers are in kcal mol^{-1} while bottom numbers in parentheses are in kJ mol^{-1}.
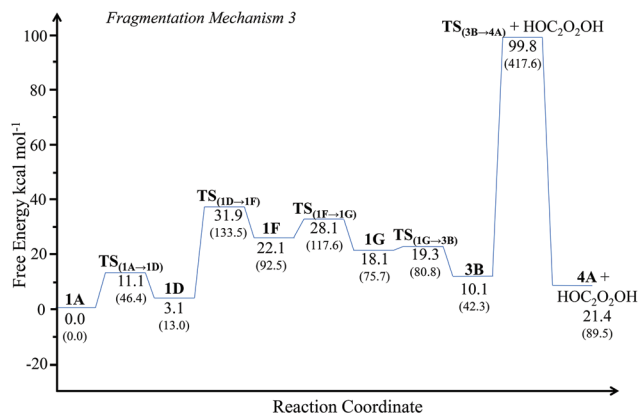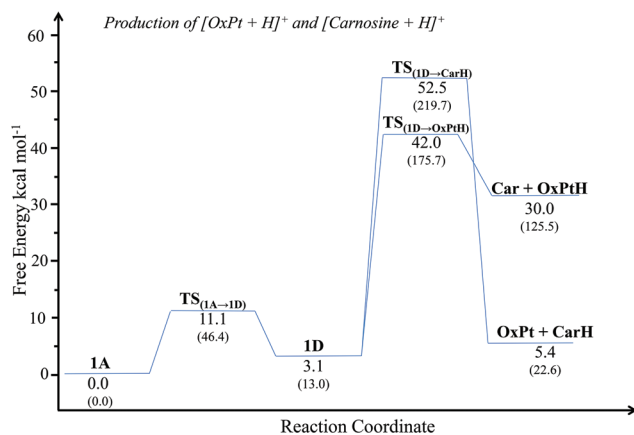

Fig. 6 Potential energy surface for the fragmentation of the protonated carnosine-oxaliplatin complex, ion **1A**. Structure labels are in bold, top numbers are in kcal mol^{-1} while bottom numbers in parentheses are in kJ mol^{-1}.

formally deprotonated oxygen atom to abstract the hydrogen atom of the OH group of the carnosine peptide. This transformation is shown to take place *via* the transition state **TS$_{(1G→3B)}$** shown in Fig. 9 and Scheme 3 with an associated free energy barrier of only 1.2 kcal mol^{-1} to produce structure **3B** in which the resulting HOC$_2$O$_2$OH fragment appears to be attached to the rest of the molecule through a single hydrogen bond formed by one of its hydrogen atoms with a carbonyl oxygen of the carnosine dipeptide. This hydrogen bond is easily broken to eliminate the HOC$_2$O$_2$OH group in order to produce the ion [carnosine + OxPt + H]$^+$. The highest free energy barrier to the formation of this ion, by following this fragmentation path, is calculated to be 31.9 kcal mol^{-1} relative to the global minimum structure **1A**, as shown in Fig. 5. This is a significantly lower barrier than those previously described in mechanisms 1 and 2 for the production of [Carnosine − H + Pt(dach)]$^+$ and is in agreement with the energy-resolved CID data that shows this ion to be easily produced at low collision

Fig. 7 Structures corresponding to the fragmentation mechanism described in Fig. 4. All structures are calculated at the B3LYP/LANL2DZ level of theory. Bond lengths are in Angstroms, relative free energies are indicated in parenthesis. Gray, red, blue and white spheres represent carbon, oxygen, nitrogen and white atoms, respectively.
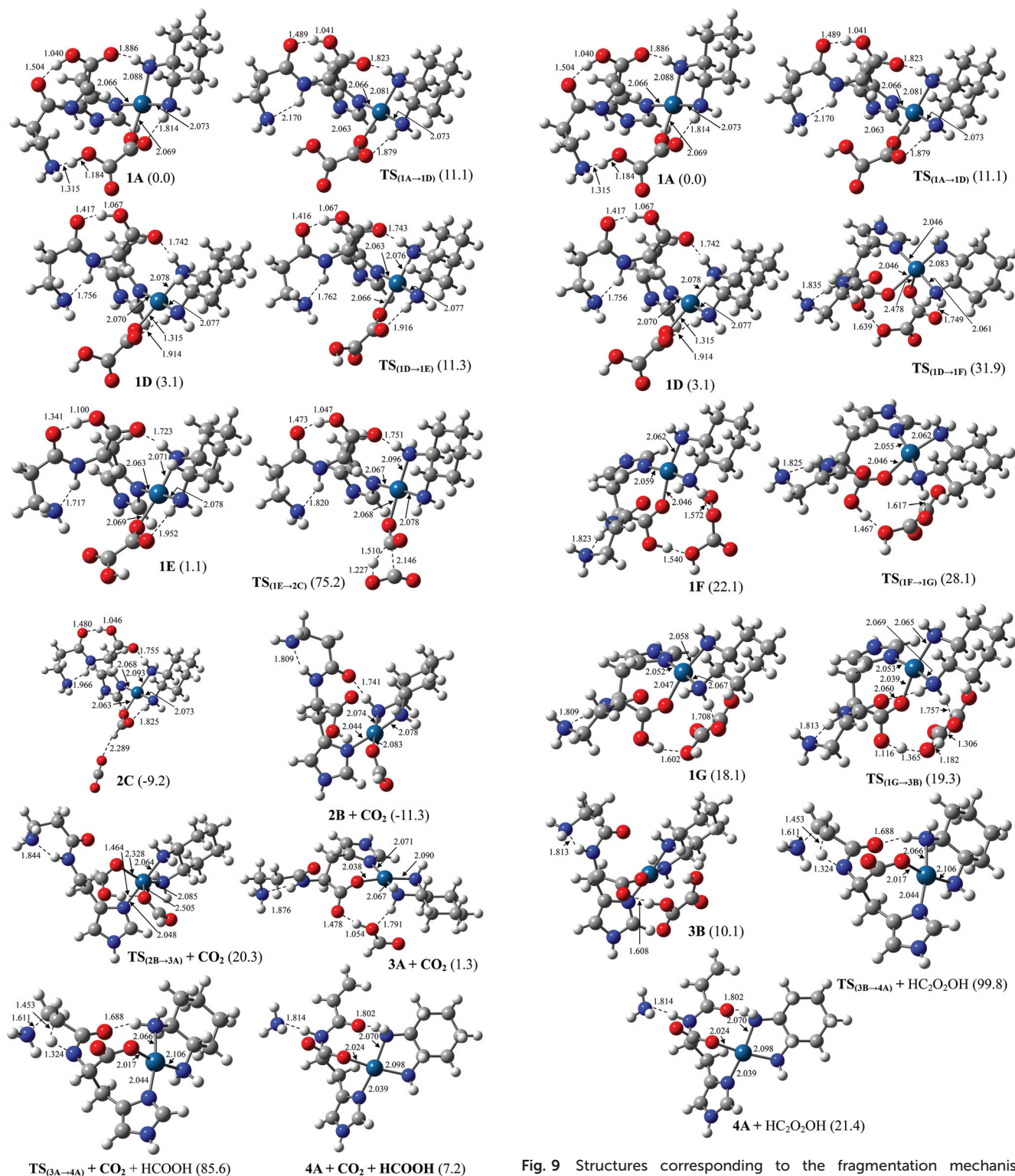
Fig. 8 Structures corresponding to the fragmentation mechanism described in Fig. 5. All structures are calculated at the B3LYP/LANL2DZ level of theory. Bond lengths are in Angstroms, relative free energies are indicated in parenthesis. Gray, red, blue and white spheres represent carbon, oxygen, nitrogen and hydrogen atoms, respectively.
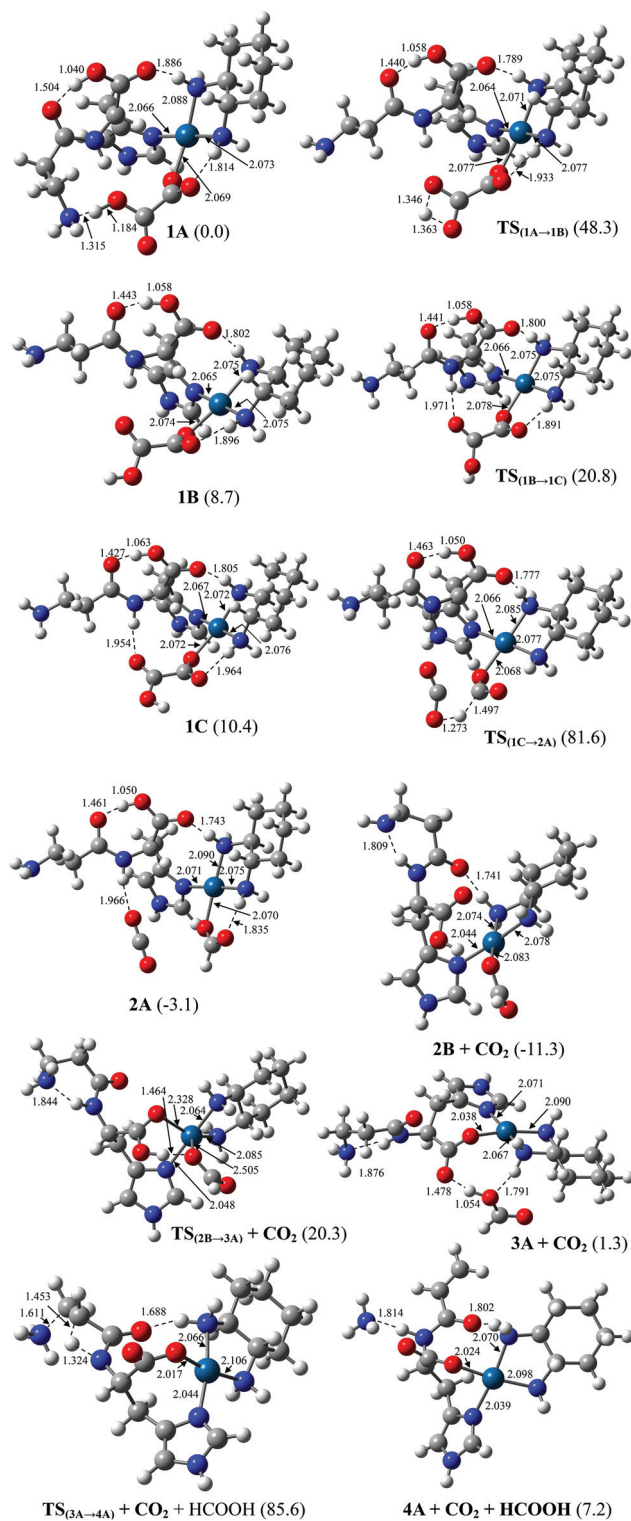
Fig. 9 Structures corresponding to the fragmentation mechanism described in Fig. 6. All structures are calculated at the B3LYP/LANL2DZ level of theory. Bond lengths are in Angstroms, relative free energies are indicated in parenthesis. Gray, red, blue and white spheres represent carbon, oxygen, nitrogen and hydrogen atoms, respectively.
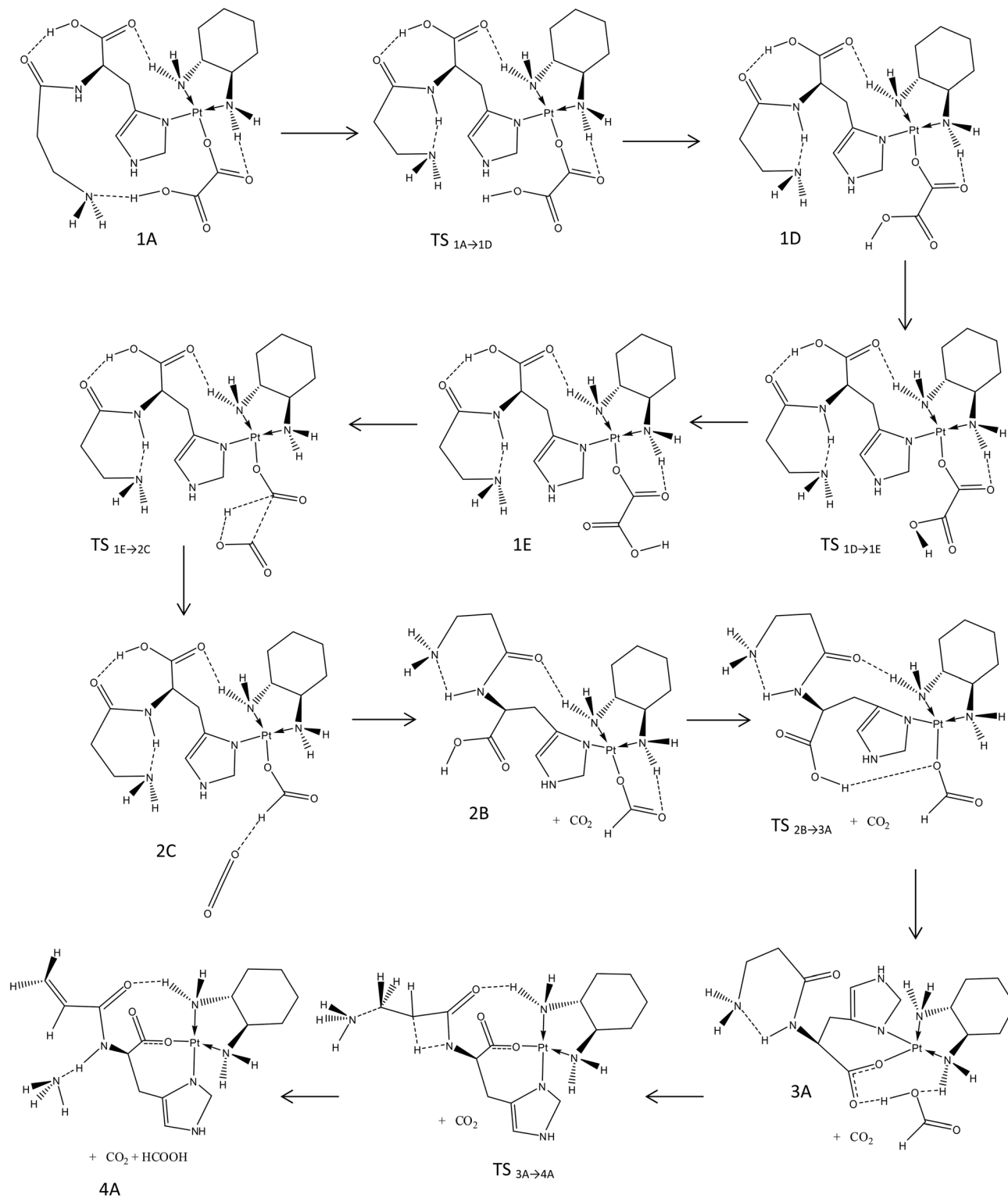
Scheme 2 Proposed mechanism 2 for the collision induced fragmentation of [Carnosine + Oxaliplatin + H]$^+$.

energies. The subsequent elimination of NH_3 from this ion to produce the ion [Carnosine − NH_3 − H + Pt(dach)]$^+$ is shown to go through the transition state $TS_{(3B→4A)}$ that possesses a relatively high free energy barrier of 99.8 kcal mol^{-1}.

Production of [OxPt + H]$^+$ and [Carnosine + H]$^+$

The energy-resolved CID data shown in Fig. 2 clearly indicates that the ion [Carnosine − H + Pt(dach)]$^+$ is the first ion that is produced from the precursor [Carnosine + OxPt + H]$^+$ ion at
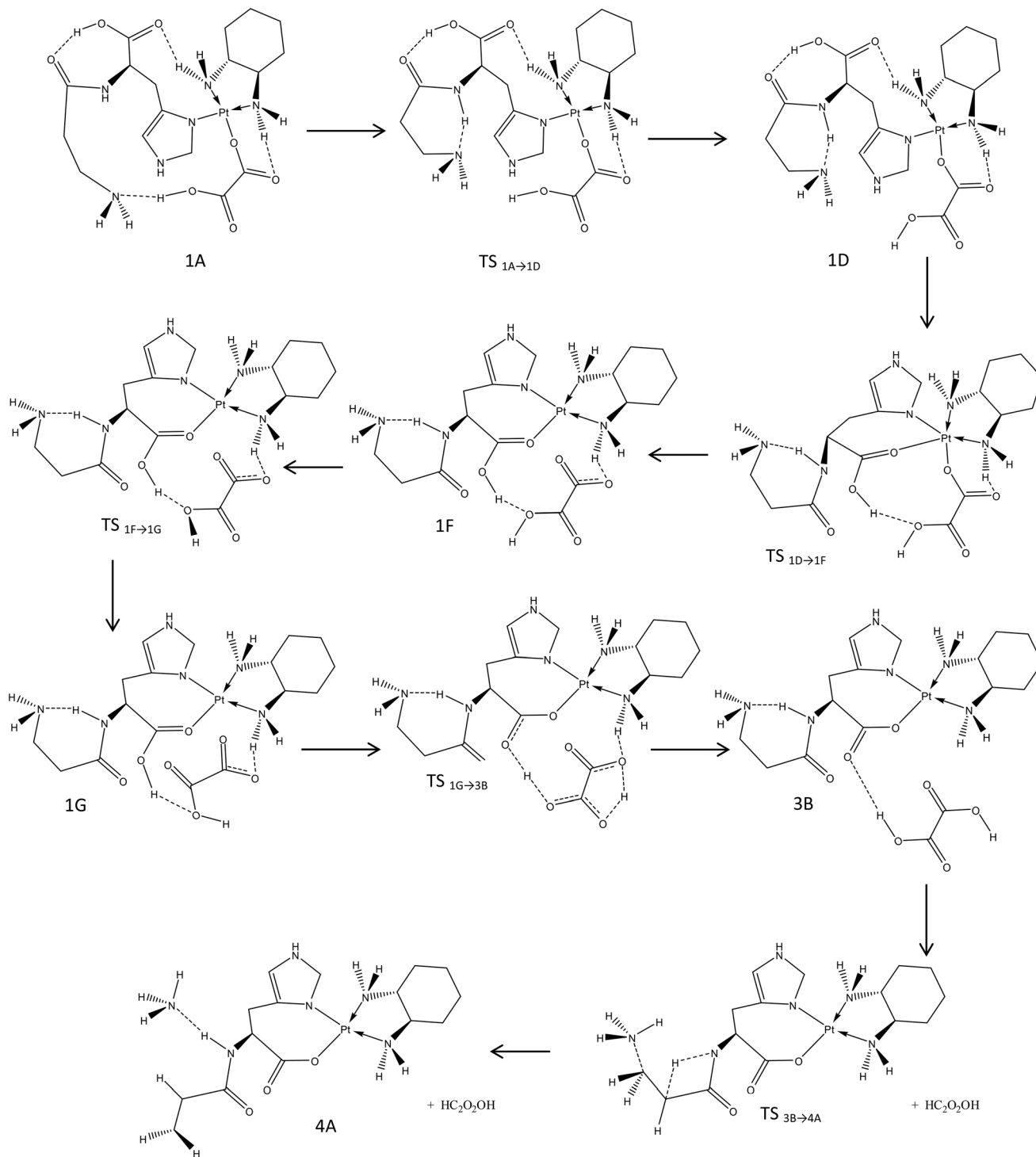
Scheme 3 Proposed mechanism 3 for the collision induced fragmentation of [Carnosine + Oxaliplatin + H]⁺.

the lowest dissociation energies. Two other ions are shown to be produced in significant abundances, but at slightly higher dissociation energies. These ions are [OxPt + H]⁺ and [Carnosine + H]⁺, which are experimentally generated from the fragmentation of the precursor ion [Carnosine + OxPt + H]⁺. The pathways to produce [OxPt + H]⁺ and [Carnosine + H]⁺ from [Carnosine + OxPt + H]⁺ were investigated and are shown in

Fig. 6, where the conformer structure **1A** of the ion [Carnosine + OxPt + H]⁺ is interconverted into structure **1D** through the transition state **TS$_{(1A→1D)}$** previously described in mechanisms 2 and 3. Here, however, structure **1D** is shown to dissociate to produce the combinations Carnosine and [OxPt + H]⁺ or OxPt and [Carnosine + H]⁺ via transition states **TS$_{(1D→OxPtH)}$** and **TS$_{(1D→CarH)}$**, calculated to be 42.0 and 52.5 kcal mol⁻¹ higher

in free energy than structure **1A**, respectively. These relatively low barriers are consistent with the relative ease of production of these two ions experimentally. The relative free energies of the barriers of $TS_{(1D \rightarrow OxPtH)}$ and $TS_{(1D \rightarrow CarH)}$ shown in Fig. 6 also predict the production of $[OxPt + H]^+$ to be more favoured at lower energies, which is corroborated by the energy-resolved CID data shown in Fig. 2.

Conclusions

In this paper, collision-induced dissociation experiments on the protonated carnosine-oxaliplatin complex, $[Carnosine + OxPt + H]^+$ using several collision energies were shown to yield nine different fragment ions. The generation of the product, $[Carnosine - H + Pt(dach)]^+$ ion from $[Carnosine + OxPt + H]^+$ is shown to be the lowest energy process. This agrees well with our calculations shown in mechanism 3, where the generation of the $[Carnosine - H + Pt(dach)]^+$ ion *via* the direct loss of HOC_2O_2OH from $[Carnosine + OxPt + H]^+$ involves the smallest energy barrier calculated here, which is 31.9 kcal mol^{-1}. Two other pathways were calculated for the generation of $[Carnosine - H + Pt(dach)]^+$ through the sequential loss of CO_2 and $HCOOH$ from $[Carnosine + OxPt + H]^+$ and were shown to involve significantly higher barriers of 81.6 and 75.2 kcal mol^{-1}, respectively, as shown in mechanisms 1 and 2. At slightly higher collision energies, the loss of neutral carnosine from $[Carnosine + OxPt + H]^+$ to produce $[OxPt + H]^+$ was experimentally observed, followed by the loss of oxaliplatin from the same precursor ion to produce $[Carnosine + H]^+$. This corresponds well with the two calculated pathways for the generation of the observed ions, where the barriers for the production of $[OxPt + H]^+$ and $[Carnosine + H]^+$ were shown to be 42.0 and 52.5 kcal mol^{-1}, respectively. At significantly higher energies, the ion $[OxPt - CO_2 + H]^+$ was shown to be initially formed, while the last two investigated ions $[Carnosine + OxPt - CO_2 + H]^+$ and $[Carnosine - NH_3 - H + Pt(dach)]^+$ did not attain any significant relative abundance. The calculated barriers for the generation of these two latter ions were shown to be 75.2 and 85.6 kcal mol^{-1}, respectively.

Acknowledgements

References

1 W. Gulewitsch and S. Amiradzibi, *Ber. Dtsch. Chem. Ges.*, 1900, **33**, 1902–1903.

2 I. Severina, O. Bussygina and N. Pyatakova, *Biochemistry*, 2000, **65**, 783–788.

3 R. Kohen, Y. Yamamoto, K. Cundy and B. Ames, *Proc. Natl. Acad. Sci. U. S. A.*, 1988, **85**, 3175–3179.

4 S. E. Gariballa and A. J. Sinclair, *Age Aging*, 2000, **29**, 207–210.

5 M. Horning, L. Blakemore and P. Trombley, *Brain Res.*, 2000, **852**, 56–61.

6 M. Nino, *J. Cosmet., Dermatol. Sci. Appl.*, 2011, **1**, 177.

7 L. J. Hobart, I. Seibel, G. S. Yeargans and N. W. Seidler, *Life Sci.*, 2004, **75**, 1379–1389.

8 A. R. Hipkiss, J. E. Preston, D. T. Himsworth, V. C. Worthington, M. Keown, J. Michaelis, J. Lawrence, A. Mateen, L. Allende, P. A. Eagles and N. J. Abbott, *Ann. N. Y. Acad. Sci.*, 1998, **854**, 37–53.

9 G. A. McFarland and R. Holliday, *Exp. Gerontol.*, 1999, **34**, 35–45.

10 V. P. Reddy, M. R. Garrett, G. Perry and M. A. Smith, *Sci. Aging Knowledge Environ.*, 2005, **18**, pe12.

11 J. Kovacs-nolan and Y. Mine, in *Animal Muscle-Based Bioactive Peptides*, Bioactive Proteins and Peptides as Functional Foods and Nutraceuticals, Wiley-Blackwell, 2010, pp. 225–231.

12 Y. Suzuki, O. Ito, N. Mukai, H. Takahashi and K. Takamatsu, *Jpn. J. Physiol.*, 2002, **52**, 199–205.

13 A. Boldyrev and S. Severin, *Adv. Enzyme Regul.*, 1990, **30**, 175.

14 M. Babizhayev, *Biochim. Biophys. Acta*, 1989, **1004**, 363–371.

15 J. Kang, K. Kim, S. Choi, H. Kwon, M. Won and T. Kang, *Mol. Cells*, 2002, **13**, 498–502.

16 C. Corona, V. Frazzini, E. Silvestri, R. Lattanzio, R. La Sorda, M. Piantelli, L. M. T. Canzoniero, D. Ciavardelli, E. Rizzarelli and S. L. Sensi, *PLoS One*, 2011, **6**, e17971.

17 K. Seto, T. Yoneta, H. Suda and H. Tamaki, *Biochem. Pharmacol.*, 1999, **58**, 245–250.

18 S. Kato, A. Tanaka, Y. Ogawa, K. Kanatsu, K. Seto, T. Yoneda and K. Takeuchi, *Med. Sci. Monit.*, 2001, **7**, 20–25.

19 A. Mahmood, A. J. FitzGerald, T. Marchbank, E. Ntatsaki, D. Murray, S. Ghosh and R. J. Playford, *Gut*, 2007, **56**, 168–175.

20 S. Stvolinsky, M. Kukley, D. Dobrota, M. Vachova, I. Tkac and A. Boldyrev, *Cell. Mol. Neurobiol.*, 1999, **19**, 45–56.

21 A. Boldyrev, S. L. Stvolinsky, O. V. Tyulina, V. B. Koshelev, N. Hori and D. O. Carpenter, *Cell. Mol. Neurobiol.*, 1997, **17**, 259–271.

22 A. Renner, N. Zemitzsch, B. Fuchs, K. D. Geiger, M. Hermes, J. Hengstler, R. Gebhardt, J. Meixensberger and F. Gaunitz, *Mol. Cancer*, 2010, **9**, 2.

23 A. Iovine, M. L. Iannella, F. Nocella, M. R. Pricolo and M. A. Bevilacqua, *Cancer Lett.*, 2012, **315**, 122–128.

24 Y. Horii, J. Shen, Y. Fujisaki, K. Yoshida and K. Nagai, *Neurosci. Lett.*, 2012, **510**, 1–5.

25 E. M. Moustafa, C. L. Camp, A. S. Youssef, A. Amleh, H. J. Reid, B. L. Sharp and T. Shoeib, *Metallomics*, 2013, **5**, 1537–1546.

26 C. G. Hartinger, M. Groessl, S. M. Meier, A. Casini and P. J. Dyson, *Chem. Soc. Rev.*, 2013, **42**, 6186.

27 M. Groessl and C. G. Hartinger, *Anal. Bioanal. Chem.*, 2013, **405**, 1791.

28 S. L. Kerr, T. Shoeib and B. L. Sharp, *Anal. Bioanal. Chem.*, 2008, **391**, 2339.

29 T. Shoeib, S. E. Taylor, G. D. Jones, A. L. Thomas, J. P. Wood, H. J. Reid and B. L. Sharp, *Int. J. Mass Spectrom.*, 2011, **307**, 70.

30 A. Zayed, G. D. Jones, H. J. Reid, T. Shoeib, S. E. Taylor, A. L. Thomas, J. P. Wood and B. L. Sharp, *Metallomics*, 2011, **3**, 991.

31 H. Li, J. R. Snelling, M. P. Barrow, J. H. Scrivens, P. J. Sadler and P. B. O'Connor, *J. Am. Soc. Mass Spectrom.*, 2014, **25**, 1217.

32 T. Zhao and F. L. King, *J. Am. Soc. Mass Spectrom.*, 2009, **20**, 1141.

33 K. Ossipov, Y. Y. Scaffidi-Dominallo, I. F. Seregina, M. Galanski, B. K. Keppler, A. R. Timerbaev and M. A. Bolshov, *J. Inorg. Biochem.*, 2014, **137**, 40–45.

34 A. R. Timerbaev, S. S. Aleksenko, K. Polec-Pawlak, R. Ruzik, O. Semenova, C. G. Hartinger, S. Oszwaldoski, M. Galanski, M. Jarosz and B. K. Keppler, *Electrophoresis*, 2004, **25**, 1988.

35 C. Brauckmann, C. A. Wehe, M. Kieshauer, C. Lanvers-Kaminsky, M. Sperling and U. Karst, *Anal. Bioanal. Chem.*, 2013, **405**, 1855–1864.

36 R. Miao, G. Yang, Y. Miao, Y. Mei, J. Hong, C. Zhao and L. Zhu, *Rapid Commun. Mass Spectrom.*, 2005, **19**, 1031–1040.

37 A. D. Becke, *J. Chem. Phys.*, 1993, **98**, 5648–5652.

38 A. Lee, W. Yang and R. G. Parr, *Phys. Rev. B: Condens. Matter*, 1988, **37**, 785–789.

39 D. Becke, *Phys. Rev. A*, 1988, **38**, 3098–3100.

40 P. J. Stephens, F. J. Devlin, C. F. Chabalowski and M. J. Frisch, *J. Phys. Chem.*, 1994, **98**, 11623–11627.

41 M. J. Frisch, G. W. Trucks, H. B. Schlegel, G. E. Scuseria, M. A. Robb, J. R. Cheeseman, G. Scalmani, V. Barone, B. Mennucci, G. A. Petersson, H. Nakatsuji, M. Caricato, X. Li, H. P. Hratchian, A. F. Izmaylov, J. Bloino, G. Zheng, J. L. Sonnenberg, M. Hada, M. Ehara, K. Toyota, R. Fukuda, J. Hasegawa, M. Ishida, T. Nakajima, Y. Honda, O. Kitao, H. Nakai, T. Vreven, J. A. Montgomery Jr., J. E. Peralta, F. Ogliaro, M. Bearpark, J. J. Heyd, E. Brothers, K. N. Kudin, V. N. Staroverov, R. Kobayashi, J. Normand, K. Raghavachari, A. Rendell, J. C. Burant, S. S. Iyengar, J. Tomasi, M. Cossi, N. Rega, J. M. Millam, M. Klene, J. E. Knox, J. B. Cross, V. Bakken, C. Adamo, J. Jaramillo, R. Gomperts, R. E. Stratmann, O. Yazyev, A. J. Austin, R. Cammi, C. Pomelli, J. W. Ochterski, R. L. Martin, K. Morokuma, V. G. Zakrzewski, G. A. Voth, P. Salvador, J. J. Dannenberg, S. Dapprich, A. D. Daniels, Ö. Farkas, J. B. Foresman, J. V. Ortiz, J. Cioslowski and D. J. Fox, *Gaussian 09, Revision A.1*, Gaussian, Inc., Wallingford, CT, 2009.

42 P. J. Hay and W. R. Wadt, *J. Chem. Phys.*, 1985, **82**, 270–283.

43 W. R. Wadt and P. J. Hay, *J. Chem. Phys.*, 1985, **82**, 284–298.

44 P. J. Hay and W. R. Wadt, *J. Chem. Phys.*, 1985, **82**, 299–310.

45 T. Shoeib, D. W. Atkinson and B. L. Sharp, *Inorg. Chim. Acta*, 2010, **363**, 184–192.

46 M. Belcastro, T. Marino, N. Russo and M. Toscano, *J. Inorg. Biochem.*, 2009, **103**, 50–57.

47 L. Salassa, H. I. A. Phillips and P. J. Sadler, *Phys. Chem. Chem. Phys.*, 2009, **11**, 10311–10316.

48 R. Wysokinski, J. Kuduk-Jaworska and D. Michalska, *J. Mol. Struct. (THEOCHEM)*, 2006, **758**, 169–179.

49 A. B. Yongye, M. A. Giulianotti, A. Nefzi, R. A. Houghten and K. Martinez-Mayorga, *J. Comput. Aided Mol. Des.*, 2010, **24**, 225–235.

50 N. T. Abdel-Ghani and A. M. Mansour, *Eur. J. Med. Chem.*, 2012, **47**, 399–411.

51 R. Wysokinski and D. Michalska, *J. Comput. Chem.*, 2001, **22**, 901–912.

52 B. Giese, G. B. Deacon, J. Jaworska and D. McNaughton, *Biopolymers*, 2002, **67**, 294–297.

53 T. C. Shore, D. Mith, D. DePrekel, S. McNall and Y. Ge, *React. Kinet. Mech. Catal.*, 2013, **109**, 315–333.

54 A. Vacher, F. Barrière, F. Camerel, J. F. Bergamini, T. Roisnel and D. Lorcy, *Dalton Trans.*, 2013, **42**, 383–394.

55 A. I. Oprea, F. Moscalu, A. Dumbrava, S. Ioannou, A. Nicolaides and M. A. Girtu, *Rom. J. Phys.*, 2011, **56**, 125–133.

56 R. J. Holmes, R. A. J. O'Hair and W. D. McFadyen, *Rapid Commun. Mass Spectrom.*, 2000, **14**, 2385–2392.

57 G.-Y. Lee and M.-S. Jun, *Bull. Korean Chem. Soc.*, 2001, **22**, 11–12.

58 Y. Kaya, C. Icsel, V. T. Yilmaz and O. Buyukgungor, *J. Organomet. Chem.*, 2014, **752**, 83–90.

59 L. Pazderski, J. Tousek, J. Sitkowski, K. Malinakova, L. Kozerski and E. Szlyk, *Magn. Reson. Chem.*, 2009, **47**, 228–238.

60 N. Moldovan, P. Lönnecke, I. Silaghi-Dumitrescu, L. Silaghi-Dumitrescu and E. Hey-Hawkins, *Inorg. Chem.*, 2008, **47**, 1524–1531.

61 A. Kerényi, V. Kovács, T. Körtvélyesi, K. Ludányi, L. Drahos and G. Keglevich, *Heteroat. Chem.*, 2010, **21**, 63–70.

62 Y.-W. Huang and S.-L. Lee, *Chem. Phys. Lett.*, 2010, **492**, 98–102.

63 T. Shoeib and B. L. Sharp, *Inorg. Chim. Acta*, 2013, **405**, 258–264.

64 J. A. R. Navarro, M. A. Romero, J. M. Salas, M. Quiros, J. El Bahraoui and J. Molina, *Inorg. Chem.*, 1996, **35**, 7829–7835.

65 R. Pazout, J. Houskova, M. Dusek, J. Maixner and P. Kacer, *Struct. Chem.*, 2011, **22**, 1325–1330.

66 R. Rajeev and R. B. Sunoj, *Dalton Trans.*, 2012, **41**, 8430–8440.

67 T. Shoeib and B. L. Sharp, *Metallomics*, 2012, **4**, 1308–1320.

68 E. M. Moustafa, M. Korany, N. A. Mohamed and T. Shoeib, *Inorg. Chim. Acta*, 2014, **421**, 123–135.

69 J. Roithová and D. Schröder, *Chem. Rev.*, 2010, **110**, 1170–1211.

70 K. Fukui, *J. Phys. Chem.*, 1970, **74**, 4161–4163.

71 C. Gonzalez and H. B. Schlegel, *J. Chem. Phys.*, 1989, **90**, 2154–2161.

Paper III

"Mass spectrometric and computational investigation of the protonated carnosine-carboplatin complex fragmentation"

Ida Ritacco, Mohamed Korany, Tamer Shoeib, Nino Russo, Emilia Sicilia.

Mass Spectrometric and Computational Investigation of the Protonated Carnosine–Carboplatin Complex Fragmentation

Ida Ritacco,[†] Emilia Sicilia,*[,†] Tamer Shoeib,*[,‡,§] Mohamed Korany,[‡] and Nino Russo[†]

[†]Dipartimento di Chimica e Tecnologie Chmiche, Università della Calabria, I-87036 Arcavacata di Rende, Italy
[‡]Department of Chemistry, The American University in Cairo, New Cairo 11835, Egypt
[§]Centre for Analytical Science, Department of Chemistry, Loughborough University, Loughborough, Leicestershire LE11 3TU, U.K.

Ⓢ *Supporting Information*

ABSTRACT: Platinum(II)-based anticancer drugs are square-planar d^8 complexes that, activated by hydrolysis, cause cancer cell death by binding to nuclear DNA and distorting its structure. For that reason, interactions of platinum anticancer drugs with DNA have been extensively investigated, aiming at disentangling the mechanism of action and toxicity. Less attention, however, has been devoted to the formation of adducts between platinum drugs with biological ligands other than DNA. These adducts can cause the loss and deactivation of the drug before it arrives at the ultimate target and are also thought to contribute to the drug's toxicity. Here are reported the outcomes of electrospray ionization mass spectrometry experiments and density functional theory (DFT) computations carried out to investigate the fragmentation pathways of the protonated carnosine–carboplatin complex, $[\text{Carnosine} + \text{CarbPt} + \text{H}]^+$. DFT calculations at the B3LYP/LANL2DZ level employed to probe fragmentation mechanisms account for all experimental data. Because of the relative rigidity of the structure of the most stable **1A** conformer, stabilized by three strong hydrogen bonds, the first step of all of the examined fragmentation pathways is the interconversion of the **1A** conformer into the less stable structure **1B**. Formation of the $[\text{Carnosine} + \text{H}]^+$ fragment from the precursor ion, $[\text{Carnosine} + \text{CarbPt} + \text{H}]^+$, is calculated to be the lowest-energy process. At slightly higher energies, the loss of two amino groups is observed to produce the $[\text{Carnosine} + (\text{CarbPt} - \text{NH}_3) + \text{H}]^+$ and $[\text{Carnosine} + (\text{CarbPt} - 2\text{NH}_3) + \text{H}]^+$ ions. At significantly higher energies, the loss of CO_2 occurs, yielding the final $[\text{Carnosine} + (\text{CarbPt} - \text{NH}_3) - \text{CO}_2 + \text{H}]^+$ and $[\text{Carnosine} + (\text{CarbPt} - 2\text{NH}_3) - \text{CO}_2 + \text{H}]^+$ products. Formation of the $[\text{CarbPt} + \text{H}]^+$ fragment from $[\text{Carnosine} + \text{CarbPt} + \text{H}]^+$, even if not hampered by a high activation barrier, is calculated to be very unfavorable from a thermodynamic point of view.
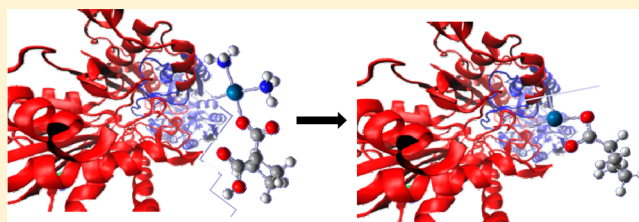
1. INTRODUCTION

Cisplatin [*cis*-diamminedichloroplatinum(II)] is the first inorganic compound introduced in clinical use for the treatment of cancer.[1−4] It is a prototype of several platinum[5−8] and other metal[9−12] coordination compounds synthesized and tested in the search for novel cytostatic agents with improved therapeutic characteristics with respect to the parent compound. Today, the most common platinum(II)-based anticancer drugs used worldwide are cisplatin, carboplatin, and oxaliplatin. These are square-planar d^8 platinum(II) complexes causing cancer cell death by binding to nuclear DNA and distorting its structure.[13,14] Carboplatin [*cis*-diammine-(cyclobutane-1,1-dicarboxylato)platinum(II)] is a platinum anticancer drug used for the treatment of many types of human cancer. Carboplatin was developed by Rosenberg and colleagues in the early 1970s to improve the clinical performance of the first-generation platinum anticancer drug cisplatin.[15,16] Carboplatin has been found to be much less oto-, neuro-, and nephrotoxic than cisplatin.[17,18] Carboplatin contains a structural feature that makes the compound much less chemically reactive than cisplatin, that is a bidentate dicarboxylate chelate leaving ligand.[18] The range of measured

values of the pseudo-first-order rate constant for the first hydrolysis reaction of carboplatin, a reaction involving the displacement of one "arm" of the cyclobutane-1,1-dicarboxylate (CBDCA) chelate ring from the Pt²⁺ ion by a water molecule, is unusually wide.[19−21] There is also an analogous discrepancy in the reported rate constant for the displacement of one of the chloro ligands of cisplatin by water.[21,22] Despite this, however, the fact that the rate constant for the hydrolysis of carboplatin is about 2 orders of magnitude smaller than the corresponding hydrolysis rate for cisplatin has encouraged investigations focused on possible activation mechanisms of carboplatin in chemotherapy. Interactions of platinum anticancer drugs with DNA to understand the mechanism of action and toxicity have been extensively investigated,[17,23−25] whereas less attention has been devoted to the undesirable interactions of platinum drugs with biological ligands other than DNA that can cause the loss and deactivation of the drug before it arrives at the ultimate target.
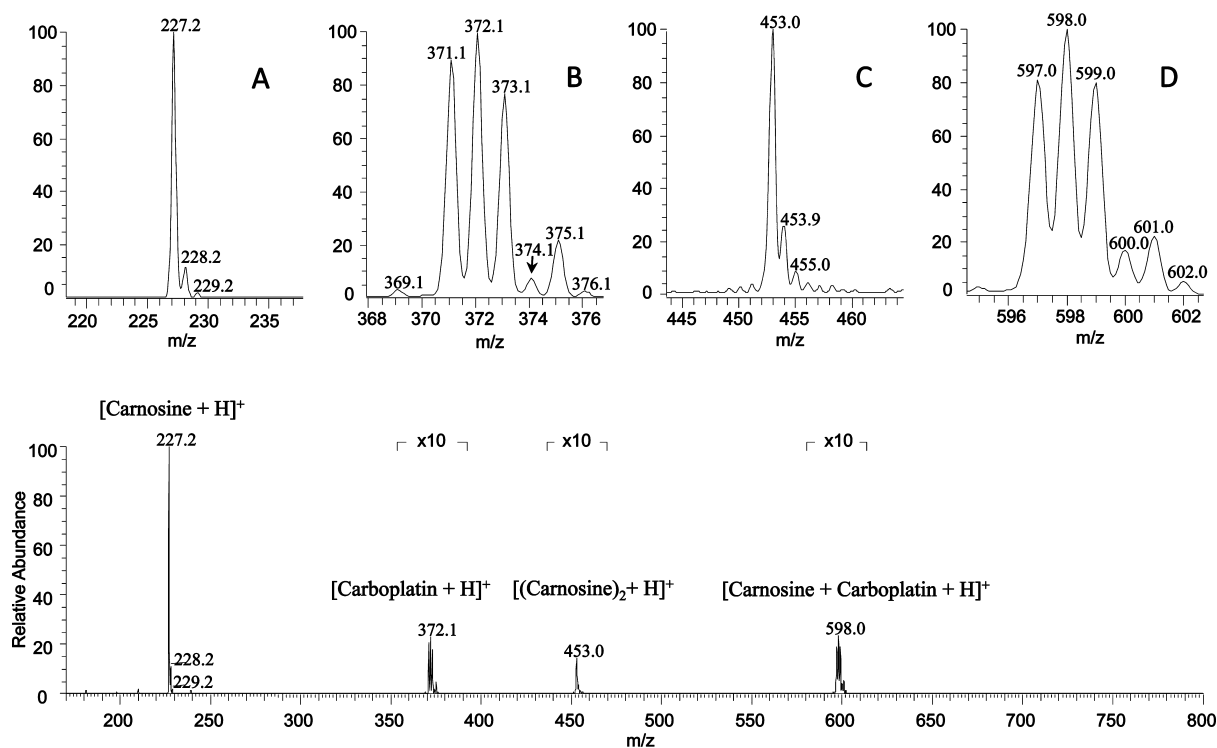
Figure 1. Full-Scan MS spectrum of a 2:1 molar ratio mixture of carnosine and carboplatin in a 1:1 (v/v) water−methanol solution as obtained on the LTQ without allowing for the incubation time. The sections of the spectrum shown under "×10" signify the magnification of the signal by 10-fold for clarity. This magnification means that, for example, the intensity of the ion at m/z 453.0 is about 2% of the base peak. The signals assigned to [Carnosine + H]$^+$, [Carboplatin − H]$^+$, [(Carnosine)$_2$ + H]$^+$, and [Carnosine + Carboplatin + H]$^+$ are each expanded and normalized to 100% in insets A−D, respectively, for clarity.

The dipeptide β-alanine-L-histidine, commonly known as carnosine, is a naturally occurring substance synthesized by endogenous carnosine synthetase. It is present at elevated levels in human skeletal and cardiac muscles as well as in brain tissue[26−30] and is typically concentrated in the cytosol of cells due to its water solubility.[31] Several possible physiological function roles have been considered since its first discovery[32,33] such as pH buffering,[34] metal chelation,[35] or neurotransmitter function.[36] Carnosine is also reported to have antioxidant activity because of its ability to react with several highly reactive species, such as hydroxyl, super oxide, and molecular oxygen free radicals, especially in the water-rich environment inside the body.[37] More recently, it has also been shown that carnosine can play a role in complexation with and sequestering of platinum anticancer drugs.[38] In vitro studies on hepatocellular carcinoma HepG2 cells have shown that carnosine may inhibit the cytotoxic action of oxaliplatin, most likely through the formation of complexes that are less cytotoxic than oxaliplatin alone.[38] The interaction between oxaliplatin and carnosine has been the subject of a recent study.[39] In this study, we offer the results of a joint theoretical and experimental study of the interactions between carboplatin and carnosine including a detailed description of the fragmentation pathways for the gas-phase dissociation of the protonated carboplatin−carnosine complex. Calculated potential energy surfaces (PESs) for the dissociation processes are compared with collision-induced dissociation (CID) experiments. Such studies are important not only to better understand the mechanism of action and toxicity of platinum anticancer drugs but also for the optimization and design of new and improved platinum-based antineoplastic agents.

2. EXPERIMENTAL SECTION

Instrumentation. An LTQ linear-ion-trap mass spectrometer with an electrospray source and a high-resolution Q-Exactive Fourier transform mass spectrometer (Thermo Electron, San Jose, CA) were used. Both instruments were calibrated using Ultramark 1621, caffeine, and Met-Arg-Phe-Ala in accordance with the manufacturer's recommendations. The Q-Exactive was equipped with a Tri-Versa NanoMate ESI chip nanospray (Advion, New York, NY). Typical resolving powers obtained from the Q-Exactive for the mass range under study were on the order of 60000. For the LTQ, resolving powers achieved were on the order of 1500, while the upper instrumental error limit in measurements was 0.2 m/z units. The LTQ autotune routine was used to obtain lens, quadrupole, and octapole voltages for maximum transmission of the ions of interest. Helium gas, admitted into the ion trap at a maintained pressure of approximately 10^{-3} torr, was used as the buffer gas to improve the trapping efficiency and as the collision gas for CID experiments performed here. Experiments designed to elucidate ion structures or fragmentation pathways on the LTQ were performed as follows: the entire isotopic envelope of the ion of interest was selected by having an isolation width set to 5 m/z units and then collisionally activated by setting the activation amplitude at 25−35% of the maximum voltage available (determined empirically), and the activation Q setting (used to adjust the frequency of the radio-frequency excitation voltage) was set at 0.25 units. Sample solutions were continuously infused at a flow rate of 5 μL min^{-1} into the pneumatically assisted electrospray probe using dry nitrogen as the nebulizing gas. Auxiliary and sheath gases were tuned daily for maximum signal transmission. The experiments reported here were all performed under multiple-collision conditions.

Reagents. Carnosine, carboplatin, HPLC-grade water, and methanol were all purchased from Sigma-Aldrich, U.K.

Computational Methods. All molecular geometries have been optimized without any geometrical constraint in the framework of the density functional theory (DFT) that is based upon a strategy of
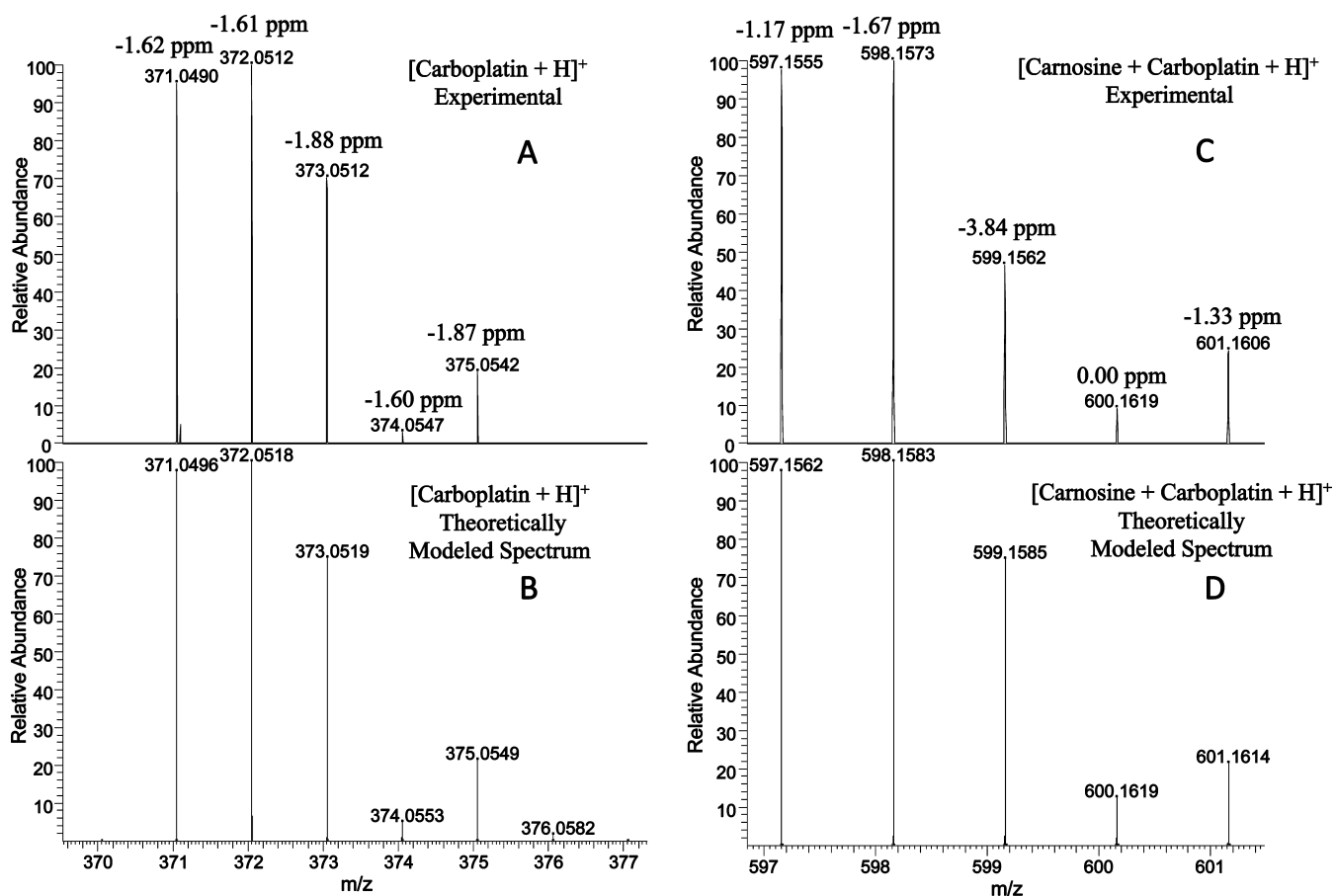
Figure 2. Full-scan MS spectrum of a 2:1 molar ratio mixture of carnosine and carboplatin in a 1:1 (v/v) water−methanol solution as obtained on the Q-Exactive FT-MS without allowing for the incubation time. The experimental signals assigned to [Carboplatin + H]⁺ and [Carnosine + Carboplatin + H]⁺ are each expanded and normalized to 100% in insets A and C, respectively, and insets B and D show the theoretically modeled spectra for [Carboplatin + H]⁺ and [Carnosine + Carboplatin + H]⁺, respectively, using the *Thermo Xcalibur* software. Errors (in ppm) are listed next to each experimental isotopic peak observed.

modeling electron correlation via the proper functionals of the electron density. The B3LYP Becke's three-parameter exchange-correlation hybrid functional with nonlocal correlation corrections, provided by Lee, Yang, and Parr, has been used in the calculations.[40−42] The LANL2DZ basis sets of Hay and Wadt have been employed for all atoms.[43−45] The successful use of the B3LYP/LANL2DZ computational protocol for the investigation of both the electronic properties and reaction pathways of transition-metal-containing compounds, including anticancer drugs, is well established.[46−57] The same protocol has been proven, recently, to give reliable results in the investigation of the fragmentation pathways of the oxaliplatin−carnosine complex.[58] Frequency calculations at the same level of theory have also been performed to identify all stationary points as minima (zero imaginary frequencies) or transition states (one imaginary frequency). The vibrational mode associated with the imaginary frequency of each intercepted transition state has been shown to correspond to the correct movement of the involved atoms. Moreover, the involved transition states have been checked by intrinsic-reaction-coordinate analysis to show the proper connection to the corresponding minima.[59,60] All of the calculations have been performed with the *Gaussian 09* software package.[61]

3. RESULTS AND DISCUSSION

Figure 1 shows the electrospray ionization mass spectrometry (ESI-MS) full-scan spectrum of a 2:1 mM solution in each of carnosine and carboplatin dissolved in a 1:1 (v/v) deionized water−methanol mixture. This figure shows a base peak at *m/z* 227 corresponding to protonated carnosine, [Carnosine + H]⁺.

The peak at *m/z* 453 and the two clusters around *m/z* 372 and 598 are assigned to the protonated carnosine dimer, [(Carnosine)₂ + H]+, protonated carboplatin, [CarbPt + H]⁺, and protonated carnosine−carboplatin complex, [Car + CarbPt + H]⁺, respectively.

The assignments of these ions have been confirmed by comparing the observed isotopic patterns to those theoretically modeled for each of the proposed species. For further confirmation, the isotopic patterns for the proposed [Carboplatin + H]⁺ and [Carnosine + Carboplatin + H]⁺ species, where the latter is the focus of this study, have been obtained on the Q-Exactive FT-MS at a resolving power of about 60000 and compared to their theoretical isotopic patterns at an equivalent resolution. The average errors obtained over all of the isotopic peaks observed were 1.72 and 1.60 ppm for [Carboplatin + H]⁺ and [Carnosine + Carboplatin + H]⁺, respectively. This mass accuracy, being below the commonly accepted 2 ppm limit and obtained without the use of lock masses, provided unequivocal identifications, as seen in Figure 2.

The mass selection and subsequent CID of the entire isotopic envelope of the ion [Carnosine + CarbPt + H]⁺ resulted in the MS² spectrum shown in Figure 3. As was previously reported in the fragmentation of other platinum drug complexes to carnosine,[58,38] here there is also no difference in the fragmentation pathway of the [Carnosine +
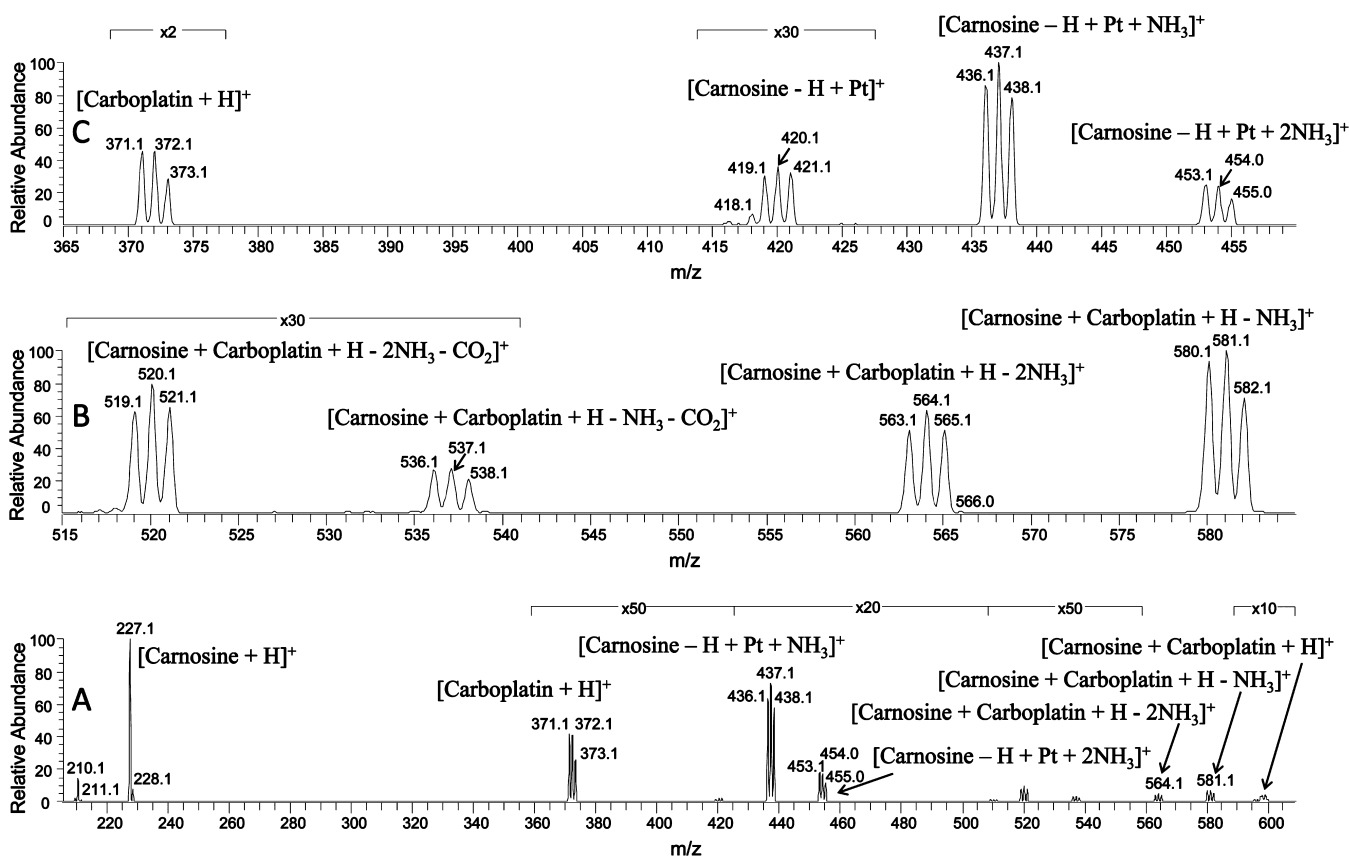
Figure 3. (A) Full scan MS^2 spectrum of the entire isotopic envelope of the ion [Camosine + Carboplatin + H]$^+$ generated at 15 eV in the laboratory frame and isolated from a (2:1) molar mixture of Camosine and Caboplatin in a (1:1) (v/v) water−methanol solution as obtained on the LTQ without allowing for the incubation time. (B and C) m/z 515−585 and 365−460 regions that are each expanded and normalized to 100%, respectively, for clarity.
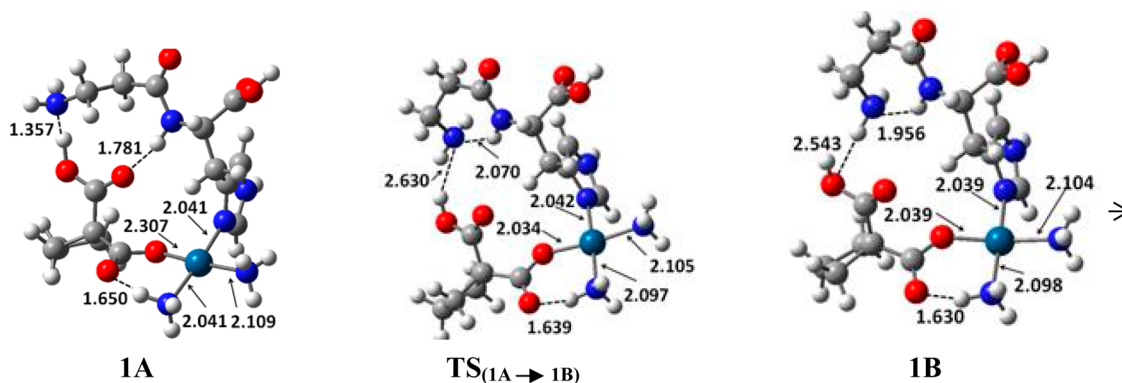

Figure 4. Geometrical structures of stationary points for the starting rearrangement of the most stable conformer **1A** into the less stable **1B** one through the **TS$_{(1A→1B)}$** transition state. Bond lengths are in angstroms. Gray, red, blue, and white spheres represent carbon, oxygen, nitrogen, and hydrogen atoms, respectively.

CarbPt + H]$^+$ complex among the different platinum isotopes. The generated product ion clusters centered around m/z 581, 564, 537, 520, 454, 437, 420, and 372 have been assigned as [Carnosine + CarbPt − NH$_3$ + H]$^+$, [Carnosine + CarbPt − 2NH$_3$ + H]$^+$, [Carnosine + CarbPt − NH$_3$ − CO$_2$ + H]$^+$, [Carnosine + CarbPt − 2NH$_3$ − CO$_2$ + H]$^+$, [Carnosine − H + Pt(NH$_3$)$_2$]$^+$, [Carnosine − H + Pt(NH$_3$)]$^+$, [Carnosine − H + Pt]$^+$, and [Carb + H]$^+$, respectively. Fragmentation pathways for the [Carnosine + CarbPt + H]$^+$ complex, leading to the experimentally determined product ions, have been theoretically investigated.

All of the reported pathways start with the structural rearrangement of the most stable conformer, labeled **1A**, of the precursor ion [Carnosine + CarbPt + H]$^+$ observed as the ion cluster around m/z 598, into conformer **1B**, being 14.0 kcal mol^{-1} higher in energy. The structures of these two minima and transition state **TS$_{(1A→1B)}$** allowing their interconversion are shown in Figure 4. Cartesian coordinates can be found (see Table S1) in the Supporting Information (SI).

It has been previously shown[55] that 46 conformers of the [Carnosine + CarbPt + H]$^+$ complex have been found to exist in a range of about 25 kcal mol^{-1}. These calculated structures
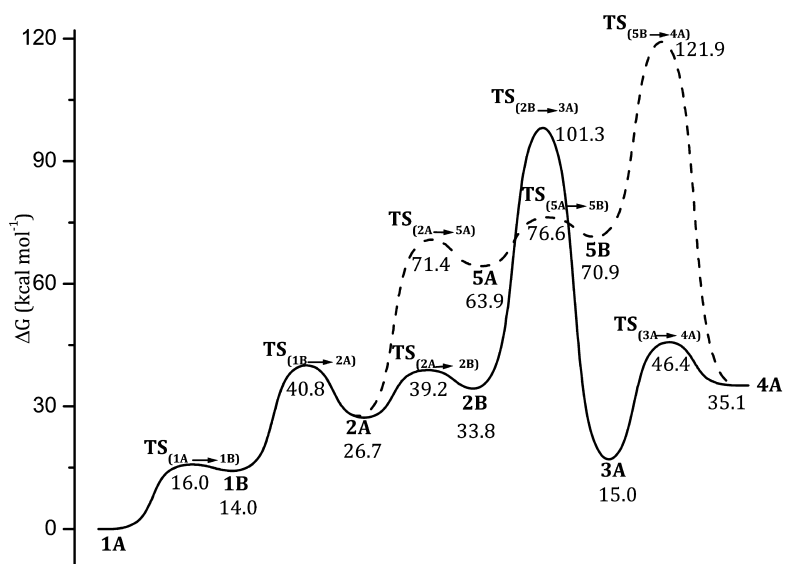
Figure 5. PES for fragmentation of the protonated carnosine−carboplatin complex: ion **1A** along pathways 1 (dashed line) and 2 (solid line). Structure labels are in bold; relative free energies are in kcal mol^{-1}.

involved either direct platinum bonding to carnosine or electrostatic interactions between protonated carnosine and CarbPt. In this figure, structure **1A** shows one of the Pt−O bonds of the CBDCA ligand to be substituted by a formal platinum coordination to the electron-rich *pros* imidazole nitrogen on the carnosine substrate. This structure is further stabilized by three hydrogen bonds. One of these is between one of the hydrogen atoms of the NH$_3$ group on platinum and the oxygen atom of one carboxylic group of the CBDCA moiety, forming a pseudo six-membered ring, another is between the hydrogen atom of the amide group and the oxygen atom of the other carboxyl group of CBDCA, and the third is between the nitrogen atom of the terminal amino group and the hydrogen atom of one of the carboxylic groups of CBDCA at 1.650, 1.781, and 1.357 Å, respectively. The number and strength of such hydrogen bonds make structure **1A** a relatively rigid conformer, and the rearrangement to **1B** is therefore required to allow for further fragmentation. The interconversion of structure **1A** into **1B** slightly shortens the length of the hydrogen bond between the amino group and the carboxyl group of CBDCA at 1.630 Å, whereas the hydrogen bond between the nitrogen atom of the terminal amino group and the OH group is no longer present. On the other hand, the bond between the nitrogen atom of the amide moiety and the other carboxyl group of CBDCA is substituted by a new hydrogen bond, at 1.956 Å, between the amide nitrogen atom and the terminal amino group. The rearrangement occurs, as shown in Figures 4 and 5, by overcoming a free-energy barrier of 16 kcal mol^{-1} for the transition state **TS**$_{(1A→1B)}$ and leads to formation of the **1B** minimum lying 14 kcal mol^{-1} above the reference energy of **1A**. The breaking of one hydrogen bond and formation of a new weaker one are partially responsible for the calculated destabilization. The fragmentation of [Carnosine + CarbPt + H]$^+$ proceeds by the loss of neutral ammonia from structure **1B** to give the fragment ion [Carnosine + (CarbPt − NH$_3$) + H]$^+$ observed as the ion cluster centered around m/z 581. Either the NH$_3$ molecules in the trans position to the CBDCA moiety of carboplatin or those in the cis position can be eliminated. Following elimination of the first NH$_3$ molecule, either the fragmentation continues with elimination of the

second carboplatin NH$_3$ molecule preceding elimination of CO$_2$ from the COOH unit of the CBDCA moiety or elimination of the CO$_2$ molecule may take place before elimination of the second NH$_3$ molecule. The peak at m/z 372 indicates that the fragment [CarbPt + H]$^+$ is formed from the precursor ion [Carnosine + CarbPt + H]$^+$ due to the loss of neutral carnosine.

Fragmentation Pathways 1 and 2: Elimination of the NH$_3$ Molecule Cis to the CBDCA Ligand. After rearrangement of the **1A** conformer to **1B**, elimination of the NH$_3$ molecule cis to the CBDCA moiety of carboplatin leads to formation of the fragment ion [Carnosine + (CarbPt − NH$_3$) + H]$^+$ observed as the ion cluster centered around m/z 581. Calculated free-energy profiles starting with elimination of the NH$_3$ molecule cis to the CBDCA moiety are depicted in Figure 5. Structure **2A** shows the initial step in the release of the NH$_3$ molecule cis to the CBDC moiety of carboplatin, with all other minima resulting from its subsequent dissociation, and the transition states leading to their formation are sketched in Figure 6. More detailed information on the geometrical parameters and Cartesian coordinates is reported in the SI (Figure S1). Elimination of the NH$_3$ molecule cis to the CBDCA moiety goes through the transition state **TS**$_{(1B→2A)}$ in which the bond between the platinum center and the *cis*-NH$_3$ is breaking and a new bond between the carbonyl oxygen atom and the platinum center is forming.

As a consequence of this rearrangement, some hydrogen bonds are broken and new ones are formed. Structure **2A** shows the released NH$_3$ molecule weakly interacting, at 1.696 Å, with the other NH$_3$ group of carboplatin. The transition state **TS**$_{(1B→2A)}$ and the minimum **2A** are calculated to be 40.8 and 26.7 kcal mol^{-1} higher in free energy relative to structure **1A**, respectively.

Along pathway 1, the reaction proceeds by a rearrangement of structure **2A**, through the transition state **TS**$_{(2A→2B)}$, into the minimum structure **2B**, where the protonated COOH unit of the CBDCA moiety reorients, allowing CO$_2$ elimination in the subsequent step. The transition state **TS**$_{(2A→2B)}$ and the **2B** minimum corresponding to the fragment ion [Carnosine + (CarbPt − NH$_3$) + H]$^+$, observed as the ion cluster centered

1B

TS$_{(1B \to 2A)}$

2A

TS$_{(2A \to 5A)}$

TS$_{(2A \to 2B)}$

5A

2B

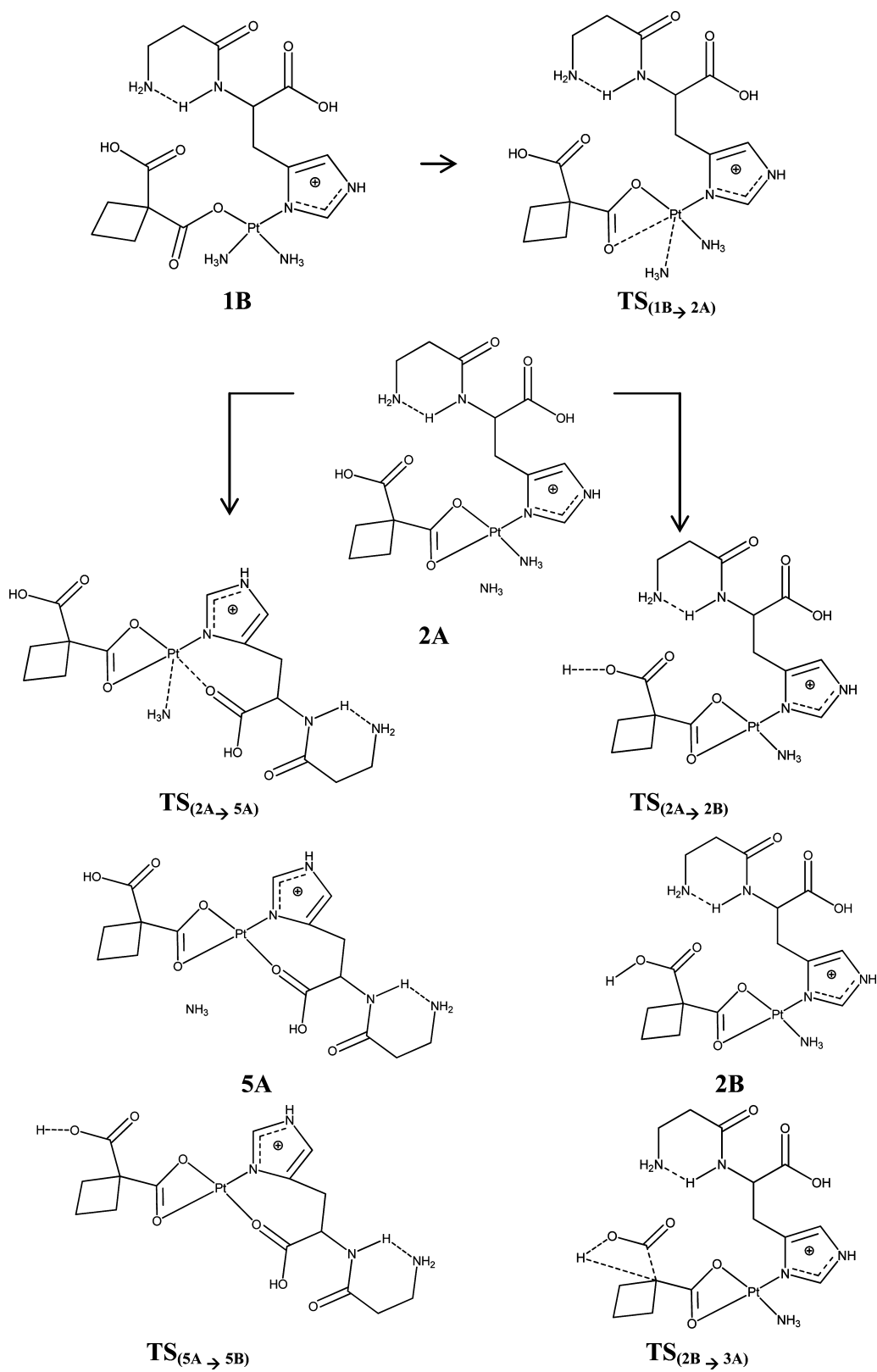**TS$_{(5A \to 5B)}$**

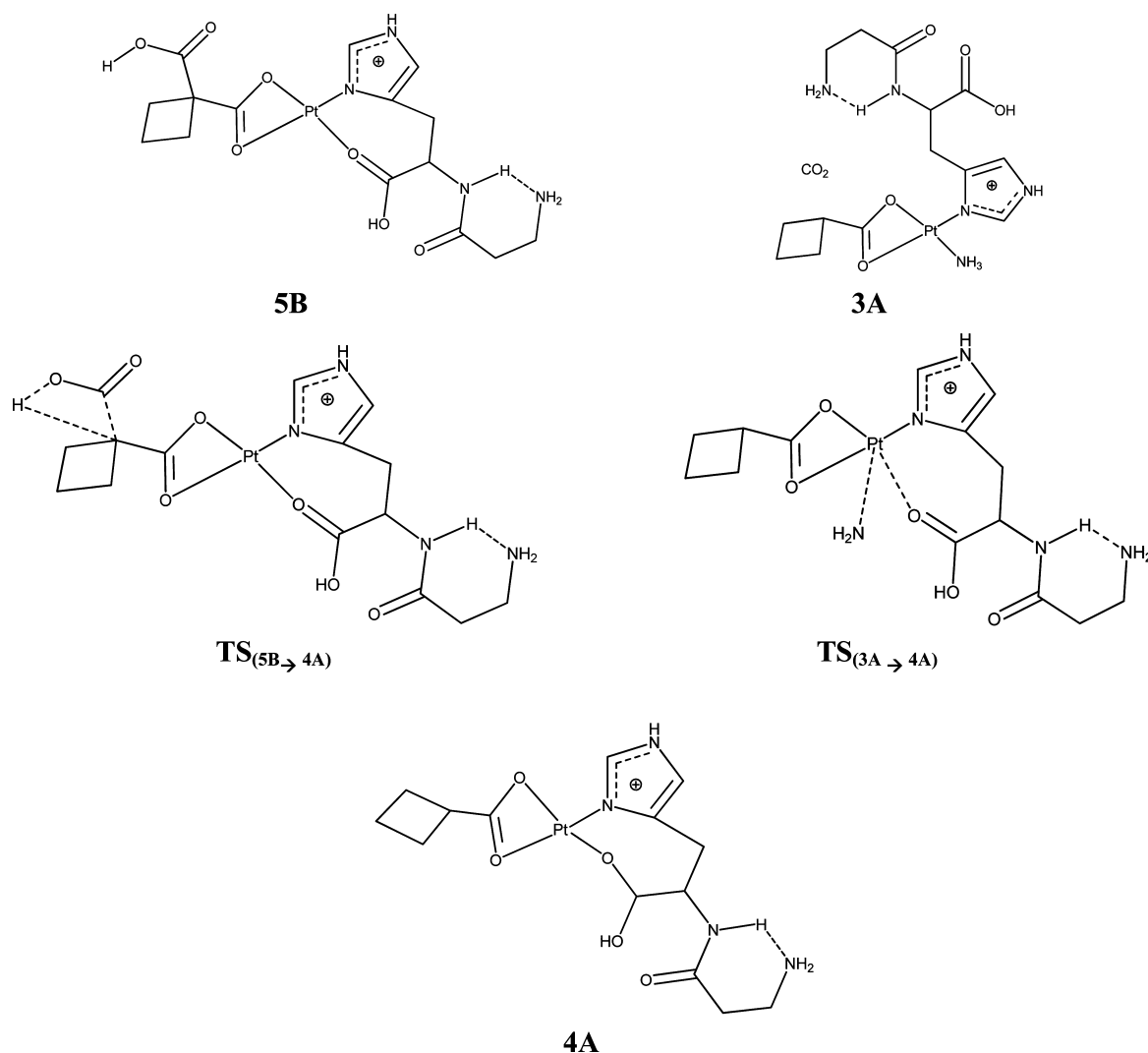**TS$_{(2B \to 3A)}$**

Figure 6. continued

Figure 6. Schematic representation of the structures of stationary points intercepted along the fragmentation Pathways 1 and 2 for the elimination of the NH_3 molecule cis to the CBDCA ligand.

around m/z 581, are calculated to be higher in energy than the reference **1A** minimum by 39.2 and 33.8 kcal mol^{-1}, respectively. In the next step, from the protonated COOH unit of the CBDCA ligand, a CO_2 molecule is eliminated to yield the minimum **3A** corresponding to the fragment ion [Carnosine + (CarbPt − NH_3) − CO_2 + H]$^+$ observed as the ion cluster centered around m/z 537. The CO_2 loss occurs by overcoming the free-energy barrier for the transition $\mathbf{TS_{(2B\to3A)}}$ of 101.3 kcal mol^{-1} relative to structure **1A**. In the transition $\mathbf{TS_{(2B\to3A)}}$, the C−C bond between the COOH unit and the quaternary carbon atom of the CBDCA moiety is broken and the proton migrates from the oxygen atom of the OH group to that carbon atom, leading to the minimum structure **3A**, whose formation is endoergic by 15.0 kcal mol^{-1} relative to the starting structure **1A**. The released CO_2 appears to be bonded to the carnosine COOH group by a relatively weak hydrogen bond with a bond length of 1.797 Å. The final step of this pathway involves further elimination of the second NH_3 from the carboplatin moiety of structure **3A** to produce the fragment ion [Carnosine + (CarbPt−2NH_3) − CO_2 + H]$^+$ observed as the ion cluster centered around m/z 520, indicated as **4A** in Figures 5 and 6.

Similar to the first NH_3 elimination, the reaction here involves the rupture of the Pt−N bond, as shown in the transition $\mathbf{TS_{(3A\to4A)}}$ with a barrier of 46.4 kcal mol^{-1} calculated with respect to the initial structure **1A**. This transition state describes the concerted breaking of two hydrogen bonds: the first is between the NH_3 molecule of carboplatin and the C=O moiety of the carnosine COOH group, while the second is between the OH group of COOH and the amide nitrogen atom of carnosine. The removal of these hydrogen bonds is followed by the subsequent rotation, and formation of a new bond between the carbonyl oxygen atom of the carnosine COOH and the platinum center gives the minimum structure **4A** having the released NH_3 molecule weakly attached to the remaining CBDCA carboxylate via a hydrogen bond of 2.194 Å. Structure **4A** is calculated to be 35.1 kcal mol^{-1} higher in energy relative to the zero reference energy of **1A**.

It is worth mentioning that the CO_2 molecule can be, alternatively, released from the carnosine moiety. The corresponding path, together with the structures of the intercepted stationary points, is displayed in the SI (Figure S2). After formation of the **2A** minimum, the reaction proceeds by rotation of the hydrogen atom of the OH group of the carnosine ligand to form, by overcoming a low barrier of 12.9
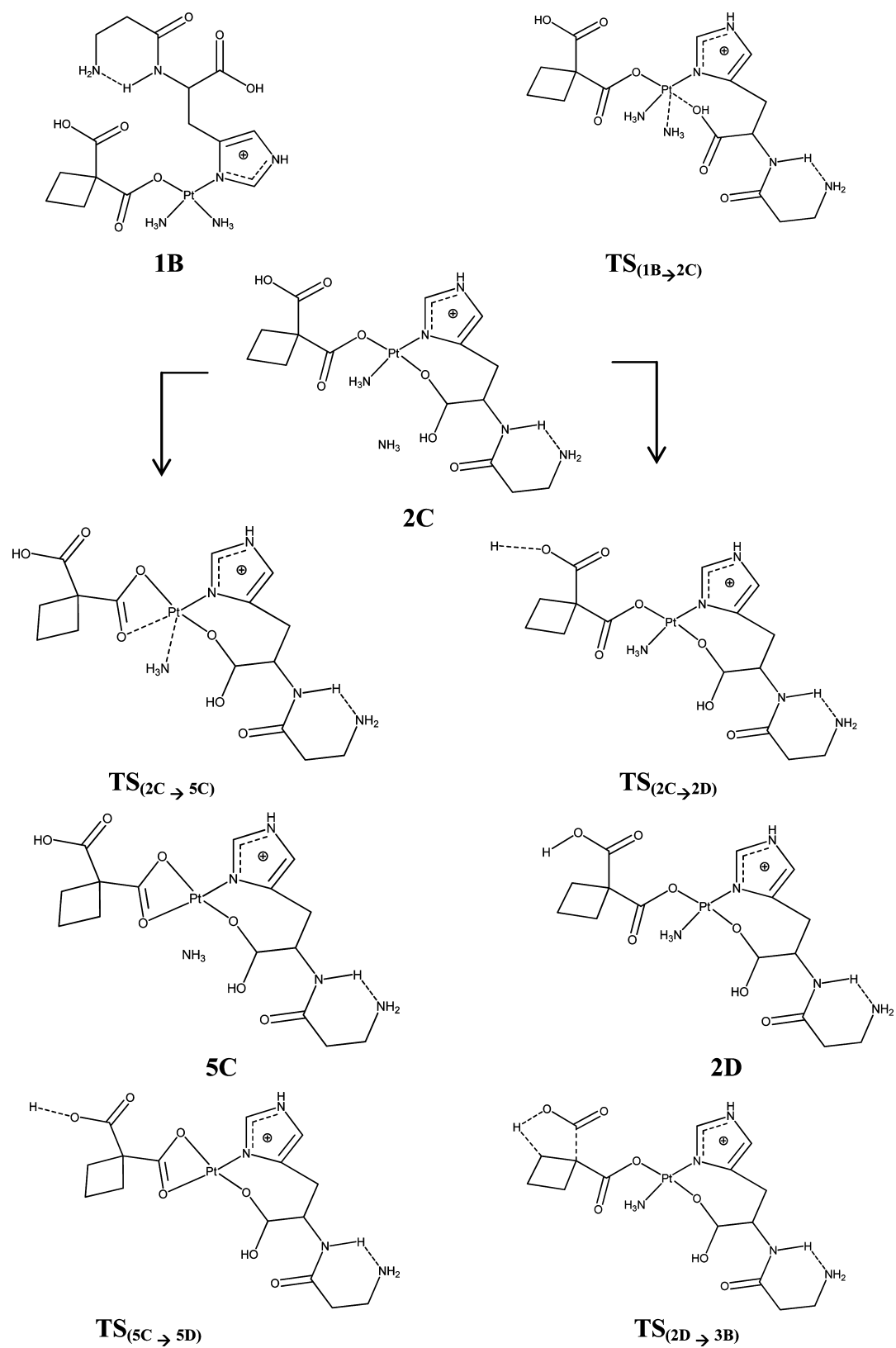
1B

TS$_{(1B \to 2C)}$

2C

TS$_{(2C \to 5C)}$

TS$_{(2C \to 2D)}$

5C

2D

TS$_{(5C \to 5D)}$

TS$_{(2D \to 3B)}$

Figure 7. continued

5D

3B

TS$_{(5D \to 4A)}$

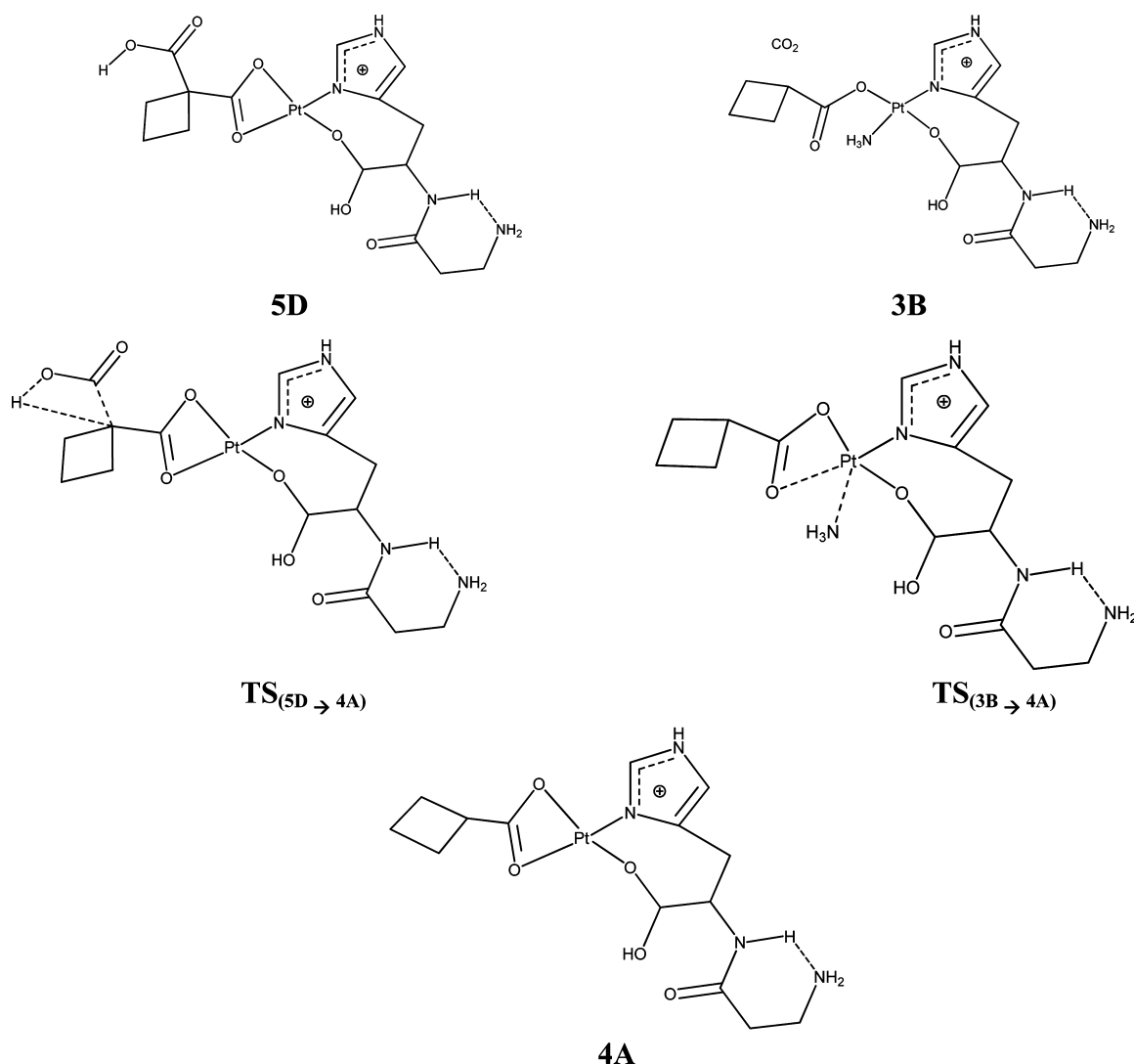**TS$_{(3B \to 4A)}$**

4A

Figure 7. Schematic representation of the structures of stationary points intercepted along the fragmentation pathways 3 and 4 for elimination of the NH_3 molecule trans to the CBDCA ligand.

kcal mol^{-1} calculated with respect to the previous minimum, the intermediate labeled **2E** lying 29.8 kcal mol^{-1} above the **1A** global minimum. The transition state **TS$_{(2E \to 3C)}$** allows OH group hydrogen transfer to the carbon atom that releases the CO_2 molecule. This rearrangement has a high energetic cost that corresponds to an activation barrier of 112.1 kcal mol^{-1} calculated with respect to the **1A** reference energy. That is, the CO_2 loss from the COOH group of the CBDC ligand appears to be more favorable and has been examined along all of the described pathways reported below.

In contrast to pathway 1, in which elimination of the cis NH_3 molecule is followed by CO_2 loss and subsequent elimination of the second NH_3, along pathway 2, elimination of the *cis*-NH_3 molecule continues with elimination of the second carboplatin NH_3, followed by the loss of CO_2 from the CBDC COOH group. Elimination of the second ammonia from structure **2A** results in the formation of structure **5A** for the fragment ion [Carnosine + (CarbPt − 2NH$_3$) + H]$^+$ observed as the ion cluster centered around *m/z* 564. This involves breaking of the Pt−N bond, as shown in transition state **TS$_{(2A \to 5A)}$**, being at a free-energy barrier of 71.4 kcal mol^{-1} relative to the starting structure **1A**. The formation of a bond between the carbonyl oxygen atom of the carnosine COOH group and the platinum

center yields the minimum structure **5A**. The released NH_3 weakly interacts, at a distance of 1.912 Å, with the terminal amino group of carnosine. Relative to **1A**, structure **5A** is calculated to be 63.9 kcal mol^{-1} higher in energy.

Similar to the rearrangement of structure **2A** into structure **2B**, here structure **5A** internally rearranges through the transition state **TS$_{(5A \to 5B)}$** to form the minimum structure **5B** prior the elimination of CO_2 in the subsequent step. The stationary points **TS$_{(5A \to 5B)}$** and **5B** are calculated to be higher in free energy than structure **1A** by 76.6 and 70.9 kcal mol^{-1}, respectively. In analogy with the same mechanism of CO_2 loss described above for pathway 1, structure **4A** is formed upon going through the transition state **TS$_{(5B \to 4A)}$**, where the C−C bond between the quaternary carbon atom and protonated COOH group of carboplatin is broken followed by proton transfer from the hydroxyl of the COOH group to the carbon atom, leading to the minimum structure **4A** corresponding to the fragment ion [Carnosine + (CarbPt − 2NH$_3$) − CO_2 + H]$^+$ observed as the ion cluster centered around *m/z* 520. This final transition state on this path, **TS$_{(5B \to 4A)}$**, is calculated to be higher in free energy relative to **1A** by 121.9 kcal mol^{-1}.

Fragmentation Pathways 3 and 4: Elimination of the NH_3 Molecule Trans to the CBDCA Ligand. Structures of
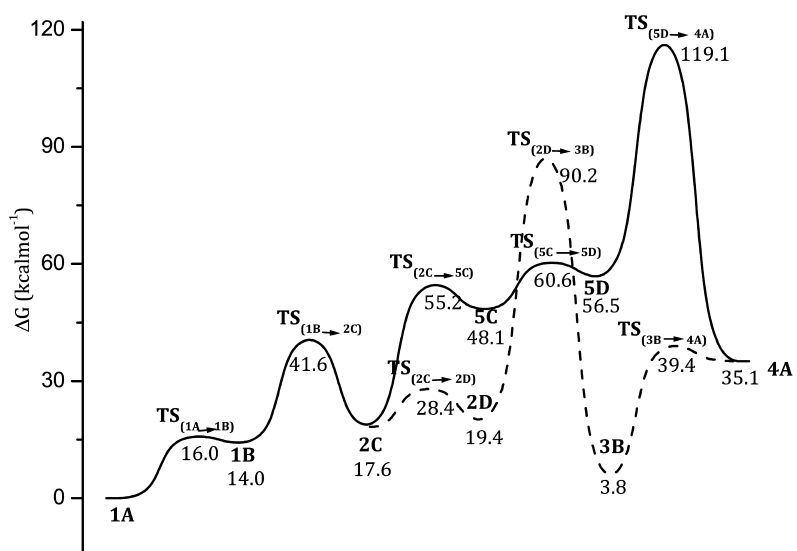
Figure 8. PES for fragmentation of the protonated carnosine–carboplatin complex, ion **1A**, along pathways 3 (solid line) and 4 (dashed line). Structure labels are in bold, and relative free energies are in kcal mol^{-1}.

all stationary points intercepted along both pathways 3 and 4 and the corresponding free-energy profiles are drawn in Figures 7 and 8. Cartesian coordinates and most relevant geometrical parameter values (Figure S3) can be found in the SI. Starting from structure **1B**, fragmentation reactions along pathways 3 and 4 involve the same initial step, which is elimination of the NH$_3$ molecule trans to the CBDCA moiety of carboplatin, resulting in the formation of structure **2C** corresponding to the ion [Carnosine + (CarbPt − NH$_3$) + H]$^+$ observed as the ion cluster centered around m/z 581. The transition state **TS$_{(1B \to 2C)}$** associated with elimination of the NH$_3$ molecule trans to the CBDCA moiety of carboplatin involves the loss of a Pt−N bond and the formation of a new bond between the carbonyl oxygen atom of the carnosine COOH group and the platinum center. The free-energy barrier of this transition state is calculated to be 41.6 kcal mol^{-1} relative to minimum **1A**. Structure **2C** formed by release of the trans NH$_3$ molecule is calculated to be higher than either precursor structure **1A** or **1B** in free energy by 17.6 and 3.2 kcal mol^{-1}, respectively. Structure **2C** may undergo rearrangement by rotation, so that the proton of the CBDCA COOH group is oriented toward the quaternary carbon atom of CBDCA for the CO$_2$ loss to occur in the next step.

This rearrangement goes through transition state **TS$_{(2C \to 2D)}$** as shown in pathway 3 in Figure 8, to give the minimum structure **2D**. Despite of this minor change in the structure, the transition state **TS$_{(2C \to 2D)}$** and the minimum **2D** are found to be 28.4 and 19.4 kcal mol^{-1} higher in free energy, respectively, relative to **1A**. Following the same mechanism of CO$_2$ elimination described in pathway 1, structure **2D** goes through transition state **TS$_{(2D \to 3B)}$**, where the C−C bond is broken and the proton of the COOH group of CBDCA is transferred to the quaternary carbon atom in order to give the minimum structure **3B** corresponding to the fragment ion [Carnosine + (CarbPt − NH$_3$) − CO$_2$ + H]$^+$ observed as the ion cluster centered around m/z 537. In analogy to the other pathways previously described, CO$_2$ elimination here requires a high energy barrier, in this case 90.2 kcal mol^{-1} for the transition state **TS$_{(2D \to 3B)}$** relative to **1A**, to be overcome.

The resulting minimum structure **3B** is, however, highly stabilized and is calculated to be only 3.8 kcal mol^{-1} above

structure **1A**. Finally, from structure **3B**, the remaining NH$_3$ molecule is released, following the same elimination mechanism in order to give structure **4A** corresponding to the fragment ion [Carnosine + (CarbPt − 2NH$_3$) − CO$_2$ + H]$^+$ observed as the ion cluster centered around m/z 520. The bond between the NH$_3$ nitrogen atom and the platinum center in structure **3B** is broken along with the formation of a new bond between the C=O group of the CBDCA moiety and the platinum atom in the transition state **TS$_{(3B \to 4A)}$** with a corresponding free-energy barrier of 39.4 kcal mol^{-1} relative to structure **1A**, leading to the formation of structure **4A**, which is 35.1 kcal mol^{-1} higher in free energy relative to **1A**.

Along pathway 4 shown in Figure 8, elimination of the first NH$_3$ molecule trans to CBDCA is followed by elimination of the other NH$_3$ molecule in order to give the minimum structure **5C** corresponding to the fragment ion [Carnosine + (CarbPt − 2NH$_3$) + H]$^+$ observed as the ion cluster centered around m/z 564. Elimination of the second NH$_3$ molecule occurs by surmounting a free-energy barrier of 55.2 kcal mol^{-1} for the transition state **TS$_{(2C \to 5C)}$**, leading to structure **5C**, which is 48.1 kcal mol^{-1} higher in energy relative to the initial structure **1A**. That is, the minimum structure **5C** is stabilized by 7.1 kcal mol^{-1} with respect to the transition state, leading to it. Structure **5C**, in turn, rearranges so that the protonated COOH moiety of CBDCA rotates to be in a suitable orientation for CO$_2$ release. This is described in transition state **TS$_{(5C \to 5D)}$**, which allows for such rearrangement and the formation of structure **5D**. These two structures are calculated to be 60.6 and 56.5 kcal mol^{-1} higher in energy with respect to **1A**, respectively. The CO$_2$ elimination mechanism, previously described, can then take place in which the C−C bond between the COOH group and the quaternary carbon atom of the CBDCA moiety is broken and the proton is transferred from the OH group to that carbon atom. As expected, the transition state **TS$_{(5D \to 4A)}$** for this transformation to finally give the minimum structure **4A** corresponding to the fragment ion [Carnosine + (CarbPt − 2NH$_3$) − CO$_2$ + H]$^+$ observed as the ion cluster centered around m/z 520 has a high energy barrier. The **TS$_{(5D \to 4A)}$** stationary point is calculated to be higher in free energy relative to the precursor structure **1A** by 119.1 kcal mol^{-1}.
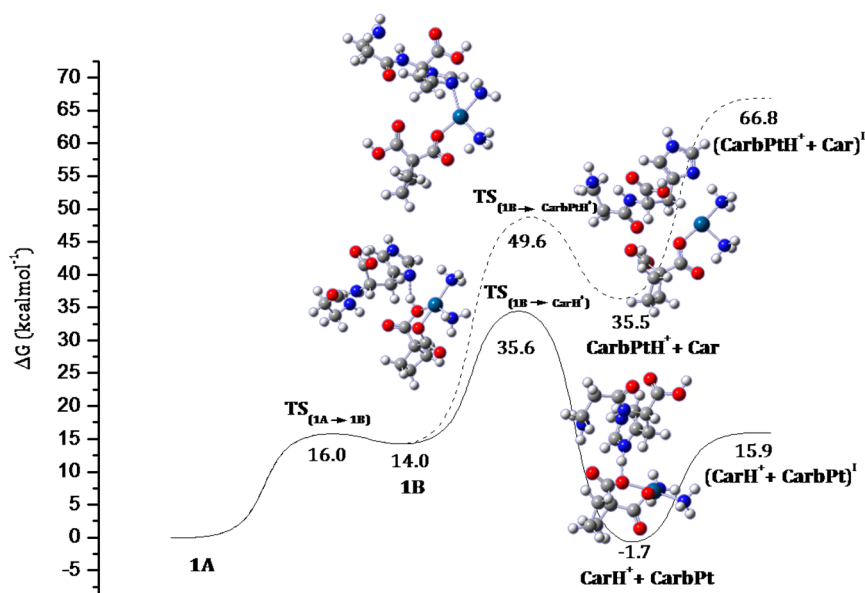
Figure 9. PES for the fragmentation of the protonated carnosine−carboplatin complex, ion **1A**, along the pathways leading to the formation of the ions [Car + H]⁺ (solid line) and [CarbPt + H]⁺ (dashed line). Structure labels are in bold, and relative free energies are in kcal mol⁻¹.

Production of [CarbPt + H]⁺ and [Carnosine + H]⁺. From the fragmentation of precursor ion [Carnosine + CarbPt + H]⁺, it is possible to generate both [Carnosine + H]⁺ and [CarbPt + H]⁺ ions. The calculated pathways to produce such ions are shown in Figure 9. The structures of intercepted stationary points are depicted in the same Figure 9, whereas their Cartesian coordinates are reported in the SI. Conversion of the conformer **1A** into **1B** is followed by dissociation of the latter to produce the combinations [Carnosine + H]⁺ and CarbPt or [CarbPt + H]⁺ and carnosine through the transition states **TS**(1B→CarH⁺) and **TS**(1B→CarbPtH⁺), which present barriers of 35.6 and 49.6 kcal mol⁻¹, respectively, relative to the minimum structure **1A** reference energy. Calculated energy barriers are consistent with the experimental findings. Overcoming the concerted transition state **TS**(1B→CarH⁺), in which the Pt−N bond with the imidazole ring is broken, the Pt−O bond with the carbonyl oxygen atom of the CBDCA COOH group is reestablished, and the hydrogen atom is transferred to the carnosine imidazole group, leads to formation of the combination Carnosine + H⁺ and neutral carboplatin, which is calculated to be exergonic by 1.7 kcal mol⁻¹ relative to structure **1A**. The final separated products, that is, the protonated carnosine fragment ion [(Carnosine + H]⁺ observed as the ion cluster centered around m/z 227 and the neutral carboplatin complex, are, instead, less stable than the **1A** minimum by 15.9 kcal mol⁻¹. The outcomes of our computational analysis show that the fragment ion [(Carnosine + H]⁺ production is the lowest-energy process, involving the lowest activation energy barrier calculated here. Overcoming the barrier relative to the transition state **TS**(1B→CarbPtH⁺), calculated to be 49.6 kcal mol⁻¹ higher in energy than structure **1A**, neutral carnosine is eliminated by breaking the Pt−N bond with the imidazole ring. The most relevant feature of the formed adduct, which is destabilized by 35.6 mol⁻¹ with respect to the **1A** minimum energy, is the interaction between the T-shaped protonated carboplatin complex and the lost carnosine ligand. Indeed, the final separated products, protonated carboplatin and neutral carnosine, because of the lack of any stabilizing interaction, lie 66.8 kcal mol⁻¹ above the reference energy of **1A**. A lot of

attempts aimed at intercepting a different transition state and a tetracoordinated minimum have systematically failed.

4. CONCLUSIONS

DFT calculations at the B3LYP/LANL2DZ level have been carried out to describe the free-energy pathways, leading to the formation of the observed fragmentation products due to the CID of the protonated carnosine−carboplatin complex, [Carnosine + CarbPt + H]⁺. Structural information and relative free energies for all intercepted stationary points, which account for all of the experimental findings, are reported. The most stable conformer **1A** of the [Carnosine + CarbPt + H]⁺ complex is relatively rigid because of the presence of three internal hydrogen bonds. Consequently, the first step of all of the examined pathways is the interconversion of **1A** into a less stable and more flexible conformer **1B**. From such a precursor ion, the two combinations CarbPt and [Carnosine + H]⁺ or Carnosine and [CarbPt + H]⁺ can be directly produced via transition states that are calculated to be 35.5 and 49.6 kcal mol⁻¹, respectively, higher in free energy than structure **1A**. Formation of the [Carnosine + H]⁺ ion from [Carnosine + CarbPt + H]⁺ appears to be the lowest-energy process, as confirmed by calculations that show generation of the protonated carnosine ion and neutral carboplatin to involve the lowest energy barrier calculated here. Although not hindered by a high activation barrier, the [CarbPt + H]⁺ ion generation is calculated to be very unfavorable from a thermodynamic point of view.

At slightly higher collision energies, the fragmentation can proceed via the loss of neutral ammonia from **1B** to give the fragment ion [Carnosine + (CarbPt − NH₃) + H]⁺ corresponding to the observed ion cluster centered around m/z 581. Both NH₃ molecules in the cis and trans positions to the CBDCA moiety of carboplatin can be eliminated. Once elimination of the first NH₃ molecule takes place, the fragmentation process can continue with either elimination of the remaining second carboplatin NH₃ molecule, followed by the elimination of CO₂ from the COOH unit of the CBDCA moiety, or the elimination of a CO₂ molecule, followed by

elimination of the second remaining NH_3 molecule of carboplatin.

■ ASSOCIATED CONTENT

Ⓢ Supporting Information

The Supporting Information is available free of charge on the ACS Publications website at DOI: 10.1021/acs.inorgchem.5b00959.

Geometrical structures of stationary points intercepted along all of the fragmentation pathways, free-energy profile for the CO_2 release from the carnosine ligand, and Cartesian coordinates (Å) and absolute energies (hartrees) of all optimized structures (PDF)

■ AUTHOR INFORMATION

Corresponding Authors

*E-mail: siciliae@unical.it.
*E-mail: t.shoeib@aucegypt.edu.

Notes

The authors declare no competing financial interest.

■ ACKNOWLEDGMENTS

■ REFERENCES

(1) Rosenberg, B.; Van Camp, L.; Krigas, T. *Nature* **1965**, *205*, 698−699.

(2) Rosenberg, B. In *Cisplatin. Chemistry and Biochemistry of a Leading Anticancer Drug*; Lippert, B., Ed.; Verlag Helvetica Chimica Acta: Zurich, Switzerland, 1999; Part 4, p 3.

(3) Cohen, S. M.; Lippard, S. J. *Progress in Nucleic Acids Research and Molecular Biology* **2001**, *67*, 93−130.

(4) Alderden, R. A.; Hall, M. D.; Hambley, T. W. *J. Chem. Educ.* **2006**, *83*, 728.

(5) Hambley, T. W. *Coord. Chem. Rev.* **1997**, *166*, 181−223.

(6) Wong, E.; Giandomenico, C. M. *Chem. Rev.* **1999**, *99*, 2451−2466.

(7) Boulikas, T.; Pantos, A.; Bellis, E.; Christofis, P. *Cancer Therapy* **2007**, *5*, 537−583.

(8) Reedijk, J. *Pure Appl. Chem.* **2011**, *83*, 1709−1719.

(9) Clarke, M. J.; et al. *Chem. Rev.* **1999**, *99*, 2511−2533.

(10) Peacock, A. F. A.; Sadler, P. J. *Chem. - Asian J.* **2008**, *3*, 1890−1899.

(11) Barnard, P. J.; Berners-Price, S. J. *Coord. Chem. Rev.* **2007**, *251*, 1889−1902.

(12) Bruijnincx, P. C. A.; Sadler, P. J. *Curr. Opin. Chem. Biol.* **2008**, *12*, 197−206.

(13) Monneret, C. *Ann. Pharm. Fr.* **2011**, *69*, 286−295.

(14) Kelland, L. *Nat. Rev. Cancer* **2007**, *7*, 573−584.

(15) Rose, W. C.; Schurig, J. E. *Cancer Treat. Rev.* **1985**, *12*, 1−19.

(16) Harrap, K. R. *Cancer Treat. Rev.* **1985**, *12*, 21−33.

(17) Knox, R. J.; Friedlos, F.; Lydall, D. A.; Roberts, J. J. *Cancer Res.* **1986**, *46*, 1972.

(18) Van der Vijgh, W. J. F. *Clin. Pharmacokinet.* **1991**, *21*, 242.

(19) Di Pasqua, A. J.; Goodisman, J.; Kerwood, D. J.; Toms, B. B.; Dubowy, R. L.; Dabrowiak, J. C. *Chem. Res. Toxicol.* **2006**, *19*, 139.

(20) Frey, U.; Ranford, J. D.; Sadler, P. J. *Inorg. Chem.* **1993**, *32*, 1333.

(21) Brandšteterová, E.; Kiss, F.; Chovancova, V.; Reichelova, V. *Neoplasma* **1991**, *38*, 415.

(22) Miller, S. E.; Gerard, K. J.; House, D. A. *Inorg. Chim. Acta* **1991**, *190*, 135.

(23) Jamieson, E. R.; Lippard, S. J. *Chem. Rev.* **1999**, *99*, 2467−2498.

(24) Tewey, K. M.; Chen, G. L.; Nelson, E. M.; Liu, L. F. *J. Biol. Chem.* **1984**, *259*, 9182−9187.

(25) Johnstone, T. C.; Park, G. Y.; Lippard, S. J. *Anticancer Res.* **2014**, *34*, 471−476.

(26) Gulewitsch, W.; Amiradzibi, S. *Ber. Dtsch. Chem. Ges.* **1900**, *33*, 1902−1903.

(27) Severina, I.; Bussygina, O.; Pyatakova, N. *Biochemistry-Moscow* **2000**, *65*, 783−788.

(28) Kohen, R.; Yamamoto, Y.; Cundy, K.; Ames, B. *Proc. Natl. Acad. Sci. U. S. A.* **1988**, *85*, 3175−3179.

(29) Gariballa, S. E.; Sinclair, A. J. *Age and Aging* **2000**, *29*, 207−210.

(30) Horning, M.; Blakemore, L.; Trombley, P. *Brain Res.* **2000**, *852*, 56−61.

(31) Nino, M.; Iovine, B.; Santoianni, P. *J. Cosmet., Dermatol. Sci. Appl.* **2011**, *1*, 177.

(32) Boldyrev, A. A. *Biochemistry (Mosc)* **2000**, *65*, 751−756.

(33) Guiotto, A.; Calderan, A.; Ruzza, P.; Borin, G. *Curr. Med. Chem.* **2005**, *12*, 2293−2315.

(34) Smith, E. C. *J. Physiol.* **1938**, *92*, 336−343.

(35) Baran, E. J. *Biochemistry (Mosc)* **2000**, *65*, 789−797.

(36) Nadi, N. S.; Hirsch, J. D.; Margolis, F. L. *J. Neurochem.* **1980**, *34*, 138−146.

(37) Kovacs-Nolan, J.; Mine, Y. *Animal Muscle-Based Bioactive Peptides*; Wiley-Blackwell: Hoboken, NJ, 2010; pp 225−231.

(38) Moustafa, E. M.; Camp, C. L.; Youssef, A. S.; Amleh, A.; Reid, H. J.; Sharp, B. L.; Shoeib, T. *Metallomics* **2013**, *5*, 1537−1546.

(39) Moustafa, E. M.; Ritacco, I.; Sicilia, E.; Russo, N.; Shoeib, T. *Phys. Chem. Chem. Phys.* **2015**, *17*, 12673−12682.

(40) Becke, A. D. *J. Chem. Phys.* **1993**, *98*, 5648−5652.

(41) Lee, A.; Yang, W.; Parr, R. G. *Phys. Rev. B: Condens. Matter Mater. Phys.* **1988**, *37*, 785−789.

(42) Becke, D. *Phys. Rev. A: At., Mol., Opt. Phys.* **1988**, *38*, 3098−3100.

(43) Hay, P. J.; Wadt, W. R. *J. Chem. Phys.* **1985**, *82*, 270−283.

(44) Wadt, W. R.; Hay, P. J. *J. Chem. Phys.* **1985**, *82*, 284−298.

(45) Hay, P. J.; Wadt, W. R. *J. Chem. Phys.* **1985**, *82*, 299−310.

(46) Yongye, A. B.; Giulianotti, M. A.; Nefzi, A.; Houghten, R. A.; Martinez-Mayorga, K. J. *J. Comput.-Aided Mol. Des.* **2010**, *24*, 225−235.

(47) Abdel-Ghani, N. T.; Mansour, A. M. *Eur. J. Med. Chem.* **2012**, *47*, 399−411.

(48) Wysokiński, R.; Michalska, D. *J. Comput. Chem.* **2001**, *22*, 901−912.

(49) Giese, B.; Deacon, G. B.; Kuduk-Jaworska, J.; McNaughton, D. *Biopolymers* **2002**, *67*, 294−297.

(50) Shore, T. C.; Mith, D.; DePrekel, D.; McNall, S.; Ge, Y. *React. Kinet., Mech. Catal.* **2013**, *109*, 315−333.

(51) Vacher, A.; Barrière, F.; Camerel, F.; Bergamini, J. F.; Roisnel, T.; Lorcy, D. *Dalton Trans.* **2013**, *42*, 383−394.

(52) Holmes, R. J.; O'Hair, R. A. J.; McFadyen, W. D. *Rapid Commun. Mass Spectrom.* **2000**, *14*, 2385−2392.

(53) Pazderski, L.; Tousek, J.; Sitkowski, J.; Malinakova, K.; Kozerski, L.; Szlyk, E. *Magn. Reson. Chem.* **2009**, *47*, 228−238.

(54) Moldovan, N.; Lönnecke, P.; Silaghi-Dumitrescu, I.; Silaghi-Dumitrescu, L.; Hey-Hawkins, E. *Inorg. Chem.* **2008**, *47*, 1524−1531.

(55) Moustafa, E. M.; Korany, M.; Mohamed, N. A.; Shoeib, T. *Inorg. Chim. Acta* **2014**, *421*, 123−135.

(56) Navarro, J. A. R.; Romero, M. A.; Salas, J. M.; Quiros, M.; El Bahraoui, J.; Molina, J. *Inorg. Chem.* **1996**, *35*, 7829−7835.

(57) Rajeev, R.; Sunoj, R. B. *Dalton Trans.* **2012**, *41*, 8430−8440.

(58) Ritacco, I.; Moustafa, E. M.; Sicilia, E.; Russo, N.; Shoeib, T. *Dalton Transactions* **2015**, *44*, 4455−4467.

(59) Fukui, K. *J. Phys. Chem.* **1970**, *74*, 4161−4163.

(60) Gonzalez, C.; Schlegel, H. B. *J. Chem. Phys.* **1989**, *90*, 2154−2161.

(61) Frisch, M. J.; Trucks, G. W.; Schlegel, H. B.; Scuseria, G. E.; Robb, M. A.; Cheeseman, J. R.; Scalmani, G.; Barone, V.; Mennucci, B.; Petersson, G. A.; Nakatsuji, H.; Caricato, M.; Li, X.; Hratchian, H. P.; Izmaylov, A. F.; Bloino, J.; Zheng, G.; Sonnenberg, J. L.; Hada, M.;

Ehara, M.; Toyota, K.; Fukuda, R.; Hasegawa, J.; Ishida, M.; Nakajima, T.; Honda, Y.; Kitao, O.; Nakai, H.; Vreven, T.; Montgomery, J. A., Jr.; Peralta, J. E.; Ogliaro, F.; Bearpark, M.; Heyd, J. J.; Brothers, E.; Kudin, K. N.; Staroverov, V. N.; Kobayashi, R.; Normand, J.; Raghavachari, K.; Rendell, A.; Burant, J. C.; Iyengar, S. S.; Tomasi, J.; Cossi, M.; Rega, N.; Millam, J. M.; Klene, M.; Knox, J. E.; Cross, J. B.; Bakken, V.; Adamo, C.; Jaramillo, J.; Gomperts, R.; Stratmann, R. E.; Yazyev, O.; Austin, A. J.; Cammi, R.; Pomelli, C.; Ochterski, J. W.; Martin, R. L.; Morokuma, K.; Zakrzewski, V. G.; Voth, G. A.; Salvador, P.; Dannenberg, J. J.; Dapprich, S.; Daniels, A. D.; Farkas, Ö.; Foresman, J. B.; Ortiz, J. V.; Cioslowski, J.; Fox, D. J. *Gaussian 09*, revision D.01; Gaussian, Inc.: Wallingford, CT, 2009.

CHAPTER IV

Platinum Complexes Hydrolysis

Introduction

Cisplatin, carboplatin and oxaliplatin are platinum-based drugs used for the treatment of various human cancers. They are square-planar d^8 Pt(II) complexes triggering cancer cell death by binding to nuclear DNA and distorting its structure [1]. Such complexes are administered intravenously, and remain in their neutral form in the bloodstream and extracellular medium. The cellular uptake occurs by passive diffusion across the membrane or actively by membrane transport proteins. Inside the cell, the sudden decrease in the chloride concentration from ~100mM to ~4mM causes hydrolysis and chloride dissociation to form the activated corresponding aquated complexes. Such positively charged complexes interact with the negatively charged DNA and form stable adducts at the N7 positions of purine bases, in particular guanine. Because platinum(II) anticancer drugs contain two labile ligands, they can form bifunctional adducts. These adducts distort DNA such that polymerases are stalled at the site of platination, resulting in an interruption of replication and transcription that ultimately triggers the cascade of events involved in apoptosis or cell-death [2-4]. Computational studies have complemented experimental efforts to understand almost every step of the mode of action of platinum(II) drugs, from hydrolysis needed to activate the drug to the binding of repair

proteins with the final adducts. In particular, many theoretical studies, mostly using DFT methods, have been devoted to the elucidation of the various aspects of the cisplatin activation process by aquation [5]. Much information on the structure of transition states for the substitution of chloride ligands with water, and on the structure of intermediates formed after hydrolysis have been supplied by these studies. However, on a quantitative level, the computed relative free energies for the transition states and products in these reactions have been, very often, only in modest agreement with experiment. In order to understand what should be the cause of such poor agreement, we have undertaken a systematic investigation of the cisplatin drug hydrolysis step to explore the agreement between experiment and theory for the reactivity and the equilibrium between the starting species and the products, in comparison also with previous theoretical studies. The results are reported in **paragraph 4.2** (manuscript in preparation).

Despite the widespread use of these drugs, the Pt(II)-based anticancer drugs present many disadvantages. For example, they can generate undesirable reactions with thiol group on proteins present in the plasma causing the deactivation of the drugs and making them toxic. Furthermore, the oral administration is limited because a large amount of Pt(II) prodrugs is lost in bloodstream before arriving at the ultimate target [6]. To

overcome these drawbacks a number of new methods are being investigated including the use of prodrugs with platinum in IV oxidation state [7-12].

These compounds are obtained by adding the axial ligands to the platinum(II) complexes through oxidative addition. Pt(IV) has a low-spin d^6 electronic configuration and exhibits octahedral geometry. This configuration makes the platinum(IV) complexes more inert than platinum(II) complexes, so they result to be more stable in biological fluids. Consequently, the reactions with biomolecules are reduced and undesired side-effects are minimized. For these reasons, the platinum(IV) complexes may reach the cellular target without prior transformation and are considered to be less toxic than platinum(II) complexes. Due to these characteristics, the platinum(IV) complexes may be administered orally.

Inside cancer cells, the Pt(IV) prodrugs can be activated selectively by reduction, releasing the axial ligands and the real drugs, that is the platinum(II) complexes. The axial ligands are also designed to increase the pharmacological properties of the prodrugs. The axial ligands mainly present in platinum(IV) prodrugs are chlorido, hydroxido or carboxylato groups [13,14]. For example, the most successful orally active Pt(IV) antitumor drug, satraplatin (JM216) has two axial acetato ligands [15].

A recent study carried out by Gibson's group [16], however, has demonstrated that Pt(IV) derivatives of cisplatin, carboplatin and oxaliplatin with acetato and haloacetato ligands, considered inert, are not very stable in biologically conditions (37 °C and neutral pH) and can undergo rapid hydrolysis. Furthermore, additional studies confirm that the platinum(IV) complexes hydrolysis could be facilitated by acidic or basic conditions. In this case, the hydrolysis could be considered as a possible prodrug activation step that precedes the reduction step [15-17,18].

4.1 Aim of the study

In this Chapter, a detailed DFT computational analysis of the first hydrolysis mechanism of cisplatin has been carried out along with implicit and hybrid explicit/implicit treatment of solvation, as well as highly accurate coupled-cluster methods to provide benchmark energetics. Outcomes have been compared with previous theoretical works performed employing several computational strategies (**paragraph 4.2**). The hydrolysis reaction for a series of Pt(IV) derivatives of cisplatin, carboplatin and oxaliplatin with acetato and haloacetato ligands has been carried out as well together with the description of the corresponding energy profiles aiming at probing their stability in biological fluids. The obtained results have been compared with

the experimental data by Gibson and coworkers (**Paper IV**). In the **Paper IV**, for the Pt(IV) derivative of cisplatin having two axial chlorido ligands the energy profiles for the hydrolysis in axial and equatorial positions and the hydrolysis mechanism assisted by Pt(II), as proposed by Basolo and coworkers [19,20] have been investigated.

Furthermore, the influence that the acidity of the biological environment can have on the activity of platinum(IV) prodrugs complexes having two carboxylates as axial ligands, in particular satraplatin, has been theoretically investigated by means of DFT (**Paper V**). In this paper, the fragmentation mechanisms of protonated satraplatin have been also investigated. The theoretical results have been compared with the experimental ones obtained by electrospray ionization mass spectrometry.

4.2 Hydrolysis of Platinum Compounds: Insights into Reactivity from Accurate Ab Initio Calculations (Manuscript in preparation).

For many anticancer drugs, in particular for cisplatin and its derivatives, the activation step coincides with the hydrolysis step. In the past, several theoretical studies about the hydrolysis mechanism have been carried out using DFT methods [5]. However, due to the modest agreement with experiment of the

computed relative free energies for the transition states and products in these reactions, in order to obtain more accurate energetics several strategies have been adopted. In some cases, for example, activation free energies have been calculated relative to incorrect reference points such as the hydrogen-bonded addition complex between the platinum drug and a water molecule [21]. In other cases, to take into account the entropy change in going from the gas to the condensed phase, somewhat arbitrary correction schemes of the entropy of the reacting species have applied.[22] For these reasons, it is not possible to establish whether the modest agreement between experiment and theory is due to the incorrect description of the solute entropy terms, the solvation free energy, the reference point in the reaction, or the level of electronic structure theory used.

With the purpose to give a contribution to the understanding of the reasons that do not allow a better agreement between measured an calculated energy values, in this study, the cisplatin hydrolysis step has been theoretically investigated by employing CCSD(T) and DFT methods. Furthermore, explicit water molecules in the optimization of the various species have been included, in order to consider all the possible weak interactions between the platinum drug and water molecules, and statistical computing techniques to minimize errors resulting from solvation have been used. The hydrolysis reaction of cisplatin

$$Pt(NH_3)_2Cl_2 + H_2O \rightleftarrows Pt(NH_3)_2Cl(OH_2)^+ + Cl^-$$

can be written as:

$$A + B \rightleftarrows C + D$$
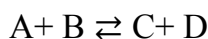
Solvation of the two species A and B with n=(l+m) water molecules (W), can be realized in different ways depending on the number of used water molecules, as it is shown in the next scheme:

A·Wl+B·Wm

A·Wm+B·Wl

A·W(m+l)+B

A+B·Wm+l·W

….
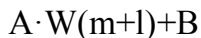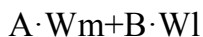
The same scheme could be applied to the C and D species.

If the continuum model works correctly, then all the possible forms should have the same free energy and the calculation of the C+D relative energy should be independent on the n+l values. As it is well known that the continuum model does not work properly, it is needed to apply correction schemes following some rules to minimize the error. The rules adopted by us are listed below:

a) n=(l+m) must be small;

b) the most strongly charged sites have to be solvated;

c) where possible, only free energies differences between species with the same total number of microsolvates have to be considered;

d) for a given state and a given n, the lowest free energy situation should be selected because the continuum model underestimates free energy of solvation for some strongly solvated species. Then, a lower free energy state with microsolvation should be somehow better.

DFT calculations have been performed employing the B3LYP and dispersion corrected [23] B3LYP-D3BJ functionals and 6-31+G* and 6-311+G** basis sets, respectively for all the atoms along with the relativistic compact Stuttgart/Dresden effective core potential in conjunction with the split valence for Pt. Such levels of theory will be indicated as B3LYP/6-31+G* and B3LYP-D3BJ/6-311+G**. Subsequently, to provide benchmark energetics CCSD(T)//B3LYP/6-31+G* calculations have been performed. The impact of solvation effects on the energy profiles has been estimated by using the Solvation Model based on Density (SMD) [24]. The results obtained adding a number n of explicit molecules from 1 to 4 are collected in Table 1. As explained above, among all the possible states for both reactants and product that at lower free energy has been selected. This approach allows identifying the proper reference state for the

calculation of relative energies. As can be inferred from the data in Table 1, both the reactants' reference state and the most stable products' state change as a function of the adopted computational protocol and the number of explicit water molecules.

The hydrolysis reaction proceeds by one step S_N2 mechanism and the relevant TS for the displacement of the chloride ligand by a water molecule adopts the shape of a substantially distorted trigonal bipyramid with significantly elongated bonds with the leaving and entering ligands. Activation free energy and reaction free energy for the first Pt-Cl bond hydrolysis calculated adopting the different computational approaches illustrated above and choosing the lower energy state for both reactants and products are collected in Table 2 and compared with the results obtained by previous theoretical investigations [21,22,25] and experimental values [26,27].

Table 1. Relative energies (in kcal mol^{-1}) with respect to the reactants'
lowest free energy state for all the microsolvated states of reactants and
products.

	B3LYP/ 6-31+G* SMD	CCSD(T)//B3LYP- 6-31+G* SMD	B3LYP-D3BJ/ 6-311+G* SMD
cisPt+H_2O	0.0	0.0	0.0
cisPt·H_2O	2.1	-4.8	-2.1
TS-Cl+H_2O	26.0	23.2	22.7
cisPt(OH_2)·Cl$^-$	7.2	3.4	3.9
cisPt(OH_2)+Cl$^-$	7.0	15.3	112.8
cisPt(OH_2)+($H2O$·Cl$^-$)	-3.2	-7.4	2.4
cisPt+2H_2O	-2.1	4.8	2.1
cisPt·H_2O +H_2O	0.0	0.0	0.0
cisPt·2H_2O	3,1	-5.7	-2.3
TS-Cl+H_2O·H_2O	25,1	23.0	21.9
cisPt(OH_2)·H_2O·Cl$^-$	8.0	5.0	3.7
cisPt(OH_2)·H_2O+Cl$^-$	6.1	14.6	14.9
cisPt(OH_2)·H_2O+($H2O$·Cl$^-$)	-5.3	-2.6	4.5
cisPt(OH_2)+H_2O+Cl$^-$	4.9	20.1	114.9
cisPt+3H_2O	-5.1	10.5	4.5
cisPt·H_2O+2H_2O	-3.1	5.7	2.3
cisPt·2H_2O+H_2O	0.0	0.0	0.0
cisPt·3H_2O	-1.1	-6.2	-4.7
TS-Cl+H_2O·H_2O	23.9	23.7	21.3
cisPt(OH_2)·2H_2O·Cl$^-$	5.3	4.9	3.2
cisPt(OH_2)·2H_2O+Cl$^-$	5.4	16.7	15.9
cisPt(OH_2)·2H_2O+($H2O$·Cl$^-$)	-8.3	3.0	6.8
cisPt(OH_2)+2H_2O+Cl$^-$	1.9	25.8	117.2
cisPt+4H_2O	-4.0	16.7	9.1
cisPt·H_2O+3H_2O	-1.9	11.9	7.0
cisPt·2H_2O+2H_2O	1.1	6.2	4.7
cisPt·3H_2O+H_2O	0.0	0.0	0.0
cisPt·4H_2O	4.3	-4.0	-0.8
TS-Cl+H_2O·H_2O	26.7	23.1	23.0
cisPt(OH_2)·3H_2O·Cl$^-$	13.9	9.5	3.8
cisPt(OH_2)·3H_2O+Cl$^-$	6.6	15.8	17.7
cisPt(OH_2)·3H_2O+($H2O$·Cl$^-$)	-7.2	9.3	11.5
cisPt(OH_2)+3H_2O+Cl$^-$	3.0	32.0	121.9

An inspection of Table 2 shows that the better agreement between theoretical values and experiment is obtained when the structures are optimized using the B3LYP-D3BJ/6-311+G** approach, whereas the inclusion into the model of two water molecules is enough for a good reproduction of the experimental values. The agreement with experiment is, instead, poor when CCSD(T) single point calculations are carried out on B3LYP optimized geometries.

The cisplatin-water complex may be viewed as a model system that can be treated by using accurate *ab initio* methods and a comparative study can provide a guide for theoretical investigations on larger transition metal containing drugs, where due to the required computational effort more modest theoretical approaches have to be used.

Table 2. Activation and reaction free energies (in kcal mol^{-1}) calculated selecting the lowest free energy state for both reactants and products compared with previous theoretical and experimental values

|	ΔE_a (kcal/mol)	ΔG_r (kcal/mol)
B3LYP/6-31+G*(SMD)	23.9 (cisPt+H_2O) 22.0 (cisPt+$2H_2O$) 25.0 (cisPt+$3H_2O$) 22.4 (cisPt+$4H_2O$)	-3.2 (cisPt+H_2O) -5.3 (cisPt+$2H_2O$) -8.3 (cisPt+$3H_2O$) -7.2 (cisPt+$4H_2O$)
CCSD(T)// B3LYP-6-31+G*(SMD)	28.0 (cisPt+H_2O) 28.7 (cisPt+$2H_2O$) 29.9 (cisPt+$3H_2O$) 27.1 (cisPt+$4H_2O$)	-7.4(cisPt+H_2O) -2.6 (cisPt+$2H_2O$) 3.0 (cisPt+$3H_2O$) 9.3 (cisPt+$4H_2O$)
B3LYP-D3/6-311+G*(SMD)	24.8 (cisPt+H_2O) 24.2 (cisPt+$2H_2O$) 26.0 (cisPt+$3H_2O$) 23.8 (cisPt+$4H_2O$)	3.9 (cisPt+H_2O) 3.7 (cisPt+$2H_2O$) 3.2 (cisPt+$3H_2O$) 3.8 (cisPt+$4H_2O$)
[a]B3LYP/6-31G**(PB)	24.9	0.1
[b]CCSD(T)//B3LYP-6-31++G**(COSMO)	22.7	6.7
[c]SCIPCM//B3P86-6-31G*	21.3	1.5
[d,e]Experimental data	23.8; 24.1	4.2; 3.6

[a]Ref.22
[b]Ref.25
[c]Ref.21
[d]Ref.26
[e]Ref.27

4.3 Investigation of the inertness to hydrolysis of platinum(IV) prodrugs (Paper IV).
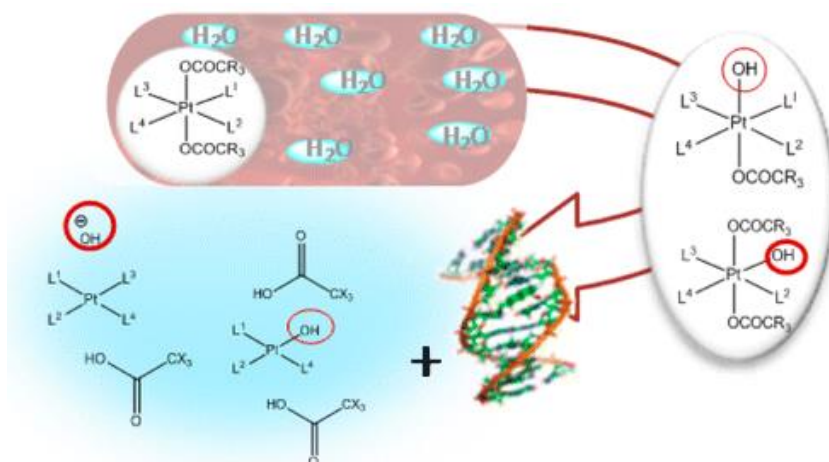
Platinum(IV) complexes are an important class of compounds that can act as pro-drugs. If correctly designed, they are more inert and consequently less toxic than platinum(II) complexes. Recently, it has been demonstrated [16] that the inertness of the platinum(IV) complexes depends on the electron withdrawing power of axial ligands. So, the presence of axial ligands strongly electron-withdrawing should make the platinum(IV) complexes less stable in biological fluids and consequently less prone to undergo chemical transformations before reaching the final target, that is the cancer cell.

The hydrolysis reaction of some platinum(IV) complexes, derivatives of cisplatin, carboplatin and oxaliplatin containing acetato (Ac), monochloroacetato (MCA), dichloroacetato (DCA)

and trifluoroacetato (TFA) ligands in axial positions has been studied aiming at probing their stability in biological fluids. For each Pt(IV) derivate having two axial carboxylato ligands, two hydrolysis mechanisms in axial position have been investigated, that is direct substitution of the axial ligand by water and attack to the carbonyl accompanied by deprotonation that can be or not assisted by the coordinated amine. Results show that the direct attack on the Pt center is the preferred mechanism. For these complexes also hydrolysis of equatorial chlorido ligands has been examined.

Furthermore, in the case of cisplatin with two chlorido ligands in axial position, axial and equatorial hydrolysis has been investigated. For this complex, Hambley and coworkers [28] have also reported that the addition of small amounts of the Pt(II) complex increases the rate of the reaction. So, the hydrolysis reaction of the cis-Pt(Cl)$_2$ complex has been theoretically investigated using the mechanism proposed by Basolo and Pearson [19,20].

From the potential energy surfaces (PES) reported in the **Paper IV** it is evident that the axial and equatorial hydrolysis of the Pt(IV) derivates takes place by means of an associative mechanism and that these complexes are, in general, more inert than the corresponding Pt(II) drugs even if inertness is lower

than expected. Furthermore, the hydrolysis reactions are influenced by both the axial and equatorial ligands.

In order to elucidate the hydrolysis reaction for platinum(IV) complexes Density Functional Theory (DFT) calculations have been performed employing the B3LYP functional. For Pt the relativistic compact Stuttgart/Dresden effective core potential has been used in conjunction with the split valence basis set. The standard 6-311+G** basis sets of Pople and co-workers have been employed for all atoms. The impact of solvation effects on the energy profiles has been estimated by using the Tomasi's implicit Polarizable Continuum Model (PCM) and the UFF set of radii has been used to build-up the cavity.

4.4 Hydrolysis in acidic environment and degradation of satraplatin: a joint experimental and theoretical investigation (Paper V)
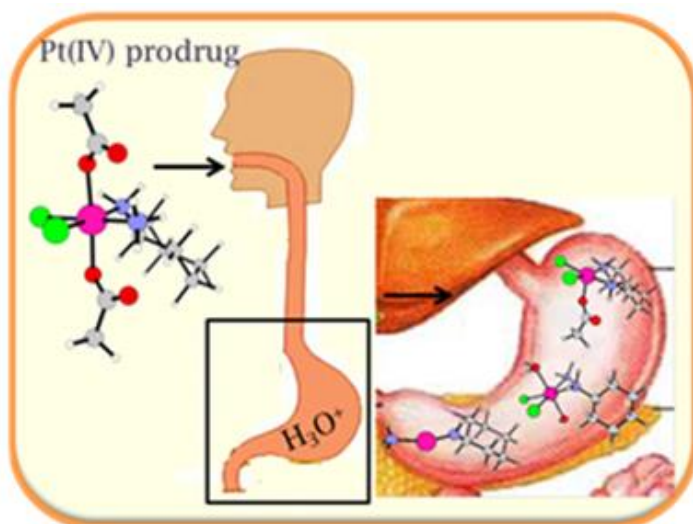
Satraplatin was the first platinum prodrug to be administered orally [29,15a]. This platinum(IV) complex is highly lipophilic and stable in biological fluids. These features favor cellular accumulation of the drug [30] and increase its oral bioavailability. Like all platinum(IV) complexes, inside cancer cells satraplatin is reduced to platinum(II) by loss of the two acetate ligands in axial position.

Generally, the prodrugs administered orally pass through the acidic environment ($1 \leq$ pH ≤ 3) of the stomach before being absorbed into the bloodstream. So, it is interesting to explore what should be the fate of these prodrugs in a very acidic environment. It is worth mentioning, however, that the study of platinum(IV) complexes hydrolysis in presence of the H_3O^+ ion is an idealization of the acidic environment of the stomach simulating a situation of very low pH.

In the **Paper V** DFT calculations have been carried out to understand if and how the acidic environment can influence the Pt(IV) prodrugs hydrolysis compared to neutral environment. Both a cisplatin derivative with axial acetato ligands and satraplatin have been examined. The results reported in this paper prove that the acidic hydrolysis of the above-mentioned prodrugs occurs faster than neutral hydrolysis. Work is in progress to examine how the presence of electron-withdrawing groups on axial carboxylato ligands and the introduction of

aliphatic carboxylato ligands with an increasing carbon atoms number in the chain can change the hydrolysis energy profile at different pH conditions.

Furthermore, the fragmentation mechanisms of the protonated satraplatin complex have been investigated through DFT calculations to rationalize the results of collision-induced dissociation experiments that prove how the first fragmentation step is the $[Sat + H - CH_3COOH]^+$ ion (445 m/z) formation by loss of protonated acetate ligand (CH_3COOH) in axial position. Subsequently, from this all the other fragments are generated. Experimental data are confirmed by theoretical investigations.

Anyway, the fragmentation profiles are useful for interpreting the protonation mechanisms and evolution of chemical species, but they are ideal pathways that concern charged molecules and which require high energy values.

Also in this case, for all calculations the Density Functional Theory (DFT) has been used, employing B3LYP functional. The relativistic compact Stuttgart/Dresden effective core potential for platinum and the standard 6-311+G** basis have been employed for all atoms. Solvation effects on the hydrolysis energy profiles has been estimated by using the Tomasi's implicit Polarizable Continuum Model (PCM) and the UFF set of radii has been used to build-up the cavity.

REFERENCES CHAPTER IV

[1] Siddik, Z. H., *Oncogene,* **2003**, 22, 7265−7279.

[2] Alberto, M. E., Butera, V., Russo, N., *Inorg. Chem.* **2011**, 50 (15), 6965-6971.

[3] Alderden, R. A., Hall, M. D., Hambley, T. W., *Journal of Chemical Education* **2006**, 83, 728-734.

[4] Lippert, B., *Cisplatin: Chemistry and Biochemistry of a Leading Anticancer Drug*, **1999,** Wiley-VCH, Weinheim, Zurich.

[5] Zhang, Y., Guo, Z., Zeng You, X., *J. Am. Chem. Soc.*, **2001**, *123* (38), 9378–9387.

[6] (a) Galluzzi, L., Senovilla, L., Vitale, I., Michels, J., Martins, I., Kepp, O., Castedo, M., Kroemer, G., *Oncogene*, **2012**, 31, 1869−1883. (b) Wexselblatt, E., Yavin, E., Gibson, D., *Inorg. Chim. Acta*, **2012**, 393, 75−83.

[7] Butler, J. S., Sadler, P. J., *Curr. Opin. Chem. Biol.*, **2013**, 17, 175− 188.

[8] Wexselblatt, E., Gibson, D., *J. Inorg. Biochem*., **2012**, 117, 220− 229.

[9] Farrell, N. P., *Curr. Top. Med. Chem*., **2011**, 11, 2623−2631.

[10] Montana, A. M., Batalla, C., *Curr. Med. Chem.*, **2009**, 16 (18), 2235−2260.

[11] Ang, W. H., Pilet, S., Scopelliti, R., Bussy, F., Juillerat-Jeanneret, L., Dyson, P. J., *J. Med. Chem.*, **2005**, 48, 8060−8069.

[12] Kelland, L. R., Sharp, S. Y., O'Neill, C. F., Raynaud, F. I., Beale, P. J., Judson, I. R., *J. Inorg. Biochem.,* **1999**, 77, 111−115.

[13] Platts, J. A., Ermondi, G., Caron, G., Ravera, M., Gabano, E., Gaviglio, L., Pelosi, G., Osella, D*., J. Biol. Inorg. Chem.*, **2011**, 16, 361−372.

[14] Gramatica, P., Papa, E., Luini, M., Monti, E., Gariboldi, M. B., Ravera, M., Gabano, E., Gaviglio, L., Osella, D., *JBIC, J. Biol. Inorg. Chem.*, **2010**, 15, 1157−1169.

[15] (a)Bhargava, A., Vaishampayan, U. N., *Expert Opin. Invest. Drugs*, **2009**, 18, 1787−1797. (b) Choy, H., *Expert Rev. Anticancer Ther.*, **2006**, 6, 973−982.

[16] (a)Wexselblatt, E., Yavin, E., Gibson, D., *Angew. Chem. Int.Ed.*, **2013**,52,6059−062. (b) Wexselblatt,E., Raveendran, R., Salameh, S., Friedman-Ezra, A., Yavin, E., Gibson, D., *Chem.- Eur. J.*, **2015**, 21, 3108−3114.

[17] Wojtkowiak, J. W., Verduzco, D., Schramm, K. J., Gillies R. J., *Mol. Pharmaceutics,* **2011**, *8*, 2032-2038.

[18] Avnet, S., Lemma, S., Cortini, M., Pellegrini, P., Perut, P., Zini, N., Kusuzaki, K., Chano, T., Grisendi, G., Dominici,

M., De Milito, A., Baldini, N., *Oncotarget*, **2016**, *7*, 63408-63423.

[19] Ellison, H. R., Basolo, F., Pearson, R. G., *J. Am. Chem. Soc.*, **1961**, 83, 3943−3948.

[20] Basolo, F., Morris, M. L., Pearson, R. G., *Discuss. Faraday Soc.*, **1960**, 29, 80−91.

[21] Chval, Z., Sip, M., *Journal of molecular structure: TEOCHEM*, **2000,** 532, 59-68.

[22] Lau, J. K-C., Deubel, D. V., *J. Chem. Theory Comput.*, **2006**, 2, 103-106.

[23] Grimme, S., Ehrlich, S., Goerigk, L., *J. Comp. Chem.*, **2011**, 32, 1456-1465.

[24] Marenich, A. V., Cramer, C. J., Truhlar, D. G., *J. Phys. Chem. B*, **2009**, 113(18), 6378-6396.

[25] Burda, J. V., Zeizinger, M., Leszczynski, J., *Journal of Computational Chemistry*, **2005**, 26, 907-914

[26] Coe, J. S., *MTP Int. Rev Sci: Inorg. Chem, Ser.2*, **1974**, 45.

[27] Perumareddi, J. R., Adamson, A. W., *J. Phys. Chem.*, **1978**, 72,414.

[28] Davies, M. S., Hall, M. D., Berners-Price, S. J., Hambley, T. W., *Inorg. Chem.*, **2008**, 47, 7673−7680.

[29] Kelland, L. R., Abel, G., McKeage, M. J., Jones, M., Goddard, P. M., Valenti, M., Murrer, B. A., Harrap, K. R., *Cancer Res.,* **1993**, 53, 2581-2586.

[30] Martelli, L., Di Mario, F., Ragazzi, E., Apostoli, P., Leone, R., Perego, P., Fumagalli, G., *Pharmacol.,* **2006**, 72, 693-700.

Paper IV

"Investigation of the inertness to hydrolysis of Platinum(IV) produgs"

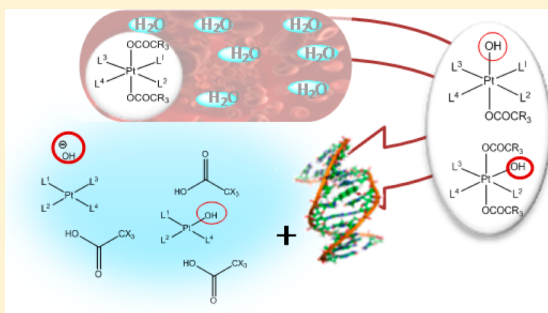Ida Ritacco, Gloria Mazzone, Nino Russo, Emilia Sicilia.

Investigation of the Inertness to Hydrolysis of Platinum(IV) Prodrugs

Ida Ritacco, Gloria Mazzone, Nino Russo, and Emilia Sicilia*

Department of Chemistry and Chemical Technologies, Università della Calabria, 87036 Arcavacata di Rende, CS, Italy

S Supporting Information

ABSTRACT: Platinum(IV) complexes are an important class of compounds that can act as prodrugs, and due to their inertness, if correctly designed, they could have low toxicity outside the cancer cell and improve the pharmacological properties of the platinum(II) anticancer agents that are currently used in the clinic. Because of the efforts that are concentrated on the use of axial ligands able to control the reduction potentials, lipophilicity, charge, selectivity, targeting, and cell uptake of the Pt(IV) complexes, we considered to be of interest to probe the inertness of such complexes that is assumed to be a fulfilled prerequisite. To this aim, a density functional theory computational analysis of the hydrolysis mechanism and the corresponding energy profiles for a series of Pt(IV) derivatives of cisplatin, carboplatin, and oxaliplatin with acetato, haloacetato, and chlorido ligands was performed to probe their stability in biological fluids. The heights of the barriers calculated along the hydrolysis pathways for the associative displacement of ligands both in axial and equatorial positions confirm that Pt(IV) complexes are, in general, more inert than the corresponding Pt(II) drugs even if inertness is lower than expected. Some exceptions exist, such as derivatives of oxaliplatin for the hydrolysis in equatorial position. The nature of the axial ligands influences the course of the hydrolysis reaction even if a decisive role is played by the ligands in equatorial positions. The mechanism of the aquation in axial position of cisplatin Pt(IV) derivative with two chlorido axial ligands assisted by Pt(II) cisplatin was elucidated, and the calculated activation energy confirms the catalytic role played by the Pt(II) complex.

■ INTRODUCTION

Cisplatin, cis-diamminedichloroplatinum(II), was the first Pt-based drug used as an anti-proliferative agent and is well-known for its high level and broad spectrum of anticancer activity.[1] Since the discovery of the anticancer activity of cisplatin by Rosenberg in the 1960s,[2] a large number of anticancer Pt(II) drugs have been found,[3] but only a few of them are used in clinical therapy.[4] Three Pt(II)-based anticancer drugs are today used worldwide: cisplatin, carboplatin, and oxaliplatin, which are square-planar d[8] Pt(II) complexes triggering cancer cell death by binding to nuclear DNA and distorting its structure.[5] However, like for many cytotoxic agents, side effects of cisplatin and related Pt(II) complexes limit their clinical usefulness. Nephrotoxicity and ototoxicity represent some of the adverse side effects ascribed to undesirable interactions with thiol groups on proteins in plasma causing deactivation of the drugs. As a large amount of Pt(II) prodrugs is lost in bloodstream before arriving at the ultimate target the bioavailability is limited, and oral administration is precluded.[6]

To overcome such drawbacks a number of new methods are being investigated including the use of prodrugs with platinum in the more inert +IV oxidation state.[7−12] The administration of nontoxic Pt(IV) prodrugs that can be activated selectively by reduction at the tumor sites might reduce unwanted reactions with biomolecules and consequently minimize undesired side effects. Even oral administration becomes feasible, since in contrast to the quite reactive Pt(II), Pt(IV) compounds are more stable in biological fluids. Degradation in the gastro-

intestinal tract is thus less likely, and the Pt(IV) prodrugs may reach the cellular target without prior transformation. Pt(IV) has a low-spin d[6] electron configuration and exhibits octahedral geometry. This configuration is relatively inert to substitution; reactions with biological nucleophiles are thus disfavored compared to Pt(II) complexes, and the lifetime in biological fluids is expected to increase. It is not yet established, however, that Pt(IV) complexes survive long enough in vivo to be delivered to the tumor sites. As intracellular activation occurs by reductive elimination, the breaking of the bond with the ligands in axial position to yield the corresponding cytotoxic square-planar Pt(II) complexes is involved. Therefore, axial ligands can be designed to favorably influence pharmacological properties of the prodrug such as solubility in biological media, redox potential, targeting functionalities, and inhibition of reactions related to resistance to the drug. Many of the axial ligands proposed to tune Pt complexes pharmacological properties are tethered to the Pt(IV) center through carboxylates.[13,14] For example, the most successful orally active Pt(IV) antitumor drug to date, satraplatin (trans,cis,cis-bis(acetato)ammine-(cyclohexylamine) dichloridoplatinum-(IV), JM216) has two axial acetato ligands.[15] Reduction potential has been demonstrated to depend on the electron-withdrawing power of axial ligands, and this is assumed to be the reason why Pt(IV) complexes with axial trifluoroacetato

ligands are more potent than their analogues with acetato ones.[16] More recently several reports have appeared in the literature dealing with the anticancer activity of *cis,trans,cis*-[Pt(NH₃)₂(OCOCHCl₂)₂Cl₂], mitaplatin, a Pt(IV) derivative of cisplatin with two dichloroacetato moieties in the axial positions.[17]

Because of the great deal of attention devoted to the design of novel anti-neoplastic agents based on Pt(IV) prodrugs and the recent reports[18] that seem to contradict the consolidated knowledge on Pt(IV) chemistry, in the present paper a density functional theory (DFT) computational analysis of the hydrolysis mechanism and the corresponding energy profiles for a series of Pt(IV) derivatives of cisplatin, carboplatin, and oxaliplatin with acetato and haloacetato ligands was performed aiming at probing their stability in biological fluids. In particular, the results presented here can be compared with the experimental findings by Gibson and co-workers,[18d,e] who demonstrated that Pt(IV) complexes considered inert, having two axial haloacetato ligands, are not very stable in biologically relevant conditions (37 °C and neutral pH) and can undergo rapid hydrolysis. Furthermore, the same authors have demonstrated that Pt(IV) derivatives of oxaliplatin that contain one hydroxido ligand, obtained by hydrolysis, and one carboxylato ligand in the axial positions, are reduced by ascorbate much more rapidly than the Pt(IV) derivatives of oxaliplatin that possess two carboxylato axial ligands, despite having more negative reduction potentials. Thus, the rapid loss of the ligands alters the physicochemical properties of such complexes. Furthermore, the stationary points along the potential energy surfaces for the replacement of ligands in equatorial position by water have been intercepted. Finally, for the Pt(IV) derivative of cisplatin having two axial chlorido ligands the energy profiles for the hydrolysis in axial and equatorial positions and the hydrolysis mechanism assisted by Pt(II), as proposed by Basolo and co-workers,[19,20] were investigated. Indeed, it has been suggested that residual amounts of Pt(II) complexes, acting as catalysts, facilitate ligand exchange on octahedral Pt(IV) complexes.[19−21]

■ RESULTS AND DISCUSSION

A systematic examination of the hydrolysis reaction for all the Pt(IV) complexes, shown in Scheme 1, was undertaken. The

Scheme 1

X= -OCOCH₃, -OCOCH₂Cl, -OCOCHCl₂, -OCOCF₃
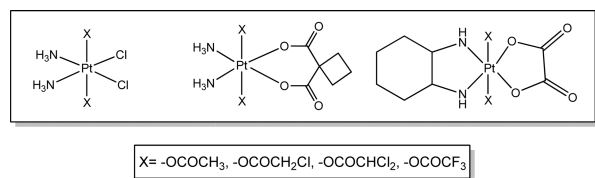
complexes are derivatives of cisplatin, carboplatin, and oxaliplatin containing acetato (Ac), monochloroacetato (MCA), dichloroacetato (DCA), and trifluoroacetato (TFA) ligands in axial positions. In addition, for cisplatin also the Pt(IV) derivative with two chlorido axial ligands was studied. Calculations were performed employing the hybrid B3LYP[22] exchange-correlation functional for a reliable comparison with the outcomes of previous investigations dealing with cisplatin hydrolysis reactions.[23]

Nevertheless, the dispersion-corrected functional B3LYP-D3[24] was used to perform additional calculations to prove whether weak interactions could influence the energetics of the studied process. Since the examined barrier heights changed only slightly and the trends remained unchanged results are not reported here. Two alternative suggested mechanisms[18d] for the hydrolysis of Pt(IV) derivatives having two axial carboxylato ligands have been explored as shown in Scheme 2, that is (a) direct substitution of the axial ligand by water and attack to the carbonyl accompanied by deprotonation that can be or not assisted by the coordinated amine. These two last alternatives are labeled (b) in the latter case and (b′) in the former. B3LYP free-energy profiles, calculated by including water solvent effects, for the hydrolysis of Pt(IV) derivative of cisplatin with two TFA axial ligands are drawn in Figure 1. The sum of complex and water reactants free energies is set to zero for the calculation of relative free energies that are expressed in kilocalories per mole. Hydrolysis of both axial TFA and equatorial chlorido ligands is reported, and for the hydrolysis in axial position all the mechanistic alternatives shown in Scheme 2 were investigated. Fully optimized structures of minima and transition states intercepted along the reported pathways are shown in Figure 1.

Complete geometries can be found in the Supporting Information (Table S1). The interaction of the entering water molecule with the Pt(IV) complex, named cisPt(TFA)₂ + H₂O, leads to the formation of the first cisPt(TFA)₂_H₂O intermediate, which is more stable than reactants by 9.5 kcal mol⁻¹. A hydrogen bond is formed by the water molecule with an amine H atom (1.836 Å). The direct coordination to the Pt center takes place overcoming a free-energy barrier of 34.2 kcal mol⁻¹ corresponding to the transition state TS1$_{cisPt(TFA)_2}$ for the associative displacement of the ligand. The imaginary frequency that confirms the nature of this stationary point is calculated to be 155.3i cm⁻¹ and corresponds to the concerted Pt−O$_{TFA}$ bond breaking, Pt−O$_{H_2O}$ bond forming, and proton transfer from water to trifluoroacetato. All the attempts to intercept minima and transition states corresponding to a dissociative mechanism were unsuccessful. Analogous results were obtained for all the Pt(IV) complexes under investigation. It is worth underlining that additional calculations including explicit water solvent molecules were executed to check the influence of their presence on the mechanism. The outcomes of such calculations clearly showed that, although hydrogen bonds are established among the explicit water molecules, the mechanism continues to be the same. One of the included water molecules attacks the Pt center displacing the ligand in an associative way. Also the energetics of the process is only a little altered by the inclusion of additional solvent molecules.

Formation of the cisPt(TFA) (OH) hydrolysis product together with the elimination of the acid is calculated to be exothermic by 7.4 kcal mol⁻¹. When the water molecule attacks on the carbonyl carbon, the calculated free-energy barrier that is necessary to surmount lies 38.4 kcal mol⁻¹ above the energy of the minimum leading to it.

In the case under investigation the coordinated amine in equatorial position catalyzes the process acting as a proton shuttle. Indeed, the normal mode associated with the imaginary frequency of 482.9i cm⁻¹ identifying the intercepted transition state TS2$_{cisPt(TFA)_2}$ corresponds to the concerted H transfer from the amine to the oxygen atom of H₂O and from the water molecule to the oxygen atom of TFA. Simultaneously, the formed OH⁻ moiety bonds to the carbonyl C atom, and the final product is formed.
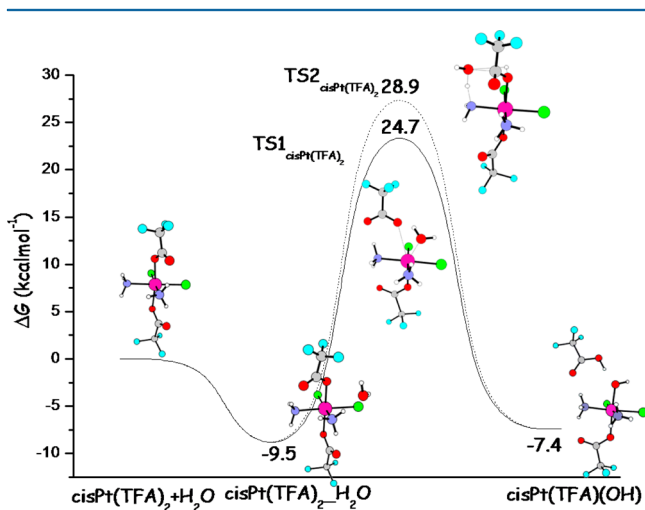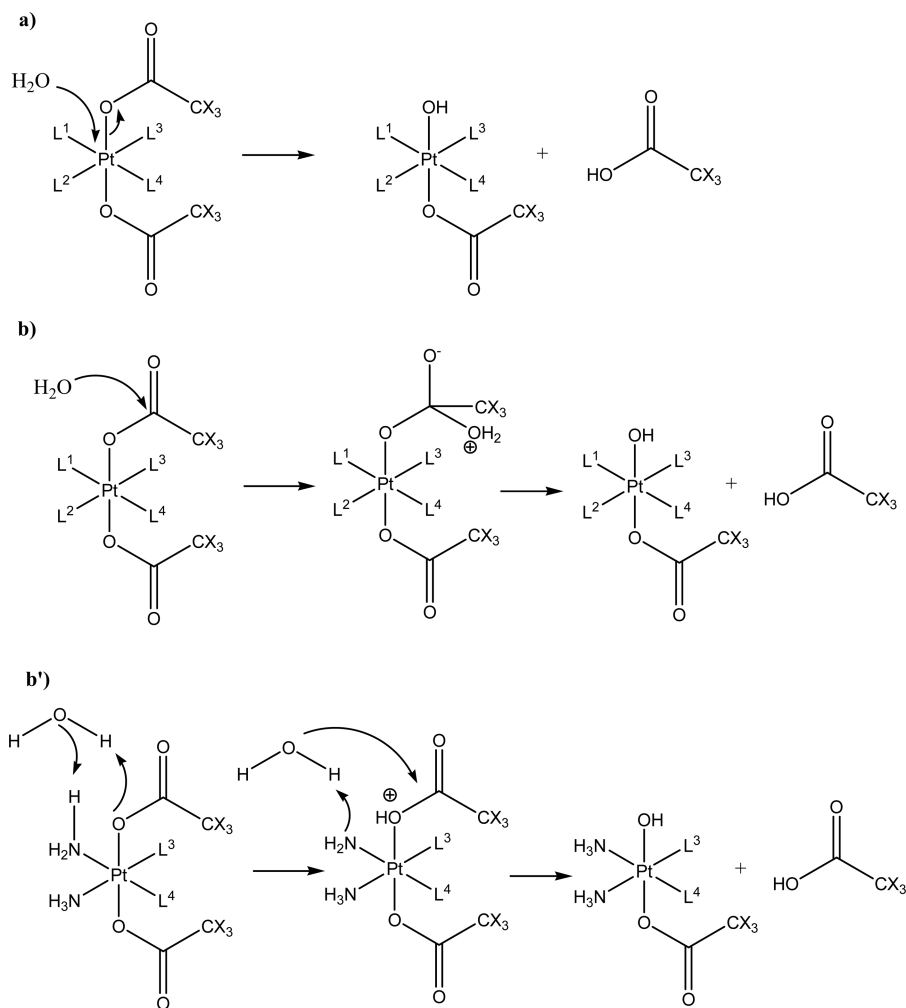
Scheme 2

Figure 1. Calculated B3LYP free-energy profiles in water for TFA axial ligand hydrolysis of the cisplatin Pt(IV) derivative with two TFA axial ligands. Results for mechanisms (a; solid line) and (b'; dashed line) are shown. Energies are in kilocalories per mole and relative to separated reactants.

From the reported data it clearly appears that the direct attack on the Pt metal center is the preferred mechanism, and analogous calculations for cisplatin derivatives containing Ac,

MCA, and DCA ligands as well as for carboplatin and oxaliplatin Pt(IV) derivatives containing Ac, MCA, DCA, and TFA ligands confirm this behavior. The outcomes of calculations performed to intercept minima and transition states along the axial ligands hydrolysis pathway for all the examined complexes and ligands are collected in Table 1. Mechanism labeled (a) was examined, whereas results for the same series of compounds for hydrolysis in axial position for the mechanisms indicated as (b) and (b') in Scheme 2 can be found in Table S2 of the Supporting Information. It is important to underline that for all the examined complexes the substitution of the ligands follows the same associative displacement mechanism and the amine in equatorial position assists the hydrogen atom transfer step (mechanism b') in Scheme 2) only in the case of cisplatin derivatives.

The main conclusion drawn on the basis of the results obtained by Gibson and co-workers[18d,e] is that, even if the hydrolysis behavior of all the examined Pt(IV) complexes containing two haloacetato ligands in axial position is not straightforward to rationalize, it seems that strong electron-withdrawing groups on acetato ligands cause a destabilization of these compounds, which can undergo fast hydrolysis. Furthermore, the nature of the ligands in the whole coordination sphere plays also an important role in influencing the behavior of the complexes. Indeed, the authors recognized that different complexes with the same ligands in axial position

Table 1. The Hydrolysis in Axial Position for Mechanism Labeled (a) for All the Pt(IV) Derivatives under Investigation[a]

Cispt(X)$_2$+H$_2$O	Cispt(X)$_2$_H$_2$O[b]	TS[c] ($\Delta E\ddagger$)	hydrolysis product[d]
X = Ac	−7.9	33.5	−7.0
X = Mca	−9.5	31.2	−12.6
X = Dca	−9.3	32.3	−9.3
X = Tfa	−9.5	34.2	−7.4
CarboPt(X)$_2$+H$_2$O	carboPt(X)$_2$_H$_2$O		
X = Ac	−9.3	35.5	−2.8
X = MCA	−10.5	40.1	−3.7
X = DCA	−8.5	39.2	−1.0
X = TFA	−8.5	35.8	−2.7
oxaPt(X)$_2$+H$_2$O	oxaPt(X)$_2$_H$_2$O		
X = Ac	−9.6	35.3	−6.0
X = MCA	−8.6	33.9	−8.1
X = DCA	−7.2	31.8	−6.4
X = TFA	−6.7	31.8	−6.7

[a]All the values are in kilocalories per mole. [b]Relative free energies of formation of the first adduct. [c]Activation energies. [d]Free energies of reaction.

showed different hydrolysis rates. The rationalization of the calculated values is difficult also from a theoretical point of view. Indeed, from the data collected in Table 1 it appears that for the cisplatin derivatives significant differences between the energy barriers do not exist. MCA and DCA barriers are even lower than those for Ac and TFA. The barriers calculated for the carboplatin derivatives are higher than those for both cisplatin and oxaliplatin Pt(IV) derivatives. In this case, the similar barriers for the Ac and TFA complexes are lower than those for MCA and DCA ligands. Finally, for the oxaliplatin derivatives the presence of more withdrawing substituents on axial acetato ligands causes a lowering of the corresponding energy barriers. This trend is that expected on the basis of the conclusions of Gibson and co-workers[18d,e] on the nature of axial ligands and the influence they have on the hydrolysis behavior. The reported values confirm that the identity of the ligands in equatorial position plays a critical role in determining the energetics of the process.

The energy profile for the hydrolysis in equatorial position that leads to the substitution of one Cl$^-$ ligand in cisPt(TFA)$_2$ derivative is reported in Figure 2. The approach of the water molecule to the complex from the side of the chlorido ligands causes a stabilization of 8.9 kcal mol^{-1}. The intercepted transition state TS3$_{cisPt(TFA)_2}$, whose structure is shown in Figure 2, has a free energy of 27.1 kcal mol^{-1}. Therefore, from the previous minimum a barrier of 36.0 kcal mol^{-1} must be overcome for the concerted breaking of the Pt−Cl bond and formation of a new bond between the Pt center and the oxygen atom of the entering water molecule to occur.

In the formed product the chlorido ligand is completely substituted by the H$_2$O molecule and interacts with the hydrogens of amine and coordinated water at distances of 1.961 and 1.742 Å, respectively. The whole process is exothermic by 0.3 kcal mol^{-1} and, then, less favored, from a thermodynamic point of view than the hydrolysis in axial position. The outcomes of analogous calculations performed to intercept minima and transition states along the aquation reaction in equatorial position for cisPt(X)$_2$, carboPt(X)$_2$, and oxaPt(X)$_2$, where X = Ac, MCA, DCA, and TFA, are gathered in Table 2.
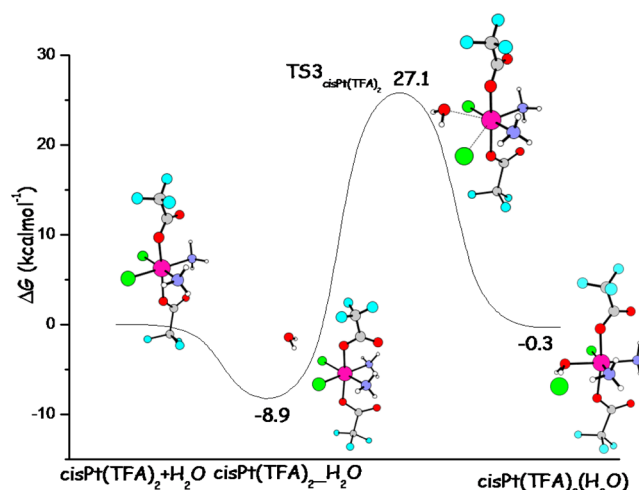

Figure 2. Calculated B3LYP free-energy profiles in water for Cl$^-$ equatorial ligand hydrolysis of the cisplatin Pt(IV) derivative with two axial TFA ligands. Energies are in kcal·mol^{-1} and relative to separated reactants.

Table 2. The Hydrolysis in Equatorial Position[a]

cisPt(X)$_2$+H$_2$O	cisPt(X)$_2$_H$_2$O[b]	TS[c] ($\Delta E\ddagger$)	hydrolysis product[d]
X = CH3COO$^-$	−7.0	31.5	−1.9
X = MCA	−8.9	33.1	−2.8
X = DCA	−8.7	35.6	0.2
X = TFA	−8.9	36.0	−0.3
carboPt(X)$_2$+H$_2$O	carboPt(X)$_2$_H$_2$O		
X = CH3COO$^-$	−8.8	36.1	−5.7
X = MCA	−9.5	38.7	−5.1
X = DCA	−8.1	39.8	−4.7
X = TFA	−8.5	40.2	−5.0
oxaPt(X)$_2$+H$_2$O	oxaPt(X)$_2$_H$_2$O		
X = CH3COO$^-$	−9.6	28.0	1.2
X = MCA	−8.6	28.3	3.2
X = DCA	−7.2	27.9	4.1
X = TFA	−6.7	27.2	5.0

[a]All the values are in kilocalories per mole. [b]Relative free energies of formation of the first adduct. [c]Activation energies. [d]Free energies of reaction.

It is worth mentioning that, for carboPt(X)$_2$ and oxaPt(X)$_2$ complexes, aquation in equatorial position involves the opening of the ring formed by malonate and oxalate ligands, respectively, with the metal center. The reported energy barrier values do not follow any specific trend as a function of the ligands in axial position. For the cisplatin and oxaliplatin derivatives, Ac and MCA ligands make the hydrolysis process more viable than DCA and TFA ligands. Furthermore, such barriers are either comparable or only slightly different with respect to the barriers for hydrolysis in axial position. The barriers for the oxaliplatin derivatives are similar among them and the lowest, even lower than those for the hydrolysis in axial position. A comparison with the available experimental and theoretical values of the activation barriers for the hydrolysis in equatorial position of the corresponding Pt(II) complexes can be helpful in rationalizing the obtained results. Many quantum chemical studies in the past have been devoted to the investigation of the hydrolysis reaction of one Pt−Cl bond of cisplatin drug.[23] The theoretical value of the activation barrier for the first hydrolysis closest to the experimentally estimated

ones (23.8^{25} and 24.1^{26} kcal mol^{-1}) has been calculated by Lau and Deubel[23] and is 25 kcal mol^{-1}. For oxaliplatin an activation barrier of 27.95 kcal mol^{-1} has been calculated[27] that agrees with the value of 26.50 kcal mol^{-1} extracted from the experimental reaction rate.[28] The ring opening process for the carboplatin drug involves the overcoming of an energy barrier calculated to be 30.1 kcal mol^{-1},[29] which is in excellent agreement with the experimentally estimated value of $\sim$30 kcal·mol^{-1}.[30] As a consequence, our calculations confirm that Pt(IV) octahedral derivatives of cisplatin and carboplatin are sensibly more inert than the corresponding square-planar Pt(II) complexes regardless of the identity of the axial ligands and the site, axial or equatorial, of hydrolysis. For oxaliplatin Pt(IV) derivatives, instead, the heights of the calculated barriers for both axial and equatorial hydrolysis are all comparable, except for the Ac ligand, and even lower than the values suggested for the aquation in equatorial position of the corresponding Pt(II) complex. Furthermore, only for oxaliplatin derivatives the trend in barrier heights confirms the behavior that can be predicted on the basis of the withdrawing power of the axial ligands.[18d,e]

Finally, in the case of cisplatin also the hydrolysis of the Pt(IV) derivative with two chlorido ligands in axial position, cisPt(Cl)$_2$, was investigated. Free-energy profiles for the first hydrolysis of both axial and equatorial chlorido ligands are reported in Figure 3 together with optimized structures of
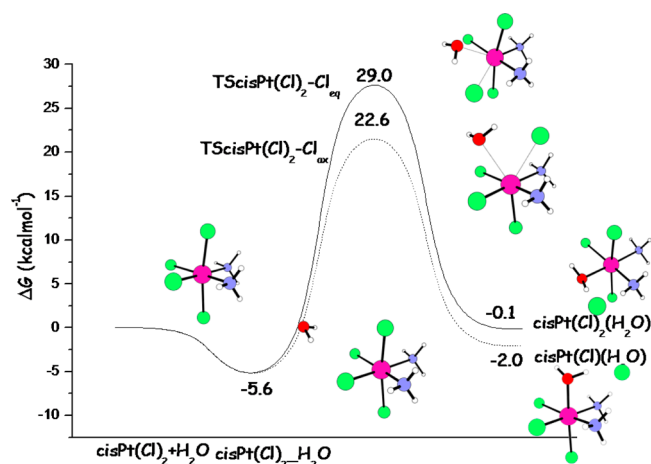
equatorial chlorido ligand for the formation of cisPt(Cl)(H$_2$O) and cisPt(Cl)$_2$(H$_2$O) products, respectively. The calculated trend of barrier heights for the aquation of cisPt(Cl)$_2$ agrees with experimental findings that show the substitution in axial position to occur before substitution in equatorial one.[21] The barriers calculated for the hydrolysis in axial and equatorial positions are lower than and comparable with, respectively, those for cisplatin derivatives having two axial carboxylato ligands. This result is a further confirmation that Pt(IV) complexes are, in general, more inert than the corresponding Pt(II) drugs. Some exceptions exist, such as derivatives of oxaliplatin for the aquation in equatorial position, and overall, inertness is lower than expected. The nature of the axial ligands can influence the course of the hydrolysis reaction, as it appears from the behaviors of cisplatin derivatives with carboxylato and chlorido axial ligands even if a decisive role is played by the ligands in equatorial positions.

Hambley and co-workers[21] have also reported that the addition of small amounts of the Pt(II) complex increases the rate of the reaction. The computed energy profile for the hydrolysis reaction of the cisPt(Cl)$_2$ complex assisted by cisplatin is depicted in Figure 4 together with the structures of located stationary points, whose Cartesian coordinates can be found in the Supporting Information.
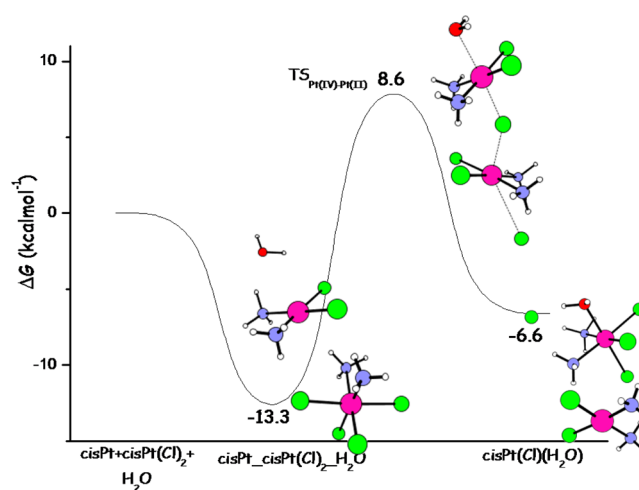

Figure 3. Calculated B3LYP free energy profiles in water for the Cl$^-$ equatorial (solid line) and axial (dashed line) ligand hydrolysis of the Pt(IV) derivative of cisplatin with two chorido axial ligands. Energies are in kilocalories per mole and relative to separated reactants.

Figure 4. Calculated B3LYP free-energy profile in water for the axial aquation of the Pt(IV) cisplatin derivative with two chlorido axial ligands assisted by the Pt(II) cisplatin complex. Energies are in kilocalories per mole and relative to separated reactants.

intercepted stationary points, whose Cartesian coordinates can be found in the Supporting Information. The reaction proceeds with the formation of the first adduct cisPt(Cl)$_2$_H$_2$O that is stabilized with respect to the reactants' zero energy by 5.6 kcal mol^{-1}. The water molecule can attack the Pt atom to substitute a chlorido ligand either in axial or equatorial positions. In the former case, the barrier that must be overcome for the TScisPt(Cl)$_2$-Cl$_{ax}$ is 28.2 kcal mol^{-1} for the associative substitution of the ligand. The lengths of the breaking Pt–Cl and forming Pt–O bonds are 3.008 and 2.898 Å, respectively. In the latter case, the transition state TScisPt(Cl)$_2$-Cl$_{eq}$ barrier is 34.6 kcal mol^{-1}. The distance between the Pt center and the oxygen of the entering water molecule is 2.627 Å, and that between Pt and the leaving chlorido is 3.062 Å. Substitution reaction is calculated to be exothermic by 2.0 kcal mol^{-1} in axial position and is thermoneutral for the displacement of an

The mechanism hypothesized by Basolo and Pearson[19,20] involves coordination of the water molecule to the Pt(II) complex to form a pentacoordinate intermediate that binds to the Pt(IV) complex through a chlorido ligand that acts as a bridge between the two Pt centers. From an inspection of the energy profile shown in Figure 4 it appears that the results of our theoretical investigation are not superimposable with the hypothesized reaction steps. Indeed, the only formed intermediate is an adduct between the water molecule and the Pt(II) and Pt(IV) complexes, which lies 13.3 kcal mol^{-1} below the energy of the entrance channel. The reaction proceeds in one step by overcoming an energy barrier of 21.9 kcal mol^{-1} for the concerted transition state TS$_{Pt(IV)-Pt(II)}$ characterized by an imaginary frequency of 57.41i cm^{-1}.

The intercepted transition state was carefully checked by IRC calculations[31] to assess its proper connection with the

corresponding minima. The normal mode associated with the imaginary frequency corresponds to the simultaneous coordination of the water molecule to the platinum center of cisplatin, detachment of one axial Cl⁻ ligands of the Pt(IV) complex, and its coordination to the Pt(II) center and release of the second axial chlorido ligand. The whole process leading to the formation of the desired hydrolysis product, the restored cisplatin complex, and the displaced Cl⁻ ligand is calculated to be exothermic by 6.6 kcal mol⁻¹. All the computational strategies employed to locate the stationary points corresponding to the mechanistic hypothesis formulated by Basolo and Pearson were unsuccessful. On this subject, it is worthwhile to underline that the results presented here agree with previous calculations that do not support the involvement of five-coordinate platinum complexes as reaction intermediates.[32] The attack on the Pt(II) center is assisted and occurs thanks to the contemporary coordination of another ligand from the opposite side to give a six-coordinate species. The barrier that is necessary to overcome for the assisted aquation in axial position is lower than that calculated when the process is not assisted, confirming the catalytic role played by residual amounts of the Pt(II) complex (21.9 vs 28.2 kcal mol⁻¹).

CONCLUSIONS

In the present paper we have undertaken a systematic examination of the hydrolysis reaction energy profiles of Pt(IV) derivatives of cisplatin, carboplatin, and oxaliplatin containing acetato, monochloroacetato, dichloroacetato, trifluoroacetato, and chlorido ligands in axial positions. For the attack to axial carboxylato ligands position, two alternatives have been explored; that is, (a) direct displacement of the axial ligand by water that simultaneously deprotonates and (b) attack to the carbonyl carbon accompanied by deprotonation that can be or not assisted by coordinated amines. Results show that the direct attack on the Pt center is the preferred mechanism. The trend of barrier heights calculated along the displacement, calculated to be associative, pathways is difficult to rationalize as a function of the nature of the axial ligands. The Pt(IV) derivatives, in general, result to be more inert than the corresponding Pt(II) complexes, even if some exception exists such as the aquation in equatorial position of Pt(IV) oxaliplatin derivatives. However, inertness is lower than expected, and the possibility that Pt(IV) prodrugs can undergo hydrolysis in biologically relevant conditions cannot be excluded. The identity of the axial ligands influences the rate of the hydrolysis reaction, but a decisive role is played by the nature of the ligands in equatorial positions. For the cisplatin derivative having two chlorido ligands in axial position the hypothesis that the cisplatin could act as catalyst has been explored, and the mechanism has been elucidated. The reaction occurs in one step, and the height of the only intercepted transition state confirms that the presence of residual amounts of the Pt(II) complex causes an enhancement of the reaction rate.

Octahedral Pt(IV) complexes act as prodrugs that are believed to be activated in the cancer cell by reductive elimination to yield the corresponding active Pt(II) congeners. Several mechanistic hypotheses have been formulated for the reductive elimination such as outer sphere reactions, inner sphere mechanisms, and Pt(II)-catalyzed reaction schemes analogous to that investigated here involving the formation of a dimer where a bridging ligand mediates the electron transfer between the Pt(II) and Pt(IV). Work is in progress to theoretically investigate for the complexes examined here what

mechanism should be responsible of the reduction of Pt(IV) prodrugs inside the cells. Moreover, once it is accepted that Pt(IV) derivatives can be hydrolyzed before entering the cancer cell, we intend to probe how the substitution of the ligands and, hence, the presence of hydroxide ligands in the coordination sphere influences the reduction process.

COMPUTATIONAL DETAILS

Geometry optimizations as well as frequency calculations for all reactants, intermediates, products, and transition states were performed at the density functional level of theory by using the B3LYP[22] functional as implemented by the Gaussian 09[33] code. For Pt the relativistic compact Stuttgart/Dresden effective core potential[34] was used in conjunction with the split valence basis set. The standard 6-311+G** basis sets of Pople and co-workers were employed for the rest of the atoms. The involved transition states were checked by intrinsic reaction coordinate (IRC) analysis.[31] For each optimized stationary point, vibrational analysis was performed to determine the character (minimum or saddle point), and zero-point vibrational energy (ZPVE) corrections were included in all relative energies. For transition states, it was carefully checked that the vibrational mode associated with the imaginary frequency corresponds to the correct movement of the involved atoms. Furthermore, the IRC[31] method was used to asses that the localized TSs correctly connect to the corresponding minima along the imaginary mode of vibration. The impact of solvation effects on the energy profiles was estimated by using the Tomasi's implicit Polarizable Continuum Model (PCM)[35] as implemented in Gaussian09. The UFF set of radii was used to build the cavity. The solvation Gibbs free energies were calculated in implicit water (ε = 78.4) at the same level performing single-point calculations on all stationary points structures obtained from vacuum calculations. Enthalpies and Gibbs free energies were obtained at 298 K and 1 atm from total energies, including zero-point, thermal, and solvent corrections, using standard statistical procedures.[36] However, such approach does not reflect the real entropic change that occurs when the solute goes from the gas to the condensed phase, and the effects are more relevant when association and dissociation are involved. Therefore, following the procedure proposed by Wertz[37] and successfully adopted formerly[38] to properly handle the change of translational and rotational entropy occurring when a solute is transferred from the gas phase into the solution phase, Gibbs free energies in solution for each species were calculated as

$$G_{298K} = E_{elec} + G_{solv} + ZPE + H_{vib} + 6kT - T(S_{vib})$$
$$- T[0.54 \times (S_{rot} + S_{trans} - 14.3) + 8.0] \quad (1)$$

where T = 298 K and the term $6kT$ accounts for the potential and kinetic energies of the translational and rotational modes.

ASSOCIATED CONTENT

S **Supporting Information**

The Supporting Information is available free of charge on the ACS Publications website at DOI: 10.1021/acs.inorgchem.5b02484.

> Cartesian coordinates (Å) of all optimized structures; relative energies of stationary points for the mechanisms labeled (b) and (b′). (PDF)

AUTHOR INFORMATION

Corresponding Author

*E-mail: emilia.sicilia@unical.it.

Notes

The authors declare no competing financial interest.

ACKNOWLEDGMENTS

■ REFERENCES

(1) Desoize, B.; Madoulet, C. *Crit. Rev. Oncol. Hematol.* **2002**, *42*, 317−325.

(2) Alderden, R. A.; Hall, M. D.; Hambley, T. W. *J. Chem. Educ.* **2006**, *83*, 728−733.

(3) (a) Rosenberg, B.; Vancamp, L.; Trosko, J. E.; Mansour, V. H. *Nature* **1969**, *222*, 385−386. (b) Rosenberg, B.; Vancamp, L.; Krigas, T. *Nature* **1965**, *205*, 698−699.

(4) Wong, E.; Giandomenico, C. M. *Chem. Rev.* **1999**, *99*, 2451−2466.

(5) Siddik, Z. H. *Oncogene* **2003**, *22*, 7265−7279.

(6) (a) Galluzzi, L.; Senovilla, L.; Vitale, I.; Michels, J.; Martins, I.; Kepp, O.; Castedo, M.; Kroemer, G. *Oncogene* **2012**, *31*, 1869−1883. (b) Wexselblatt, E.; Yavin, E.; Gibson, D. *Inorg. Chim. Acta* **2012**, *393*, 75−83.

(7) Butler, J. S.; Sadler, P. J. *Curr. Opin. Chem. Biol.* **2013**, *17*, 175−188.

(8) Wexselblatt, E.; Gibson, D. *J. Inorg. Biochem.* **2012**, *117*, 220−229.

(9) Farrell, N. P. *Curr. Top. Med. Chem.* **2011**, *11*, 2623−2631.

(10) Montana, A. M.; Batalla, C. *Curr. Med. Chem.* **2009**, *16* (18), 2235−2260.

(11) Ang, W. H.; Pilet, S.; Scopelliti, R.; Bussy, F.; Juillerat-Jeanneret, L.; Dyson, P. J. *J. Med. Chem.* **2005**, *48*, 8060−8069.

(12) Kelland, L. R.; Sharp, S. Y.; O'Neill, C. F.; Raynaud, F. I.; Beale, P. J.; Judson, I. R. *J. Inorg. Biochem.* **1999**, *77*, 111−115.

(13) Platts, J. A.; Ermondi, G.; Caron, G.; Ravera, M.; Gabano, E.; Gaviglio, L.; Pelosi, G.; Osella, D. *JBIC, J. Biol. Inorg. Chem.* **2011**, *16*, 361−372.

(14) Gramatica, P.; Papa, E.; Luini, M.; Monti, E.; Gariboldi, M. B.; Ravera, M.; Gabano, E.; Gaviglio, L.; Osella, D. *JBIC, J. Biol. Inorg. Chem.* **2010**, *15*, 1157−1169.

(15) (a) Bhargava, A.; Vaishampayan, U. N. *Expert Opin. Invest. Drugs* **2009**, *18*, 1787−1797. (b) Choy, H. *Expert Rev. Anticancer Ther.* **2006**, *6*, 973−982.

(16) Choi, S.; Filotto, C.; Bisanzo, M.; Delaney, S.; Lagasee, D.; Whitworth, J. L.; Jusko, A.; Li, C. R.; Wood, N. A.; Willingham, J.; Schwenker, A.; Spaulding, K. *Inorg. Chem.* **1998**, *37*, 2500−2504.

(17) (a) Dhar, S.; Lippard, S. J. *Proc. Natl. Acad. Sci. U. S. A.* **2009**, *106*, 22199−22204. (b) Johnstone, T. C.; Kulak, N.; Pridgen, E. M.; Farokhzad, O. C.; Langer, R.; Lippard, S. J. *ACS Nano* **2013**, *7*, 5675−5683. (c) Liu, W.; Su, J.; Jiang, J.; Li, X.; Ye, Q.; Zhou, H.; Chen, J.; Li, Y. *Sci. Rep.* **2013**, *3*, 2464−2470. (d) Xue, X.; You, S.; Zhang, Q.; Wu, Y.; Zou, G. Z.; Wang, P. C.; Zhao, Y. L.; Xu, Y.; Jia, L.; Zhang, X.; Liang, X. *Mol. Pharmaceutics* **2012**, *9*, 634−644.

(18) (a) Sinisi, M.; Intini, F. P.; Natile, G. *Inorg. Chem.* **2012**, *51*, 9694−9704. (b) Nemirovski, A.; Vinograd, I.; Takrouri, K.; Mijovilovich, A.; Rompel, A.; Gibson, D. *Chem. Commun.* **2010**, *46*, 1842−1844. (c) Zhang, J. Z.; Wexselblatt, E.; Hambley, T. W.; Gibson, D. *Chem. Commun.* **2012**, *48*, 847−849. (d) Wexselblatt, E.; Yavin, E.; Gibson, D. *Angew. Chem., Int. Ed.* **2013**, *52*, 6059−062. (e) Wexselblatt, E.; Raveendran, R.; Salameh, S.; Friedman-Ezra, A.; Yavin, E.; Gibson, D. *Chem. - Eur. J.* **2015**, *21*, 3108−3114.

(19) Ellison, H. R.; Basolo, F.; Pearson, R. G. *J. Am. Chem. Soc.* **1961**, *83*, 3943−3948.

(20) Basolo, F.; Morris, M. L.; Pearson, R. G. *Discuss. Faraday Soc.* **1960**, *29*, 80−91.

(21) Davies, M. S.; Hall, M. D.; Berners-Price, S. J.; Hambley, T. W. *Inorg. Chem.* **2008**, *47*, 7673−7680.

(22) (a) Becke, A. D. *J. Chem. Phys.* **1993**, *98*, 5648−5652. (b) Lee, C.; Yang, W.; Parr, R. G. *Phys. Rev. B: Condens. Matter Mater. Phys.* **1988**, *37*, 785−789.

(23) Lau, J. K-C.; Deubel, D. V. *J. Chem. Theory Comput.* **2006**, *2*, 103−106 and references therein..

(24) Grimme, S.; Antony, J.; Ehrlich, S.; Krieg, H. *J. Chem. Phys.* **2010**, *132*, 154104.

(25) Coe, J. S. In *MTP International Review of Science, Inorganic Chemistry Series Two*; Tobe, M. L., Ed.; Butterworths: London, 1974, Vol. *9*, p 45.

(26) Perumareddi, J. R.; Adamson, A. W. *J. Phys. Chem.* **1968**, *72*, 414−420.

(27) Lucas, M. F. A.; Pavelka, M.; Alberto, M. E.; Russo, N. *J. Phys. Chem. B* **2009**, *113*, 831−838.

(28) Jerremalm, E.; Videhult, P.; Alvelius, G.; Griffiths, W. J.; Bergman, T.; Eksborg, S.; Ehrsson, H. *J. Pharm. Sci.* **2002**, *91*, 2116−2121.

(29) Pavelka, M.; Lucas, M. F.; Russo, N. *Chem. - Eur. J.* **2007**, *13*, 10108−10116.

(30) Hay, R. W.; Miller, S. *Polyhedron* **1998**, *17*, 2337−2343.

(31) (a) Fukui, K. *J. Phys. Chem.* **1970**, *74*, 4161−4163. (b) Gonzalez, C.; Schlegel, H. B. *J. Chem. Phys.* **1989**, *90*, 2154−2161.

(32) Mazzone, G.; Russo, N.; Sicilia, E. *Inorg. Chem.* **2011**, *50*, 10091−10101.

(33) Frisch, M. J.; Trucks, G. W.; Schlegel, H. B.; Scuseria, G. E.; Robb, M. A.; Cheeseman, J. R.; Scalmani, G.; Barone, V.; Mennucci, B.; Petersson, G. A.; Nakatsuji, H.; Caricato, M.; Li, X.; Hratchian, H. P.; Izmaylov, A. F.; Bloino, J.; Zheng, G.; Sonnenberg, J. L.; Hada, M.; Ehara, M.; Toyota, K.; Fukuda, R.; Hasegawa, J.; Ishida, M.; Nakajima, T.; Honda, Y.; Kitao, O.; Nakai, H.; Vreven, T.; Montgomery, J. A., Jr.; Peralta, J. E.; Ogliaro, F.; Bearpark, M.; Heyd, J. J.; Brothers, E.; Kudin, K. N.; Staroverov, V. N.; Kobayashi, R.; Normand, J.; Raghavachari, K.; Rendell, A.; Burant, J. C.; Iyengar, S. S.; Tomasi, J.; Cossi, M.; Rega, N.; Millam, J. M.; Klene, M.; Knox, J. E.; Cross, J. B.; Bakken, V.; Adamo, C.; Jaramillo, J.; Gomperts, R.; Stratmann, R. E.; Yazyev, O.; Austin, A. J.; Cammi, R.; Pomelli, C.; Ochterski, J. W.; Martin, R. L.; Morokuma, K.; Zakrzewski, V. G.; Voth, G. A.; Salvador, P.; Dannenberg, J. J.; Dapprich, S.; Daniels, A. D.; Farkas, Ö.; Foresman, J. B.; Ortiz, J. V.; Cioslowski, J.; Fox, D. J. *Gaussian 09*, Revision D.01; Gaussian, Inc: Wallingford, CT, 2009.

(34) Andrae, D.; Hüßermann, U.; Dolg, M.; Stoll, H.; Preuß, H. *Theor. Chim. Acta* **1990**, *77*, 123−141.

(35) (a) Cances, M. T.; Mennucci, B.; Tomasi, J. *J. Chem. Phys.* **1997**, *107*, 3032−3041. (b) Cossi, M.; Barone, V.; Mennucci, B.; Tomasi, J. *Chem. Phys. Lett.* **1998**, *286*, 253−260. (c) Mennucci, B.; Tomasi, J. *J. Chem. Phys.* **1997**, *106*, 5151−5158.

(36) McQuarrie, D. A.; Simon, J. D. *Molecular Thermodynamics*; University Science Books: Sausalito, CA, 1999.

(37) Wertz, D. H. *J. Am. Chem. Soc.* **1980**, *102*, 5316−5322.

(38) Cheng, M.-J.; Nielsen, R. J.; Goddard, W. A., III *Chem. Commun.* **2014**, *50*, 10994−10996.

Paper V

"Hydrolysis in acidic environment and degradation of satraplatin: a joint experimental and theoretical investigation"

Ida Ritacco, Tamer Shoeib, Nino Russo, Emilia Sicilia.

Hydrolysis in acidic environment and degradation of satraplatin: a joint experimental and theoretical investigation

Ida Ritacco,[§] Merriam Al Assy [‡], Nino Russo[§] Tamer Shoeib,*[‡,†] and Emilia Sicilia*[§]

[§]Department of Chemistry and Chemical Technologies, University of Calabria, Arcavacata di Rende, 87036 Italy.

[‡] Department of Chemistry, The American University in Cairo, New Cairo 11835, Egypt

[†]Centre for Analytical Science, Department of Chemistry, Loughborough University, Loughborough, Leicestershire LE11 3TU, U.K.

ABSTRACT: In the effort to synthesize and select active platinum-based anticancer drugs performing better than cisplatin and its analogues, six-coordinate octahedral Pt(IV) complexes appear to be promising candidates as, being kinetically more inert and more resistant to ligand substitution than four-coordinate Pt(II) centers, are able to minimize unwanted side reactions with biomolecules prior to DNA binding. Due to their kinetic inertness Pt(IV) complexes have been also exploited to bypass inconvenient intravenous administration. The most prominent example is satraplatin that is the first platinum antineoplastic agent reported to have oral activity. The present paper deals with a theoretical DFT investigation of the influence that the acidity of the biological environment can have on the activity of satraplatin and analogous octahedral Pt(IV) complexes having two carboxylates as axial ligands. Moreover, here the outcomes of a joint electrospray ionization mass spectrometry and DFT investigation of the fragmentation pathways of the protonated satraplatin are reported. Calculations show that the simulated acidic environment has an important impact on the satraplatin reactivity causing a significant lowering of the barrier that is necessary to overcome for the hydrolysis of the first acetate ligand to occur. Electrospray ionization experiments confirm that the loss of CH_3COOH from the protonated satraplatin ion $[Sat + H]^+$ takes place almost immediately upon dissolution of satraplatin in the used methanol-water solution at room temperature.

1. INTRODUCTION

   Platinum-based drugs are used widely in chemotherapy. The clinically approved platinum complexes cis-diamminedichloridoplatinum(II), cisplatin, and its direct analogues cis-diammine-[1,1-cyclobutanedicarboxylato]platinum(II), carboplatin, and 1R,2R-diaminocyclohexane oxalatoplatinum(II), oxaliplatin, are the majorly used chemotherapeutic agents. Application of such three worldwide approved platinum(II)-based cytostatics, however, is limited by their severe side effects, intrinsic and/or acquired therapy resistance and the inconvenient way of intravenous administration.[1-5] To overcome these drawbacks a great deal of efforts has been concentrated on the search for improved metal-based anticancer agents including prodrugs in the more inert +IV oxidation state.[6-11] Since Pt(IV) complexes are kinetically more inert, they have been exploited for oral
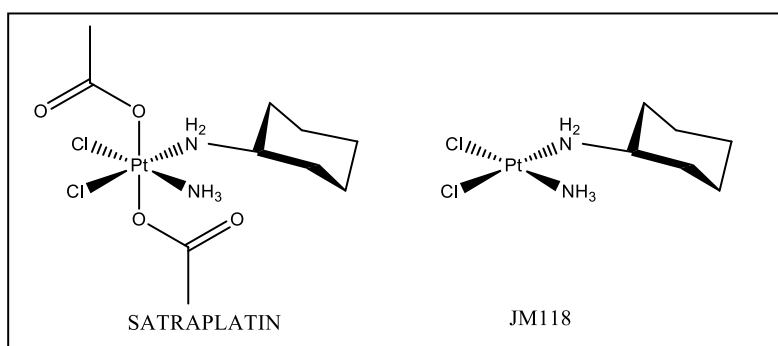
Scheme 1. Chemical structures of satraplatin and JM118

administration. The most prominent example is satraplatin, *trans,cis,cis*-bis(acetato)ammine-cyclohexylaminedichloroplatinum(IV) (Scheme 1), the first platinum agent reported to have oral activity.[12,13] It has been rationally designed for its lipophilicity and stability to be suitable for oral administration. The lipophilic character of satraplatin favors cellular accumulation of the

drug[14] and increases its oral bioavailability. Satraplatin complex exerts its antitumor activity by a generally accepted intracellular mechanism that entails: cellular entry and activation typically involving reduction of Pt(IV) to Pt(II) and, in analogy to cisplatin, aquation by substitution of chloride ligands. Six distinct platinum(II) species can be formed, where *cis*-ammine(cyclohexylamine)-dichloroplatinum(II) (JM118, Scheme 1) derived from the loss of the two acetate ligands is the major metabolite. Consequent DNA binding and initial cellular responses to the DNA damage ultimately lead to cellular death.[15-17] Satraplatin and its JM118 metabolite have shown antitumor effects *in vitro*, *in vivo*, and in clinical trials.[4] Advantages of using satraplatin as an alternative platinum antitumor agent, besides convenience of oral administration, include milder toxicity profile, lack of cross-resistance with cisplatin, and activity in cancers that are nonresponsive to conventional platinum drugs used in the clinic. Despite these advantages and the positive outcome of Phase III clinical trials, satraplatin has not been approved by the FDA as it did not show a convincing benefit in terms of overall survival.[18] As a consequence, clinical studies with satraplatin are still ongoing.[1]

In the framework of a more extended project aimed at investigating one aspect that is triggering increasing attention,[19-22] that is how the pH, both in acidic and basic conditions, of the biological environment can influence the activity of anticancer drugs, in the present paper we report the outcomes of a theoretical density functional theory (DFT) study of the acidic environmental conditions influence on the cytotoxicity of satraplatin and analogous octahedral Pt(IV) complexes having two carboxylates as axial ligands. Furthermore, electrospray ionization mass spectrometry experiments and DFT computations have been carried out to investigate the fragmentation pathways of the protonated satraplatin to allow identification and structural characterization of metabolites.

2. COMPUTATIONAL AND EXPERIMENTAL DETAILS

2.1 Computational methods.

The geometry optimization of all the compounds located along the calculated energy profiles have been carried out by means of the Gaussian09 software package[23] in the framework of the density functional theory employing the hybrid three-parameters B3LYP[24] functional. To describe Pt the relativistic compact Stuttgart/Dresden effective core potential[25] has been used in conjunction with its split valence basis set. Standard 6-311+G** basis set of Pople has been employed for the rest of the atoms, except C and H atoms of the cyclohexylamine ligand in order to reduce the computational effort. To describe such atoms the smaller 6-31G basis set has been employed. Vibrational analysis for each optimized stationary point has been performed to determine its minimum or saddle point nature and to calculate zero-point vibrational energy corrections included in all relative energies. For the intercepted transition states, it has been carefully checked that the vibrational mode associated with the imaginary frequency corresponds to the correct movement of the involved atoms. Furthermore, the IRC[26] method has been used to asses that the localized TSs correctly connect to the corresponding minima along the imaginary mode of vibration. The influence of the aqueous environment has been taken into account by means of the implicit Polarizable Continuum Model (PCM)[27] as implemented in Gaussian09 with $\varepsilon=78.35$. To build up the cavities, which solvent molecules are accommodated in, the UFF radii have been used. The solvation Gibbs free energies have been calculated in implicit water at the same level performing single-point calculations on structures obtained from gas-phase optimizations. Enthalpies and Gibbs free energies have been obtained at 298 K and 1 atm from total energies, including zero-point, thermal and solvent corrections, using standard statistical

procedures.[28] Gas-phase reaction free energy (ΔG_{gas}) and a solvation-reaction free-energy terms calculated with the continuum approach (ΔG_{solv}) have been summed up to calculate reaction Gibbs free energies in solution (ΔG_{sol}). However, the real entropic change that occurs when the solute goes from the gas- to the condensed-phase is not properly handled, and the effects are more prominent when dissociation and association reactions are involved. Therefore, to appropriately take into account the translational and rotational entropy change occurring when a solute is transferred from the gas phase into the solution phase, the procedure proposed by Wertz[29] and successfully employed formerly,[30] has been adopted and Gibbs free energies in solution for each species, have been calculated as:

$$G_{298K} = E_{elec} + G_{solv} + ZPE + H_{vib} + 6\,kT - T(S_{vib}) - T[0.54 \times (S_{rot} + S_{trans} - 14.3) + 8.0] \quad (1)$$

where the potential and kinetic energies of the translational and rotational modes are taken into consideration by the $6kT$ term and T=298K.

2.2 Mass Spectrometry.

A triple quadrupole mass spectrometer, (Acquity TQ, Waters, MA, USA) equipped with an electrospray ionisation source was used here. The instrument was operated in the positive ion mode, with typical values of cone and extractor voltages set to 35, and 3 respectively. The capillary voltage was optimised each day for maximum signal transmission and spray stability, the optimised range was typically 2200-2500 volts. The de-solvation gas was usually set at a flow of 200-250 L h^{-1} at a temperature of 150 ºC. Argon was used as the collision gas at a flow rate of about 0.15 ml min^{-1}. Ions sampled from the electrospray suffered many collisions in an attempt to achieve effective thermalization in the lens region, being from the orifice/skimmer to the first r.f. only quadrupole. The bias potential in this lens region was set up to strike a

compromise between signal transmission and minimal collisional heating. The precursor ions underwent multiple collisions with argon to produce product ion spectra obtained at collision energies in the range 0-25 eV in the lab frame having both Q1 and Q3 operated at unit resolution with typical a dwell time of 25 millisecond per transition.

2.3 Reagents

Satraplatin was obtained from Sanofi-Synthelabo Ltd, and Shandong Boyuan Pharmaceutical Co. Ltd., HPLC-grade water and methanol were all purchased from Sigma-Aldrich.

3. RESULTS AND DISCUSSION

3.1 Hydrolysis in water and acidic media of Pt(IV) complexes with carboxylato axial ligands.

The increased stability and bioavailability of platinum(IV) complexes, which allow oral application and reduce significantly side effects, is assumed also to aid the survival of such compounds in the acidic environment of the stomach before being absorbed into the blood stream. In particular, for satraplatin, the only orally administered platinum complex with documented efficacy, it is important to gain information concerning the fate of the drug after its oral assumption and the influence the low pH can have on its activity. On the other hand, the belief is increasing that the acidic environment can induce resistance to chemotherapeutic drugs that could be overcome using proton pump inhibitors in combination to conventional anticancer agents.[31,32] Furthermore, since *in vivo* activation by reduction inside the tumor cell to the corresponding platinum(II) analogs is essential for the anticancer activity of Pt(IV) compounds, it is speculated that when the axial ligands are carboxylates the acidity of the tumor

microenvironment favors the reduction process by ligands loss.[33] By performing a systematic exploration of the hydrolysis energy profiles of Pt(IV) derivatives of cisplatin, carboplatin, and oxaliplatin containing acetate (Ac) and haloacetato ligands in axial positions, we have already demonstrated that inertness is lower than expected, and the possibility that Pt(IV) prodrugs can undergo hydrolysis of axial ligands in biologically relevant conditions cannot be excluded.[34] The aquation in equatorial position is calculated to be, as expected, an unfavorable process.[34,35] In the present paper DFT calculations have been performed to investigate how the hydrolysis energy profiles of Pt(IV) complexes change in going from neutral to acidic environments. Both cisplatin derivative with axial acetato ligands and satraplatin have been examined. Free energy profiles for the hydrolysis by reaction with water and H_3O^+, mimicking the acidic environment, of the axial Ac ligands of the Pt(IV) cisplatin derivative, named cisPt(Ac)$_2$ are drawn in Figure 1. The sum of reactants free energies, that is complex and water or complex and H_3O^+, is set to zero for the calculation of relative free energies that are expressed in kcal mol^{-1}. Relative gas-phase zero-point corrected energies are also reported in parentheses. Fully optimized structures of minima and transition states intercepted along the reported pathways are shown in the same Figure 1, whereas complete geometries can be found in Table S1 of the Supporting Information (SI). The suggested alternative mechanisms for the hydrolysis of carboxylates in axial position, that is: direct water substitution of axial ligands or attack to the carbonyl accompanied by deprotonation have been already investigated by us.[34] The former is the preferred mechanism, which involves water attack on the Pt center and displacement of the ligand in an associative way. The interaction of the entering water molecule with the cisPt(Ac)$_2$ complex leads to the formation of the first cisPt(Ac)$_2$_H$_2$O intermediate, that is more stable than reactants by 7.9 kcal mol^{-1}. The direct coordination to the Pt center takes place overcoming a free energy barrier of 33.5 kcal mol$^-$

[1] corresponding to the transition state $TS1_{cisPt(Ac)_2}$ for the associative displacement of the ligand. The imaginary frequency that confirms the nature of this stationary point corresponds to the concerted $Pt - O_{Ac}$ bond breaking, $Pt - O_{H_2O}$ bond forming and proton transfer from water to the acetate ligand.
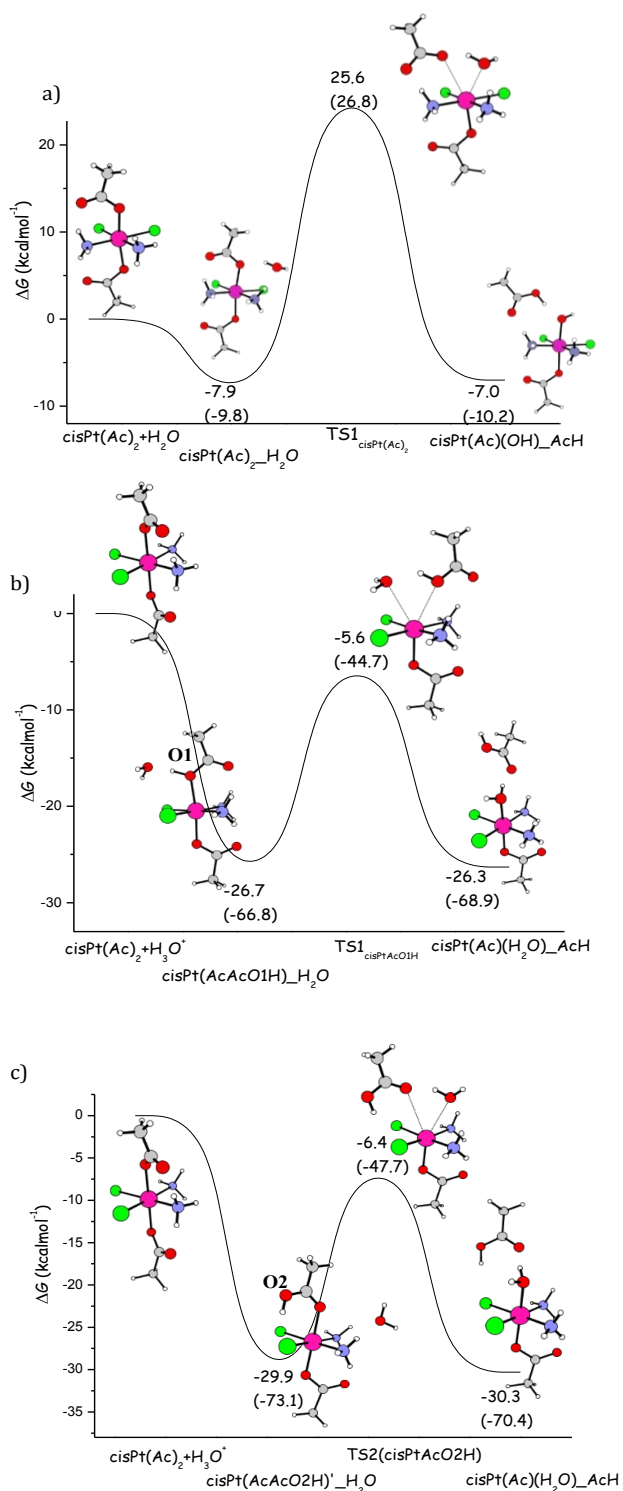
Figure 1. Calculated B3LYP energy profiles for the hydrolysis of Ac ligand in axial position of the Pt(IV) derivative of cisplatin in a) neutral and b) and c) acidic environments. Relative ZPE-corrected electronic energies (in parentheses) and Gibbs free energies at 298.15 K in water solvent are in kilocalories per mole.

When the interaction with the H_3O^+ ion, mimicking the acidic environment, is examined the barrier lowers notably. First of all, the energy of the adduct formed by the complex and the H_3O^+ ion cannot be calculated because during the optimization the proton is transferred to the Ac ligand. As the transfer of the proton can occur to both oxygen atoms, labeled O1 and O2 in Figure 1, of the Ac ligand, the hydrolysis pathways have been examined for both complexes. When the proton is transferred to the O1 atom coordinated to the metal center, the formation of the first cisPt(AcAcO1H)_H_2O adduct is exothermic by 26.7 kcal mol^{-1}. The barrier for the transition state TS1$_{cisPtAcO1H}$ that allows the displacement of the protonated Ac ligand and coordination of water is 21.1 kcal mol^{-1}. The products, hydrolyzed complex and AcH, are calculated to be more stable by 26.3 kcal mol^{-1} than the reactants' energy. The process is calculated to be less kinetically, even if more thermodynamically, favorable if the proton is transferred to the O2 atom, as the height of the barrier for the transition state TS1$_{cisPtAcO2H}$ is 23.5 kcal mol^{-1}. The first adduct lies 29.9 kcal mol^{-1} below the entrance channel and the overall process for the elimination of an acetic acid molecule is exothermic by 30.3 kcal mol^{-1}.

Analogous calculations have been carried out for satraplatin. The energy profiles describing the hydrolysis process in presence of water and H_3O^+ are depicted in Figure 2 together with the fully optimized structures of intercepted stationary points. More information on the geometry of such species can be found in the SI (Table S2). The hydrolysis of both axial ligands has been examined, whereas, according to the results for the Pt(IV) cisplatin derivative, only the pathway involving proton transfer to the O1 oxygen atom of the Ac ligand, which has been calculated to be more favorable from a kinetic point of view, is described. In the neutral environment, after the

slightly endothermic formation (2.1 kcal mol^{-1}) of the first complex/water adduct the barrier that

is necessary to overcome for the associative displacement of the Ac ligand is calculated to be

38.0 kcal mol^{-1}. The formed complex from which an acetic acid molecule is released is

destabilized with respect to reactants by 7.2 kcal mol^{-1}. The displacement of the second Ac axial

ligand by water requires 32.8 kcal mol^{-1} to occur leading to the formation of the corresponding

di-hydroxo complex, which lies 10.4 kcal mol^{-1} above the reference reactants' energy.
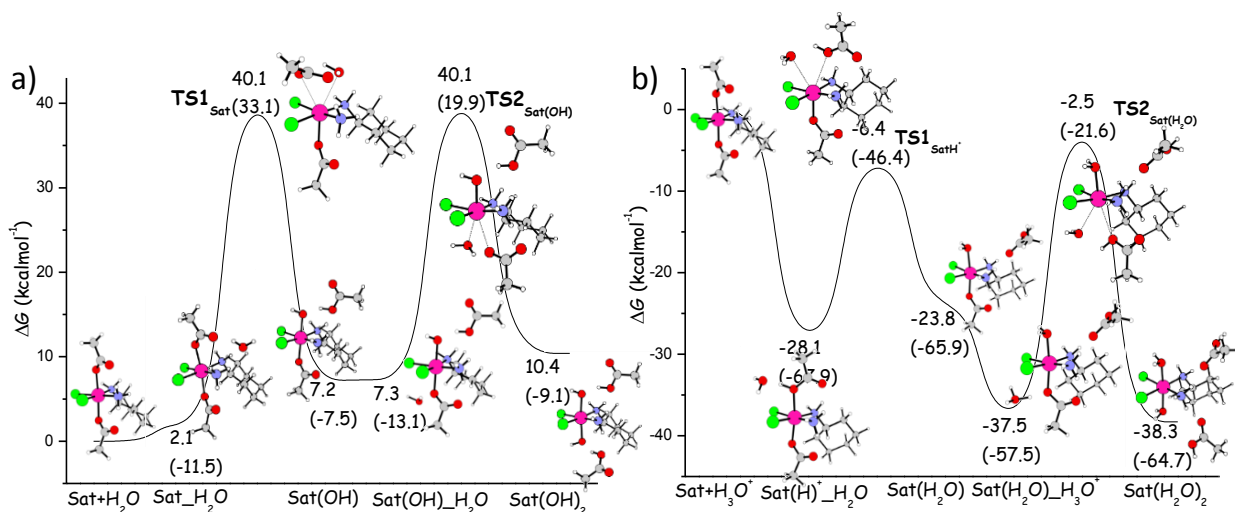
Figure 2. Calculated B3LYP energy profiles for the hydrolysis of Ac ligand in axial position of satraplatin in a) neutral and b) acidic environments. Relative ZPE-corrected electronic energies (in parentheses) and Gibbs free energies at 298.15 K in water solvent are in kilocalories per mole.

Comparison with the reaction profile describing the reaction with H_3O^+ shows a drastic change

of the energetics of the process. As reported above for the cisplatin derivative, during the

optimization a proton is transferred to the Ac ligand to form the first adduct, $Sat(H)^+\_H_2O$,

which is more stable than reactants by 28.1 kcal mol^{-1}. The associative substitution of the AcH

ligand requires 21.7 kcal mol^{-1} to occur and leads to the formation of the hydrolyzed product that

together with the AcH ligand lies 23.8 kcal mol^{-1} below the energy of the entrance channel. The

addition of a second H_3O^+ ion further stabilizes the system by 13.7 kcal mol^{-1}. One of the protons

of the oxonium ion forms a hydrogen bond with O1 atom and is definitively transferred in the transition state together with the substitution of the second axial ligand in *trans* to the water molecule. For such concerted rearrangement to occur it is necessary to surmount a high energy barrier of 35.0 kcal mol^{-1}. The di-hydrated complex together with released AcH molecules lies 38.3 kcal mol^{-1} below the reactants' reference energy.

For both cisplatin derivative and satraplatin the outcomes of our calculations show that the simulated acidic environment has a remarkable impact on the height of the barrier that is necessary to surmount for the hydrolysis of the first acetate ligand to occur. Indeed, the barrier lowers by 12.4 kcal mol^{-1} and by 14.6 kcal mol^{-1} for the model cisplatin derivative system and satraplatin, respectively with respect to the barriers calculated in neutral environment. As a consequence, more attention should be devoted to the transformations that the orally administered drug undergoes in the acidic environment of the stomach. Moreover, the acidic environment existing in tumors,[36] that favors the reduction process of the prodrugs,[33] could have an effect on the ligand elimination step by changing the nature of the ligands in the coordination sphere of the metal. Such results could be useful in understanding the observed differences between *in vitro* and *in vivo* anticancer activity of Pt(IV)-based cytostatics.[37]

3.2 Fragmentation pathways of protonated satraplatin

In this section the outcomes are reported of a detailed analysis of the collision induced dissociation (CID) products of protonated satraplatin and a quantum mechanical investigation of the fragmentation pathways leading to the experimentally determined product ions.

Electrospraying a 1mM solution of satraplatin in a 1:1 (v/v) methanol-water in the positive ion mode without allowing for any incubation time generated the mass spectrum shown in Figure 3.

The signal for the protonated satraplatin [Sat + H]$^+$ being the most dominant species appears as the cluster of peaks centered around m/z 501 (m/z 499-505). Complexes of satraplatin with both sodium and potassium ions being ubiquitous in water can be clearly observed as the cluster of peaks centered around m/z 523 (m/z 521-527) in the case of [Sat + Na]$^+$ and the cluster of peaks
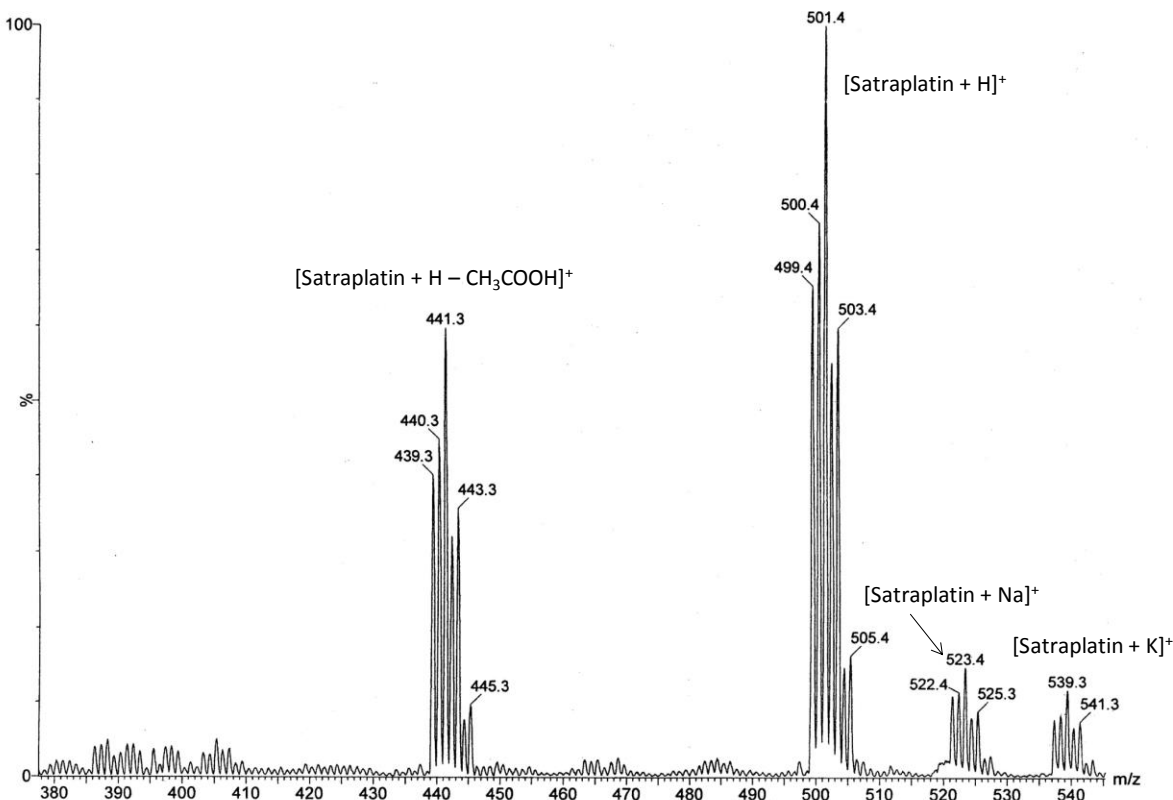

Figure 3. Full MS spectrum of a 1 mM satraplatin solution in (1:1) (v/v) water-methanol without allowing for incubation time.

centered around m/z 539 (m/z 537-543) in the case of [Sat + K]$^+$. The only other major species observed in Figure 3 appears as the cluster of peaks centered around m/z 441 (m/z 439-445) as is assigned to be due to the loss of CH_3COOH from protonated satraplatin, [Sat + H − CH_3COOH]$^+$. The presence of this species in some significant abundance in the MS spectrum shown in Figure 3 suggests that the species [Sat + H − CH_3COOH]$^+$ may be present in an appreciable concentration in the initial satraplatin methanol-water solution. This in turn implies

13

that the loss of CH_3COOH from $[Sat + H]^+$ takes place almost immediately upon dissolving satraplatin in the methanol-water solution at room temperature as used here, making it a low barrier, kinetically favored process. The observation of $[Sat + H - CH_3COOH]^+$ in Figure 3 may also indicate that the CH_3COOH is lost from the precursor ion $[Sat + H]^+$ due to collisions in the lens region. This possibility might suggest that the gas phase process of CH_3COOH loss from the ion $[Sat + H]^+$ involves a low energy barrier that would be accessible due the multiple collisions suffered by the precursor species in an attempt to achieve effective thermalization in the lens region. It is worth noting that all species observed in Figure 3 have isotopic patterns consistent with the presence of a single platinum atom with its three most abundant isotopes (being ^{194}Pt (32.9%), ^{195}Pt (33.8%) and ^{196}Pt (25.3%)) as well as two chloride atoms with their two most abundant isotopes ^{35}Cl (75.7%) and ^{37}Cl (24.2%). This indicates that the loss of either of the chloride ions from the precursor $[Sat + H]^+$ is a process that involves a larger energy barrier than the loss of CH_3COOH from the same precursor. The mass selection and subsequent collision induced dissociation (CID) of the ion $[Sat + H]^+$ as represented by the m/z 505 isotope resulted in the MS^2 spectra shown in Figure 4.

Performing the CID experiments on any of the isotopic peaks of the $[Sat + H]^+$ (m/z 499-505) resulted in same fragmentation pattern with only shifts in the m/z values of some product ions accounting for the m/z of the ion used as a precursor which confirms that there is no difference in the fragmentation pathways among the three platinum and two chlorine isotopes. The MS^2 spectra of the ion $[Sat + H]^+$ as represented by the m/z 505 isotope presented in Figure 4 shows a signal at m/z 445 assigned as $[Sat + H - CH_3COOH]^+$. This ion was also observed in the full scan MS shown in Figure 3 and assumed to involve a low energy process as discussed earlier. It is also interesting to note that energy resolved CID curve shown in Figure 5 clearly indicates that
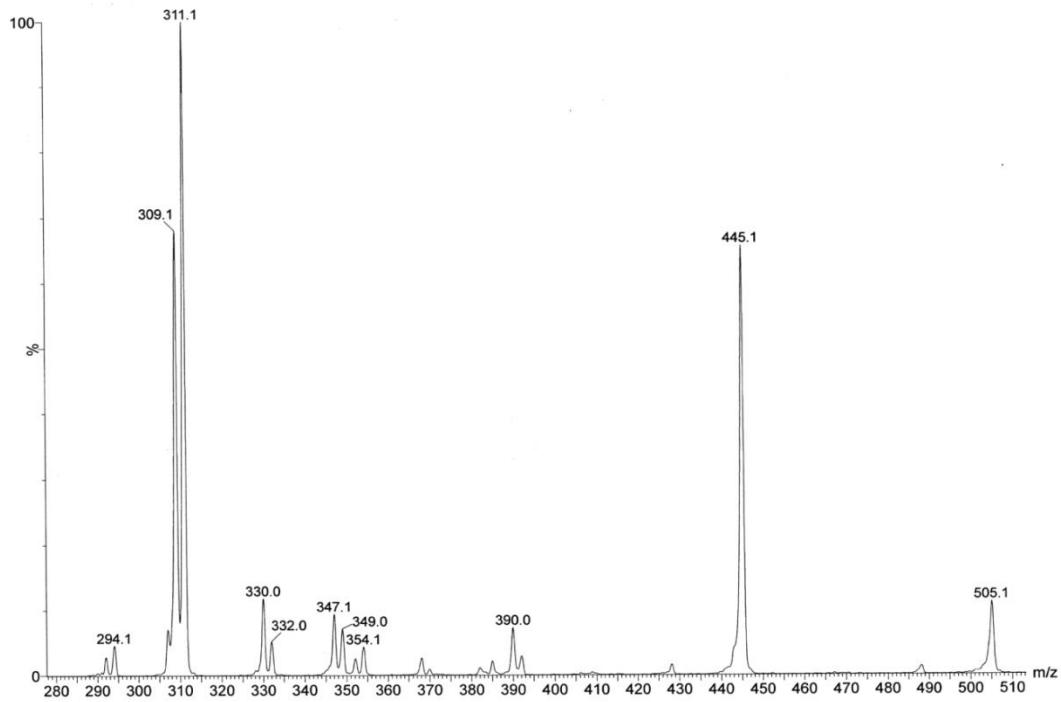
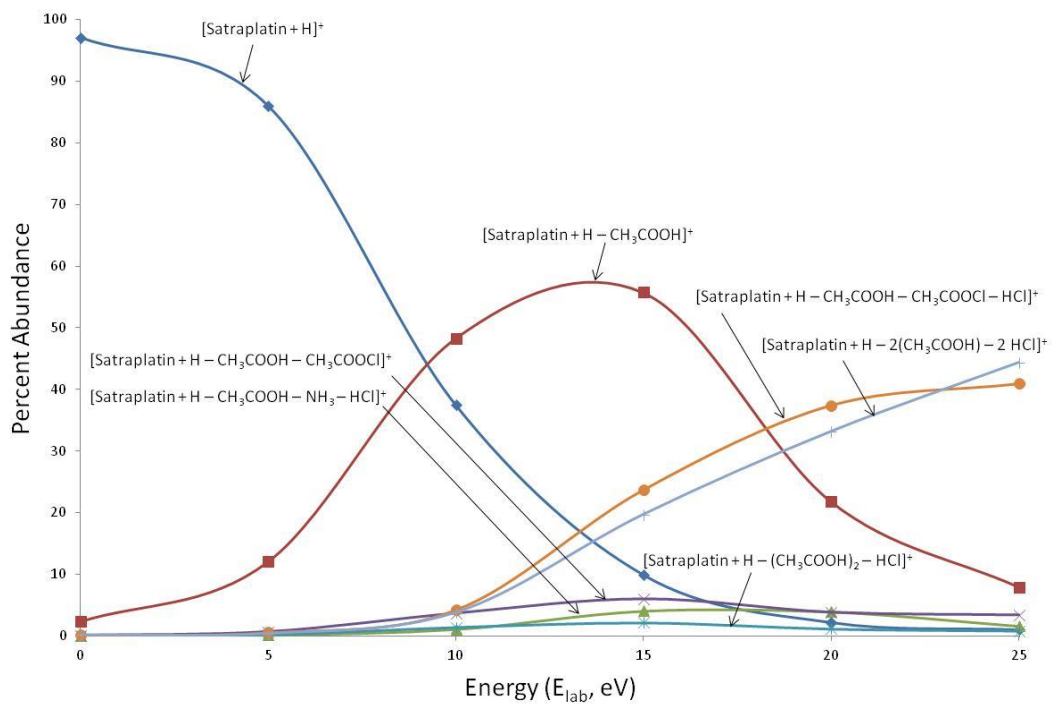**Figure 4**. MS^2 spectrum of the ion [Satraplatin + H]$^+$ generated at 20 eV in the lab frame.

Figure 5: Energy resolved collision-induced dissociation of [Satraplatin + H]$^+$

the product ion $[Sat + H - CH_3COOH]^+$ at m/z 441 resulting from the CH_3COOH loss from the precursor ion $[Sat + H]^+$ at m/z 501 involves the lowest energy process of any of the product ions observed in the MS^2 of $[Sat + H]^+$ shown in Figure 4. It is also clear from Figure 5 that the ion $[Sat + H - CH_3COOH]^+$ at m/z 441 initially increases in abundance as the energy employed increases reaching its maximum intensity at around 12 eV and then decreases in abundance at even higher energies. This indicates that the ion $[Sat + H - CH_3COOH]^+$ at m/z 441 is most likely involved in the production of ions of smaller m/z values observed in the MS^2 spectra of the ion $[Sat + H]^+$ presented in Figure 4. This is further confirmed in the MS^2 spectra and the energy resolved CID curve of $[Sat + H - CH_3COOH]^+$ shown in Figures 6 and 7 respectively. The

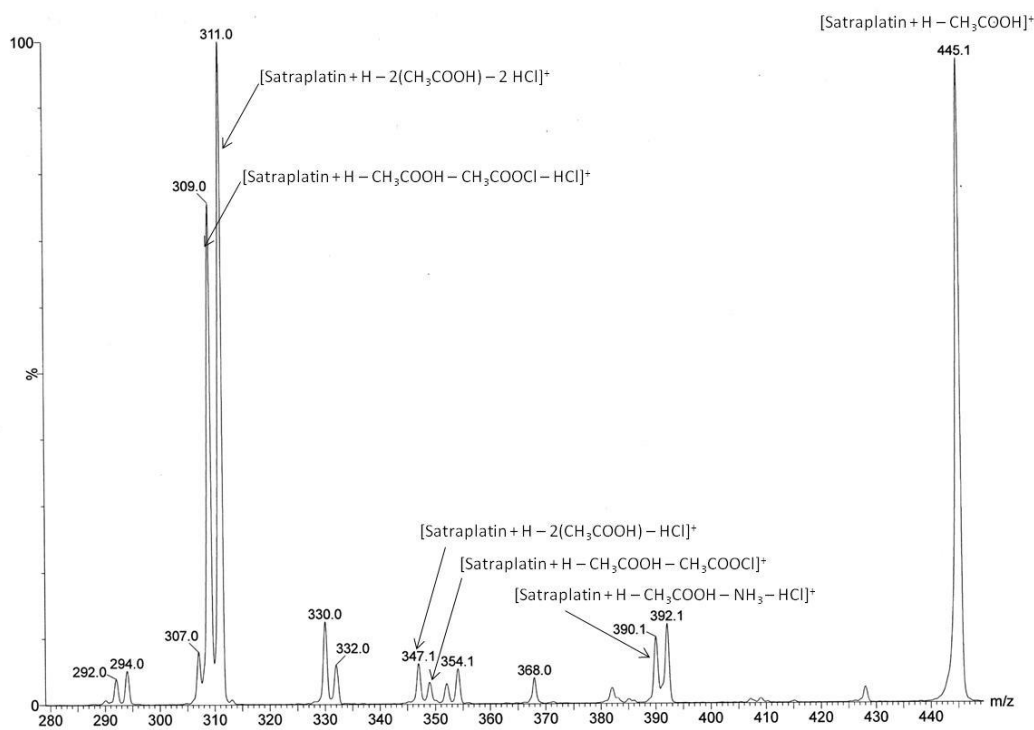**Figure 6**: MS^2 spectrum of the ion $[Satraplatin + H - CH_3COOH]^+$ generated at 15 eV in the lab frame.

intensity of the ion $[Sat + H - CH_3COOH]^+$ in Figure 7 was initially maximized through significantly increasing the bias potential in the lens region to allow for the dissociation of $[Sat +$

H]$^+$ thus in effect each point in the curve presented in Figure 7 is due to a pseudo MS^3 and thus only information pertaining to ion lineage may be ascertained while no significant energetic information may be obtained from the figure as the initial ion entering the reaction is not thermalized.

The MS^2 spectra of the ion [Sat + H]$^+$ shown in Figure 4 shows a signal at m/z 390 observed at about 10% relative abundance and assigned as [Sat + H – CH$_3$COOH – NH$_3$ – HCl]$^+$ most likely due to the simultaneous losses of NH$_3$ and HCl from the ion [Sat + H – CH$_3$COOH]$^+$ at m/z 445.

The losses of CH$_3$COOCl in one instant and the combination of CH$_3$COOH and HCl in the other
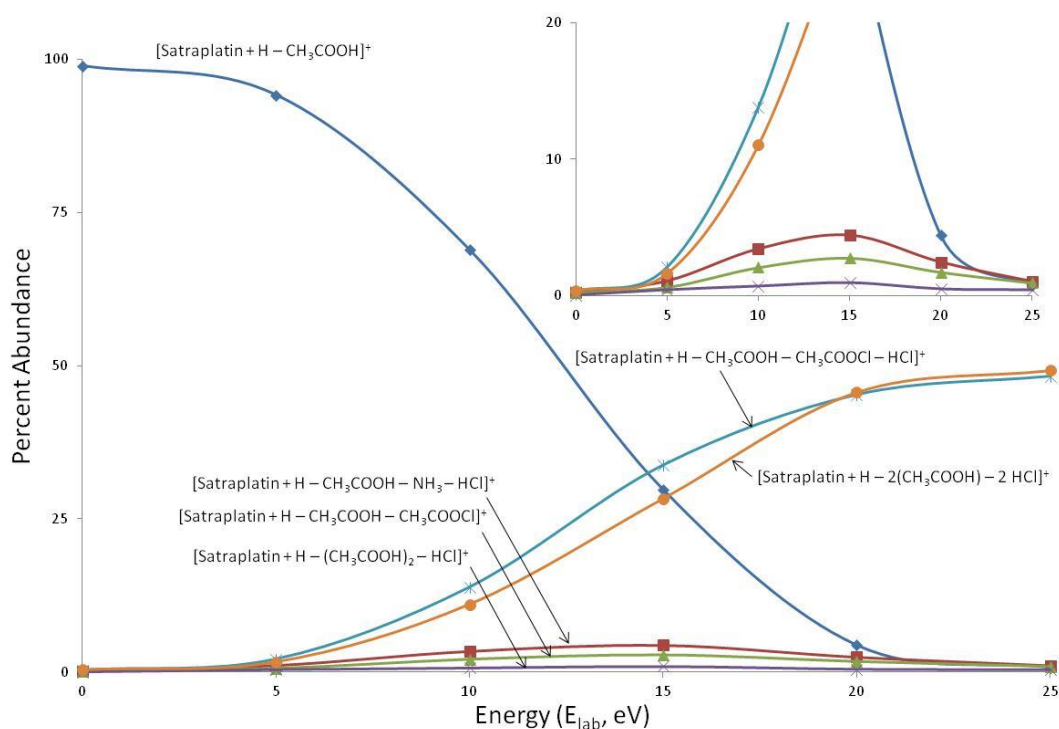

Figure 7: ~~Energy resolved~~ collision-induced dissociation of [Satraplatin + H – CH$_3$COOH]$^+$ curve. Main figure shows the full curve while the insert in the top right hand corner shows an expanded view for clarity.

from the ion [Sat + H – CH$_3$COOH]$^+$ at m/z 445 are most likely the processes involved in the production of the ions observed at m/z 349 and 347 being assigned as [Sat + H – CH$_3$COOH –

CH$_3$COOCl]$^+$ and [Sat + H – (CH$_3$COOH)$_2$ – HCl]$^+$, respectively. The two signals with the largest relative abundances observed at m/z 311 and 309 are most likely due to the subsequent losses of HCl from the ions [Sat + H – CH$_3$COOH – CH$_3$COOCl]$^+$ and [Sat + H – (CH$_3$COOH)$_2$ – HCl]$^+$ at m/z 349 and 347 respectively.

3.2.1 Low energy generation of the [Sat + H – CH$_3$COOH]$^+$ ion

The fragmentation pathways leading to the formation of the observed product ions have been theoretically explored. The Cartesian coordinates of all the intercepted stationary points are available in Table S3 of the SI. All of the reported pathways start with the structural rearrangement of the most stable isomer **1A** of the precursor ion [Sat + H]$^+$ obtained by protonation of the O2 oxygen atom non bonded to the Pt center into the isomer, protonated on the O1 atom, labeled **1B** lying 8.6 kcal mol^{-1} higher in energy. In the former minimum the H atom bonded to the O2 atom favorably interacts with the chlorine atoms in equatorial position, whereas in the latter such interaction is lost due to an upward rotation of the H atom. The interconversion between these two minima occurs going through the **TS$_{1A-1B}$** transition state overcoming an energy barrier of 16.4 kcal mol^{-1}. A further rearrangement leads to formation of the **1C** isomer in which the CH$_3$COOH ligand is coordinated to the Pt center through the O1 oxygen atom. The imaginary frequency that characterizes the **TS$_{1B-1C}$** transition state allowing this rearrangement corresponds to the concerted Pt-O2 bond breaking and Pt-O1 bond forming. The structures of the minima and transition states are depicted in Figure 8 along the energy profile that describes the fragmentation process that after the formation of the **1C** isomer proceeds with the release of the protonated Ac ligand. For the loss of a CH$_3$COOH molecule to

occur it is necessary to overcome a barrier of 22.9 kcal mol^{-1} calculated with respect to the energy of the most stable isomer, which is clearly accessible according to the experimental findings. The formed penta-coordinated intermediate, labeled **445** from the corresponding m/z value in Figure 4, lies 21.6 kcal mol^{-1} above the energy of the entrance channel and all the other fragments are released starting from such intermediate confirming that CH$_3$COOH release occurs directly from the [Sat + H]$^+$ precursor and involves the lowest energy process of any of the observed product ions.
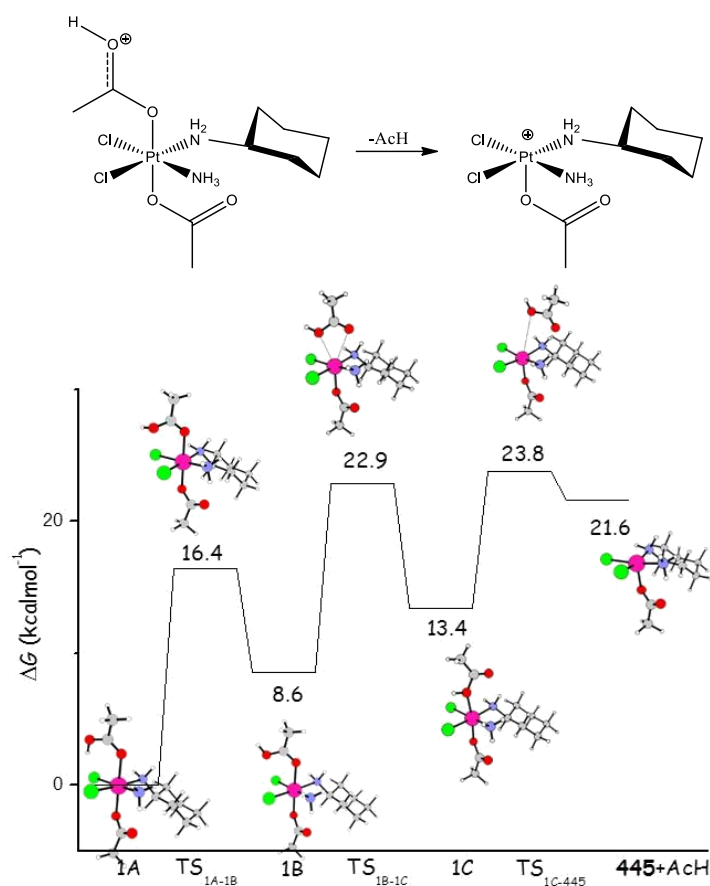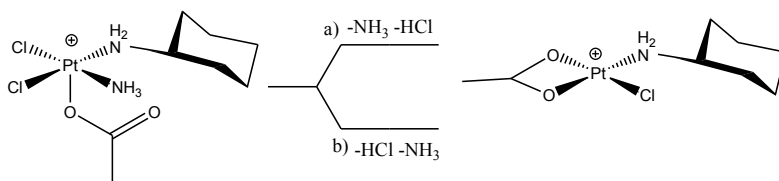

Figure 8. Calculated free energy profile for fragmentation of the protonated satraplatin complex, ion **1A**, to give the fragment [Sat + H − CH$_3$COOH]$^+$ observed at m/z=445 in Figure 4. Relative Gibbs free energies at 298.15 K are in kilocalories per mole.

For further fragmentations the outcomes obtained following the indications coming from experiments are illustrated in the next sections. It is worth mentioning that minima and transition states leading to the formation of the **445** fragment have been intercepted along a higher energy fragmentation pathway reported in Figure S1 of the SI. From the precursor ion [Sat + H]$^+$ a new isomer, named **1D**, is formed in which the favorable interaction of the H atom of the CH$_3$COOH ligand with equatorial chlorine ligands is broken due to an upward rotation of the molecule. The energetic cost for this rearrangement is low as only 10.9 kcal mol^{-1} are required and the formed isomer is less stable by 6.4 kcal mol^{-1} than the reference **1A** compound. The hydrogen shift from the oxygen atom labeled O2 to the O1 atom takes place surmounting an energy barrier of 43.5 kcal mol^{-1} and leads to formation of a very unstable isomer in which once again the CH$_3$COOH ligand is coordinated to the metal center through the protonated O1 atom. From this isomer, indicated as **1E**, lying 22.3 kcal mol^{-1} above the entrance channel energy the CH$_3$COOH ligand can be released to yield the key **445** fragment going through the corresponding **TS$_{1E-445}$** at 32.5 kcal mol^{-1}. Furthermore, an alternative viable pathway has been explored involving, after the formation of the **1B** isomer, the coordination of the acetate ligand in an η^2 fashion that causes the concerted elimination of the acetic acid unit and the displacement of the NH$_3$ ligand from the equatorial to the axial position. As shown in Figure S2 of SI, the transition state **TS$_{1B-445'}$** through which such rearrangement occurs is higher by 40.3 kcal mol^{-1} than the reference energy of the **1A** isomer. The **445'** fragment formed by loss of the acetic acid ligand, lying only 4.3 kcal mol^{-1} above the entrance channel energy, is noticeably more stable than the **445** isomer. The higher calculated barrier for the **TS$_{1B-445'}$** transition state and the stabilization of the **445'** minimum that hampers the next fragmentation steps, as probed by the very numerous attempts carried out to generate the experimentally observed product ions, confirm the **445** isomer to be the key species

for the following fragmentation pathways that we are going to describe. A superimposable description is obtained when, as a result of the η^2 coordination of the acetate ligand and acetic acid elimination, displacement of the cyclohexylamine ligand from the equatorial to the axial position occurs. Finally, it is worth of mention that the analogous possibility for the chloride ligand to transfer from the equatorial to the axial position, as a consequence of the acetate ligand η^2 coordination, has been unsuccessfully explored.

3.2.2 $[Sat + H - CH_3COOH - NH_3 - HCl]^+$

After the formation of the **445** penta-coordinated intermediate, the subsequent elimination of NH_3 and HCl produces the $[Sat + H - CH_3COOH - NH_3 - HCl]^+$ ion observed at m/z 390. As the fragmentation can proceed by either elimination of NH_3 followed by HCl release or in reversed order, that is elimination of HCl followed by NH_3 loss, both alternatives have been examined. The calculated pathways are reported in Figure 9 together with optimized structures of intercepted stationary points. The ammonia elimination directly from the **445** intermediate occurs (see Figure 9a) going through the $TS_{445-428}$ transition state with an associated barrier of 47.3 kcal mol^{-1}. The imaginary frequency confirming the nature of this transition state corresponds to the concerted formation of a new Pt-O bond with the Ac ligand that coordinates to the metal center in a chelating fashion and breaking of the Pt-N bond. The new formed intermediate **428** is more stable than the transition state leading to it by 4.3 kcal mol^{-1}. The next elimination of a HCl molecule takes place by a hydrogen atom shift from the NH_2 group to one of the chlorine atoms and occurs surmounting an energy barrier for the $TS_{428-390}$ transition state of 74.5 kcal mol^{-1} above the reference energy of the most stable isomer of the protonated satraplatin.
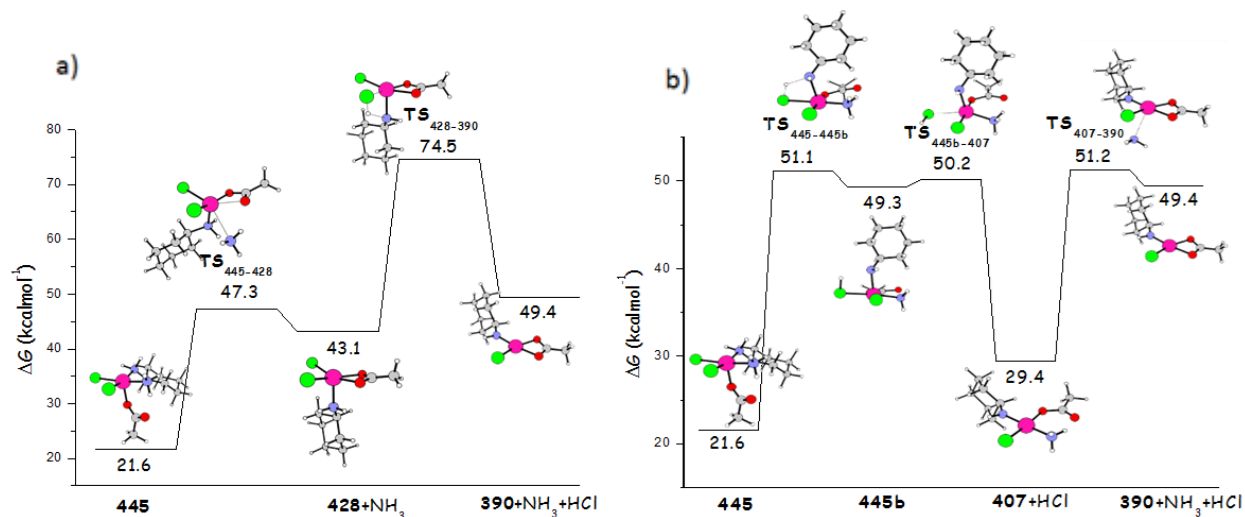
Figure 9. Calculated free energy profiles for fragmentation process that from the ion at m/z 445 leads to the fragment [Sat + H − CH$_3$COOH− NH$_3$ − HCl]$^+$ at m/z=390. Both sequential a) NH$_3$ and HCl and b) HCl and NH$_3$ release are reported. Relative Gibbs free energies at 298.15 K are in kilocalories per mole and calculated with respect the precursor ion **1A**.

The final product ion at m/z 390, is destabilized by 49.4 kcal mol^{-1} with respect to the entrance channel energy and its geometry is square planar with the acetate ligand coordinated to the metal center in a η^2 fashion.

The loss of HCl and NH$_3$ in reversed order, as shown in Figure 9b, proceeds by the preparatory H shift from the NH$_2$ group to a chlorine atom in equatorial position that requires overcoming an energy barrier of 51.1 kcal mol^{-1} for the **TS$_{445-445b}$** transition state and leads to the formation of the **445b** intermediate that is more stable by only 1.8 kcal mol^{-1} than the previous transition state. The formed HCl moiety is released going through the TS$_{445b-407}$ transition state destabilized by only 0.9 kcal mol^{-1} than the **445b** minimum. The fragmentation product at m/z 390, is obtained by release of a NH$_3$ molecule with an energetic cost of 51.2 kcal mol^{-1} corresponding to height of

the barrier for the $TS_{407\text{-}390}$ calculated with respect to zero energy of the scale and a whole destabilization, as described above, of 49.4 kcal mol^{-1}. From the outcomes of this computational analysis of the fragmentation mechanisms can be deduced that the sequential release of HCl and NH$_3$ is less energetically demanding than the NH$_3$ and HCl loss in inverted order.

3.2.3 [Sat + H – 2(CH$_3$COOH) – HCl]$^+$ and [Sat + H – 2(CH$_3$COOH) – 2HCl]$^+$

Starting from the same penta-coordinated fragment at m/z 445 the observed ion [Sat + H – (CH$_3$COOH)$_2$ – HCl]$^+$ with m/z 347 can be obtained by sequential loss of both CH$_3$COOH and HCl and viceversa of HCl and CH$_3$COOH. From such ion the further loss of a second HCl molecule generates the fragment corresponding to the peak observed at m/z 309. The energy profiles describing both alternatives can be compared in Figure 10. The former alternative, reported in Figure 10a, involves the transfer of a hydrogen atom from the NH$_3$ ligand to the uncoordinated oxygen atom of the Ac ligand. This rearrangement leads to the formation of a new isomer, **445c**, less stable by 4.1 kcal mol^{-1} of the **445** fragment and requires 48.7 kcal mol^{-1} to occur. The reaction proceeds with the interconversion between the two intermediates **445c** and **445d**, differing for their coordination to the metal center by the O2 atom in the former and O1 in the latter. The height of the barrier that separates these two isomers is 41.3 kcal mol^{-1}. From the **445d** isomer the acetic acid molecule is lost going through the $TS_{445d\text{-}385}$ transition state that lies 46.8 kcal mol^{-1} above the global **1A** minimum. With respect to **1A**, the structure labeled **385** is destabilized by 33.2 kcal mol^{-1}. The subsequent loss of the first HCl molecule requires that an H atom is transferred from the NH$_2$ group to one of the chlorine atoms. This transfer occurs in two steps: from N to Pt and from Pt to Cl.

Figure 10. Calculated free energy profiles for fragmentation process that from the ion at m/z 445 leads to the fragment [Sat + H − (CH$_3$COOH)$_2$ − HCl]$^+$ at m/z=347. Both sequential a) AcH and HCl and b) HCl and AcH release are reported. Relative Gibbs free energies at 298.15 K are in kilocalories per mole and calculated with respect the precursor ion **1A**.

The subsequent loss of the first HCl molecule requires that an H atom is transferred from the NH$_2$ group to one of the chlorine atoms. This transfer occurs 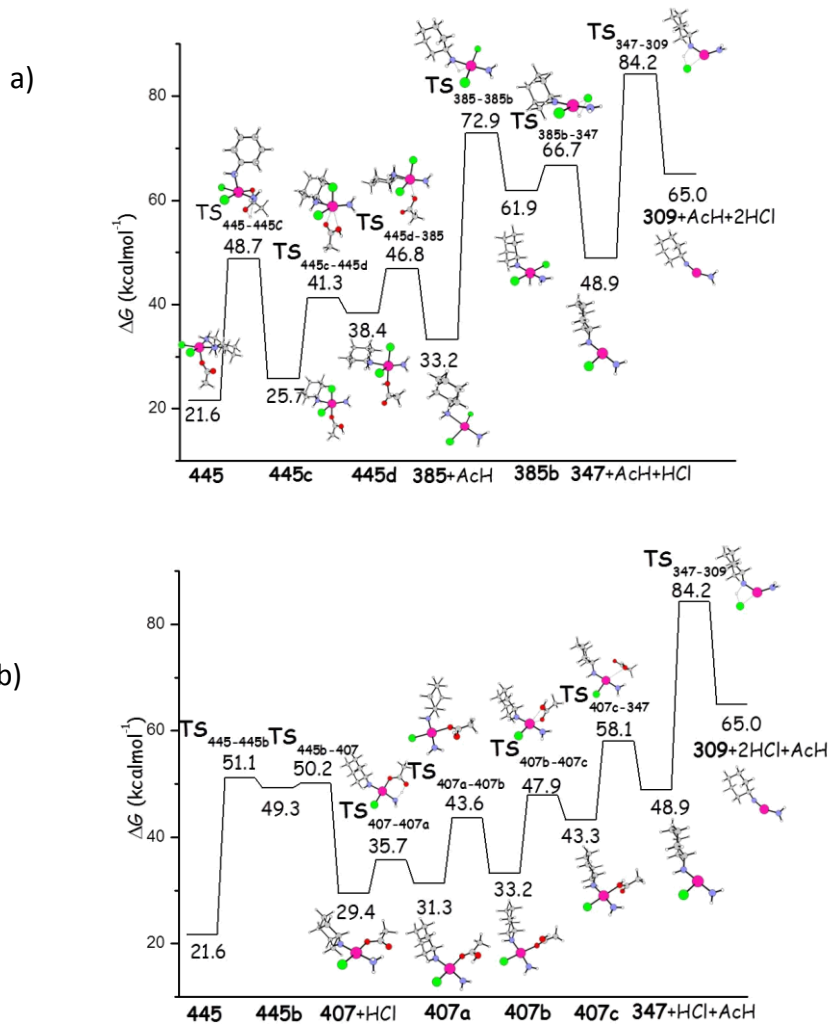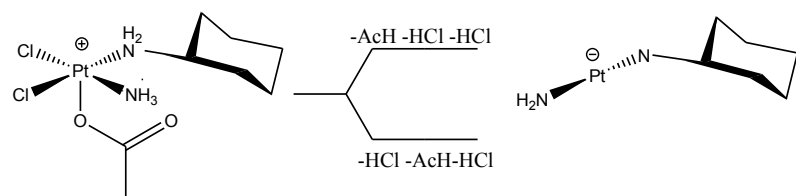in two steps: from N to Pt and from Pt to Cl. The first shift takes place going through the **TS$_{385-385b}$** with a barrier of 72.9 kcal mol^{-1}

and yields the minimum at 61.9 kcal mol^{-1}, whereas the shift from Pt to Cl causes the detachment of the HCl molecule requiring 66.7 kcal mol^{-1} to occur and leads to the formation of the corresponding ion [Sat + H − (CH$_3$COOH)$_2$ − HCl]$^+$ at m/z 347. In order to eliminate an HCl unit first, as illustrated in Figure 10b, the pathway follows the same steps described in Figure 9b leading to the formation of the ion [Sat + H − CH$_3$COOH − HCl]$^+$. The successive loss of the second CH$_3$COOH molecule goes through a series of steps that allow the hydrogen atom shift from the NH$_3$ ligand to the acetate: upward rotation of such H atom to avoid stabilizing hydrogen bond interactions, decoordination of the non-protonated O1 atom and coordination of the coordinated O2 one and finally the release of the acetic acid molecule. The calculated heights of the barriers are 35.7, 43.6, 47.9 and 58.1 kcal mol^{-1}, respectively for each of the described steps, whereas the corresponding minima lie 31.3, 33.2, 43.3 and 48.9 kcal mol^{-1} above the zero energy of the global **1A** minimum. The fragmentation process terminates, along both pathways reported in figure 10, with the elimination of the second HCl molecule and generation of the [Sat + H − (CH$_3$COOH)$_2$ − 2HCl]$^+$ ion at m/z 309. The reaction proceeds by the concerted shift of the remaining H atom on the nitrogen atom of the NH$_2$ group and the elimination of the formed HCl unit. The barrier to overcome for this rearrangement to occur is 84.2 kcal mol^{-1} and the formation of the [Sat + H − (CH$_3$COOH)$_2$ − HCl]$^+$ ion is calculated to be endothermic by 65.0 kcal mol^{-1}. From a comparison between the two free energy profiles shown in Figure 10 it appears that the sequential HCl and CH$_3$COOH elimination is energetically more amenable than the elimination in reversed order of CH$_3$COOH and HCl.

3.2.4 [Sat + H − CH$_3$COOH − CH$_3$COOCl]$^+$, [Sat + H − CH$_3$COOH − CH$_3$COOCl − HCl]$^+$ and [Sat + H − CH$_3$COOH − CH$_3$COOCl − HCl − NH$_3$]$^+$

From the fragment ion [Sat + H – CH$_3$COOH]$^+$ at m/z 445, a CH$_3$COOCl unit can be eliminated following the fragmentation path, illustrated in Figure 11, that entails several steps to achieve the final aim. First of all, an internal rearrangement of the penta-coordinated **445** fragment is required, which occurs going through the transition state **TS$_{445-445e}$** located 31.9 kcal mol^{-1} above the zero energy of the scale. Such rearrangement causes the movement of one of the Cl ligands from the *cis* position to the *trans* one with respect to the Ac ligand. The new formed intermediate **445e** is less stable by 4.9 kcal mol^{-1} than the most stable **445** isomer. In the next step the Cl atom is transferred to the Ac ligand to form the AcCl unit overcoming a barrier of 38.2 kcal mol^{-1}. The produced intermediate **445f** is slightly more stable, by 2.3 kcal mol^{-1}, than the previous **445e** one. From this intermediate the AcCl species is released, being 37.1 kcal mol^{-1} the height of the barrier for the corresponding **TS$_{445f-349}$** transition state. The formed fragment, that is the [Sat + H – CH$_3$COOH – CH$_3$COOCl]$^+$ ion at m/z 349, is more stable than the previous transition state by only 3.00 kcal mol^{-1}. The further fragmentation, as illustrated in Figure 11, involves the loss of an HCl molecule that generates the peak observed at m/z 311. The required steps to obtain the **311** fragment are three: transfer of a hydrogen atom from the amino group to the metal centre, H transfer from the Pt centre to the Cl ligand and release of the formed HCl species. The barriers for such isomerizations to occur are calculated to be 88.4, 84.3 and 76.6 kcal mol^{-1}, respectively with respect to the **1A** global minimum. The two isomeric forms of the **349** intermediate, named **349a** and **349b**, and the **311** fragment lie at 72.7, 73.9 and 72.2 kcal mol^{-1} above the reference zero energy.
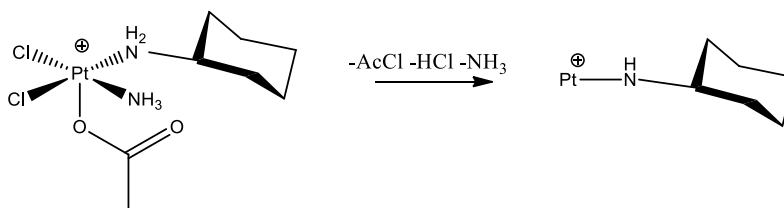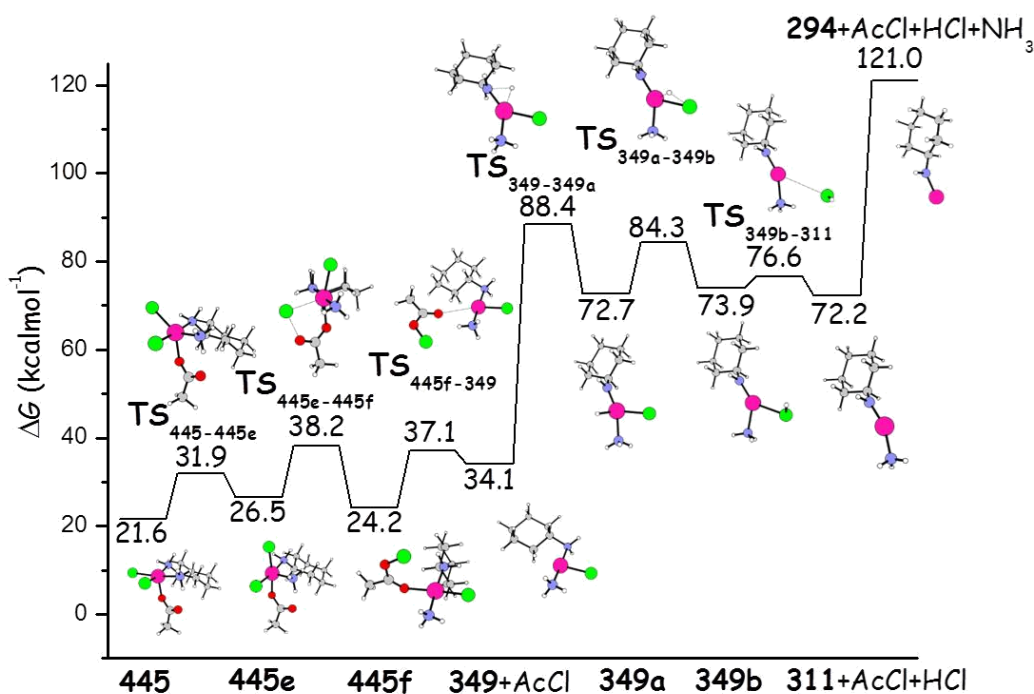
Figure 11. Calculated free energy profile for the degradation process that from the ion at m/z 445 leads to the $[Sat + H - CH_3COOH - CH_3COOCl]^+$ fragment ion at m/z 349 and by sequential release of HCl and NH_3 to the fragment $[Sat + H - CH_3COOH - CH_3COOCl - HCl - NH_3]^+$ at m/z=294. Relative Gibbs free energies at 298.15 K are in kilocalories per mole and calculated with respect the precursor ion **1A**.

To account for the peak observed at m/z 294 many attempts to eliminate a NH_3 unit have been carried out. In the same Figure 11b is reported the barrierless step that leads to the stationary point located at 121.0 kcal mol^{-1} above the entrance channel, which corresponds to the cleavage of the Pt-N bond and the formation of the **294** ion.

3.4 CONCLUSIONS

The theoretical DFT investigation presented here of the influence that acidic environments can have on the activity of octahedral six-coordinate Pt(IV) complexes having carboxylate ligands in

axial positions working as anticancer prodrugs, prove how the hydrolysis barriers of the first axial carboxylate ligand significantly lower in going from neutral to acidic solutions. Collision-induced dissociation experiments on the protonated satraplatin complex $[Sat + H]^+$ show to yield several different fragment ions, whose fragmentation pathways have been investigated and rationalized by quantum mechanical calculations. The generation of the $[Sat + H - CH_3COOH]^+$ ion at m/z 445 is shown to be the lowest energy process that takes place almost immediately after dissolution of satraplatin in the methanol-water solution at room temperature and all the other detected fragments may be generated starting from such ion. The corresponding degradation pathways have been quantum mechanically explored and for the generation of the ion at m/z 445 by loss of a protonated Ac ligand calculations confirm that the lowest energy barriers calculated here are involved. Work is in progress to analyze how the presence of electron-withdrawing groups on axial carboxylato ligands as well as the introduction of aliphatic carboxylato ligands with an increasing carbon atoms number in the chain can change the hydrolysis energy profile at different pH conditions.

Supporting Information. Cartesian coordinates (Å) of all optimized structures and additional computational and experimental results. This material is available free of charge via the Internet at http://pubs.acs.org.

AUTHOR INFORMATION

Corresponding Author

* E-mail for E.S.: emilia.sicilia@unical.it.

* E-mail for T.S.: T.Shoeib@aucegypt.edu.

Author Contributions

The manuscript was written through contributions of all authors. All authors have given approval to the final version of the manuscript.

Notes

The authors declare no competing financial interest.

REFERENCES

(1)   Wheate, N.J.; Walker, S., Craig, G.E., Oun, R. The status of platinum anticancer drugs in the clinic and in clinical trials. *Dalton Trans.* **2010**, 39, 8113-8127.

(2)   Yao, X.; Panichpisal, K.; Kurtzman, N.; Kenneth, N. Cisplatin nephrotoxicity: a review. *Am. J. Med. Sci.* **2007**, *334*, 115-124.

(3)   Heffeter, P.; Jungwirth, U.; Jakupec, M.; Hartinger., C; Galanski, M.; Elbling, L.; Micksche, M.; Keppler, B.; Berger, W. Resistance against novel anticancer metal compounds: differences and similarities. *Drug Resist. Updat.* **2008**, 11, 1-16.

(4)   Kelland, L.R. The resurgence of platinum-based cancer chemotherapy. *Nat. Rev. Cancer.* **2007**, *7*, 573-584.

(5)   Jakupec, M.A.; Galanski, M.; Arion, V.B.; Hartinger, C.G.; Keppler, B.K. Antitumour metal compounds: more than theme and variations. *Dalton Trans.* **2008**, *2*, 183-194.

(6)   Butler, J.S.; Sadler, P.J. Targeted delivery of platinum-based anticancer complexes. *Curr. Opin. Chem. Biol.* **2013**, *17*, 175-188.

(7)   Wexselblatt, E.; Gibson, D. What do we know about the reduction of Pt(IV) pro-drugs?. *J. Inorg. Biochem.* **2012**, *117*, 220-229.

(8)   Farrell, N.P. Platinum formulations as anticancer drugs clinical and pre-clinical studies. *Curr. Top. Med. Chem.* **2011**, *11*, 2623-2631.

(9)   Montana, A.M.; Batalla, C. The Rational Design of Anticancer Platinum Complexes: The Importance of the Structure-Activity Relationship. *Curr. Med. Chem.* **2009**, *16* (18) 2235-2260.

(10)   Ang, W.H.; Pilet, S.; Scopelliti, R.; Bussy, F.; Juillerat-Jeanneret, L.; Dyson, P.J. Synthesis and characterization of platinum(IV) anticancer drugs with functionalized aromatic carboxylate ligands: influence of the ligands on drug efficacies and uptake. *J. Med. Chem.* **2005**, *48*, 8060-8069.

(11)   Kelland, L.R.; Sharp, S.Y.; O'Neill, C.F.; Raynaud, F.I.; Beale, P.J.; Judson, I.R. Mini-review: discovery and development of platinum complexes designed to circumvent cisplatin resistance. *J. Inorg. Biochem.* **1999**, *77*, 111-115.

(12)   Kelland, L. R.; Abel, G.; McKeage, M. J.; Jones, M.; Goddard, P. M.; Valenti, M.; Murrer, B. A.; Harrap, K. R. Preclinical antitumor evaluation of bis-acetato-ammine-

dichloro-cyclohexylamine platinum(IV): an orally active platinum drug. *Cancer Res.* **1993**, *53*, 2581-2586.

(13)   Bhargava, A.; Vaishampayan, U. N. Satraplatin: leading the new generation of oral platinum agents. *Expert Opin. Invest. Drugs* **2009**, *18*, 1787-1797.

(14)   Martelli, L.; Di Mario, F.; Ragazzi, E.; Apostoli, P.; Leone, R.; Perego, P.; Fumagalli, G. Different accumulation of cisplatin, oxaliplatin and JM216 in sensitive and cisplatin-resistant human cervical tumour cells, *Pharmacol.* **2006**, 72, 693-700.

(15)   Brabec, V. DNA modifications by antitumor platinum and ruthenium compounds: their recognition and repair. *Prog. Nucleic Acid Res. Mol. Biol.* **2002**, *71*, 1-68.

(16)   Wang, D.; Lippard, S. J. Cellular processing of platinum anticancer drugs. *Nat. Rev. Drug Discovery* **2005**, *4*, 307–320.

(17)   Lovejoy, K. S.; Todd, R. C.; Zhang, S. Z.; McCormick, M. S.; D'Aquino, J. A.; Reardon, J. T.; Sancar, A.; Giacomini, K. M.; Lippard, S. J. cis-Diammine(pyridine)chloroplatinum(II), a monofunctional platinum(II) antitumor agent: Uptake, structure, function, and prospects. *Proc. Natl. Acad. Sci. U.S.A.* **2008**, *105*, 8902-8907.

(18)   Sternberg, C. N.; Petrylak, D. P.; Sartor, O.; Witjes, J. A.; Demkow, T.; Ferrero, J. M. J.; Eymard, C.; Falcon, S.; Calabro, F.; James, N.; Bodrogi, I.; Harper, P.; Wirth, M.; Berry, W.; Petrone, M. E.; McKearn, T. J.; Noursalehi, M.; George, M.; Rozencweig, M. Multinational, Double-Blind, Phase III Study of Prednisone and Either Satraplatin or Placebo in Patients With Castrate-Refractory Prostate Cancer Progressing After Prior Chemotherapy: The SPARC Trial. *J. Clin. Oncol.* **2009**, *27*, 5431–5438.

(19)   Wexselblatt, E.; Yavin, E.; Gibson, D. Platinum(IV) Prodrugs with Haloacetato Ligands in the Axial Positions can Undergo Hydrolysis under Biologically Relevant Conditions *Angew. Chem. Int. Ed.* **2013**, *52*, 6059-6062.

(20)   Wexselblatt, E.; Raveendran, R.; Salameh, S.; Friedman-Ezra, A.; Yavin, E.; Gibson, D. On the Stability of PtIV Pro-Drugs with Haloacetato Ligands in the Axial Positions *Chem. Eur. J.* **2014**, 20, 1-8.

(21)   Lugini, L.; Federici, C.; Borghi, M.; Azzarito, T.; Marino, M. L.; Cesolini, A.; Spugnini; E. P.; Fais, S. Proton pump inhibitors while belonging to the same family of generic drugs show different antitumor effect, *J. Enzyme Inhib. Med. Chem.*, 2016, *31*, 538-545.

(22)   Ding, S.; Bierbach, U. Target-selective delivery and activation of platinum-based anticancer agents *Future Med. Chem.* **2015**, 7, 911-927.

(23)   Frisch, M. J.; Trucks, G. W.; Schlegel, H. B.; Scuseria, G. E.; Robb, M. A.; Cheeseman, J. R.; Scalmani, G.; Barone, V.; Mennucci, B.; Petersson, G. A.; Nakatsuji, H.; Caricato, M.; Li, X.; Hratchian, H. P.; Izmaylov, A. F.; Bloino, J.; Zheng, G.; Sonnenberg, J. L.; Hada, M.; Ehara, M.; Toyota, K.; Fukuda, R.; Hasegawa, J.; Ishida, M.; Nakajima, T.; Honda, Y.; Kitao, O.; Nakai, H.; Vreven, T.; Montgomery, J. A., Jr.; Peralta, J. E.; Ogliaro, F.; Bearpark, M.; Heyd, J. J.; Brothers, E.; Kudin, K. N.; Staroverov, V. N.; Kobayashi, R.; Normand, J.; Raghavachari, K.; Rendell, A.; Burant, J. C.; Iyengar, S. S.; Tomasi, J.; Cossi, M.; Rega, N.; Millam, J. M.; Klene, M.; Knox, J. E.; Cross, J. B.; Bakken, V.; Adamo, C.; Jaramillo, J.; Gomperts, R.; Stratmann, R. E.; Yazyev, O.; Austin, A. J.; Cammi, R.; Pomelli, C.; Ochterski, J. W.; Martin, R. L.; Morokuma, K.; Zakrzewski, V. G.; Voth, G. A.;

Salvador, P.; Dannenberg, J. J.; Dapprich, S.; Daniels, A. D.; Farkas, Ö.; Foresman, J. B.; Ortiz, J. V.; Cioslowski, J.; Fox, D. J. *Gaussian 09*, Revision D.01; Gaussian, Inc: Wallingford, CT, **2009**.

(24)　a) Becke, A. D. Density-functional thermochemistry. III. The role of exact exchange. *J. Chem. Phys.* **1993**, *98*, 5648-5652; b) Lee, C.; Yang, W.; Parr, R. G. Development of the Colle-Salvetti correlation-energy formula into a functional of the electron density. *Phys. Rev. B: Condens. Matter Mater. Phys.* **1988**, *37*, 785-789.

(25)　Andrae, D.; Hüßermann, U.; Dolg, M.; Stoll, H.; Preuß, H. Energy-adjusted *ab initio* pseudopotentials for the second and third row transition elements. *Theor. Chim. Acta* **1990**, *77*, 123-141.

(26)　a) Fukui, K. A formulation of the reaction coordinate. *J. Phys. Chem.* **1970**, *74*, 4161-4163; b) Gonzalez, C.; Schlegel, H.B. An improved algorithm for reaction path following. *J. Chem. Phys.* **1989**, *90*, 2154 –2161.

(27)　Tomasi, J.; Mennucci, B.; Cammi, R. Quantum mechanical continuum solvation models. *Chem. Rev.* **2005**, *105*, 2999-3093.

(28)　McQuarrie, D. A.; Simon, J. D. *Molecular thermodynamics*; University Science Books: Sausalito, CA, **1999**.

(29)　Wertz, D.H. Relationship between the gas-phase entropies of molecules and their entropies of solvation in water and 1-octanol. *J. Am. Chem. Soc.* **1980**, *102*, 5316-5322.

(30)　a) Cheng, M.-J.; Nielsen, R. J.; Goddard III, W. A. A homolytic oxy-functionalization mechanism: intermolecular hydrocarbyl migration from M–R to vanadate oxo. *Chem. Commun.* **2014**, *50*, 10994-10996; b) Butera, V.; Russo, N.; Cosentino, U.; Greco, C.; Moro, G.; Pitea, D., Sicilia, E. Computational insight on CO_2 fixation to produce styrene

carbonate assisted by a single centre Al(III) catalyst and quaternary ammonium salts. *ChemCatChem* **2016**, *8*, 1167-1175.

(31)   Avnet, S.; Lemma, S.; Cortini, M., Pellegrini, P.; Perut, P.; Zini, N.; Kusuzaki, K.; Chano, T.; Grisendi, G.; Dominici, M.; De Milito, A.; Baldini, N. Altered pH gradient at the plasma membrane of osteosarcoma cells is a key mechanism of drug resistance. *Oncotarget*, **2016**, *7*, 63408-63423.

(32)   Wojtkowiak, J. W.; Verduzco, D.; Schramm, K. J.; Gillies R. J. drug resistance and cellular adaptation to tumor acidic pH microenvironment *Mol. Pharmaceutics* **2011**, *8*, 2032-2038.

(33)   Gabano, E.; Ravera, M.; Osella, D. Pros and cons of bifunctional platinum(IV) antitumor prodrugs: two are (not always) better than one. *Dalton Trans.*, **2014**, *43*, 9813-9820.

(34)   Ritacco, I.; Mazzone, G.; Russo, N.; Sicilia, E. Investigation of the Inertness to Hydrolysis of Platinum(IV) Prodrugs. *Inorg. Chem.* **2016**, *55*, 1580-1586.

(35)   Bradáč, O.; Zimmermann, T.; Burda J. V. Can Satraplatin be hydrated before the reduction process occurs? The DFT computational study. *J. Mol. Model.* **2013**, *19*, 4669-4680.

(36)   van Sluis, R.; Bhujwalla, Z.M.; Raghunand, N.; Ballesteros, P.; Alvarez, J.; Cerdan, S.; Galons, J.P.; Gillies, R. J. In vivo imaging of extracellular pH using ^{1}H MRSI. *Magn. Reson. Med.* **1999**, *41*, 743-750.

(37)   Theiner, S.; Varbanov, H. P.; Galanski, M.; Egger, A. E.; Berger, W.; Heffeter, P.; Keppler, B. K. Comparative in vitro and in vivo pharmacological investigation of platinum(IV) complexes as novel anticancer drug candidates for oral application. *J. Biol. Inorg. Chem.*, **2015**, *20*, 89-99.

For Table of Content Only

A joint theoretical and experimental investigation of the influence that acidic environments can have on the reactivity of the anticancer prodrug satrapaltin and of analogous octahedral Pt(IV) complexes having two carboxylates as axial ligands has been carried out. Such study sheds some light on the fate of the drugs, synthetized to be orally administered, after their assumption.

TOC graphics
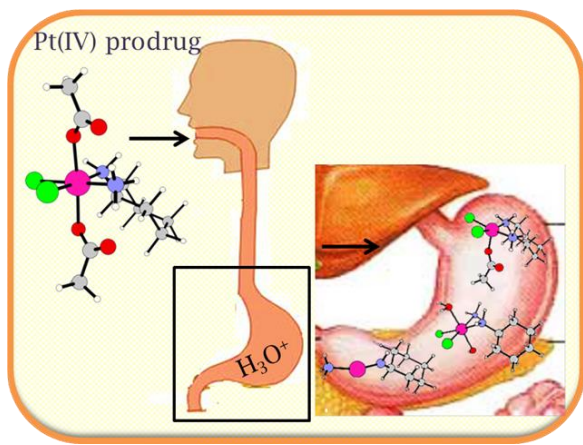
CHAPTER V

A New Class of Anticancer Drugs: Organoiridium(III) Complexes

Introduction

After the discovery of the anticancer activity of cisplatin by Rosenberg in the 1960s [1], a large number of platinum anticancer drugs have been synthesized and tested for their biological activity. However, the remarkable versatility and the side-effects of cisplatin and its derivatives have motivated the exploration of non platinum metal antitumor agents. These new anticancer drugs show reduced side effects and resistance, greater efficacy towards a wider range of human cancers and they can have various mechanisms of action [2]. In fact, their mechanism of action may involve both an attack on DNA and a perturbation of the redox status of cancer cells. Generally, cancer cells exhibit high oxidative stress with an increased production of reactive oxygen species (ROS). Oxidative stress, so the ROS production, causes the diseased cells to undergo apoptosis. Aim of these non-platinum metal antitumor agents is to catalyze the formation of ROS in order to increase oxidative stress and promote the cancer cells death. In this respect iridium complexes appear to be excellent candidates. Initially, attention was focused on d^8 Ir(I) square-planar complexes with square-planar geometry similar to cisplatin [3,4]. More recently, iridium(III) complexes have shown promising antiproliferative activity toward cancer cells [5]. Ir(III) is often considered to be one of the most inert low-spin d^6 metal ions. Generally,

iridium(III) complexes are very inert, so they possess a low reactivity. Introducing proper ligands is possible to increase the reactivity of these complexes and improve their anticancer properties [6,7]. Iridium(III) complexes of general formula [(η^5-Cp^x)Ir(III)(X^Y)Z]$^{0/+}$ appear to be potent anticancer agents [8]. Commonly, these complexes are called half-sandwich organoiridium(III) complexes.

A recent study carried out by Sadler's group has confirmed the high reactivity of the organoiridium(III) complexes [(η^5-Cp^{xbiph})Ir-(phpy)(Cl)] (**1-Cl**) and [η^5-Cp^{xbiph})Ir-(phpy)(py)] (**1-py**) which contain the C^N-chelated phenylpyridine (phpy) and π-bonded biphenyltetramethylcyclopentadienyl (Cp^{xbiph}) ligands. This complex should cause an increase of the oxidative stress through reactive oxygen species (ROS) production.

5.1 Aim of the study

In this Chapter for the two complexes **1-Cl** and **1-py**, with the aid of the DFT calculations, the mechanisms of the hydrolysis reaction, H_2O_2 ROS production by assisted hydride transfer from NADH to molecular oxygen, interaction with adenine, guanine and very abundant in cells glutathione have been theoretically investigated. Furthermore, the reaction mechanism for the oxidation of the formed sulfur-coordinated thiolate to the

corresponding sulfenato complex has been investigated. Then, a comparison between the calculated potential energy surfaces (PESs) for all the involved processes and the experimental observations will be reported (**Paper VI**).

5.2 DFT investigation of the mechanism of action of organoiridium(III) complexes as anticancer agents (Paper VI).
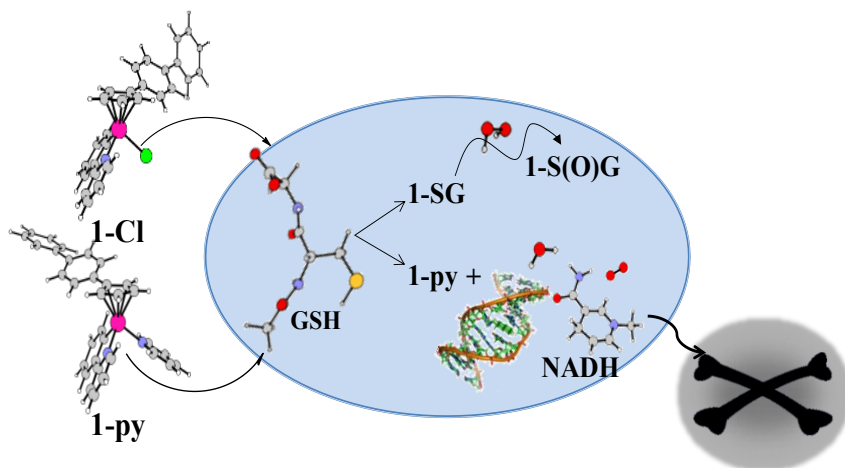
Experimental data show that inside the human body the organoiridium complex $[(\eta^5\text{-Cp}^{xbiph})\text{Ir-(phpy)(Cl)}]$ (**1-Cl**) can undergo rapid hydrolysis and consequent deactivation. The organoiridium complex $[(\eta^5\text{-Cp}^{xbiph})\text{Ir-(phpy)(py)}]$ (**1-py**), instead, hydrolyzes slowly and exhibits high anticancer activity. For this reason, Sadler and his coworkers thought to protect the complex **1-Cl** from deactivation by replacing the chlorido ligand with pyridine ligand [9]. Therefore, aiming at confirming the

experimental data, the ability to undergo hydrolysis of the two complexes **1-Cl** and **1-py** has been theoretically investigated. According to Sadler's group studies, in the cancer cells **1-Cl** e **1-py** can react with glutathione and affect their anticancer activity. To understand the role of glutathione in differentiating anticancer activity of **1-Cl** and **1-py** complexes the interaction between the tripeptide and the two half-sandwich Ir complexes, through the use of computational techniques has been investigated. From this interaction, by substitution of the chlorido and pyridine ligands in the anticancer complexes **1–Cl** and **1–py** with glutathione, the complex $[(\eta^5\text{-}Cp^{xbiph})Ir(phpy)(SG)]^-$, **1-SG**, is formed. The theoretical data, in agreement with experimental data, confirm that the reaction with the glutathione (GSH) is very rapid for the **1-Cl** complex, but very slow for the **1-py** complex.

Furthermore, to prove that these iridium(III) complexes are oxidant drugs, the reaction between **1-py** and **1-Cl** complexes with the coenzyme nicotinamide adenine dinucleotide, NADH, which leads to the H_2O_2 ROS formation has been examined. In addition to this mechanism, called primary mechanism, a secondary mechanism, according to which the two complexes **1-Cl** and **1-py** interact with the DNA of the cancer cells has been also explored.

Finally, the oxidation potential energy surface (PES) of the complex **1-SG** to **1-S(O)G**, through interaction with H_2O_2 produced via hydride transfer from coenzyme NADH to iridium and then to O_2 has been reported [10]. According to Liu and Sadler, this new adduct can play a role in the anticancer activity of such iridium complexes.

In order to elucidate the MoA of **1-Cl** and **1-py** iridium complexes DFT calculations have been performed employing M06-L functional. For Ir the relativistic compact Stuttgart/Dresden effective core potential has been used in conjunction with the split valence basis set, while the standard triple-ζ quality basis sets 6-311+G** have been used for the atoms directly participating in the process. For peripheral C and H atoms the smaller 6-31G basis sets have been used. The impact of solvation effects on the energy profiles has been estimated by using the Tomasi's implicit Polarizable Continuum Model (PCM) and the UFF set of radii has been used to build-up the cavity.

REFERENCES CHAPTER V

[1] Rosenberg, B., Van Camp, L., Krigas, T., *Nature,* **1965**, *205*, 698– 699

[2] a)Giraldi, T., Sava, G., Mestroni, G., Zassinovich, G., Stolfa, D., *Chem.-Biol. Interact.,* **1978**, *22*, 231-238.
b)Sava,G., Zorzet, S., Perissin, L., Mestroni, G., Zassinovich, G., Bontempi, A., *Inorg. Chim. Acta,* **1987**, *137*, 69-71.

[3] Trachootham, D., Alexandre, J., Huang, P., *Nat. Rev. Drug Discovery*, **2009**, *8*, 579–591.

[4] (a) Liu Z., Sadler, P. J., *Acc. Chem. Res.*, **2014**, *47*, 1174-1185.(b)Wirth, S., Rohbogner, C. Cieslak, M., Kazmierczak-Baranska, J., Donevski, S., Nawrot, B., Lorenz, I.-P., *J. Biol. Inorg. Chem.*, **2010**, *15*, 429-440. (c)Casini, A., Edafe, F., Erlandsson, M., Gonsalvi, L., Ciancetta, A., Re, N., Ienco, A., Messori, L., Peruzzini, M., Dyson, P. J., *Dalton Trans.,* **2010**, *39*, 5556-5563. (d)Gras, M., Therrien, B., Süss-Fink, G., Casini, A., Edafe, F., Dyson, P. J., *J. Organomet. Chem.*, **2010**, *695*, 1119-1125.(e)Ruiz, J., Rodriguez, V., Cutillas, N., Samper, K. G., Capdevila, M., Palacios, O., Espinosa, A., *Dalton Trans.*, **2012**, *41*, 12847-12856.(f)Lo, K. K.-W., Zhang, K. Y., *RSC Adv.*, **2012**, *2*, 12069-12083;(g)Gasser, G., Ott, I., Metzler-Nolte, N. *J., Med. Chem.*, **2011**, *54*, 3-25.

[5] (a) Wilbuer, A., Vlecken, D. H., Schmitz, D. J., Kräling, K., Harms, K., Bagowski, C. P., Meggers, E., *Angew. Chem., Int. Ed. Engl.,* **2010**, *49*, 3839-3842. (b) Messori, L. Marcon, G., Orioli, P., Fontani, M., Zanello, P., Bergamo, A., Sava, G., Mura, P., *J. Inorg. Biochem.,* **2003**, *95*, 37-46.(c) Marcon, G., Casini, A., Mura, P., Messori, L., Bergamo, A., Orioli, P., *Metal-Based Drugs,* **2000**, *7*, 195-200.

[6] Cusanelli, A., Frey, U., Richens, D. T., Merbach, A. E., *J. Am.Chem. Soc.,* **1996**, *118*, 5265-5271.

[7] Poth, T., Paulus, H., Elias, H., Dücker-Benfer, C., van Eldik, R., *Eur. J. Inorg. Chem.,* **2001**, 1361-1369.

[8] (a)Liu, Z., Sadler, P., J. *Acc. Chem. Res.,* **2014**, *47*, 1174-1185.(b) Hearn, J., RomeroCanelón, I., Qamar, B.,Liu, Z., Hands-Portman, I., Sadler, P.J.,*ACSChem. Biol.,* **2013**, *8*,1335-1343.(c)Liu, Z., Habtemariam, A., Pizarro, A.M., Fletcher, S. A., Kisova, A., Vrana, O., Salassa, L., Bruijnincx, P.C.A., Clarkson, G.J., Brabec, V., Sadler, P.J., *J.Med.Chem.,* **2011**, *54*,3011-3026. (d)Liu, Z., Salassa, L., Habtemariam, A., Pizarro, A. M., Clarkson, G. J., Sadler, P.J., *Inorg. Chem.,* **2011**, *50*, 5777-5783. (e)Liu, Z., Romero-Canelón,I., Habtemariam, A., Clarkson,G. J., Sadler, P. J. *Organometallics* **2014**, *33*, 5324-5333. (f)Ali Nazif, M,

Bangert, J.-A., Ott, I., Gust, R., Stoll, R, Sheldrick, W. S., J. *Inorg. Biochem,* **2009**, *103*, 1405-1414.

[9] Liu, Z., Romero-Canelón, I., Qamar, B., Hearn, J. M., Habtemariam, A., Barry, N. P. E., Pizarro, A. M., Clarkson G. J., Sadler, P. J., *Angew. Chem., Int. Ed.,* **2014**, *53*, 3941-3946.

[10] Liu, Z., Sadler P. J., *Inorg. Chem. Front.*, **2014**, *1,* 668-672.

Paper VI

"DFT Investigation of the Mechanism of Action of Organoiridium(III)Complexes As Anticancer Agents"

Ida Ritacco, Nino Russo, Emilia Sicilia.

DFT Investigation of the Mechanism of Action of Organoiridium(III) Complexes As Anticancer Agents

Ida Ritacco, Nino Russo, and Emilia Sicilia*

Dipartimento di Chimica e Tecnologie Chimiche, Università della Calabria, Ponte P. Bucci, Cubo 14cI-87030, Arcavacata di Rende, Italy

S *Supporting Information*

ABSTRACT: The potential use of synthetic metal complexes able to catalyze chemical transformations in living organisms is currently attracting a great deal of attention. Recently, organometallic ruthenium and iridium complexes have revealed an unexpected ability to modulate the redox status of cancer cells. In particular, half-sandwich organoiridium(III) cyclopentadienyl complexes of general formula $[(\eta^5\text{-}Cp^x)Ir(III)\text{-}(X^\wedge Y)Z]^{0/+}$, where Cp^x = Cp*, Cp^{xph} (tetramethyl-(phenyl)-cyclopentadienyl) or Cp^{xbiph} (tetramethyl(biphenyl)-cyclopentadienyl), $X^\wedge Y$ = bidentate ligand with nitrogen, oxygen, and/or carbon donor atoms, and Z = Cl, H_2O, or pyridine (py) have shown promising antiproliferative activity toward cancer cells, higher potency than cisplatin, and a different mechanism of action due to the increase of the oxidative stress in cells. As such, complexes can belong to the class of DNA interacting compounds and attack on DNA can represent a secondary mechanism of action. We have explored here by means of density functional calculations (M06-L) and with the support of experimental observations for both $[(\eta^5\text{-}Cp^{xbiph})Ir\text{-}(phpy)\ (Cl)]$, **1-Cl**, and $[(\eta^5\text{-}Cp^{xbiph})Ir\text{-}(phpy)\ (py)]$, **1-py**, complexes the mechanistic aspects of the hydrolysis reaction, H_2O_2 ROS production by assisted hydride transfer from NADH to molecular oxygen, interaction with purine nucleobases adenine and guanine as well as gluthatione, that is highly abundant in cells, alongside the reaction mechanism for the oxidation of the formed sulfur-coordinated thiolate to the corresponding sulfenato complex. The comparison between kinetic and thermodynamic parameters calculated for all the involved processes shows that, according to the hypothesis based on experimental findings, the interaction with the tripeptide glutathione causes deactivation of **1-Cl**, whereas **1-py**, in both its aquated and nonaquated form, can induce cell apoptosis in a dual manner: DNA damage and H_2O_2 ROS production to increase oxidative stress.
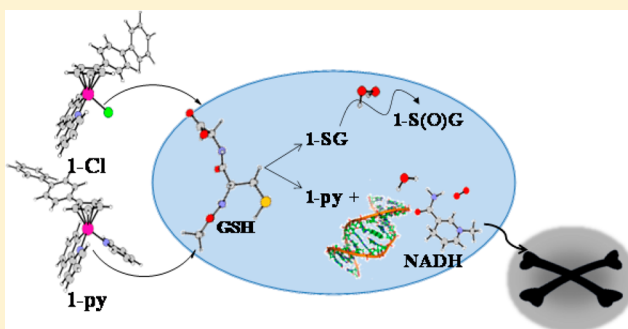
INTRODUCTION

Cisplatin, *cis*-diamminedichloroplatinum(II), was the first Pt-based complex used as an antiproliferative agent and is well-known for its high level and broad spectrum of anticancer activity.[1] Since the serendipitous discovery of the anticancer activity of cisplatin by Rosenberg in the 1960s,[1a] a large number of anticancer Pt(II) drugs have been synthesized and tested for their biological activity,[2] but only a few of them, like carboplatin and oxaliplatin, are used in clinical therapy for applying to various types of cancers.[2a,3] Pt(II)-based anticancer drugs are square-planar d^8 complexes that activated by hydrolysis trigger cancer cell death by binding to nuclear DNA and distorting its structure.[4] However, in spite of their remarkable versatility, side effects of cisplatin and related Pt(II) complexes limit their clinical usefulness and represent a continuing challenge.[5] Both clinical success and drawbacks of Pt antineoplastic compounds have motivated the exploration of non-platinum metal antitumor agents having reduced side effects, lower resistance, and efficacy toward a wider range of cancers and different mechanisms of action (MoA).[6] Over the past decade, increased efforts have been devoted toward targeting redox alterations in cancer[7] because tumors frequently exhibit high oxidative stress with an increased production of reactive oxygen species (ROS). The consequential increased vulnerability of cancer cells to modulations of the ROS homeostasis has therefore been exploited with oxidative stress promoting redox catalysts. Iridium complexes are particularly promising in this respect even if initial efforts have been concentrated on d^8 Ir(I) square—planar complexes in analogy with cisplatin.[8] More recently, encouraging antiproliferative activity toward cancer cells of organometallic complexes of the Ir(III) low-spin d^6 ion have been investigated.[9] Iridium(III) complexes are generally thought to be too inert to possess high reactivity, and even hundreds of years can be required to exchange ligands.[10] However, the introduction of proper ligands can significantly increase the ligands exchange rate and modulate inertness and stability that might also be suitable properties for anticancer drugs.[11] A series of half-sandwich cyclopentadienyl anticancer complexes of general formula $[(\eta^5\text{-}Cp^x)Ir(III)(X^\wedge Y)Z]^{0/+}$,

where the Cp^x ligand can be a pentamethylcyclopentadienyl (Cp*), phenyltetramethylcyclopentadienyl (Cp^{xph}), or biphenyltetramethylcyclopentadienyl (Cp^{xbiph}) moiety, X^Y is a chelating ligand, and Z is Cl or pyridine (py), has been synthesized and characterized as potential anticancer agents.[12] The general structure of such complexes is shown in Scheme 1.

Scheme 1. General Structure of Ir(III) Cyclopentadienyl Complexes
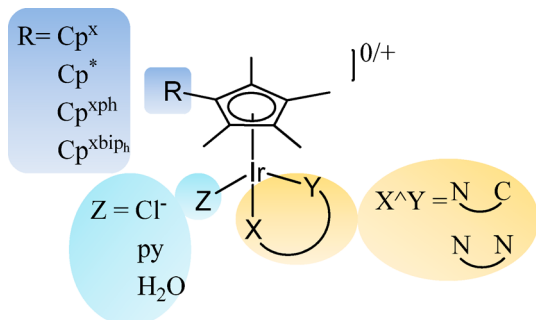
The extended arene in the functionalized Cp* ligand may play a role in interactions with a target. The chelating ligand X^Y affords additional stability to the complex and contributes to tuning the electronic properties of the iridium center. The monodentate ligand Z, such as chloride, can provide a labile site for substitution reactions with target sites.

Very recently, Sadler's group[13] has reported an investigation of the organoiridium(III) complex [(η^5-Cp^{xbiph})Ir-(phpy)(Cl)], containing the C^N-chelated phenylpyridine (phpy) and π-bonded biphenyltetramethylcyclopentadienyl (Cp^{xbiph}) ligands, as a model of a new generation of anticancer drugs, which should cause an increase of the oxidative stress owing to both production of reactive oxygen species (ROS) and diminished ability to scavenge ROS.

On the basis of the results of such investigation, Sadler and co-workers have demonstrated that the organoiridium complex [(η^5-Cp^{xbiph})Ir-(phpy)(Cl)], for which we adopt the same label used in the reference paper, **1-Cl**, undergoes rapid hydrolysis of the chlorido ligand. The pyridine analogue [(η^5-Cp^{xbiph})Ir-(phpy)(py)], synthesized starting from **1-Cl**, instead, hydrolyzes slowly. As a consequence, the authors have hypothesized that replacement of the chlorido ligand with pyridine (py) protects the complex from deactivation. Also, the reaction with

the abundant intracellular thiol glutathione (GSH), that is very rapid for the **1-Cl** complex, becomes very slow for the pyridine complex, **1-py**. Evaluation tests of the antiproliferative activity suggest that, even if **1-py** is more potent than **1-Cl**, the MoA of both complexes is different from that of cisplatin and other platinum complexes. Aiming at proving that the anticancer activity of such complexes should be that expected for oxidant drugs, the authors have investigated whether the reaction of **1-py** and **1-Cl** complexes with the coenzyme nicotinamide adenine dinucleotide, NADH, can lead to the production of ROS. The ability of both **1-py** and **1-Cl** to catalytically transfer a hydride from NADH to molecular oxygen forming H_2O_2 has been demonstrated. Such results suggest the primary mechanism of action of this class of iridium complexes to be perturbation of the redox status of cells, whereas attack on DNA and its damage should represent the secondary mechanism. Indeed, the investigation[12c,d] of adduct formation with both 9-ethylguanine (9-EtG) and 9-methyladenine (9-MeA) has shown that the monodentate ligand, such as chloride and py, can provide a labile site for substitution reactions with the potential DNA target site. Finally, very recently, Liu and Sadler have shown that the iridium glutathione adduct, indicated from now on as **1-SG**, formed by substitution of the chlorido or pyridine ligands in **1-Cl** and **1-py**, respectively, by S-bound glutathione can be readily oxidized to the sulfenato complex **1-S(O)G** by H_2O_2 produced via hydride transfer from coenzyme NADH to iridium and then to O_2.[14] The authors suggest that the new adduct can play a role in the anticancer activity of such iridium complexes.

With the aim to elucidate the MoA of **1-Cl** and **1-py** iridium complexes and to rationalize a great deal of experimental data, we have performed density functional theory (DFT) calculations, which can provide valuable information exploitable in optimizing the design of this class of anticancer complexes. For both the **1-Cl** complex and **1-py** analogue, the mechanistic routes of the hydrolysis reaction and H_2O_2 ROS production by hydride transfer from NADH to molecular oxygen have been theoretically explored. Interactions with GSH as well as purine nucleobases adenine (A) and guanine (G) have been also investigated alongside the reaction mechanism for the formed **1-SG** oxidation to **1-S(O)G**. Our study shows that the primary MoA of both **1-Cl** and **1-py** complexes should be the increase of the oxidative stress. According to the hypothesis formulated on the basis of the experimental findings,[13] it seems to be the interaction with the tripeptide glutathione that plays a crucial
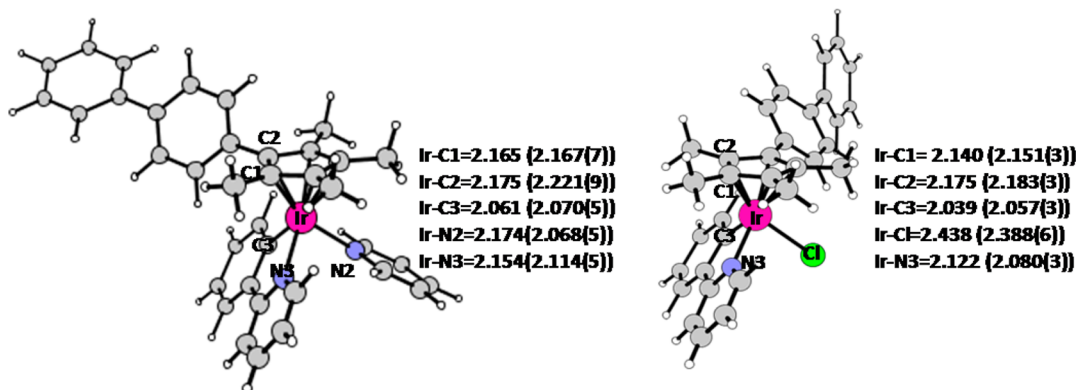

Figure 1. Fully optimized structure of **1-Cl** and cationic portion of **1-py** complexes. Selected bond lengths (in Å) are compared with available experimental values (in parentheses).

role in influencing both the fate and the potency of the two complexes, causing deactivation of the **1-Cl** in comparison to the less reactive **1-py**.

■ RESULTS AND DISCUSSION

M06-L fully optimized structure of the **1-Cl** and **1-py** complexes are shown in Figure 1, where the experimental and theoretical values of the most significant geometrical parameters are compared. Calculated geometrical parameters agree with those extracted from the crystallographic characterization[13,15] of the complexes, indicating a good modeling of the investigated systems. Supporting Information (SI) gives atomic coordinates for the complexes (Table S1).

1. Hydrolysis of Chloride, 1-Cl, and Pyridine, 1-py, Complexes. Given that metal aqua complexes are often more reactive than their equivalent nonaqua complexes and hydrolysis can represent an activation step for transition metal anticancer compunds[12c,16] as for Pt drugs,[17] the ability to undergo hydrolysis of the M−Z bond has been investigated also for half-sandwich cyclopentadienyl anticancer complexes.[13,15] Such studies have shown as the presence of the strongly bound pyridine ligand slows down the hydrolysis reaction by several orders of magnitude compared to that of its chlorido analogue **1-Cl**.

M06-L free energy profiles in solvent for the aquation reaction of the chloride complex **1-Cl** and the corresponding pyridine complex **1-py** are compared in Figure 2. Fully
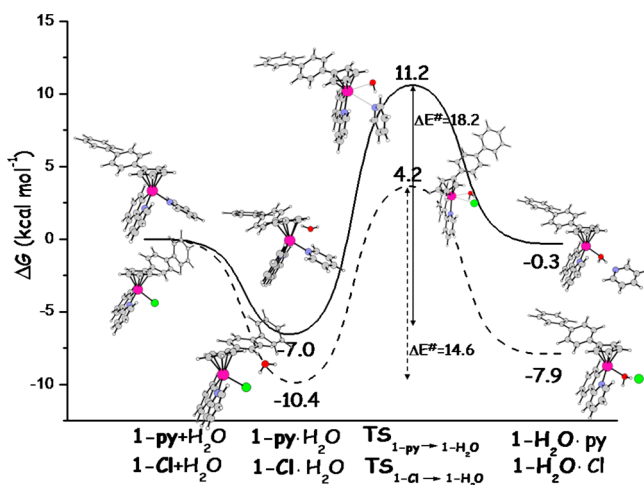

Figure 2. Calculated M06-L free energy profiles in water for the hydrolysis of **1-py** (solid line) and **1-Cl** (dashed line). Energies are in kcal·mol^{-1} and relative to separated reactants.

optimized geometrical structures of all intercepted stationary points are sketched in the same figure. Minima and transition states Cartesian coordinates can be found in the SI. According to the previous theoretical investigations,[18] several water attack modes have been explored and only one of them, the lowest energy one, has been reported. For both complexes, the reaction proceeds by formation of a first adduct in which the water molecule interacts with the chlorine atom of **1-Cl** complex and nitrogen atom of the py ligand in **1-py** complex. Adducts are more stable than separated reactants by 10.4 kcal mol^{-1} in the former case and 7.0 kcal mol^{-1} in the latter. The reaction proceeds by second-order nucleophilic substitution (SN2), that is an exchange of two ligands, the chlorine anion and py, with the water molecule. The transition state structures

for the associative displacement of chlorine and py ligands lie 4.2 and 11.2 kcal mol^{-1} above the reactants reference energy, respectively, that is, the barrier that is necessary to overcome is 14.6 kcal mol^{-1} for the displacement of the Cl^{-} and 18.2 kcal mol^{-1} for the py ligand. The substitution reaction is calculated to be exothermic by 7.9 kcal mol^{-1} for the displacement of chorine anion and almost thermoneutral for the displacement of the py ligand. The hydrolysis reaction of the **1-Cl** complex is calculated to be more favored from both kinetic and thermodynamic points of view according to experimental findings that show how the substitution of the Cl^{-} ligand with pyridine slows down the rate of the hydrolysis reaction.

Because the methyl groups of the Cp^{xbiph} ligand have been substituted with hydrogen atoms with the purpose to reduce the computational cost, the effects of such substitution have been preliminarily checked. In the SI (Figure S1) is reported a comparison between the energy profiles for chloride and py ligands substitution by water when both biphenyltetramethyl-cyclopentadienyl (**1*-Cl** and **1*-py**) and biphenylcyclopenta-dienyl (**1-Cl** and **1-py**) ligands are used. Such comparison shows that the presence of methyl groups on the Cp^{xbiph} ligand has little effect on the course of the reaction. The more electrodonating CH$_3$ groups on the Cp ring increase the lability of the monodentate Z ligand with a consequent lowering of the barriers by about 2 kcal mol^{-1}. However, as can be deduced by both NBO charge analysis (Table S2 in the SI) and molecular electrostatic potential (MEP) calculations (Figure S2) for the four complexes **1*-Cl**, **1*-py**, **1-Cl**, and **1-py**, methyl groups on the Cp ligand mainly increase the electron density on both biphenyl substituent and C^N-chelated phenylpyridine ligand. This effect is more evident for the **1-py** complex. As expected, in the region of the Z ligand, the surface of chlorido complexes is much more negative than their pyridine analogues.

2. Interactions with Nucleobases. DNA is usually a potential target for transition metal anticancer drugs, as platinum-based drugs that have chiefly contributed to cancer chemotherapy in the last 30 years.[2] Although it has been proved that the underlying biological effects of **1-Cl**, **1-py**, and analogous half-sandwich Ir(III) complexes do not correlate with that of cisplatin,[12a,b,13] interactions with DNA have been equally well investigated,[12,13] as they should represent one of the factors involved in their mechanism of action.

Because, in analogy with Pt-based anticancer drugs, aqua complexes appear to react more readily with nucleobases,[12c] the interaction of the aqua complex **1-H₂O** with a purine base site of DNA has been studied computationally using adenine and guanine as model reactants. Calculated free energy profiles for the interaction with the **1-H₂O** complex are depicted in Figure 3a for guanine and Figure 3b for adenine. Optimized structures of intermediates and transition states intercepted along the guanine and adenine coordination pathways are shown in the same figures, whereas Cartesian coordinates can be found in Table S1 of the SI. Previous investigations[12d] have shown that Ir metal center reacts with guanine via N7 and forms adenine adducts via both N1 and N7, with the N1 interaction adduct being the major product. In addition, investigated Ir complexes showed a higher affinity for guanine in comparison with adenine. The free energy profiles in Figure 3a show that the interaction with guanine stabilizes the formed adduct by 19.2 kcal mol^{-1}. The transition state for the associative displacement of the water molecule and coordination of guanine through the N7 binding site lies 7.6 kcal mol^{-1} above, whereas the whole process leading to the final N7-coordinated guanine complex
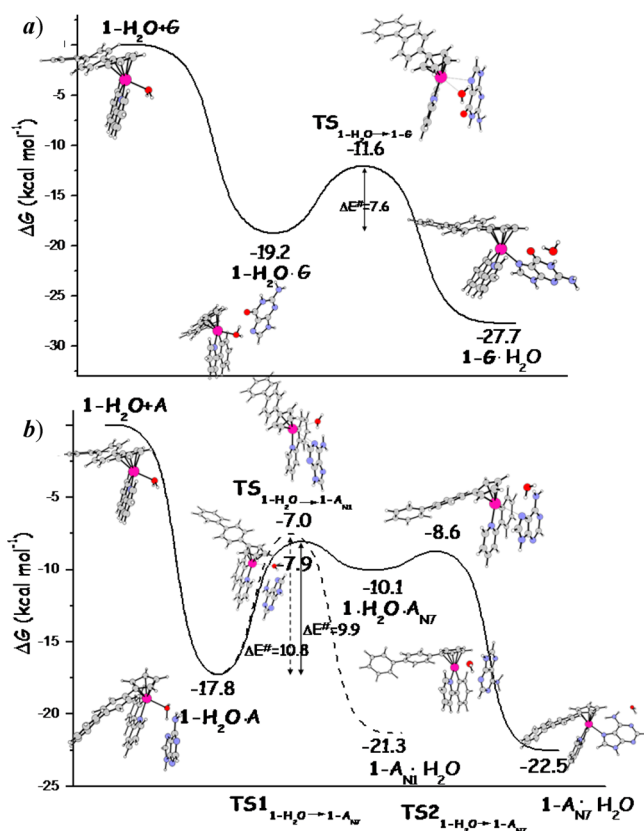
Figure 3. Calculated M06-L free energy profiles in water for the coordination of guanine (a, upper) and adenine (b, lower) to the aqua complex **1-H$_2$O**. For adenine both N7 (solid line) and N1 (dashed line), coordination sites have been considered. Energies are in kcal·mol^{-1} and relative to separated reactants.

formation is calculated to be exothermic by 27.7 kcal mol^{-1}. Along the analogous pathways for the coordination of adenine, the interaction between the **1-H$_2$O** complex and adenine leads to the formation of the first intermediate that is stabilized by 17.8 kcal mol^{-1} with respect to reactants' reference energy. Displacement of the water ligand by adenine takes place by following two different mechanisms for binding to N1 and N7 sites: a one-step associative in the former case and a two-step dissociative mechanism in the latter. For the associative displacement of the water molecule and coordination of the N1 site the intercepted transition lies 7.0 kcal mol^{-1} below the entrance channel and then 10.8 kcal mol^{-1} above the first adduct. Product formation is exothermic by 21.3 kcal mol^{-1}. For the dissociative mechanism allowing coordination of the N7 site, the first transition state for the release of H$_2$O is formed overcoming an energy barrier of 9.9 kcal mol^{-1} and the formed intermediate is calculated more stable by only 2.2 kcal mol^{-1}. The height of the free energy barrier for the next transition state, which allows the N7 site adenine coordination, is only 1.5 kcal mol^{-1}. The process occurs in a stepwise manner even if this region of the surface is very flat. The overall substitution process is exothermic by 22.5 kcal mol^{-1}. The results of our computational analysis do not clearly discriminate between the N1 and N7 modes of coordination neither from a kinetic nor thermodynamic point of view, whereas the preferential binding with guanine in respect to adenine is confirmed.

To check whether the direct interaction of **1-Cl** and **1-py** complexes with nucleobases is less favorable than the interaction of their corresponding aquated complexes, potential energy surfaces (PESs) for the displacement of Cl$^-$ and py ligands and coordination of guanine have been calculated (see Figure 4).
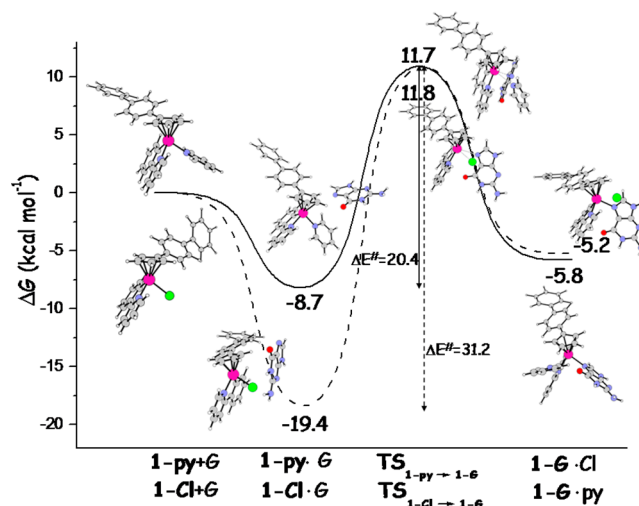

Figure 4. Calculated M06-L free energy profiles in water for guanine coordination to **1-py** (solid line) and **1-Cl** (dashed line). Energies are in kcal·mol^{-1} and relative to separated reactants.

The first formed adduct along the pathway for chloride anion substitution is stabilized by 19.4 kcal mol^{-1} with respect the reference energy of separated reactants, whereas the transition state for the associative guanine substitution lies 11.8 kcal mol^{-1} above. That is, an activation barrier of 31.2 kcal mol^{-1} hampers the displacement process that is calculated to be exothermic by 5.2 kcal mol^{-1}. The relative energies of the first adduct and the transition state for the associative mechanism of displacement with respect to separated reactants along the analogous pathway for the **1-py** complex are −8.7 and 11.7 kcal mol^{-1}, respectively. Therefore, the py ligand substitution takes place overcoming an activation barrier of 20.4 kcal mol^{-1} and leads to the formation of the **1-G** complex that is more stable by 5.8 kcal mol^{-1} than separated reactants. Calculations confirm that, in analogy with other metal anticancer drugs, hydrolysis represents the activation step for DNA binding when the **1-Cl** complex is the cytotoxic agent as the formed **1-H$_2$O** complex reacts more readily with nucleobases than **1-Cl**. In the case of **1-py**, instead, it is more difficult to select the preferred mechanism. Indeed, the height of the calculated barrier for the activation of **1-py** by hydrolysis, 18.2 kcal mol^{-1}, is only by about 2 kcal mol^{-1} lower than that, of 20.4 kcal mol^{-1}, for the direct guanine coordination by displacement of the py ligand.

3. Reaction with Glutathione Tripeptide. The tripeptide c-L-glutamyl-L-cysteinyl-glycine (glutathione or GSH) is the most abundant low-molecular-weight thiol containing molecule in human cells and it is believed to form with cisplatin complexes that are a significant cellular sink of the Pt drug, causing its inactivation by forming stable adducts, thus preventing the drug from reaching and binding to DNA.[19] Moreover, reactions of metal complexes with GSH can affect the redox state of cells[20] due to its antioxidant properties, which prevent damage to cellular components caused by reactive oxygen species.[21] Thus, the possible role that could be played
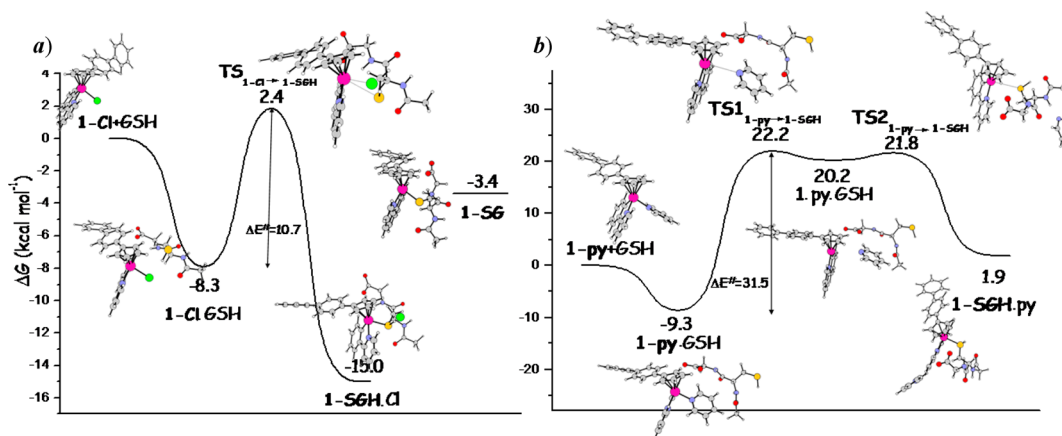
Figure 5. Calculated M06-L free energy profiles in water for the coordination of GSH to the **1-Cl** (a, left) and **1-py** (b, right) complexes. Energies are in kcal·mol^{-1} and relative to separated reactants.

by both GSH in differentiating anticancer activity of **1-Cl** and **1-py** complexes[13] and thiol-mediated redox reactions in the MoA of half-sandwich Ir complexes[15] has been investigated. By substitution of the chlorido and pyridine ligands in the anticancer complexes **1-Cl** and **1-py** with glutathione, the complex $[(\eta^5\text{-Cp}^{xbiph})\text{Ir}(\text{phpy})\,(\text{SG})]^-$, **1-SG**, is formed. With respect to the reaction of **1-Cl** with GSH, the presence of the py ligand in **1-py** slows down the rate of the substitution reaction by several orders of magnitude.

The outcomes of our exploration of the interaction mechanism of GSH with both **1-Cl** and **1-py** are displayed in Figure 5 for both free energy profiles and stationary point optimized geometries. At physiological pH, the GSH tripeptide assumes zwitterionic form at the glutamyl residue, the cysteine moiety has neutral thiol (SH) side chain and the carboxyl group of the glycine fragment is deprotonated. The computational requirements have been reduced cutting the glutamyl residue. The interaction between **1-Cl** and GSH leads to the formation of an adduct that is more stable than separated reactants by 8.3 kcal mol^{-1}. The favored coordinating mode of GSH to the metal center is through the thiol group that is still protonated. The transition state structure leading to the formation of the HS-bound thiol complex, **1-SGH**, characterized by an imaginary frequency describing the formation of the Ir–S bond and the breaking of the Ir–Cl bond, lies only 2.4 kcal mol^{-1} above the reference energy of dissociated reactants. That means that the free energy barrier for the formation of the substitution product is 10.7 kcal mol^{-1}. The formed product is stabilized by 15.0 kcal mol^{-1} with respect to reactants. Along the analogous pathways for the displacement of the py ligand, the first intermediate is calculated to lie 9.3 kcal mol^{-1} below the entrance channel of the reaction, whereas the substitution of py with GSH proceeds following a dissociative mechanism involving two transition states and a minimum separating them. The height of the barrier to overcome for the first transition state, **TS1**$_{1\text{-py}\rightarrow1\text{-SGH}}$, is 31.5 kcal mol^{-1} for the release of the py ligand. The next minimum lies only 2.0 kcal mol^{-1} below the energy of the transition state, leading to it and the barrier of the second transition state, **TS2**$_{1\text{-py}\rightarrow1\text{-SGH}}$, for the coordination of glutathione is only 1.6 kcal mol^{-1}. As it clearly appears from Figure 5b, this region of the potential energy profile is very flat and the geometry of the **TS1**$_{1\text{-py}\rightarrow1\text{-SGH}}$ transition state is very close to that of the next intermediate. Therefore, as the ligand displacement does not take place in a concerted manner,

decoordination of the py ligand represents the slow step that slows down the GSH coordination reaction. The final product lies 1.9 kcal mol^{-1} above the reactants' reference energy. The outcomes of our computations confirm that the energetic cost for the displacement of the py ligand by GSH is remarkably higher than that required to substitute the chloride ligand. Formation of **1-SGH** product complex from **1-Cl** is also favored from a thermodynamic point of view. It is worth emphasizing that, from a comparison of such barriers with the corresponding barriers for the aquation reactions, the glutathione interaction with the **1-Cl** complex involves the lowest energy barrier. Hydrolysis of **1-py**, on the contrary, is more favorable than py ligand displacement by GSH and, mainly, interaction with GSH, much more than aquation, differentiates the behaviors of **1-Cl** and **1-py** complexes.

The final complex **1-SG** is formed by cysteine thiol group SH deprotonation that should be facilitated by coordination to the iridium center also in a nonalkaline medium, as we are going to prove. The equation $\text{GSH}_{(\text{solv})} \rightarrow \text{GS}^-_{(\text{solv})} + \text{H}^+_{(\text{solv})}$ for the isolated glutathione and $\textbf{1-SGH}_{(\text{solv})} \rightarrow \textbf{1-SG}^-_{(\text{solv})} + \text{H}^+_{(\text{solv})}$ for the HS-bound glutathione complex have been employed together with the experimental value of -269.0 kcal mol^{-1} for the aqueous solvation free energy of the proton, including conversion of the ΔG_{gas} reference state (24.46 L at 298.15 K) from 1 atm to 1 M.[22] The calculated values of the reaction free energy for the equations reported above measuring the deprotonating ability of isolated and Ir-coordinated cysteine thiol − SH group are 14.2 and -3.4 kcal mol^{-1}, respectively, that means about 11 pk_a units.

4. Oxidation of NADH to NAD$^+$ and Generation of ROS. The studies carried out recently by Sadler's group demonstrate that Ir anticancer complexes such those under investigation are able to accept hydride from NADH in aqueous solution and the hydride in turn can be transferred to oxygen to generate H_2O_2.[12a,13] The use of organometallic complexes and intracellular antioxidants allows generating ROS in cancer cells that causing oxidative stress can provide an effective strategy for curing cancer. Experiments have demonstrated that both **1-Cl** and **1-py** are able to accept a hydride from NADH and successively generate the H_2O_2 ROS even if the reaction of **1-py** appears to be slower. The authors have suggested that this difference in behavior maybe due to the difference in hydrolysis rate of the two complexes.

Scheme 2. Proposed Mechanisms for Hydride Transfer from MNH to 1-Z Complexes
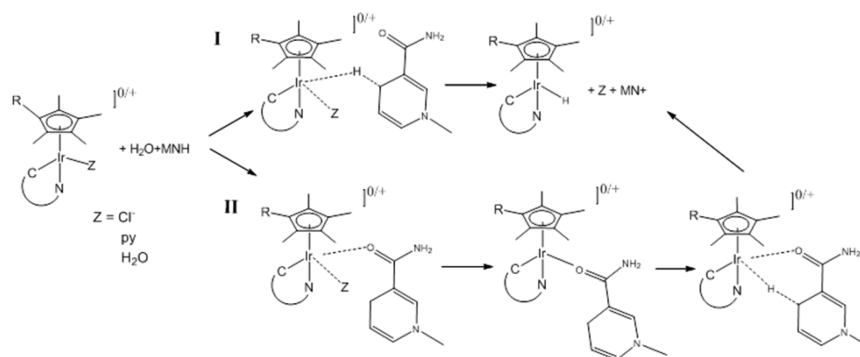
To simulate the hydride transfer reaction from NADH to the **1-Z** complexes (Z = H$_2$O, Cl, py), two likely mechanisms have been explored (see Scheme 2). Mechanism labeled **I** involves direct transfer of the hydride from NADH to the metal center concomitant to the displacement of the Z ligand. Mechanism labeled **II** occurs in two steps: displacement of the Z ligand and coordination of the carbonyl oxygen of NADH followed by hydride transfer to form the **1-H** complex and the NADH oxidized form NAD$^+$. Potential energy surfaces calculated at M06-L level for the hydride transfer from NADH to the hydrolyzed complex **1-H$_2$O** following **I** and **II** mechanisms are shown Figure 6. To reduce the computational cost, the model
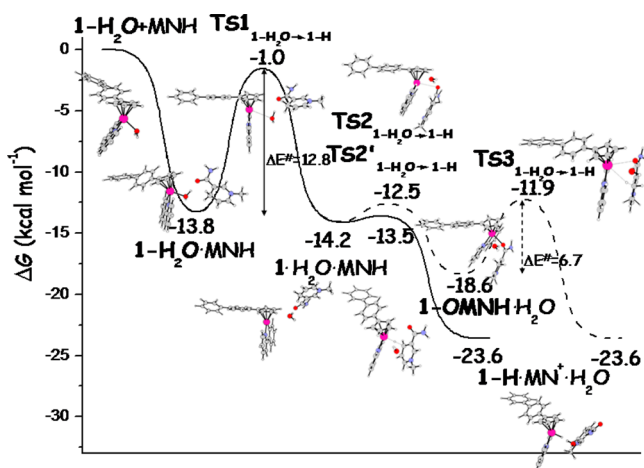

Figure 6. Calculated M06-L free energy profiles in water for the coordination of MNH to the **1-H$_2$O** along **I** (solid line) and **II** (dashed line) pathways. Energies are in kcal·mol^{-1} and relative to separated reactants.

N-methyl-1,4-dihydronicotinamide, MNH, has been used for mimicking NADH. Analogous calculations carried out for hydride transfer to **1-Cl** and **1-py** are reported and commented below.

Along both **I** and **II** pathways, in the first step, the interaction between **1-H$_2$O** complex and MNH leads to the formation of the corresponding adduct stabilized by 13.8 kcal mol^{-1} with respect to separated reactants. The next step should be displacement of H$_2$O and coordination of either the hydride along the path **I** or MNH through the carbonyl oxygen along the path **II**. The substitution occurs following a dissociative mechanism that entails first the elimination of the water molecule overcoming an energy barrier of 12.8 kcal mol^{-1} and formation of a coordinatively unsaturated intermediate that is

more stable by only 0.4 kcal mol^{-1} than the previous minimum. Conversion of MNH into its corresponding oxidized form MN$^+$ through direct hydride transfer to the metal center to form the Ir hydride complex **1-H** requires to occur the overcoming of a very low, only 0.7 kcal mol^{-1}, free energy barrier. The imaginary frequency, calculated to be 282i cm^{-1}, corresponds to the movement of the hydrogen atom detaching from carbon and bonding to Ir.

The overall process is calculated to be exothermic by 23.6 kcal mol^{-1}. Along the path **II** for the coordination of the carbonyl oxygen of MNH to the metal center to occur, it is necessary to surmount a very low energy barrier of 1.7 kcal mol^{-1}. The calculated imaginary frequency of 50i cm^{-1} describes the movement for the formation of a new Ir−O bond. The formed intermediate is stabilized by 18.6 kcal mol^{-1} with respect to the reference energy and by 4.4 kcal mol^{-1} than the previous minimum. The final step leading to formation of the **1-H** complex takes place with the hydride transfer from the CH$_2$ moiety of MNH at an energetic cost of 6.7 kcal mol^{-1} for the transition state **TS3$_{1\text{-H2O}\rightarrow1\text{-H}}$**. From such exploration of the probable mechanisms results that the hydride transfer reaction from NADH to Ir center and formation of NAD$^+$, very likely, occurs by initial dissociative displacement of the H$_2$O ligand and direct hydride transfer from the CH$_2$ group of NADH.

For the sake of completeness, we have carried out analogous calculations for the oxidation of MNH to MN$^+$ in the presence of **1-Cl** and **1-py** to confirm that, as it is reported in the literature,[8a,23,24] the **1-H$_2$O** aqua complex is the oxidizing agent that accepts the hydride from MNH. Both mechanisms named **I** and **II** in Scheme 2 have been explored. Calculated free energy profiles for the **II** mechanism are depicted in Figure 7, whereas the mechanism **I** appears to be not viable because water competes for coordination and substitution of Cl$^−$ and py ligands with a water molecule occurs in state of the hydride transfer. Along path **II** the first step is adduct formation that occurs with an energy gain of 28.2 kcal mol^{-1} for **1-Cl** and 17.3 kcal mol^{-1} for **1-py**. Next, the second-order nucleophilic substitution of chloride and pyridine ligands and formation of a new Ir−O bond with the carbonyl oxygen of MNH takes place. The activation energies are calculated to be 14.8 and 15.1 kcal mol^{-1} for the **1-Cl** and **1-py** complexes, respectively. The formed intermediates lye 22.4 and 10.7 kcal mol^{-1} below the entrance channel for Cl$^−$ and py substitution, respectively. The subsequent decoordination of MNH and hydride transfer from the CH$_2$ group to the metal center to form MN$^+$ requires 5.9 and 8.2 kcal mol^{-1} along the pathways starting from the **1-Cl** and **1-py** complexes, respectively. The product of the process, the iridium hydride complex **1-H**, lies 25.6 and 23.4 kcal mol^{-1}
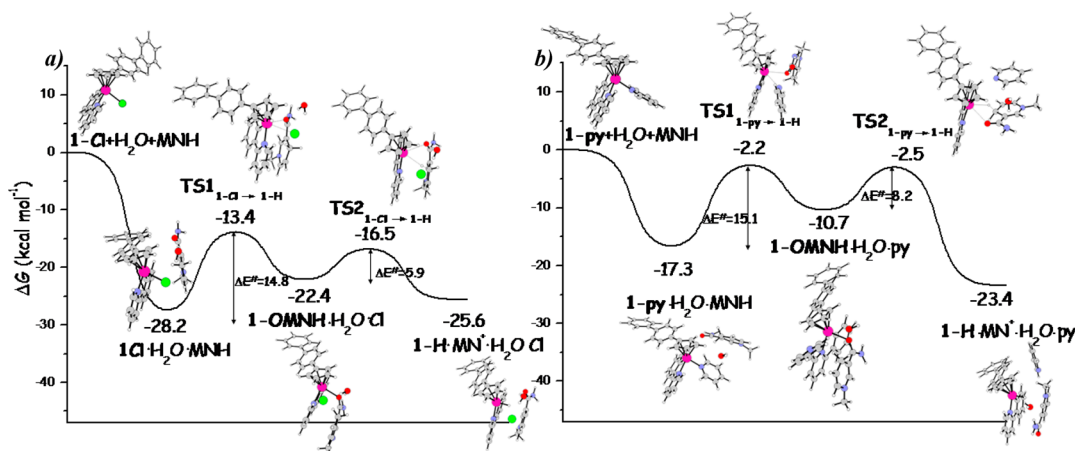
Figure 7. . Calculated M06-L free energy profiles in water for the coordination of MNH to the **1-Cl** (a left) and **1-py** (b right) along the pathway named **II**. Energies are in kcal·mol^{-1} and relative to separated reactants.

below the reference energy of separated **1-Cl** and **1-py** reactants, respectively.

To summarize, the **1-H$_2$O** aqua complex interacts with NADH, modeled by MNH, for the hydride transfer and formation of the corresponding hydride complex more favorably than **1-Cl** and **1-py** complexes. The difference in the activation energies for aquation is therefore responsible for the observed difference in the rates of NADH oxidation reaction for the two complexes. If the direct interaction of **1-Cl** and **1-py** complexes with NADH is taken into consideration, the stepwise oxidation described in Figure 7 is calculated to be, in any case, more favorable for **1-Cl**.

Once the **1-H** complex is formed in the presence of molecular oxygen, the ROS H$_2$O$_2$ can be produced. Both singlet and triplet M06-L PESs for the oxygenation process of **1-H** are drawn in Figure 8. For the triplet multiplicity, only
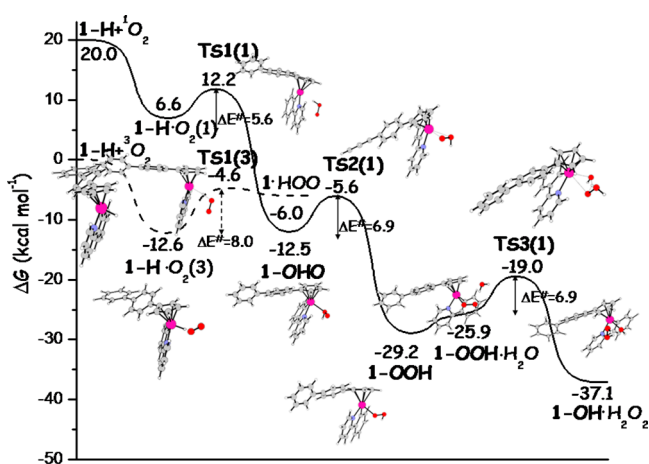

Figure 8. Singlet and triplet calculated M06-L PESs in water solvent for the oxygenation process of **1-H** to produce the H$_2$O$_2$ ROS. Energies are in kcal·mol^{-1} and relative to **1-H** + ^{3}O$_2$ ground state reactants.

stationary points involved in the surface crossing are displayed. Cartesian coordinates can be found in the SI (see Table S1). Relative free energies in solution have been calculated with respect to the ground-state reactants asymptote **1-H** + ^{3}O$_2$.

The addition of triplet molecular oxygen yields the adduct **1-H·O$_2$(3)**, whose formation is exothermic by 12.6 kcal mol^{-1}.

The optimized structure of the corresponding complex in a singlet state **1-H·O$_2$(1)** lies at 6.6 kcal mol^{-1} above the entrance channel of separated reactants. The next step of the process involves the abstraction of the hydrogen atom from the iridium center by O$_2$. Along the triplet pathway, the activation barrier of 8.0 kcal mol^{-1} corresponds to the formation of the **TS1(3)** transition state. The imaginary frequency, calculated to be 1207i cm^{-1}, corresponds to the movement of the hydrogen atom detaching from Ir and bonding to the next oxygen. As a result, an intermediate is formed, **1·(HOO)**, that lies 1.4 kcal mol^{-1} below the **TS1(3)**, in which the peroxyl HOO radical is coordinating with the metal center of the complex through a weak interaction between Ir and hydrogen atoms. On the other hand, along the singlet pathway, a transition state, **TS1(1)**, is intercepted and characterized where the distance between the hydrogen atom and the closest oxygen is 1.361 Å. This transition state lies 12.2 kcal mol^{-1} above the reactants' reference energy and is characterized by an imaginary frequency of 773i cm^{-1}. The reaction proceeds with the formation of the intermediate **1-(OHO)**, whose formation is exothermic by 12.5 kcal mol^{-1}. The most important feature of this intermediate, in analogy with our previous theoretical investigations,[25] is that the hydrogen atom is bonded to the proximal oxygen, whereas the distal oxygen atom is rotated upward. Because the singlet structure of the **1-(OHO)** complex is more stable than the **1-(OOH)** triplet intermediate, in this region of the PES, a spin inversion has to occur after the passage of the **TS1(3)** transition state. However, such a kind of spin crossing occurring after formation of the transition state does not play a critical role in influencing the rate of the reaction.[26]

After the crossing, the reaction proceeds along the singlet path with the formation of the final Ir−hydroperoxo complex and the overall process is calculated to be exothermic by 29.2 kcal mol^{-1}. The reaction evolves through the breaking of the bond between the proximal oxygen and the Ir center that makes a new bond with the distal oxygen. The corresponding transition state **TS2(1)**, lying 5.6 kcal/mol below the reactants dissociation limit, has been intercepted and confirmed by IRC analysis.

The last step of the process leads to the release of H$_2$O$_2$ from the hydroperoxide complex. Generation and release of hydrogen peroxide is simulated by considering the interaction with an additional explicit water molecule that interacts with the complex causing a destabilization of 3.3 kcal mol^{-1}. The

water oxygen atom coordinates to the metal center and simultaneously transfers one of the H atoms to the OOH group. The height of the barrier for this rearrangement is 6.9 kcal mol^{-1} with respect to the energy of the H_2O and hydroperoxide adduct leading to it. The imaginary frequency that confirms the nature of this stationary point is $199i$ cm^{-1} and corresponds to the simultaneous shift of one of the water hydrogen atoms to oxygen to yield a H_2O_2 molecule and form a new bond between the Ir center and the OH$^-$ moiety. The overall process that leads to the production of the H_2O_2 ROS together with formation of a hydroxide complex is exothermic by 37.1 kcal mol^{-1}. As suggested by the authors, in the presence of acidic species a water molecule should be released and the initial Ir complex regenerated.

5. Oxidation of the Ir-SG Complex to the Sulfenato Ir−S(O)G Complex.

Very recently, Sadler and co-workers have reported that the formation of the complex **Ir-SG** by substitution of the chlorido and pyridine ligands in the anticancer complexes **Ir-Cl** and **Ir-py** with glutathione can explain the observed differences in potency.[14] The addition of NADH to a solution containing 95% **Ir-SG** and 5% **Ir-py** causes the oxidation of NADH to NAD$^+$ and subsequent oxidation of the **1-SG** complex to the corresponding sulfenato $[(\eta^5\text{-Cp}^{xbiph})\text{Ir-(phpy)S(O)G}]^-$, **1-S(O)G**, complex.

Here are illustrated the outcomes of the calculation of the PES, reported in Figure 9, describing the oxidation of the **1-SG** complex by the produced H_2O_2 ROS.
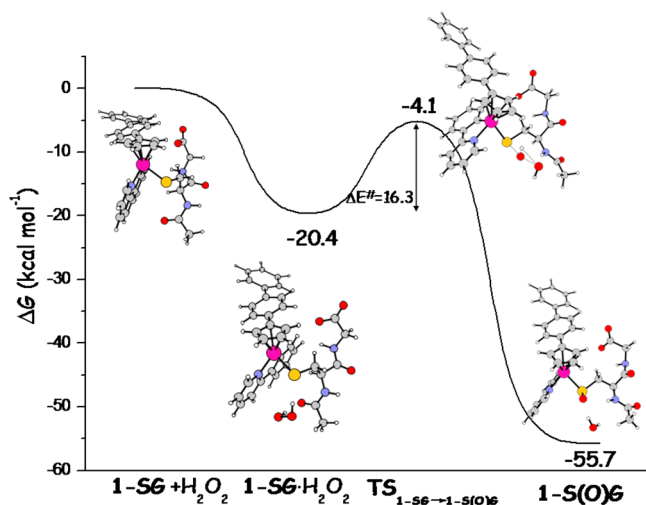

Figure 9. M06-L PES for the oxidation of the **1-SG** complex by the H_2O_2 ROS. Energies are in kcal·mol^{-1} and relative to separated reactants.

The interaction of the sulfur-coordinated thiolate **1-SG** complex with H_2O_2 leads to a stabilization of the corresponding adduct, **1-SG·H_2O_2**, by 20.4 kcal mol^{-1} with respect to the entrance channel. The next step is the conversion of the thiolate adduct to the sulfenato complex **1-S(O)G**, occurring by transfer of one of the oxygen atoms of H_2O_2 to the sulfur atom concomitant to formation of H_2O. The height of the barrier for such rearrangement is 16.3 kcal mol^{-1}, whereas the sulfenato product is formed with an energy gain of 55.7 kcal mol^{-1}. The outcomes of our computations corroborate the hypothesis that the gluthatione complex formed by substitution of the chloride or pyridine ligands in half-sandwich **1-Cl** and **1-py** complexes, respectively by S-bound gluthatione might be not a dead-end

product. Owing to driving force of the process, that is, the large calculated exothermicity, the **1-SG** complex can be quite rapidly oxidized and the formed hydrogen peroxide, which should be responsible of the increased ROS oxidative stress in cancer cells as a new strategy for curing cancer, consumed.

6. MoA of Half-Sandwich Cyclopentadienyl 1-Cl and 1-py Anticancer Complexes.

All the outcomes of our computational analysis of the water reactivity of the two **1-Cl** and **1-py** complexes illustrated in the previous sections can serve to draw some general conclusions about their MoA as anticancer drugs and to rationalize the observed differences in behavior, mainly the higher potency of **1-py** with respect **1-Cl**.

First, the hydrolysis, that is very often the necessary activation step for metal-based anticancer drugs preluding to the interaction with biological targets, has been examined. Both **1-Cl** and **1-py** complexes undergo hydrolysis even if the substitution of Cl$^-$ in **1-Cl** by water proceeds more rapidly and is more exothermic. The interaction of the formed aqua complex **1-H_2O** with a purine base site of DNA has been studied computationally using adenine and guanine as model reactants. Calculations confirm that the aqua complex readily binds to both purines. As direct interaction of **1-Cl** with guanine is hampered by a very high energy barrier, hydrolysis represents the activation step for DNA binding when the **1-Cl** complex is the cytotoxic agent. The barriers, instead, that are necessary to overcome for the displacement of py ligand in **1-py** by water, is by only 2 kcal mol^{-1} lower than that for guanine.

The process that really differentiates the behaviors of the two complexes and can influence their fate and potency is the interaction with gluthatione. Indeed, the energetic cost for the displacement of the py ligand by gluthatione is remarkably higher (31.5 kcal mol^{-1}) than that required to substitute the chloride ligand (10.7 kcal mol^{-1}) and formation of the corresponding **1-SG** product complex from **1-Cl** is also favored from a thermodynamic point of view. Deactivation of **1-Cl** by gluthatione appears, therefore, to be very likely.

The **1-H_2O** aqua complex as well as **1-Cl** and **1-py** are able to accept a hydride from NADH, causing its conversion into its oxidized form NAD$^+$. The activation by water and subsequent hydride transfer from the aqua complex is the preferred reaction pathway. The formed hydride complex reacts with triplet molecular oxygen to form the corresponding hyroperoxide complex and after that to release hydrogen peroxide by surmounting low energy barriers. The process involves a surface crossing that does not represent a bottleneck for the reaction.

At last, the oxidation reaction of the formed **1-SG** complex by H_2O_2 has been calculated to occur easily enough consuming the produced ROS hydrogen peroxide that should be the species responsible of the increased oxidative stress in cells.

In summary, it is very likely deactivation of **1-Cl** to occur by interaction with gluthatione, whereas the **1-py** complex does not undergo analogous deactivation and can, both in its aquated and nonaquated form, induce apoptosis in dual manner: by both DNA damage and H_2O_2 ROS production to increase oxidative stress.

■ CONCLUSIONS

On the basis of the experimental observations and formulated hypotheses on the mechanism of action, we have theoretically investigated with the aid of the density functional theory calculations the aqueous chemistry of the two half-sandwich organoiridium(III) cyclopentadienyl complexes **1-Cl** and **1-py**. The mechanism of the hydrolysis reaction, H_2O_2 ROS

production by hydride transfer from NADH to molecular oxygen, interaction with gluthatione and purine nucleobases adenine and guanine alongside the reaction mechanism for the oxidation of the formed sulfur-coordinated thiolate to the corresponding sulfenato complex, have been studied in detail. From the outcomes of our computational analysis, we can assume that the process clearly differentiating the behaviors of the two complexes is the interaction with gluthatione tripeptide. Coordination of gluthatione that occurs very rapidly for the **1-Cl** complex causes its deactivation, whereas a very high energy barrier hampers the process in the case of **1-py**. Both complexes can undergo hydrolysis that leads to the formation of the corresponding aqua complex. For the 1-Cl complex, in analogy with other metal-based anticancer agents, aquation represents the necessary activation step allowing coordination of purine guanine and adenine bases, whereas for **1-py**, the barrier for the aquation is lower than that for guanine coordination by only 2 kcal mol^{-1}. Interaction with NADH to form the corresponding hydride complex occurs preferentially with the aqua complex even if direct interaction with **1-Cl** and **1-py** cannot be excluded. Reaction of the formed hydride with molecular oxygen leads to the production of H$_2$O$_2$ ROS, that should be the real cytotoxic agent but that could be consumed to oxidize the formed gluthatione adduct into the corresponding sulfenato complex. Deactivation of **1-Cl** appears to be very likely. The **1-py** action, instead, is not disturbed by gluthatione interaction and can induce cell apoptosis by both DNA damage and H$_2$O$_2$ ROS production.

COMPUTATIONAL DETAILS

All molecular geometries were optimized using Truhlar's meta-GGA functional M06-L[27] that was designed to be as good as possible for the study of organometallic systems.[27] Frequency calculations at the same level of theory were also performed to identify all stationary points as minima (zero imaginary frequencies) or transition states (one imaginary frequency). The involved transition states were checked by IRC (intrinsic reaction coordinate) analysis.[28−30] For Ir, the relativistic compact Stuttgart/Dresden effective core potential[31] was used in conjunction with the split valence basis set, while the standard triple-ζ quality basis sets 6-311+G** basis sets of Pople and co-workers were used for the atoms directly participating in the process. For peripheral C and H atoms of both xbiph and phpy, the smaller 6-31G basis sets were used. All the calculations have been carried out employing the Gaussian09 software package.[32]

To reduce the computational cost, the methyl groups of the Cp^{xbiph} ligand were substituted with hydrogen atoms. Therefore, because preliminary calculations have clearly shown that the replacement of methyl groups with hydrogen atoms does not introduce any significant change in energetics, simplified models were adopted for all the studied complexes. Along the pathway for the hydride transfer from NADH to triplet molecular oxygen assisted by iridium complexes, both triplet and singlet multiplicities were examined for all the involved species. $\langle S^2 \rangle$ values were checked to assess whether spin contamination can influence the quality of the results. The method proposed by Ovchinnikov and Labanowski[33] was used for correcting the mixed spin energies and removing the foreign spin components for singlet structures that appeared to be contaminated. For molecular oxygen, for example, the adoption of the mentioned correction scheme, allowed correction of the contaminated singlet wave function and calculate a triplet-singlet energy gap of O$_2$ of 20.0 kcal mol^{-1}, which is in good agreement with the experimental value.[34]

The impact of solvation effects on the energy profiles was estimated by using the Tomasi's implicit polarizable continuum model (PCM)[35] as implemented in Gaussian09. The UFF set of radii was used to build up the cavity. The solvation Gibbs free energies were calculated in implicit water ($\varepsilon = 78.4$) at the same level by performing single-point

calculations on all stationary points structures obtained from vacuum calculations. Enthalpies and Gibbs free energies were obtained at 298 K at 1 atm from total energies, including zero-point, thermal, and solvent corrections, using standard statistical procedures.[36] However, such an approach does not reflect the real entropic change that occurs when the solute goes from the gas to the condensed phase, and the effects are more relevant when association and dissociation are involved. Therefore, following the procedure proposed by Wertz[37] and successfully adopted formerly[38] to properly handle the change of translational and rotational entropy occurring when a solute is transferred from the gas phase into the solution phase, Gibbs free energies in solution for each species, have been calculated as

$$G_{298K} = E_{elec} + G_{solv} + ZPE + H_{vib} + 6kT - T(S_{vib})$$
$$- T[0.54 \times (S_{rot} + S_{trans} - 14.3) + 8.0] \quad (1)$$

where T = 298 K and the term $6kT$ accounts for the potential and kinetic energies of the translational and rotational modes. More details can be found in the Supporting Information.

NBO charge analysis[39] and electrostatic potential calculation were carried out on the structures of some intercepted stationary points.

ASSOCIATED CONTENT

ⓢ Supporting Information

The Supporting Information is available free of charge on the ACS Publications website at DOI: 10.1021/acs.inorg-chem.5b01832.

Cartesian coordinates (Å) and absolute energies (Hartrees) of all optimized structures; additional energy profiles; NBO charge analysis; maps of the molecular electrostatic potential (PDF)

AUTHOR INFORMATION

Corresponding Author
*E-mail: siciliae@unical.it.

Notes
The authors declare no competing financial interest.

ACKNOWLEDGMENTS

REFERENCES

(1) (a) Rosenberg, B.; Van Camp, L.; Krigas, T. *Nature* **1965**, *205*, 698−699. (b) Rosenberg, B. In *Cisplatin: Chemistry and Biochemistry of a Leading Anticancer Drug*; Lippert, B., Ed.; Verlag Helvetica Chimica Acta: Zurich, 1999; Part 4, p 3. (c) Cohen, S. M.; Lippard, S. J. *Prog. Nucleic Acid Res. Mol. Biol.* **2001**, *67*, 93−130. (d) Alderden, R. A.; Hall, M. D.; Hambley, T. W. *J. Chem. Educ.* **2006**, *83*, 728−734.

(2) (a) Weiss, R. B.; Christian, M. C. *Drugs* **1993**, *46*, 360−377. (b) Hambley, T. W. *Coord. Chem. Rev.* **1997**, *166*, 181−223. (c) Wong, E.; Giandomenico, C. M. *Chem. Rev.* **1999**, *99*, 2451−2466. (d) Boulikas, T.; Pantos, A.; Bellis, E.; Christofis, P. *Cancer Ther.* **2007**, *5*, 537−583. (e) Reedijk, J. *Pure Appl. Chem.* **2011**, *83*, 1709−1719. (e1) Kelland, L. *Nat. Rev. Cancer* **2007**, *7*, 573−584. (f) Monneret, C. *Ann. Pharm. Fr.* **2011**, *69*, 286−295.

(3) Siddik, Z. *Oncogene* **2003**, *22*, 7265−7279.

(4) (a) Sherman, S. E.; Lippard, S. J. *Chem. Rev.* **1987**, *87*, 1153−1181. (b) Reedijk, J. *Proc. Natl. Acad. Sci. U. S. A.* **2003**, *100*, 3611−3616. (c) Bruijnincx, P. C. A.; Sadler, P. J. *Curr. Opin. Chem. Biol.* **2008**, *12*, 197−206.

(5) (a) Garbutcheon-Singh, K. B.; Grant, M. P.; Harper, B. W.; Krause-Heuer, A. M.; Manohar, M.; Orkey, N.; Aldrich-Wright, J. R. *Curr. Top. Med. Chem.* **2011**, *11*, 521−542. (b) Hannon, M. J. *Pure Appl. Chem.* **2007**, *79*, 2243−2261. (c) Fu, Y.; Habtemariam, A.; Pizarro, A. M.; Van Rijt, S. H.; Healey, D. J.; Cooper, P. A.; Shnyder, S. D.; Clarkson, G. J.; Sadler, P. J. *J. Med. Chem.* **2010**, *53*, 8192−8196.

(d) Fu, Y.; Habtemariam, A.; Basri, A. M. B. H.; Braddick, D.; Clarkson, G. J.; Sadler, P. J. *Dalton Trans.* **2011**, *40*, 10553−10562. (e) Park, G. Y.; Wilson, J. J.; Song, Y.; Lippard, S. J. *Proc. Natl. Acad. Sci. U. S. A.* **2012**, *109*, 11987−11992. (f) Pracharova, J.; Zerzankova, L.; Stepankova, J.; Novakova, O.; Farrer, N. J.; Sadler, P. J.; Brabec, V.; Kasparkova. *Chem. Res. Toxicol.* **2012**, *25*, 1099−1111. (g) Castonguay, A.; Doucet, C.; Juhas, M.; Maysinger, D. *J. Med. Chem.* **2012**, *55*, 8799−8806. (h) Hartinger, C. G.; Phillips, A. D.; Nazarov, A. A. *Curr. Top. Med. Chem.* **2011**, *11*, 2688−2702. (i) Liu, Z.; Habtemariam, A.; Pizarro, A. M.; Fletcher, S. A.; Kisova, A.; Vrana, O.; Salassa, L.; Bruijnincx, P. C. A.; Clarkson, G. J.; Brabec, V.; Sadler, P. J. *J. Med. Chem.* **2011**, *54*, 3011−3026.

(6) (a) Giraldi, T.; Sava, G.; Mestroni, G.; Zassinovich, G.; Stolfa, D. *Chem.-Biol. Interact.* **1978**, *22*, 231−238. Sava, G.; Zorzet, S.; Perissin, L.; Mestroni, G.; Zassinovich, G.; Bontempi, A. *Inorg. Chim. Acta* **1987**, *137*, 69−71.

(7) Trachootham, D.; Alexandre, J.; Huang, P. *Nat. Rev. Drug Discovery* **2009**, *8*, 579−591.

(8) (a) Liu, Z.; Sadler, P. J. *Acc. Chem. Res.* **2014**, *47*, 1174−1185. (b) Wirth, S.; Rohbogner, C.; Cieslak, M.; Kazmierczak-Baranska, J.; Donevski, S.; Nawrot, B.; Lorenz, I.-P. *JBIC, J. Biol. Inorg. Chem.* **2010**, *15*, 429−440. (c) Casini, A.; Edafe, F.; Erlandsson, M.; Gonsalvi, L.; Ciancetta, A.; Re, N.; Ienco, A.; Messori, L.; Peruzzini, M.; Dyson, P. J. *Dalton Trans.* **2010**, *39*, 5556−5563. (d) Gras, M.; Therrien, B.; Süss-Fink, G.; Casini, A.; Edafe, F.; Dyson, P. J. *J. Organomet. Chem.* **2010**, *695*, 1119−1125. (e) Ruiz, J.; Rodriguez, V.; Cutillas, N.; Samper, K. G.; Capdevila, M.; Palacios, O.; Espinosa, A. *Dalton Trans.* **2012**, *41*, 12847−12856. (f) Lo, K. K.-W.; Zhang, K. Y. *RSC Adv.* **2012**, *2*, 12069−12083. (g) Gasser, G.; Ott, I.; Metzler-Nolte, N. *J. Med. Chem.* **2011**, *54*, 3−25.

(9) (a) Wilbuer, A.; Vlecken, D. H.; Schmitz, D. J.; Kräling, K.; Harms, K.; Bagowski, C. P.; Meggers, E. *Angew. Chem., Int. Ed.* **2010**, *49*, 3839−3842. (b) Messori, L.; Marcon, G.; Orioli, P.; Fontani, M.; Zanello, P.; Bergamo, A.; Sava, G.; Mura, P. *J. Inorg. Biochem.* **2003**, *95*, 37−46. (c) Marcon, G.; Casini, A.; Mura, P.; Messori, L.; Bergamo, A.; Orioli, P. *Metal-Based Drugs* **2000**, *7*, 195−200.

(10) Cusanelli, A.; Frey, U.; Richens, D. T.; Merbach, A. E. *J. Am. Chem. Soc.* **1996**, *118*, 5265−5271.

(11) Poth, T.; Paulus, H.; Elias, H.; Dücker-Benfer, C.; van Eldik, R. *Eur. J. Inorg. Chem.* **2001**, *2001*, 1361−1369.

(12) (a) Liu, Z.; Sadler, P. J. *Acc. Chem. Res.* **2014**, *47*, 1174−1185. (b) Hearn, J.; Romero-Canelón, I.; Qamar, B.; Liu, Z.; Hands-Portman, I.; Sadler, P. J. *ACS Chem. Biol.* **2013**, *8*, 1335−1343. (c) Liu, Z.; Habtemariam, A.; Pizarro, A. M.; Fletcher, S. A.; Kisova, A.; Vrana, O.; Salassa, L.; Bruijnincx, P. C. A.; Clarkson, G. J.; Brabec, V.; Sadler, P. J. *J. Med. Chem.* **2011**, *54*, 3011−3026. (d) Liu, Z.; Salassa, L.; Habtemariam, A.; Pizarro, A. M.; Clarkson, G. J.; Sadler, P. J. *Inorg. Chem.* **2011**, *50*, 5777−5783. (e) Liu, Z.; Romero-Canelón, I.; Habtemariam, A.; Clarkson, G. J.; Sadler, P. J. *Organometallics* **2014**, *33*, 5324−5333. (f) Ali Nazif, M.; Bangert, J.-A.; Ott, I.; Gust, R.; Stoll, R.; Sheldrick, W. S. *J. Inorg. Biochem.* **2009**, *103*, 1405−1414.

(13) Liu, Z.; Romero-Canelón, I.; Qamar, B.; Hearn, J. M.; Habtemariam, A.; Barry, N. P. E.; Pizarro, A. M.; Clarkson, G. J.; Sadler, P. J. *Angew. Chem., Int. Ed.* **2014**, *53*, 3941−3946.

(14) Liu, Z.; Sadler, P. J. *Inorg. Chem. Front.* **2014**, *1*, 668−672.

(15) Liu, Z.; Habtemariam, A.; Pizarro, A. M.; Clarkson, G. J.; Sadler, P. J. *Organometallics* **2011**, *30*, 4702−4710.

(16) (a) Martin, R. B. In *Cisplatin: Chemistry and Biochemistry of a Leading Anticancer Drug*; Lippert, B., Ed.; Verlag Helvetica Chimica Acta: Zurich, 1999; pp 181−205. (b) Hohmann, H.; Hellquist, B.; van Eldik, R. *Inorg. Chem.* **1992**, *31*, 345−351.

(17) Pizarro, A. M.; Habtemariam, A.; Sadler, P. J. In *Medicinal Organometallic Chemistry*, 1st ed.; Topics in Organometallic Chemistry; Jaouen, G., Metzler-Nolte, N., Eds.; Springer-Verlag: Heidelberg, Germany, 2010; Vol. 32, pp 21−56.

(18) Wang, H. L.; De Yonker, N. J.; Gao, H.; Tan, C. P.; Zhang, X. T.; Ji, L. N.; Zhao, C. Y.; Mao, Z. W. *RSC Adv.* **2012**, *2*, 436−446.

(19) (a) Dolphin, D.; Avramović, O.; Poulson, R. *Glutathione: Chemical, Biochemical, And Medical Aspects*; Wiley, New York, 1989;.

(b) Hwang, C.; Sinskey, A. J.; Lodish, H. F. *Science* **1992**, *257*, 1496−1502. (c) Corazza, A.; Harvey, I.; Sadler, P. J. *Eur. J. Biochem.* **1996**, *236*, 697−705. (d) Bibhesh, K. S. *Asian J. Chem.* **2005**, *17*, 1−32. (e) Zhang, K.; Mack, P.; Wong, K. P. *Int. J. Oncol.* **1998**, *12*, 871−882.

(20) (a) Valko, M.; Morris, H.; Cronin, M. T. D. *Curr. Med. Chem.* **2005**, *12*, 1161−1208. (b) Romero-Canelón, I.; Sadler, P. J. *Inorg. Chem.* **2013**, *52*, 12276−12291.

(21) Sies, H. *Free Radical Biol. Med.* **1999**, *27*, 916−921.

(22) Liptak, M. D.; Shields, G. C. *J. Am. Chem. Soc.* **2001**, *123*, 7314−7319.

(23) Betanzos-Lara, S.; Liu, Z.; Habtemariam, A.; Pizarro, A. M.; Qamar, B.; Sadler, P. J. *Angew. Chem., Int. Ed.* **2012**, *51*, 3897−3900.

(24) Liu, Z.; Deeth, R. J.; Butler, J. S.; Habtemariam, A.; Newton, M. E.; Sadler, P. J. *Angew. Chem., Int. Ed.* **2013**, *52*, 4194−4197.

(25) Chowdhury, S.; Himo, F.; Russo, N.; Sicilia, E. *J. Am. Chem. Soc.* **2010**, *132*, 4178−4190.

(26) Schröder, D.; Shaik, S.; Schwarz, H. *Acc. Chem. Res.* **2000**, *33*, 139−145.

(27) Zhao, Y.; Truhlar, D. G. *J. Chem. Phys.* **2006**, *125*, 194101−194118.

(28) Zhao, Y.; Truhlar, D. G. *Theor. Chem. Acc.* **2008**, *120*, 215−241.

(29) Fukui, K. *J. Phys. Chem.* **1970**, *74*, 4161−4163.

(30) Gonzalez, C.; Schlegel, H. B. *J. Chem. Phys.* **1989**, *90*, 2154−2161.

(31) Andrae, D.; Hüßermann, U.; Dolg, M.; Stoll, H.; Preuß, H. *Theor. Chim. Acta* **1990**, *77*, 123−141.

(32) Frisch, M. J.; Trucks, G. W.; Schlegel, H. B.; Scuseria, G. E.; Robb, M. A.; Cheeseman, J. R.; Scalmani, G.; Barone, V.; Mennucci, B.; Petersson, G. A.; Nakatsuji, H.; Caricato, M.; Li, X.; Hratchian, H. P.; Izmaylov, A. F.; Bloino, J.; Zheng, G.; Sonnenberg, J. L.; Hada, M.; Ehara, M.; Toyota, K.; Fukuda, R.; Hasegawa, J.; Ishida, M.; Nakajima, T.; Honda, Y.; Kitao, O.; Nakai, H.; Vreven, T.; Montgomery, J. A., Jr.; Peralta, J. E.; Ogliaro, F.; Bearpark, M.; Heyd, J. J.; Brothers, E.; Kudin, K. N.; Staroverov, V. N.; Kobayashi, R.; Normand, J.; Raghavachari, K.; Rendell, A.; Burant, J. C.; Iyengar, S. S.; Tomasi, J.; Cossi, M.; Rega, N.; Millam, J. M.; Klene, M.; Knox, J. E.; Cross, J. B.; Bakken, V.; Adamo, C.; Jaramillo, J.; Gomperts, R.; Stratmann, R. E.; Yazyev, O.; Austin, A. J.; Cammi, R.; Pomelli, C.; Ochterski, J. W.; Martin, R. L.; Morokuma, K.; Zakrzewski, V. G.; Voth, G. A.; Salvador, P.; Dannenberg, J. J.; Dapprich, S.; Daniels, A. D.; Farkas, Ö.; Foresman, J. B.; Ortiz, J. V.; Cioslowski, J.; Fox, D. J. *Gaussian 09*, revision D.01; Gaussian, Inc.: Wallingford CT, 2009.

(33) Ovchinnikov, A. A.; Labanowski, J. K. *Phys. Rev. A: At., Mol., Opt. Phys.* **1996**, *53*, 3946−3952.

(34) Weissbluth, M. *Atoms and Molecules*; Academic Press: New York, 1978; p 587.

(35) Scalmani, G. M.; Frisch, J. *J. Chem. Phys.* **2010**, *132*, 114110−114112.

(36) McQuarrie, D. A.; Simon, J. D. *Molecular Thermodynamics*; University Science Books: Sausalito, CA, 1999.

(37) Wertz, D. H. *J. Am. Chem. Soc.* **1980**, *102*, 5316−5322.

(38) Cheng, M.-J.; Nielsen, R. J.; Goddard, W. A., III *Chem. Commun.* **2014**, *50*, 10994−10996.

(39) Stephens, P. J.; Devlin, F. J.; Chabalowski, C. F.; Frisch, M. J. *J. Phys. Chem.* **1994**, *98*, 11623−11627.

ACKNOWLEDGEMENTS

I would like to thank all the people who in these three years have enriched my personal and professional life.

First of all, I want to thank my Supervisor, Professor Emilia Sicilia. In these three years, she has been my inspiration source, she has taught me that everything is possible and she has enriched my personal and cultural fund.

I want to thank Professor Nino Russo. He has always been present and he has given me the opportunity to work in a team with highly work experienced.

I want to thank my colleagues, especially Dr. Gloria Mazzone. She has always been close to me in difficulty and discouragement moments.

Finally, I want to thank my husband, Christopher, and my beautiful daughter, Francesca Pia.